STUDY OF SORPTION, HEAT AND MASS TRANSFER DURING CONDENSED MODE OPERATION OF GAS PHASE ETHYLENE POLYMERIZATION ON SUPPORTED CATALYST

By

Arash Alizadeh

A thesis submitted to the Department of Chemical Engineering

In conformity with the requirements for

the degree of Doctor of Philosophy

Queen's University

Kingston, Ontario, Canada

July 2014

This work is part of the Research program of the Dutch Polymer Institute, PO Box 902, 5600AX, Eindhoven, The Netherlands, project nr. # 709.

Abstract

In the current thesis study it is intended to investigate the potential effect of the inert condensing agent (ICA) of *n*-hexane used in condensed mode operation on the solubility of ethylene in produced polyethylene (PE) and consequently the quality and rate of gas phase ethylene polymerization on supported catalyst under reactive conditions. This is the first time for such a study. Performing the set of designed polymerization reaction experiments using a lab-scale stirred-bed gas phase reactor, it is observed that the instantaneous rate of ethylene polymerization increases in the presence of *n*-hexane, thus supporting the initial speculation of the effect of *n*-hexane on the enhancement of the ethylene solubility in polymer known as "cosolubility" phenomenon. In order to have a better picture and understanding, the averaged instantaneous rate of polymerization in presence of *n*-hexane is normalized with the one without any *n*-hexane. Consequently, this helps to see that while the effect of *n*-hexane increases proportionally to its partial pressure in the gas phase composition, this effect is more pronounced at the initial steps during the course of polymerization.

In the current thesis study for the first time, the Sanchez-Lacombe EOS as one of the most widely applied thermodynamic models in polymer industry is adapted and developed in order to study not only the solubility but also concentration of ethylene in polyethylene in the absence and presence of an inert condensing agent in order to quantify the speculated cosorption phenomenon under the reactive polymerization condition. By incorporating this thermodynamic model to describe the solubility of ethylene in polymer into a single particle model like Polymer Flow Model (PFM) to estimate the concentration and temperature gradient through a growing polymer particle, it is ultimately attempted to predict the effect of change in the process operating condition by addition of *n*-hexane as the ICA to the gas phase composition.

Finally in the current thesis study, it is demonstrated how the thermal effect associated with the heat of sorption of ICAs can have a positive effect in terms of avoiding particle over-heating under certain circumstances like its temporary exposition to the defluidized regions inside a fluidized bed reactor (FBR) as a possible undesirable operating condition for this type of reactor set-ups.

Co-Authorship

The bulk of the research work presented in the current thesis study was carried out by me under supervision of Dr. Timothy F.L. McKenna. The materials presented in Chapter 3, 5, and 6 are published in the journals of *Macromolecular Symposia*, *Macromolecular Chemistry and Physics*, and *Macromolecular Reaction Engineering*, respectively. The details about each of the aforementioned publications are provided at the beginning of the corresponding chapter in the thesis. While the set of experiments presented in Chapter 5 has been designed and analyzed by me, they were performed by Mr. Montree Namkajorn as a visiting scientist to the Laboratory of Chemistry and Processes of Polymerization (LCPP) in University of Lyon I, France. The preparation and editing of the current thesis manuscript was performed by me under the supervision of the Dr. Timothy F.L. McKenna.

Acknowledgments

It is a pleasure to thank those who made this thesis possible. Before anyone else, I would like to express my deepest gratitude to my supervisor, Dr. McKenna, for his excellent guidance, caring, patience, and providing me with an excellent atmosphere for doing research. I would also like to thank Dr. Boisson from University of Lyon I and Dr. Guay from Queen's University for accepting to co-supervise my thesis with guiding my research for the past several years.

Advices and comments given by Dr. Spitz has been a great help during the progress of my research and I am very grateful to him. In addition, discussions with Dr. Monteil have been very illuminating for me from practical perspective and I would like to thank him for his interest and eagerness in dedicating his time for these discussions.

This dissertation would not have materialized, without persistent support of the technical staff at LCPP namely Mr. Broyer, Dr. Norsic and Mr. Dugas and I am particularly thankful for their assistances.

I would also like to express my gratitude to Dutch Polymer Institute (DPI) for the financial support of this project. I would like to specially thank Dr. Stamhuis and Dr. Busico who were of great support and help during the transition between the Queen's University and University of Lyon I. I would like to also show my appreciation to the industrial correspondents of the project in the DPI from the different industrial companies including SABIC Europe, Borealis and Exxon Mobil, in particular, Dr. Brinen and Dr. Walzer from Exxon Mobil who gave insightful comments and suggestions during the DPI meetings in the course of progress of my project.

Special thanks to all of my colleagues in LCPP including Montree, Julien, Miloud, Qiao, Solmaz, Muhammad Ahsan, Ravindra, Estevan, Elena, Ana, Guilhem, Benoit and many others who brought different tastes to the lab environment and made my Ph.D journey more pleasant and enjoyable.

Finally, I would like to express the deepest appreciations to my parents and elder brother. They were always supporting me and encouraging me with their best wishes.

Table of Contents

APPENDICES

List of Figures

List of Tables

List of Abbreviations

List of symbols

C^*	concentration of polymerization active sites, (mol site/m^3 cat)
C_0^*	concentration of polymerization active sites at time zero, (mol site/m^3 cat)
$C_{p,g}$	heat capacity of gas phase, (J/kg.K)
$C_{p,pol}$	heat capacity of polymer, (J/kg.K)
D_1	dimensionless diffusivity of ethylene, (dimensionless)
D_2	dimensionless diffusivity of ICA, (dimensionless)
$D_{ov.1}$	overall diffusivity of ethylene through the polymer particle, (m^2/sec)
$D_{ov.2}$	overall diffusivity of ICA through the polymer particle, (m^2/sec)
d_p	diameter of polymer particle, (m)
E_a	activation energy for propagation, (J/mol)
E_d	activation energy for catalyst deactivation, (J/mol)
h	heat transfer coefficient, (J/m^2.sec.K)
k	dimensionless rate coefficient for ethylene polymerization, (dimensionless)
$k_{c,g}$	thermal conductivity of gas phase, (J/m.sec.K)
$k_{c,p}$	thermal conductivity of polymer, (J/m.sec.K)
k_d	deactivation constant, (1/sec)
$k_{d,ref}$	deactivation constant at reference temperature, (1/sec)
k_{ij}	binary interaction parameter, (dimensionless)
k_p	propagation constant, (m^3 tot/mol site.sec)
$k_{p,ref}$	propagation constant at reference temperature, (m^3 tot/mol site.sec)
M_1	dimensionless ethylene concentration in the polymer particle, (dimensionless)
M_2	dimensionless ICA concentration in the polymer particle, (dimensionless)
$[M]_{eq.1}$	equilibrium concentration of ethylene in the polymer phase, (mol/m^3 pol)
$[M]_{eq.2}$	equilibrium concentration of ICA in the polymer phase, (mol/m^3 pol)
$[M]_{ov.1}$	overall concentration of ethylene in the polymer particle, (mol/m^3 tot)

$[M]_{ov.2}$	overall concentration of ICA in the polymer particle, (mol/m^3 tot)
$[M]_{ov.eq.1}$	overall equilibrium concentration of ethylene in whole particle considering its porosity (mol/m^3 tot)
$[M]_{ov.eq.2}$	overall equilibrium concentration of ICA in whole particle considering its porosity (mol/m^3 tot)
MW_1	molecular weight of ethylene, (gr/mol)
m_{pol}	mass of polymer produced, (gr)
N	number of grids, (dimensionless)
Nu	Nusselt number, (dimensionless)
Pr	Prandtl number, (dimensionless)
Re	Reynolds number, (dimensionless)
R_g	universal gas constant, (J/mol.K)
R_l	particle radius, (m)
R_p	equivalent radius of "polymer-only" particle without considering porosity, (m)
R_{pol}	rate of polymerization at the catalyst particle surface, (mol/m^3 cat.sec)
R_{pol}^{ins}	instantaneous rate of polymerization, (gr pol/gr cat.hr)
R_v	volumetric rate of ethylene polymerization inside growing polymer particle, (mol/m^3 tot.sec)
r	dimensionless radial position, (dimensionless)
r_{cat}	radius of initial catalyst particle, (m)
r_l	radial position inside the spherical polymer particle, (m)
T	temperature, (K)
T_b	bulk temperature, (K)
T_r	dimensionless temperature, (dimensionless)
T_{ref}	reference temperature, (K)
$T_{r,ref}$	dimensionless reference temperature, (dimensionless)
t	time, (sec)
t_{char}	characteristic time, (sec)
t_{react}	polymerization reaction time, (sec)
u	gas-particle superficial velocity, (m/sec)
V_{cat}	total catalyst volume, (m^3)
$V_{cat\,i}$	volume of catalyst dispersed in grid i, (m^3)
V_{pol}	volume of polymer, (m^3)
V_{tot}	total particle volume including its porosity, (m^3)
v_i	dimensionless volume of grid i, (dimensionless)

Greek letters

α	dimensionless thermal diffusivity of the particle, (dimensionless)
α_{ov}	overall thermal diffusivity of the particle, (m^2/sec)
β	dimensionless clustered function, (dimensionless)
γ	dimensionless clustered function, (dimensionless)
ΔH_{pol}	enthalpy of ethylene polymerization, (J/mol)
$\Delta H_{sorp,2}$	enthalpy of sorption of ICA in the polymer phase, (J/mol)
ϵ	porosity of polymer particle, (dimensionless)
μ	gas phase viscosity, (kg/m.sec)
ρ_{cat}	catalyst density, (kg/m^3)
ρ_g	gas phase density, (kg/m^3)
ρ_{ov}	overall particle density, (kg/m^3)
ρ_{pol}	polymer density, (kg/m^3)
τ	dimensionless time, (dimensionless)
τ_{react}	dimensionless polymerization reaction time, (dimensionless)
ϕ	overall growth factor, (dimensionless)

Chapter 1

Introduction

1. Inroduction

The polymerization of ethylene on supported catalyst in gas phase fluidized bed reactors (FBRs) continues to be the predominant process for production of linear low density polyethylene (LLDPE) and also represents a considerable portion of the installed high density polyethylene (HDPE) plants worldwide. However, due to the highly exothermic nature of the polymerization, the rate of polymer production in these reactors can be severely limited by the rate at which the heat of the polymerization can be removed. One means of increasing the capacity for heat removal, and thus obtaining higher production rates, is to use what is commonly referred to as condensed mode cooling. In condensed mode operation, in addition to containing ethylene, nitrogen, hydrogen and eventually a comonomer, the gas phase feed stream of the FBR also contains an inert condensing agent (ICA) such as *iso*-pentane or *n*-hexane. In this configuration, the feed stream is partially liquefied in an external heat exchanger by cooling it below the dew point of the heavier components and the liquefied portion of the feed stream is injected into the reactor in the form of small droplets. The droplets of liquid then heat up and vaporize in the reactor. In this manner the latent heat of vaporization is used to absorb a significant portion of the heat of reaction in the bottom part of the reactor, thereby making it possible to polymerize at higher rates than would be possible with a completely dry feed stream.

While it is clear that evaporation of condensable components will ultimately help to control the temperature in the zones where these components are injected, the evaporation process will be relatively fast and it is unlikely that these components remain in the liquid state much more than few seconds. In Chapter 3, it will be shown that the lifetime of a reasonably sized droplet would be on the order of a second in the reactor environment. This means that the ICAs are present in the vapor phase for a much longer time than they are in the liquid phase. Thus, it is interesting to ask whether or not their presence has any additional influence on the polymerization.

In order to answer this question, one needs to think about how the reaction proceeds on the supported catalysts used in this type of reaction: the catalytic sites are deposited inside the pores of a highly porous solid, typically made of $MgCl_2$ in the case of Ziegler-Natta catalysts or silica for metallocene or chromium-based catalysts. The particles are injected into the reactor, where ethylene rapidly polymerizes in the pores. The stress created by this initial polymerization causes the initial structure of the support to fragment and the particle is transformed into a polymer particle where the semi-crystalline polyethylene forms the continuous phase with the fragments of the support dispersed therein. The reaction continuous as monomer diffuses into the pores of the particle, sorbs in the polymer layer covering the active sites,

and then diffuses once more toward the active centers where it reacts. The continuous formation of polymer causes the particle to expand as the reaction proceeds. As the polymer layer covering the active sites is essentially made of amorphous material, the rate of reaction will be determined by the concentration of monomer in the amorphous phase of the semi-crystalline PE.

This profound importance of the sorption process during the gas phase polymerization has motivated many experimental studies in order to measure the solubility of the different species present in the gas phase composition by implementing different experimental methods in the course of last few decades. However, most of these measurements were conducted for the sorption of a single solute like ethylene in a polymer like polyethylene as a binary system, while as mentioned earlier, the feed stream of polyethylene FBR is a mixture of different components having different functionalities during the process. This implies that, for instance, the solubility of reactant ethylene in produced polyethylene in the reactor condition might actually differ from the values obtained from the binary sorption measurements of single ethylene solute in polyethylene. In fact, the presence of a heavier component in the gas phase composition is believed to enhance the solubility of lighter component of ethylene monomer in the polymer phase, which is referred to as "cosolubility" effect. A non-negligible cosolubility effect would in turn result in higher rate of polymerization thanks to the higher availability of ethylene at the active sites even if the cosolvent did not directly impact the behavior of the active sites. Thus the physical cosolubility phenomenon is obviously different from the well-known comonomer effect.

In Chapter 4, the effect of *n*-hexane as one of the most commonly used inert condensing agents (ICA) on the solubility and more importantly concentration of ethylene in amorphous phase of polyethylene is explored using the equilibrium solubility data for the binary systems of ethylene-PE and *n*-hexane-PE, and the ternary system of ethylene-*n*-hexane-PE which are measured by implementing pressure-decay technique. The Sanchez-Lacombe EOS is one of the most widely applied and popular thermodynamic models in simulation of polymerization processes due to its excellent predictive capabilities and also relative mathematical simplicity compared to the other classes of thermodynamic models for the systems including a polymer component. As a result, in Chapter 4, for the first time to the best of our knowledge, the application of Sanchez-Lacombe EOS is extended from the binary system of ethylene-PE to the ternary system of ethylene-*n*-hexane-PE, in order to describe the change in concentration of ethylene in the amorphous phase of polyethylene in the absence and presence of *n*-hexane in the gas phase composition, respectively. Consequently, the predictive performance of Sanchez-Lacombe EOS in describing the solubility of ethylene and *n*-hexane in the ternary system of ethylene-*n*-hexane-PE is evaluated against the solubility set of data obtained experimentally. Finally, a method is proposed to have

the best fitting of Sanchez-Lacombe EOS prediction for the ethylene and *n*-hexane solubility to the experimental data simultaneously which would eventually lead to a more accurate estimation of ethylene concentration in the amorphous phase of PE.

Regarding the related literature survey on sorption studies of mixture of solutes in polymer and cosolubility phenomenon, it can be deduced that the all of the academics studies available in open literature in this field aimed at quantifying the cosolubility effect during the sorption process of solutes in the polymer powder under non-reactive condition and in the equilibrium state. As a result, Chapter 5 investigates the potential effect of the inert condensing agent of *n*-hexane used in condensed mode operation on the solubility of ethylene in produced polyethylene and consequently the quality and rate of gas phase ethylene polymerization on supported catalyst under reactive conditions, for the first time in this field. Performing the set of designed polymerization reaction experiments using a lab-scale stirred-bed gas phase reactor, it is observed that the instantaneous rate of ethylene polymerization increases in the presence of *n*-hexane, thus supporting the initial speculation of the effect of *n*-hexane on the enhancement of the ethylene solubility in polymer.

While the experimental studies in the lab-scale reactors provide extremely valuable insight and understanding about the expected kinetic and thermal behavior of the studied catalytic system in the commercial scale fluidized bed reactors, however, the reliable experimental studies of gas phase ethylene polymerization process with different gas phase compositions which induce different operating conditions are found to be very time consuming. As a result, being capable to predict how the quality and rate of gas phase ethylene polymerization would evolve upon imposing a change in the process operating condition, here by addition of an ICA to the gas phase composition, appears to be of profound importance and interest from practical point of view during the operation of a FBR.

In order to achieve this level of predictive capability, at the first step, one needs to be able to describe the solubility behavior of ethylene in PE in the presence of the additional solute component of ICA by implementing the related experimental solubility data under equilibrium condition into the thermodynamic model like Sanchez-Lacombe EOS which is found to be capable to properly capture the speculated cosolubility phenomenon in the Chapter 4. By incorporating this thermodynamic model to describe the solubility of ethylene in polymer into a single particle model like Polymer Flow Model (PFM) to estimate the concentration and temperature gradient through a growing polymer particle, it is ultimately possible to theoretically predict the effect of change in the process operating condition by addition of an ICA to the gas phase composition.

It is found that at the later steps of polymerization, in which the growing polymer particle has reached its thermal stability and the solubility of solutes in the polymer phase are closer to the equilibrium condition, the prediction of the approach developed in the current study matches with the experimental rates of polymerization in an excellent manner of almost perfect fit. This remarkably good predictive capability originates from the reasonable estimation of the local concentration of reactant ethylene and local temperature inside the particle by the PFM model. In the case of local concentration, in combination with the adapted simplified diffusivity model, it demonstrates the outstanding predictive capability of the Sanchez-Lacombe model which has been developed and fitted to the experimentally obtained set of solubility data in the ternary system of ethylene-*n*-hexane-PE in order to describe the effect of *n*-hexane on the concentration of ethylene in the amorphous phase of polyethylene. However, the general modeling approach at its current development state appears to underestimate the rate of gas phase ethylene polymerization in the presence of *n*-hexane at initial steps during the course of polymerization. This discrepancy between the model prediction and experimentally obtained rates of polymerization on the effect of *n*-hexane is an indicator of some phenomena that are not captured appropriately in the developed model. These phenomena may include (but are not limited to) the evolution of morphology and porosity of catalyst/polymer particle during the polymerization reaction, and the quality and exact mechanism of processes of reactant sorption and diffusion in the absence and presence of ICA during the initial moments of polymerization in which the catalyst/polymer particle rapidly evolves in terms of its size, structure, and thermal behavior.

Finally in Chapter 6, it is intended to demonstrate how the thermal effect associated with the heat of sorption of ICAs can have a positive effect in terms of avoiding particle over-heating under certain circumstances like its temporary exposition to the defluidized regions inside a FBR as a possible undesirable operating condition for this type of reactor set-ups. Simulated thermal behavior of the particle during transition period of its temporary exposition to the defluidized region demonstrated that the rate of increase in the particle temperature is lower in the presence of *n*-hexane; as the particle starts to heat up due to the accumulation of polymerization energy, part of this energy is consumed in order to partially desorb the condensable *n*-hexane solubilized in the particle leading to lower rate of particle temperature rise. As a result, it is concluded that the probability of the particle temperature to reach its fusion temperature and consequently the probability of the resultant polymer agglomerate formation due to the local defluidization inside the FBR becomes lower in the presence of condensable *n*-hexane.

Chapter 2

Background
and
Literature Review

2. Literature review

2.1. Introduction to polyolefins

2.1.1. General aspects

Polyolefins include different types of polymers, however, in terms of production volume the most important are polyethylene (PE) and polypropylene (PP), and the variants of these two classes of polymers by addition of comonomers like 1-butene or 1-hexene. Polyethylene, the focus of the current thesis, is generally classified in three different families: high density polyethylene (HDPE), linear low density polyethylene (LLDPE), and low density polyethylene (LDPE). Figure 2.1 demonstrates the global consumption of polyolefins in 2009 and the share of each type of polyolefins in the global consumption worldwide.

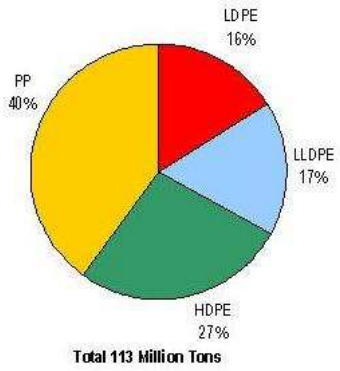

Figure 2.1. Global polyolefin consumption in 2009.[1]

Despite the enormous market for polyolefins, the global consumption of this class of polymers is expected to grow over the next decade as presented in Figure 2.2.

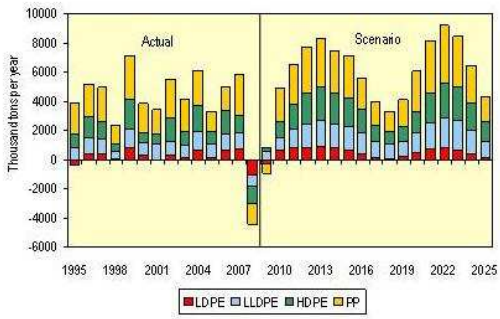

Figure 2.2. Polyolefins consumption growth (1995-2025).[1]

Polyolefins continue to hold a major portion of the market share of the commodity plastics worldwide. For instance, the market demand for LLDPE alone is expected to grow by 6.2 percent per year over the period to 2015.[1] This is in fact mainly due to their low production costs and tremendous range of achievable properties which can find a variety of applications in different sectors. Innovative materials with desirable properties for specific applications can be synthesized through state of the art tailoring of the microstructure of the polymer chains. New, more flexible processes are continuously being developed in order to produce polymers with specific properties to meet the requirements of different end-use products. In addition, due to the ever increasing demand for PE, there is a real economic driving force to increase the productivity and space-time yield in existing processes in order to expand production. Given the high exothermicity of ethylene polymerization reactions, heat removal is one of the main upper limitations on permissible production rates, so the use of techniques such condensed mode cooling is becoming more and more important.

2.1.2. Processes for production of polyolefins

Polyolefins are produced with different well-established processes in industry. Free radical polymerization (FRP) at high pressures is only used to produce LDPE as propylene decomposes before it can react under the necessary conditions. In the FRP process, the polymerization reaction is carried out in the pressure range of 1200-3500 bars and temperature range of 150-350 °C.[2] The high pressure free radical polymerization of ethylene is out of the scope of the current study and will not be discussed further here.

In addition, olefins can be polymerized catalytically at lower temperature and pressures using transition metals. In this case, the catalytic polymerization of olefins is carried out in three main types of processes depending on the phase of the continuous medium in which the reaction takes place: solution, slurry, and gas phase.[3,102]

In the solution process, the polymerization reaction is carried out at temperatures on the order of 170-250 °C. This is in order to keep the polymer produced in solution, and, along with pressures on the order of 40-60 bars, to maintain high specific reaction rates.

In a slurry process, the solid catalyst and growing polymer particles are dispersed in a continuous phase composed of a hydrocarbon diluent such as *iso*-butane or heavier alkanes. In the case of PP production the continuous phase can also be liquid propylene monomer.

Finally, in the gas phase polymerization process, the catalyst and polymer particles are dispersed and in continuous motion inside the reactor by an agitator or a fluidizing gas flow depending on the reactor

configuration.[3] In the case of PE, only fluidized bed reactors are used commercially, because of heat transfer limitations imposed by stirred bed reactors.

All of these three types of processes for catalytic polymerization of olefins offer a range of advantages and limitations. The most appropriate reactor configuration to be used in or as a part of the process to produce the final polymeric product will be determined by many factors including (but are not limited to) economic constraints, process limitations (e.g. heat transfer), the production capacity of process, equipment and operating costs of process, the desired level of flexibility of process in producing different grades of polymer depending on the changes in the market demand, and finally the target properties of final polymeric material designed for the specific end-use product.

The focus of the current study is the gas phase polymerization of ethylene on supported catalyst inside a fluidized bed reactor (FBR). After a brief introduction to the types of catalyst used in these reactors, we will discuss them in greater detail.

2.1.3. Catalysts for polymerization of olefins

There are three major types of catalytic systems which are used for the polymerization of olefins: Ziegler-Natta, metal oxides (commonly called Phillips catalysts), and metallocene catalysts.

Ziegler-Natta catalysts generally consist of a transition metal salt of groups IV-VIII and a metal alkyl of group I-III which acts as the co-catalyst. The most commonly used transition metals are titanium and vanadium.[4] Upon exposition of the transition metal to the co-catalyst, the polymerization active sites are created in a two-step process involving alkylation and reduction of the transition metal centers. Ziegler-Natta catalysts have evolved significantly since their first commercial use over sixty years ago: the first generation of Ziegler catalysts had a very low productivity of about 2 kg polymer/gr catalyst, today for its fifth generation, the productivity as high as 100 kg polymer/gr catalyst is achieved thanks to continuous improvements in catalyst chemistry and control of the evolution of particle morphology during the reaction.[4]

Phillips catalysts are composed of chromium oxide (CrO_x) or vanadium oxide (VO_x) which is generally impregnated on a silica support.[5] The Phillips catalysts are activated in-situ by ethylene during the polymerization, and unlike Ziegler-Natta catalysts there is no need for a co-catalyst. However, this in-situ activation step causes a certain induction time during the polymerization. While the exact mechanism by which the active polymerization sites are being generated still remains unknown, it appears that the metal that forms the active sites for polymerization can exist in different oxidation states.

Metallocene catalysts are basically organometallic compounds which have one or two cyclopentadienyl rings or substituted cyclopentadienyl rings bound to a central transition metal atom.[6,7] For most of metallocene catalysts, an activator like methylaluminoxane (MAO) is required, although with the recent progress now it is also possible to use metallocene catalysts without MAO.[6,7]

Both Ziegler-Natta and metallocene catalysts are used industrially in either supported (heterogeneous) or non-supported (homogenous as soluble in reaction medium) form, while the Phillips catalyst only exists in the supported form. The two most commonly used materials for catalyst supports are magnesium dichloride ($MgCl_2$) and silica (SiO_2).

The presence of more than one type of active sites in heterogeneous Ziegler-Natta and Phillips catalysts results in a wide molecular weight distribution (MWD) and chemical composition distribution (CCD) of produced polymer with a polydispersity index between 4-10 for Ziegler-Natta catalyst and 15-30 for Phillips catalysts. On contrary, homogeneous Ziegler-Natta catalysts generally based on vanadium can make polymer with uniform microstructure. Finally, the metallocene catalyst in both homogeneous and heterogeneous form can produce polymers with properties that are considerably more uniform in comparison with those made with Phillips or heterogeneous Ziegler-Natta catalysts.

In the current thesis study, the conventional Ziegler-Natta catalyst of $TiCl_4$ supported on $MgCl_2$ with triethylaluminium (TEA) as co-catalyst will be used as the catalytic system in the related experimental investigations during the gas phase ethylene polymerization.

2.2. Gas phase ethylene polymerization on supported catalyst in fluidized bed reactors

2.2.1. Process overview

The polymerization of ethylene on supported catalysts in gas phase fluidized bed reactors (FBRs) continues to be the predominant process for production of linear low density polyethylene (LLDPE), and also represents a considerable portion of the installed high density polyethylene (HDPE) capacity worldwide. Figure 2.3 shows a schema of a typical continuous FBR for polymerization of ethylene on supported catalyst, and of the different levels of complexity that need to be considered. One injects a feed gas below the distributor plate which is specially designed to appropriately distribute the gas in the reactor zone. The gas rises through the bed, which is typically 10-15 m in height, in a more or less plug-flow-like manner. As it rises, it fluidizes and mixes the solid particles in the bed. The particle, or powder phase is a mixture of freshly injected catalysts or prepolymers plus the growing polymer particles. It circulates in the bed with a CSTR-like residence time distribution. The top of the reactor is wider than the main reaction

zone. This is to cause the velocity to drop and is intended to help prevent any fine particles from leaving the reactor.

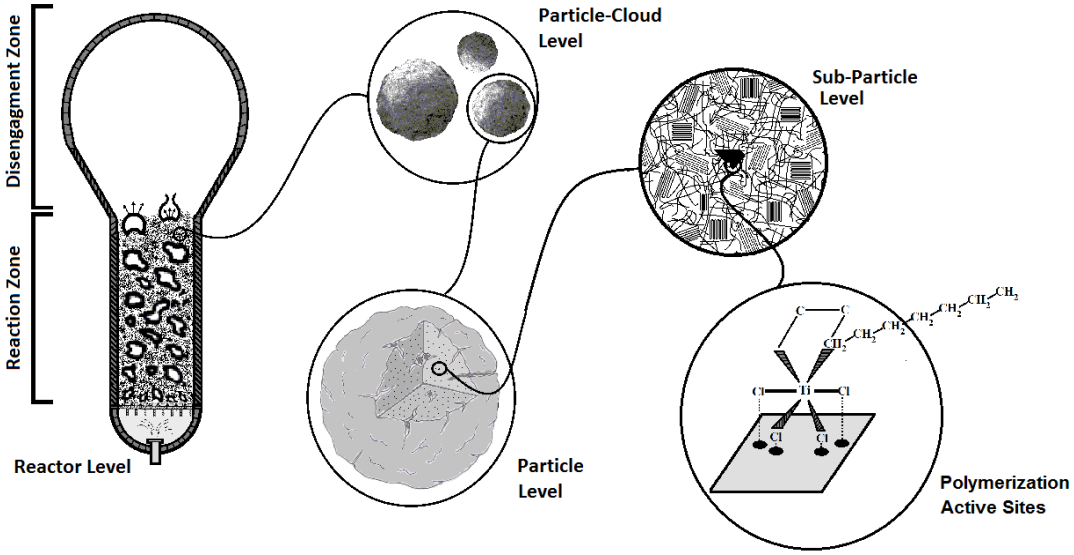

Figure 2.3. FBR and definition of different length scales corresponding to the different phenomena in the reactor.

The full modelling of this process is very complex as many different phenomena are occurring at different length scales: (a) it is at the reactor scale (macro-scale) that one needs to be able to describe the reactor hydrodynamics in order to comprehend the phenomena related to the quality of mixing and the bed stability; (b) at the intermediate scale (meso-scale) we find phenomena related to the particle interactions and intra-particle transport phenomena; (c) finally, it is at the micro-scale that one needs to be able to accurately describe the phenomena related to the sorption of monomer(s) and other species from gas phase into polymer phase, their diffusion through the generated polymer phase to reach the active sites, and ultimately the chemistry and kinetics of polymerization at the active sites which have been created and immobilized on the surface of the catalyst support material. Obviously heat transfer in the case of this highly exothermic reaction occurs in the opposite direction.

The focus of the current thesis is on the elucidation of the effect of changes in certain process conditions in a fluidized bed reactor that are associated with condensed mode cooling. In other words, we will concentrate on the effect of changing the gas phase composition on the quality and rate of ethylene polymerization on supported catalysts. Consequently, we will be looking at how the polymerization proceeds in the particles, and thus at the phenomena related to the micro-scale at the particle and sub-particle level as illustrated in Figure 2.3.

2.2.2. Single particle growth during gas phase ethylene polymerization on supported catalysts

As has already been mentioned, the polymerization of ethylene in the process of interest takes place at the "active sites" which have been chemically created and immobilized on interior pore surfaces of an inorganic support. Upon introduction of the active catalyst particle into the reactor, ethylene molecules start to diffuse from the continuous, or bulk phase of the reactor, through the pores of the particle until they reach the active sites where the polymerization reaction takes place. As the polymerization proceeds, polymer starts to accumulate in the pores of the catalyst particle, leading to the build-up of stress locally. When this stress exceeds certain level, the initial catalyst particle undergoes a process referred as "fragmentation". During the fragmentation process, the initial porous structure of the catalyst disintegrates into smaller fragments. However, the particle keeps its integrity thanks to the entangled network of produced polymers. The schematic 3D-cut presentation of the initial catalyst particle evolution during the course of the polymerization reaction with the characteristic diameter at each step is provided in Figure 2.4.

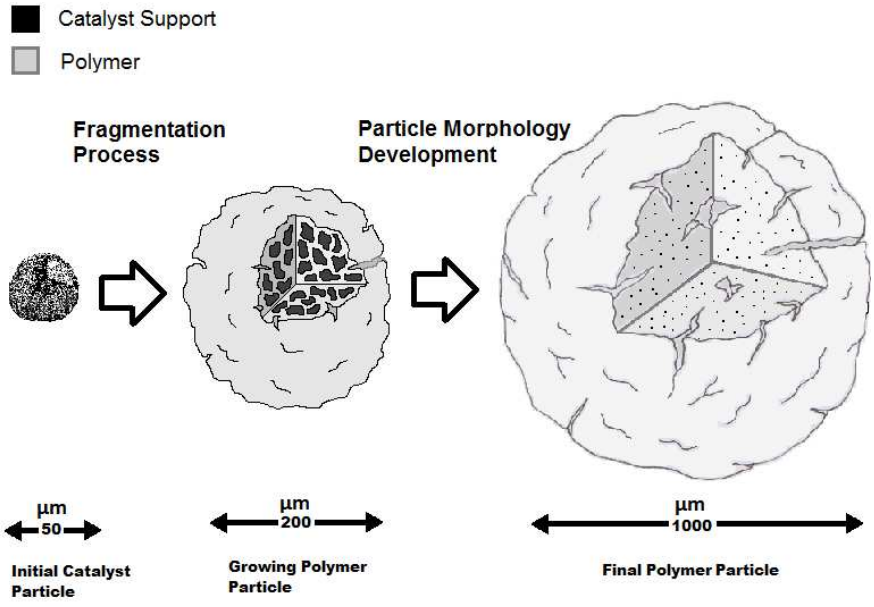

Figure 2.4. Schematic representation of a single particle evolution during the course of ethylene polymerization on the supported catalyst.

By completion of the fragmentation step, the active sites located on the fragments of initial catalyst support are completely surrounded by semi-crystalline polymer. As a result, the monomer species must diffuse through the macropores of the particle then be sorbed from the gas phase into the polymer phase. Once the monomer species are sorbed, they must diffuse through the polymer phase to reach the surface

of the catalyst fragment where the polymerization takes place. Since the polymerization reaction is exothermic, the heat produced at the active sites needed to be transferred the other way; through the polymer layer and structure of particles to the particle surface; and from the surface, through the boundary layer to the bulk phase, as presented in Figure 2.5.

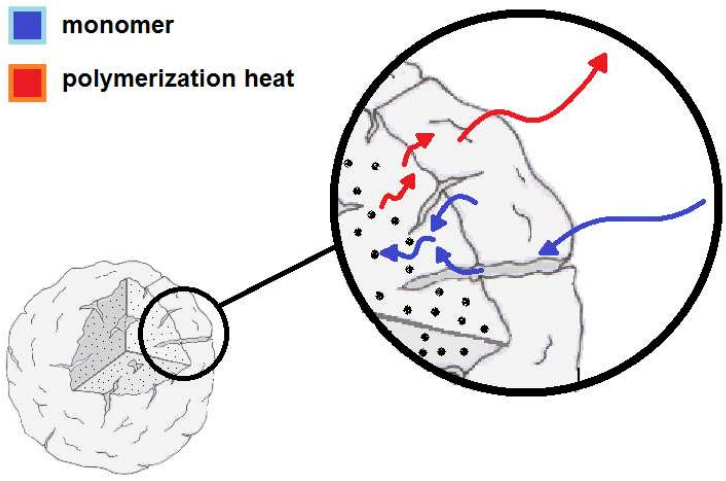

Figure 2.5. Conceptual representation of ethylene monomer sorption and diffusion in produced polymer and evacuation of released polymerization heat by convection mechanism from a single polymer particle during gas phase ethylene polymerization on supported catalyst.

This will result in the concentration and temperature gradient through the growing particle as depicted schematically in Figure 2.6.

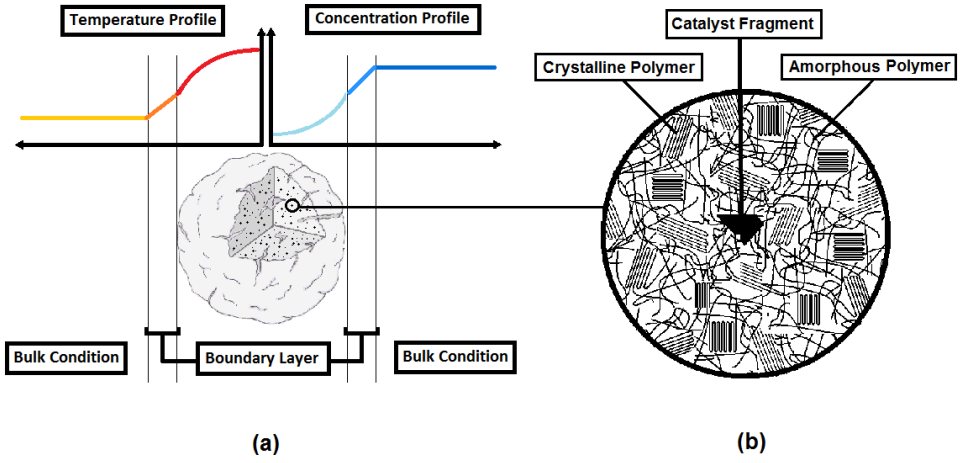

Figure 2.6. The schematic representation of (a) concentration and temperature gradient at the particle level and (b) catalyst fragment encapsulated by the produced amorphous and crystalline polymer at the sub-particle level.

2.2.3. Single particle modeling for the polymerization of olefins on supported catalysts

In the last three decades, an enormous amount of effort has been directed towards modeling and understanding the physical and chemical phenomena which take place simultaneously during the process of olefin polymerization on the supported catalytic systems at the single particle level.[3] It is out of scope of main subject of current thesis study to explore the different single particle modeling approaches developed and designed to capture and describe specific physical and/or chemical phenomena during the course of heterogeneous olefin polymerization. However, a brief overview on the different classes of single particle models is presented hereunder. In particular we will discuss the capabilities and limitations of the Polymer Flow Model, the single particle model which has been adapted for the purposes of the current thesis.

In short, the single particle models proposed and developed during the course of last three decades can be classified into two major categories: particle morphology models and particle performance models. The main goal of morphology models[8-16] is to be able to describe the evolution of particle morphology during the course of polymerization beginning with the fragmentation step, and to be able to predict the morphology of final polymer particle under specific process condition utilizing specific type of catalytic system. Performance models[17-23] are primarily aimed at simulating a specific process which takes place in a single polymer particle with a well-defined morphology. This process can be monomer diffusion in a growing particle during the polymerization, monomer degassing from the polymer particle after polymerization, or simply the sorption of monomer from gas phase into the polymer particle under the non-reactive condition. Model outputs can be polymerization rates, molecular weight distributions, etc.

The Polymer Flow Model (PFM) and Multi Grain Model (MGM) can be considered as the most commonly considered particle performance models. In the PFM model,[18] the single growing polymer particle is treated as a pseudo-homogeneous continuum through which the polymerization active sites are dispersed homogeneously. By assuming diffusion-controlled polymerization reaction within the particle, the model is able to predict the concentration gradient of reactant monomer and temperature gradient inside the growing particle at each moment during the course of polymerization. The MGM model[17] takes into account the heterogeneous nature of growing particle by assuming two levels of heat and mass transfer. The growing catalyst/polymer particle called macro-particle is assumed to be formed by agglomeration of micro-particles. Each micro-particle consists of a fragment of the original catalyst particle with all active sites on its external surface, surrounded by dead and living polymer chains. Monomer diffuses through the pores of the macro particles, adsorbs on the layer of polymer surrounding

the catalyst fragment in the micro-particles and diffuses through this layer to the active sites on the surface of the fragments, where polymerization eventually takes place. PFM and MGM models are schematically presented in Figure 2.7.

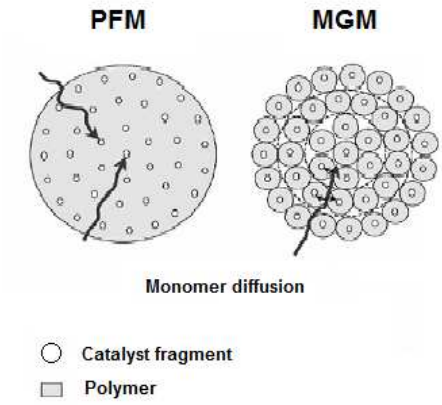

Figure 2.7. Schematic representation of PFM and MGM models.

PFM model is adapted in the current study in order to investigate the effect of local monomer concentration and temperature at the active sites dispersed inside the growing particle on the quality and rate of gas phase ethylene polymerization upon imposing a change in the process operating condition by varying the gas phase composition. This is due to the major capabilities of PFM model as explained before and considering its relative simplicity compared to the other single particle models available in the particle performance category. As a result, regarding the context of current thesis study, the use of a more complex single particle model is not justified. The polymer flow model (PFM) and the assumptions made explicitly or implicitly during its development and application will be provided in details in the corresponding section.

2.3. Condensed mode operation of gas phase ethylene polymerization on supported catalyst in FBRs

2.3.1. Introduction to condensed mode operation

The process of gas phase ethylene polymerization on supported catalyst inside FBRs offers a range of advantages including lower operational cost and more flexibility in terms of producing different polymer grades compared to the other conventional processes. However, because of the exothermic nature of the polymerization reaction, the rate of the polymer production in these reactor set-ups is limited by the rate

at which the heat of the polymerization can be removed. Increasing the polymer production rate, without the capability to remove the associated heat release would result in a dramatic increase in the reactor temperature and consequently the polymer fusion, agglomeration, and finally the reactor shut down.[24]

It is possible to increase the rate of heat removal from particles with the convection mechanism by increasing the gas superficial velocity. However, there is a limit for the increase of gas flow rate because of higher possibility of the entrainment of catalyst and polymer particles out of bed at higher gas flow rates.[25]

One can also increase the heat capacity of the gas phase by changing its composition, which would lead to higher capacity of gas phase in order to evacuate the polymerization heat from the growing particles inside the bed. Certain commercial processes like Spherilene[102] use propane instead of N_2 to achieve this. Obviously economic factors limit the degree to which we can do this in a real FBR.

One can also use what is referred to as condensed mode operation.[25-32] In the condensed mode operation of ethylene polymerization in FBRs, the gas phase feed stream of the reactor contains not only ethylene, nitrogen, hydrogen and eventually a comonomer but also an inert condensing agent (ICA) such as *iso*-pentane or *n*-hexane. In this configuration, as demonstrated schematically in Figure 2.8, the feed stream is partially liquefied in an external heat exchanger by cooling it below the dew point of the heavier components (inert and comonomers in the reactor). The vaporization of the liquid phase inside the reactor allows one to increase the amount of heat which can be removed from the reaction environment thanks to the associated latent heat of vaporization, providing the possibility to achieve higher space yield for the same reactor set-up and consequently higher production rate than is possible in “dry mode”. While it is clear that evaporation of condensable components will ultimately help to control the temperature in the zones where these components exist in liquid form, once they are vaporized these heavy components are still present in the gas phase of the reactor, and can continue to exert other influences in the reaction zone of the FBR.

In order to be able to produce the condensate in the heat exchanger by cooling, the dew point of the recycle gas must be increased. There are different ways proposed in patents; like increasing the pressure or decreasing the percentage of non-condensable components in the stream, but the most importantly and widely used is to increase the percentage of condensable components in the recycle gas stream. The preferred inert condensable components are saturated C_5 and C_6.[25-32]

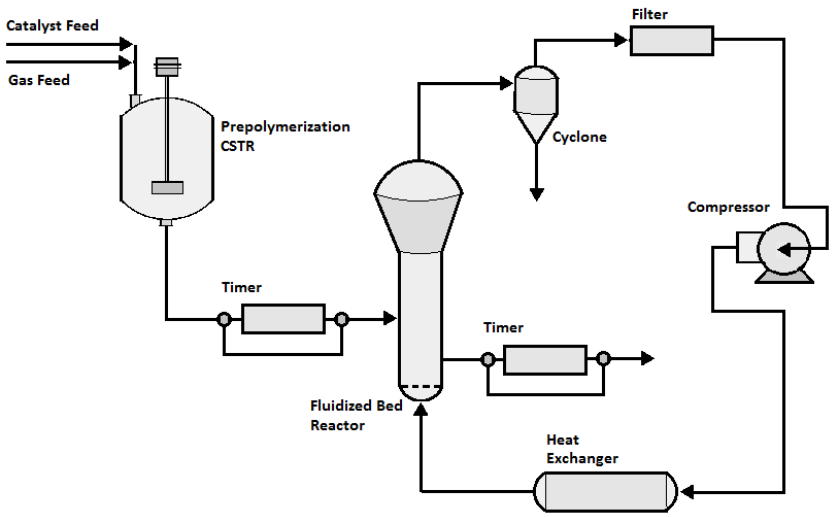

Figure 2.8. Process overview of gas phase ethylene polymerization on supported catalyst inside FBR.

2.3.2. Different configurations of condensed mode operation

There are different methods for introducing the generated liquid phase to the FBR which has been described in a range of patents.[25-32] Despite all the differences in the proposed and practiced configurations in the related condensed mode patents for gas phase ethylene polymerization in FBR, all of these condensed mode configurations are designed and developed in a manner to meet the following requirements for the operation of the process: (a) the liquid phase should be vaporized quickly in the fluidized bed, (b) the liquid accumulation should be prevented because of the possibility of production of polymer agglomerates, (c) liquid should be introduced to the bed in a manner to have the minimum effect in the fluidization behavior and stable operation of the bed, and (d) the properties of the polymer product must be consistent during the condensed mode operation. In the following section, we will briefly take a closer look on the some of the important condensed mode patents which we believe to be the most commonly practiced ones in the industry.

In the Union Carbide Patents,[25,31,32] the two phase stream obtained from cooling the recycle gas in the heat exchanger is directly fed to the bottom of the reactor as illustrated in Figure 2.9. In this design, a flow deflector is associated with entry conduit to provide upward and outward fluid flow path. This assures that the liquid and gas phases are well-mixed and the continuous suspension of entrained liquid in the gas stream. It is recommended in these patents that the weight fraction of condensed liquid not to exceed 20% wt of the recycle stream.

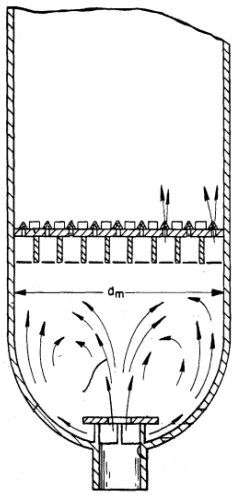

Figure 2.9. Reactor configuration for the condensed mode operation of gas phase ethylene polymerization in FBR in Union Carbide patents, adapted from Reference.[31]

Exxon patents[29,30] applied on the preceding reactor configuration, attempt to determine the stable operating conditions of the fluidized bed reactor. For instance, it is recommended that the mole fraction of *iso*-pentane as the inert condensing agent (ICA) in the recycle gas stream should not exceed 15% otherwise it will lead to instability in the fluidization or even defluidization of the bed. These patents provide information about operational aspects of the condensed mode operation of polyethylene reactors, from gas phase composition to superficial gas velocity which will be used in upcoming theoretical discussions in the next chapter.

A BP Patent[28] provides another possible configuration for the condensed mode where the liquid phase is separated from the gas phase after the heat exchanger and is injected into the bed as schematically depicted in Figure 2.10. The injection device can be an atomizer nozzle or liquid only nozzle. The atomizer nozzle is capable of producing smaller droplets. The injection means can be arranged to protrude substantially into the bed either vertically or horizontally. In order to have the fast vaporization, it is important to achieve good dispersion and penetration of liquid in the bed in this configuration.

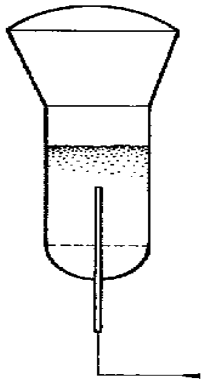

Figure 2.10. Pilot reactor configuration for the condensed mode operation of gas phase ethylene polymerization in FBR in BP patent, adapted from Reference.[28]

There are also other patents available in this field which mainly differ in the technique of separation and introduction of the liquid phase to the bed. The patent of Basell[27] introduces an innovative method of using the space below the distributor plate to serve as a "liquid-cyclone". The liquid separated is then transported with an external pipe to the top of the reactor thanks to higher pressure at the bottom of the reactor without any need to additional pump. In another patent by Union Carbide,[26] the liquid phase is separated and injected directly into the peripheral region around the fluidized bed or onto the walls of the expanded section of the reactor to form a liquid film flowing down the wall of the reactor. This method is claimed to have less effect on the fluidization behavior of the bed.

After looking at some of the important industrial patents, the related systematic studies that are available in the academic literature about condensed mode operation of gas phase polyolefin reactors or injection of a condensate into a FBR in general will be reviewed in the following section. This will eventually help us to analyze the current understanding in the academic literature about the different phenomena associated with the condensed mode operation of gas phase polyethylene reactors.

2.3.3. Theoretical studies in the literature about condensed mode operation

Despite the industrial attractiveness and numerous patents available in the field of condensed mode operation of polyolefin reactors, very few scholarly articles have been found in the open literature which addresses this subject for PE processes. We have therefore turned to experiences with other processes to begin our analysis.

The group of Briens[33] studied the possibility of agglomeration in the fluidized bed of Fluid Catalytic Cracking (FCC) catalyst particles due to the presence of large droplets of different liquids by coupling

modeling and experimental analysis. Their model simply claims that there will be the possibility of agglomeration if "the liquid droplet per mass of particles is larger than the amount of liquid which vaporizes because of instantaneous heat conduction from particle to liquid plus particle pore filling liquid". Yang et al.[34] had a similar target of analyzing the bed stability and compared the relative order of magnitude of the force related to interfacial tension between particles because of presence of liquid and drag force imposed to these particles because of fluidization. In order to have a stable fluidization, the drag force should be larger than sticky interfacial force to avoid the possibility of agglomeration.

Mirzaei et al.[35] and Utikar et al.[36] independently provided a reactor scale model for polyolefin fluidized bed reactor taking into account an "immediate" vaporization of introduced liquid into the bed during the condensed mode operation. Both of the models can be considered as an extension to the original model of McAuley et al.[24] These models all consider the reactor bed to be constituted from a bubble and an emulsion phase. The only modification in References[35,36] was to introduce additional terms in energy balance of each phase because of condensate vaporization.

The research group of McAuley studied the heat exchanger unit of the condensed mode process in a series of papers.[37-39] Their analysis provides some interesting recommendations from a process point of view. For example, it has been found that in order to optimize the rate of heat removal, the makeup ethylene should be added after the heat exchanger unit while the makeup hexene as a condensable agent should be added before the heat exchanger.

Hutchinson et al.[40] performed a modeling analysis in order to investigate the effect of condensed mode operation on the prevention of particle heat-up. Using a quasi-steady state assumption in which the heat of polymerization is removed by convection and evaporation, their simulation indicates that the condensed mode cooling has little effect on small particles which are more prone to overheating.

The presented overview of the related academic studies for the condensed mode operation of gas phase polyolefin FBRs, reveals that the most of these studies are intended to analyze the phenomena related to macro-scale of the process including: the effect of presence of condensate on the stable operation of the FBR, the influence of vaporization of condensate on controlling the overall temperature of the FBR having higher productivity, and finally, the optimization study of the heat exchanger unit of the process in which the partial condensation of reactor feed stream takes place.

On the other hand, in the appropriate operation of condensed mode polyethylene FBRs, the introduced liquefied portion of the feed stream is expected to vaporize fast in order to have minimum effect on the stable fluidization of the reactor.[25,28] Consequently, the inert condensable components will be present in

the vapor phase for a much longer time than they are in the liquid phase, in the reaction zone of a FBR. Thus, in order to develop a sound understanding about the condensed mode operation, we need to ask whether or not the presence of inert condensing agents (ICA) such as *iso*-pentane or *n*-hexane in the gas phase composition has any additional influence on the quality of polymerization. In order to answer this question, one needs to think about how the reaction proceeds on the supported catalysts used in this type of reaction at the single particle level. As presented in the previous section, the active sites located on the fragments of initial catalyst support are surrounded by the produced semi-crystalline polymer. Since the polymer layer immediately covering the active sites is essentially made of amorphous material,[41] the rate of reaction will be primarily determined by the concentration of monomer in the amorphous phase of the semi-crystalline PE. The profound importance of sorption process during the gas phase polymerization has inspired many experimental and modeling studies in this field in the course of last few decades in order to measure and describe the solubility of different species present in the gas phase composition.

In the next section, we present a review of the successive improvements in measurement and modeling of the process of sorption of a gaseous solute in a polymeric material by time, while exploring the current understanding about the potential effect of the presence of an additional solute like *n*-hexane as ICA on the solubility of ethylene in the produced semi-crystalline polyethylene.

2.4. Sorption process: from experimental measurements to modeling analyses

2.4.1. Experimental methods for sorption measurements

There are different experimental techniques[42,103] that can be used to measure the solubility of a gaseous solute in a polymer: (a) gravimetric techniques in which the weight of polymer sample is directly measured during the sorption process. In gravimetric methods, the sorption of a single solute or of a mixture of solutes is carried out by exposing a pre-weighed polymer sample to the gas phase in a well-controlled manner and continuously monitoring its weight until the sorption equilibrium is achieved; (b) pressure-decay techniques in which the amount of the solute species sorbed into polymer phase is obtained from continuous measurement of pressure decrease in a vessel with constant volume containing the polymer sample and the known amount of gaseous solute; (c) flow measurement methods such as inverse gas chromatography, in which the gas solubility in a polymer is interpreted from the measurement of partitioning of the penetrant between the mobile gas phase and the stationary polymer one; and (d) oscillating techniques in which the increase in mass of polymer sample due to the sorption of solute species is interpreted from the resonance characteristics of a vibrating support. Each of these experimental

methods possesses a number of advantages and limitations. Further details about methods of solubility measurement are not presented here; however, an interesting review about these methods with the recent advances in this field in order to acquire more precise measurement of solubility of solutes by coupling two different techniques like the pressure-decay method with the oscillating one is provided in details in Reference.[103]

In the following sections we will review experimental studies on sorption measurement for a binary system of a gaseous solute and a polymer in general; however focus will be essentially on ethylene and polyethylene in particular.

2.4.2. Sorption studies of a single solute in polymer

To the best of our knowledge, Rogers et al.[43] were the first to study (in 1959) the sorption of thirteen common organic vapors in three different polyethylene samples with different density and crystallinity at temperatures between 0-25 °C by means of a quartz helix microbalance. In this study, it was confirmed that the crystalline phase of the polyethylene is physically impenetrable to the solute molecules. In other studies by this group,[43,44] it was observed that, at low pressures, the solubility of a given solute in the polymer phase follows Henry's law. However, as the pressure of the solute increases, a higher amount of solute is solubilized in the polymer phase resulting in considerable plasticization of polymer chains. At this point, the solubility of the solute starts to increase exponentially with respect to its pressure and deviates significantly from the prediction of Henry's law. For systems of several penetrants and polyethylene in which the solubility does not obey Henry's law, Rogers et al.[44] proposed a correlation for dependency of solubility of solute to its concentration to be $S = S_0 \exp(\sigma c)$, where S_0 is the solubility coefficient from intercept at $c=0$ and σ is a constant characterizing the concentration dependency of the solubility.

Similarly, Michaels and Bixler[45] confirmed that there is no solubility in the crystalline phase of polyethylene, even for small molecules like Helium. They attempted to describe the temperature dependency of the solubility constant over the range of 10-50 °C with an Arrhenius type of correlation. They also provided a predictive correlation for estimation of solubility constant of different gases based on the Lennard-Jones potential energy as the available parameters of the gases at the time.

Li and Long[46] studied the solubility of different gases of nitrogen, methane, and ethylene at the pressures up to 100 bars, well above their critical pressure, with a quartz spring balance. In their study ethylene solubility was reported to increase exponentially with increasing pressure, while solubility of nitrogen and

methane increased asymptotically toward a saturation value. They also suggested that the deviation from the Henry's law becomes considerable at pressure higher than the critical pressure of the solute gas.

Stern et al.[47] studied the sorption data reported by several research groups implementing different experimental techniques. By analyzing these data, they discovered two common trends in all of them: first, in the limit of Henry's law the solubility of solute increases with its critical temperature and second, the pressure at which the deviation from Henry's law becomes considerable decreases as the critical temperature of solute increases. Based on the analyzed data, they proposed the following correlation for the temperature dependency of solubility of gases in the limit of Henry's law:

$$logS_0 = -5.64 + 1.14(T_c/T)^2 \qquad (2.1)$$

in which T and T_c are the solubility measurement temperature and critical temperature of the solute, respectively. The solubility of the solute in the limit of Henry's law is represented by S_0*[=]moles sorbed/(gr amorphous polymer.atm).*

In addition, they also proposed a useful correlation for the estimation of the pressure of the solute at which the deviation of solubility of solute from the prediction of Henry's law becomes appreciable (defined as 5% of deviation), P_s:

$$\log(P_s/P_c) = 3.025 - 3.5(T_c/T) \qquad (2.2)$$

in which P_c is the critical pressure of solute.

Kulkarni and Stern[48] studied the diffusivity and solubility of CO_2, CH_4, C_2H_4, and C_3H_8 in the polyethylene. At temperatures between 5-35 °C and pressures up to 40 bars, the solubility of all of the penetrants obeyed the Henry's law. Castro et al.[49] studied the solubility of *n*-butane, *n*-pentane, *n*-hexane, and *n*-heptane vapors in polyethylene with an electrobalance. The temperature range in their study was from -15 to 45 °C, at pressures up to of 0.95 relative to the vapour pressure of the hydrocarbon at that temperature. The results were analyzed attempting to establish a unique expression to predict the solubility of these hydrocarbon vapors in spite of the remarkable deviation of the experimental results from the Henry's law.

In another comprehensive analysis, Hutchinson et al.[50] investigated the accuracy of the correlation proposed by Stern et al.[47] by analysing the sorption data available in the literature reported from different research groups and found these data consistent with predictive correlation of Stern.

The effect of the copolymer composition on the solubility of ethylene, propylene, and 1-butene have been investigated by Yoon et al.[51] using quartz spring balance. The Henry's constant was found to be almost independent of the copolymer composition for ethylene and propylene while that of 1-butene showed a slight dependency on copolymer composition. As the continuation of their first work, Yoon et al.[52] found a strong dependency of the solubility of 1-hexene and 1-octene on the composition of the random ethylene/α-olefin copolymers. Jin et al.[53] measured the solubility of 1-hexene in LLDPE with a quartz spring balance at 50, 60, and 70 °C and pressures up to 0.4 bars. Their sorption data was fitted well to the prediction of Flory-Huggins theory with a constant interaction parameter χ. The measured solubility values for 1-hexene by Jin et al.[53] were consistent with the values reported in the earlier work of Yoon et al.[52]

Moore et al.[54] measured the solubility of ethylene at temperatures between 30-90 °C and the pressures up to 35 bars in polyethylene and confirmed that it obeys Henry's law in the range of studied pressure and temperature. The Henry's coefficient was found to decrease by increasing the temperature and polymer crystallinity. Regarding that the solubility coefficient was expressed in terms of mass of solute sorbed per mass of amorphous phase polyethylene, the decrease in the solubility by increasing the crystallinity was ascribed to the crystallites effect which limits the maximum of swelling and sorption for the amorphous phase. Kiparissides et al.[55] studied the sorption of ethylene in polyethylene samples at 80 °C and at elevated pressures up to 60 atm. Their measurement also showed a decrease in the solubility with increasing temperature, as expected.

While the wide range of the available solubility data acquired from the different experimental techniques provides a reliable base for evaluating and consequently implementing these data in the analyses related to the intrinsic activity of a catalytic system and reactor productivity, one must bear in mind that these measurements were conducted for sorption of a single solute like ethylene in a polymer like polyethylene as a binary system. However, as mentioned earlier, the feed stream of polyethylene fluidized bed reactor contains not only ethylene but also α-olefins like 1-butene or 1-hexene as comonomer, saturated alkanes like *iso*-pentane or *n*-hexane as inert condensing agent (ICA), hydrogen as an agent to control the molecular weight distribution of the produced polymer and finally nitrogen as an inert. This implies that, for instance, the solubility of ethylene in produced polyethylene in the reactor condition might actually differ from the values obtained from the binary sorption measurements of single ethylene solute in polyethylene, depending on the composition of the feed stream to the reactor.

In fact, it is extremely important to dispose of solubility measurements for a gas phase composed of a mixture of different solute components. The solubility measurements of a gas phase as mixture of solutes

in polymer would provide a valuable insight and understanding on how the solubility of a single gaseous solute in polymer is expected to evolve by introducing a second solute component to the gas phase composition. In the next section, we will look at the related sorption studies of a gas phase as a mixture of solutes in polymer in this field. This will eventually lead us to the main subject of the current thesis study as exploring the potential effect of the presence of inert condensing agents like *n*-hexane in the gas phase composition on the solubility and as a result quality and rate of gas phase ethylene polymerization on supported catalyst during the condensed mode operation of FBR.

2.4.3. Sorption studies of mixture of solutes in polymer

According to the experimental sorption studies of mixture of solutes in polymer, the presence of a heavier component in the gas phase composition is believed to enhance the solubility of lighter component of ethylene monomer in the polymer phase. This increase in the solubility of one species due to the presence of another is referred to as the "cosolubility" effect.[46,51,54,57-65] This could be quite important since if there is a cosolubility effect, for instance of *n*-hexane on ethylene, one could expect to see a higher rate of polymerization in condensed mode than in dry mode due to the higher availability of ethylene at the active sites. This physical "cosolubility" phenomenon is obviously different from the well-known comonomer effect in which the rate of ethylene polymerization is boosted due to the modifications in the chemical nature of catalyst active sites in presence of comonomer molecules.[56]

To the best of our knowledge, the first experimental study which partially addressed the cosolubility phenomenon was reported in 1968 by Robeson and Smith.[57] In this study, the permeation of mixtures of ethane and butane through a polyethylene film was investigated using a permeation cell apparatus. The permeability of both ethane and butane in semi-crystalline PE in the temperature range of 20-80 °C and at the mixture vapour pressure equal to the atmospheric pressure was found to increase by increasing the butane concentration in the gas phase mixture. However, the solubility of ethane was found to rise only at a lower temperature range of 20-30 °C as a result of the plasticizing effect of butane. This could be attributed to the fact that at lower temperature the natural mobility of the polymer chains are much less and as a result the plasticizing effect of more soluble component (butane) produces more pronounced effect at lower temperatures. This is in addition to the fact that higher amount of butane is solubilized in polymer at lower temperatures.

Li and Long[46] measured the total solubility of methane-ethylene, methane-nitrogen, and ethylene-nitrogen mixtures in PE. In all of the experiments, the overall solubility of gas phase mixture measured was found to be higher than the solubility expected by individual sorption measurement of each single

component and considering their partial pressure in the gas phase mixture. They explained this phenomenon by the plasticizing effect of more soluble component which raises the solubility of less soluble component in PE and consequently raises the total gas phase solubility.

Yoon et al.[51] reported a similar trend in the gas phase mixture of ethylene-propylene. They also found that keeping constant total pressure and increasing partial pressure of more soluble component (propylene), the cosolubility effect becomes more pronounced. On contrary, they found that keeping partial pressure of more soluble component constant and raising the partial pressure of less soluble component of ethylene did not affect the difference between the solubility of gas phase mixture and the one predicted from the sorption measurements of individual gases. They concluded that this observation indicates that the solubility of propylene in PE is not affected by the partial pressure of ethylene in the gas phase mixture.

McKenna[58] experimentally measured the cosolubility phenomenon in the gas phase as a mixture of ethylene and 1-butene being solubilized in polyethylene. Based on the experimental results, it was concluded that the presence of 1-butene did not affect the solubility behavior of ethylene in PE, but this was attributed to the very low partial pressure of 1-butene used in this set of experiments.

Moore and Wanke reported some preliminary cosorption studies using an electro microbalance apparatus as an attempt to explore the counter effects of ethylene and 1-hexene on the solubility of each other in polyethylene.[54] In these experiments, the admission of olefins to the measurement chamber was performed sequentially rather than simultaneously due to the technical limitations as highlighted by authors; first 1-hexene is introduced to the measurement chamber in which the polymer sample is placed. After reaching the equilibrium condition, this is followed by introduction of ethylene. It is observed that by admission of ethylene, first the sample weight decreased very rapidly, which was attributed to the partial desorption of the 1-hexene from the sample. Subsequently, the measured weight started to increase by resorption of 1-hexene. This increase in weight of sample continued even after 70 hours when the measurement was stopped without reaching the equilibrium condition. While this set of experiments shed some light on the effect of complex interactions between olefin molecules on their solubility behavior in polymer phase, it could not totally succeed to capture the cosolubility phenomenon due to inability to reach the equilibrium condition for the ternary system of study.

In order to explore the cosolubility phenomenon, Novak et al.[59] similarly performed sorption measurements by the gravimetric technique of suspension magnetic balance with the gas phase as a mixture of ethylene and the heavier component of 1-hexene. In their study, it was reported that the

solubility of gas phase as the mixture of solute components was less than the summation of the individual independent measured solubility of ethylene and 1-hexene at the same condition. Using modeling analysis, this observation was explained by claiming that the decrease in the solubility of 1-hexene due to the presence of ethylene (anti-solvent effect of ethylene) is larger than the increase in ethylene solubility in presence of 1-hexene (cosorption effect of 1-hexene).

Finally, Yao et al.[60] investigated the effect of presence of *iso*-pentane and *n*-hexane as two major inert condensing agents (ICA) in the gas phase composition on the solubility of ethylene in polyethylene powder by using a pressure decay method. An enhancement in ethylene solubility in polyethylene was observed in the presence of both ICAs of *iso*-pentane and *n*-hexane in their study.

Regarding the related literature survey on sorption studies of mixture of solutes in polymer and cosolubility phenomenon, it can be deduced that most of the academic studies available in the open literature in this field aimed at quantifying the cosolubility effect during the sorption process of solutes in the polymer powder under non-reactive conditions and in the equilibrium state. However, in the current thesis we wish to investigate the potential effect of an inert condensing agent on the solubility of ethylene under reactive conditions. Thus we will be obliged to use this equilibrium data for certain modeling studies, however in order to be more realistic, details about a series of designed experiments with the associated results in order to capture the speculated cosolubility phenomenon under the reactive conditions will be provided in the related Chapter 5.

The experimental studies in lab-scale reactors used to investigate the effect of changes in the process operating conditions, for instance here by varying the gas phase composition during ethylene polymerization on a supported catalyst, provide extremely valuable insight and understanding about the expected kinetic and thermal behavior of the studied catalytic system in the commercial scale fluidized bed reactors while experiencing similar imposed changes in the operating condition of the process.

Nevertheless, reliable experimental studies of gas phase ethylene polymerization process with different gas phase compositions which induce different operating conditions are very time consuming. As a result, we would like to be capable of predicting how the quality and rate of gas phase ethylene polymerization would evolve upon imposing a change in the process operating condition using a process model.

In order to achieve this level of predictive capability, one needs first to be able to describe the cosolubility behavior by using an appropriate thermodynamic model which is capable to properly capture the equilibrium phenomenon. Then, incorporating this thermodynamic model in a single particle model like

the PFM to estimate the concentration and temperature gradient through a growing polymer particle should allow us to predict the effect of change in the process operating condition by addition of an ICA to the gas phase composition.

In the next section, we will have a brief overview of the major thermodynamic models that are applied in the polymer industry in general and in the polyolefin sector in particular. The thermodynamic model which is adapted in the current thesis study in order to quantify the solubility behavior of ethylene in polyethylene in presence of the studied inert condensing agent is highlighted while the details about the development and application of this thermodynamic model is provided in Appendix A and Chapter 4, respectively.

2.4.4. Thermodynamic models to describe the sorption equilibrium

In the solubility studies for sorption of a single solute in polymer, it was demonstrated that the solubility of heavy components, especially at higher pressures, deviates significantly from the prediction of Henry's law. In addition, Henry's law is incapable of describing the solubility of a gas phase as a mixture of components in polymer. It is therefore necessary to use a more advanced thermodynamic model for a more precise description of the sorption process.

Generally, the advanced thermodynamic models for treating the phase equilibria of the solution can be classified into two major categories: (a) activity coefficient relations; and (b) equations of state. For the systems of solvent-polymer, equations of state (EOS) are preferred over the activity coefficient models[66] because the EOS can capture and describe the dependency of phase volume on pressure, which is of profound importance in estimating the solubility of solute and swelling degree of the polymer phase due to the sorption. As a result, the activity coefficient models are not presented here, however an interesting review about this category of the thermodynamic models is provided in Reference.[66]

In this section, an overview of the equations of state (EOS) applied in the polymer industry will be presented. There are two major classes of thermodynamic equations of state which have been subject to substantial improvements over the course of last three decades, and currently have found a wide range of application fields in the polymer industry due to their excellent predictive capabilities: (a) perturbation theory models with the PC-SAFT model as its most recent and widely applied version; and (b) lattice models with Sanchez-Lacombe EOS as its most widely applied version.[67]

2.4.4.1. Perturbation theory models and PC-SAFT EOS

In the perturbation theory, the main assumption is that the residual part of the Helmholtz energy of a system, A^{res}, as its difference from an ideal gas can be expressed as the summation of different contributions, whereas the main contribution is covered by the Helmholtz energy of a chosen reference system, A^{ref}. Contributions to the Helmholtz energy that are not covered by the reference system are considered as perturbation terms, A^{pert}:

$$A = A^{id} + A^{res} = A^{id} + A^{ref} + A^{pert} \qquad (2.3)$$

For the small molecules, an appropriate reference system is the hard sphere system. In a hard sphere system, the molecules are assumed to be spheres of a fixed diameter, which do not have any attractive interactions. The hard-sphere system covers the repulsive interactions among the molecules that are considered to mainly contribute to the thermodynamic properties. However, the thermodynamic properties of real molecules can deviate from the reference system due to attractive interactions (dispersion), formation of hydrogen bonds (association), or non-spherical shape of molecules. These contributions are generally accepted to be independent of each other and therefore are accounted for by different perturbation terms. Depending on the type of the considered perturbation term and the expression used to describe, different thermodynamic models have been developed based on the perturbation theory.[68-73]

Statistical Associating Fluid Theory (SAFT) was one of the first models derived from the idea of the perturbation theory.[68-71] A widely applied model of this family of models is the Perturbed Chain SAFT (PC-SAFT) model which was particularly developed to improve the modeling of systems including polymeric components.[72,73] The different versions of SAFT family have been applied widely in the polymer industry in order to describe the phenomena related to the phase equilibria. In particular, in the polyolefin sector, it has been implemented to study the phase diagrams in polymer-solvent systems which play an important role during the stable operation of solution and slurry polymerization processes.[74-80] In addition to describe the solubility of single solutes in polymer, the PC-SAFT model has been specifically extended to study the sorption behavior of gas phase as a mixture of ethylene and 1-hexene in LLDPE.[59]

The detailed description of the models based on the perturbation theory including the different developed versions of SAFT family can be found in References[81,82] and will not be elucidated further here.

2.4.4.2. Lattice models and Sanchez-Lacombe EOS

In the lattice models, it is assumed that the molecules have one or more segments and the partition function of the system can be calculated by counting the number of possible configurations when these segments are arranged in hypothetical cells, which resemble the crystal lattice of a solid. The thermodynamic properties can then be obtained by using formalism of statistical mechanics. The lattice can be considered to be compressible or incompressible. The incompressible lattices are generally used to model liquids at low pressures while the compressible lattices result in the equations of state based on lattice model like the lattice fluid theory of Sanchez and Lacombe.[83-85] The Sanchez-Lacombe EOS is similar and can be considered as the continuation of Flory-Huggins theory. The most important improvement is that Sanchez-Lacombe theory introduces holes into the hypothetical lattice to account for the variation in compressibility and consequently density.[83-85]

The Sanchez-Lacombe model has been applied in the polyolefin industry in order to describe the phase diagrams of polymer-solvent systems[86-93] and also the solubility of different single solutes in polymer.[42,94-100] More recently, Bashir et al.[101] extended the Sanchez-Lacombe EOS to describe the solubility of a gas phase as a mixture of two solute components in the polyolefins. According to their analysis, it was found that the Sanchez-Lacombe EOS is capable of predicting the cosolubility phenomenon for the different systems which have been analyzed.

In the current thesis study, and for the first time, the Sanchez-Lacombe EOS is adapted and developed to study not only the solubility but also concentration of ethylene in polyethylene in the absence and presence of an inert condensing agent in order to quantify the speculated cosorption phenomenon under the reactive polymerization condition. This is regarding the wide range of application of this thermodynamic model in order to describe the solubility of different solutes of interest in polyolefins which is originated from its excellent predictive capability and also relative simplicity compared to the other class of equations of state (EOS), e.g. PC-SAFT. The further details about the development and application of this thermodynamic model are provided in Appendix A and Chapter 4, respectively.

2.5. Conclusion

In the current chapter, it was intended to provide an introduction to the polyolefins as the category of polymers with the largest market share among other commodity plastics worldwide. The different commonly used catalytic systems and established processes in industry for polymerization of olefins have been briefly reviewed, while the gas phase ethylene polymerization on supported catalyst has been

elucidated in more detail as the focus of current thesis study. The different phenomena occurring simultaneously at different length scales during the gas phase ethylene polymerization in FBRs have been highlighted. The quality of a single catalyst particle growth from the time of its exposure to the reaction environment until its withdrawal from the reactor as a fully grown polymer particle was explained in details. This was followed by an overview on the modeling approaches developed in this field like PFM and MGM models in order to capture the physical and/or chemical phenomena occurring at the single particle level as the main interest of current thesis study.

The process of gas phase ethylene polymerization on supported catalysts in FBRs offers a range of advantages. However, because of the exothermic nature of the polymerization reaction, the rate of the polymer production in these reactor set-ups is limited by the rate at which the heat of the polymerization can be removed. On the other hand, due to the ever-increasing demand for polyethylenes, there is a real economic driving force to increase the productivity and space time yield in the existing processes in order to expand the production. The condensed mode operation and its most important configurations have been introduced in this chapter as a commonly practiced method in industry in order to achieve higher productivity of gas phase ethylene polymerization in existing FBR set-ups. In the condensed mode operation of FBRs, an inert condensing agent(s) such as *iso*-pentane or *n*-hexane is added to the gas phase composition. As a result, the feed stream could be partially liquefied in an external heat exchanger by cooling it below the dew point of the gas phase mixture. By vaporization of the liquid phase inside the reactor higher amount of heat can be removed from the reaction environment thanks to the associated latent heat of vaporization, providing the possibility to achieve higher space yield for the same reactor set-up.

The presented review of the related academic studies for the condensed mode operation of gas phase polyolefin reactors revealed that most of these studies were intended to analyze the phenomena related to macro-scale of the process including the effect of the presence of condensate on the stable operation of FBR, the influence of vaporization of condensate on controlling the overall temperature of FBR, and so on. While it is clear that the evaporation of condensable components will ultimately help to control the temperature in the zones where these components exist in liquid form, once they are vaporized these inert condensing agents are still present in the gas phase of the reactor. Therefore, in order to develop a sound understanding about the condensed mode process, it is important to ask whether or not their presence has any additional influence. In order to able to answer this question, one needs to think about how the polymerization reaction proceeds on supported catalysts at the single particle scale (and not the macro-scale) in this process. As presented in details in this chapter, during the gas phase polymerization of

ethylene on supported catalyst and by completion of the fragmentation process during the early stages, the active sites located on the fragments of the initial catalyst support are completely surrounded by the produced semi-crystalline polymer. Since the polymer layer immediately covering the active sites is essentially made of amorphous material, the quality and rate of polymerization reaction will be primarily determined by the solubility or in more accurate terms the concentration of monomer in the amorphous phase of the semi-crystalline polyethylene. According to the experimental sorption studies as presented in the current chapter, the presence of a heavier component is believed to enhance the solubility of the lighter component of ethylene monomer in the polymer which is referred to as "cosolubility" effect. Regarding the related literature survey on sorption studies of mixture of solutes in polymer and cosolubility phenomenon, it is deduced that most of the published academic studies in this field aimed at quantifying the cosolubility effect during the sorption process of solutes in the polymer powder under non-reactive conditions and in the equilibrium state. However, in the current thesis we wish to investigate the potential effect of an inert condensing agent on the solubility of ethylene under reactive conditions. Thus we will be obliged to use this equilibrium data for certain modeling studies, however in order to be more realistic, details about a series of designed experiments with the associated results in order to capture the speculated cosolubility phenomenon under the reactive conditions will be provided in the related Chapter 5.

The experimental studies in lab-scale reactors used to investigate the effect of changes in the process operating conditions, for instance here by varying the gas phase composition during ethylene polymerization on a supported catalyst, provide extremely valuable insight and understanding about the expected kinetic and thermal behavior of the studied catalytic system in the commercial scale fluidized bed reactors while experiencing similar imposed changes in the operating condition of the process. Nevertheless, reliable experimental studies of gas phase ethylene polymerization process with different gas phase compositions which induce different operating conditions are very time consuming. As a result, we would like to be capable of predicting how the quality and rate of gas phase ethylene polymerization would evolve upon imposing a change in the process operating condition using a process model.

In order to achieve this level of predictive capability, one needs first to be able to describe the cosolubility behavior by using an appropriate thermodynamic model which is capable to properly capture the equilibrium phenomenon. The Sanchez-Lacombe EOS is adapted for this purpose in the current study. Then, incorporating this thermodynamic model in a single particle model like the PFM to estimate the concentration and temperature gradient through a growing polymer particle should allow us to predict the

effect of change in the process operating condition by addition of an ICA to the gas phase composition during the condensed mode operation.

After defining the framework of the current thesis study by reviewing the current understanding about condensed mode operation of gas phase ethylene polymerization on supported catalysts in FBRs and the related phenomena, we will start our study by analyzing the process of evaporation of liquefied portion of feed stream inside the FBR in the next chapter.

2.6. References

1. www.chemsystems.com. **2014**.
   Ref Type: Online Source

2. Woodbrey, J. C.; Ehrlich, P. The Free Radical, High Pressure Polymerization of Ethylene. II. The Evidence for Side Reactions from Polymer Structure and Number Average Molecular Weights. *J. Am. Chem. Soc.* **1963,** *85* (11), 1580-1584.

3. McKenna, T. F.; Soares, J. B. P. Single particle modelling for olefin polymerization on supported catalysts: A review and proposals for future developments. *Chemical Engineering Science* **2001,** *56* (13), 3931-3949.

4. Albizzati, E.; Galimberti, M. Catalysts for olefins polymerization. *Catalysis Today* **1998,** *41* (1-3), 159-168.

5. Thune, P. C.; Loos, J.; de Jong, A. M.; Lemstra, P. J.; Niemantsverdriet, J. W. Planar model system for olefin polymerization: the Phillips CrOx /SiO2 catalyst. *Topics in Catalysis* **2000,** *13* (1-2), 67-74.

6. Mulhaupt, R. Catalytic Polymerization and Post Polymerization Catalysis Fifty Years After the Discovery of Ziegler's Catalysts. *Macromol. Chem. Phys.* **2003,** *204* (2), 289-327.

7. Hlatky, G. G. Heterogeneous Single-Site Catalysts for Olefin Polymerization. *Chem. Rev.* **2000,** *100* (4), 1347-1376.

8. Di Martino, A.; Weickert, G.; Sidoroff, F.; McKenna, T. F. L. Modelling Induced Tension in a Growing Catalyst/Polyolefin Particle: A Multi-Scale Approach for Simplified Morphology Modelling. *Macromolecular Reaction Engineering* **2007,** *1* (3), 338-352.

9. Kittilsen, P.; Svendsen, H. F.; McKenna, T. F. Viscoelastic model for particle fragmentation in olefin polymerization. *AIChE J.* **2003,** *49* (6), 1495-1507.

10. Horácková, B.; Grof, Z.; Kosek, J. Dynamics of fragmentation of catalyst carriers in catalytic polymerization of olefins. *Chemical Engineering Science* **2007,** *62* (18-20), 5264-5270.

11. Grof, Z.; Kosek, J.; Marek, M. Modeling of morphogenesis of growing polyolefin particles. *AIChE J.* **2005,** *51* (7), 2048-2067.

12. Grof, Z.; Kosek, J.; Marek, M.; Adler, P. M. Modeling of morphogenesis of polyolefin particles: Catalyst fragmentation. *AIChE J.* **2003,** *49* (4), 1002-1013.

13. Merquior, D. M.; Lima, E. L.; Pinto, J. C. Modeling of Particle Fragmentation in Heterogeneous Olefin Polymerization Reactions, 2. *Macromol. Mater. Eng.* **2005,** *290* (6), 511-524.

14. Chiovetta, M. G.; Estenoz, D. A. Behavior of Active Sites in a Changing, Supported Metallocene Catalyst Particle: Modeling Monomer Transport and Kinetics. *Macromol. Mater. Eng.* **2004,** *289* (11), 1012-1026.

15. Estenoz, D. A.; Chiovetta, M. G. A structural model for the catalytic polymerization of ethylene using chromium catalysts. Part I: Description and solution. *Polym Eng Sci* **1996,** *36* (17), 2208-2228.

16. Ferrero, M. A.; Chiovetta, M. G. Catalyst fragmentation during propylene polymerization: Part I. The effects of grain size and structure. *Polym Eng Sci* **1987,** *27* (19), 1436-1447.

17. Hutchinson, R. A.; Chen, C. M.; Ray, W. H. Polymerization of olefins through heterogeneous catalysis X: Modeling of particle growth and morphology. *J. Appl. Polym. Sci.* **1992,** *44* (8), 1389-1414.

18. Kanellopoulos, V.; Dompazis, G.; Gustafsson, B.; Kiparissides, C. Comprehensive Analysis of Single-Particle Growth in Heterogeneous Olefin Polymerization: The Random-Pore Polymeric Flow Model. *Ind. Eng. Chem. Res.* **2004,** *43* (17), 5166-5180.

19. Agarwal, U. S. Modeling Polyolefin Deformation Resistance in a Growing Microparticle. *Ind. Eng. Chem. Res.* **2004,** *43* (23), 7275-7281.

20. Seda, L.; Zubov, A.; Bobak, M.; Kosek, J.; Kantzas, A. Transport and Reaction Characteristics of Reconstructed Polyolefin Particles. *Macromolecular Reaction Engineering* **2008,** *2* (6), 495-512.

21. Bobak, M.; Gregor, T.; Bachman, B.; Kosek, J. Estimation of Morphology Characteristics of Porous Poly(propylene) Particles from Degassing Measurements. *Macromolecular Reaction Engineering* **2008,** *2* (2), 176-189.

22. Kanellopoulos, V.; Tsiliopoulou, E.; Dompazis, G.; Touloupides, V.; Kiparissides, C. Evaluation of the Internal Particle Morphology in Catalytic Gas-Phase Olefin Polymerization Reactors. *Ind. Eng. Chem. Res.* **2007,** *46* (7), 1928-1937.

23. Patzlaff, M.; Wittebrock, A.; Reichert, K.-H. Sorption studies of propylene in polypropylene. Diffusivity in polymer particles formed by different polymerization processes. *J. Appl. Polym. Sci.* **2006,** *100* (4), 2642-2648.

24. McAuley, K. B.; Talbot, J. P.; Harris, T. J. A comparison of two-phase and well-mixed models for fluidized-bed polyethylene reactors. *Chemical Engineering Science* **1994,** *49* (13), 2035-2045.

25. Jenkins J.M.; Jones R.L.; Jones T.M. Fluidized Bed Reaction Systems. US 4,543,399, **1985**.

26. Brown R.C.; Balmer N.L.; Simpson L.L. Gas Phase Polymerization Process. US 6,306,981, **2001**.

27. Penzo G.; Mei G.; Meier G. Gas-Phase Olefin Polymerization Process. US 7,482,411, **2009**.

28. Chinh J-C.; Filippelli M.C.H; Newton D.; Power M.B. Polymerization Process. US 5,541,270, **1996**.

29. Griffin J.R.; DeChellis M.L.; Muhle M.E. Process for Polymerizing Monomers in Fluidized Beds. US 5,462,999, **1995**.

30. DeChellis M.L.; Griffin J.R. Process for Polymerizing Monomers in Fluidized Bed. US 5,352,749, **1994**.

31. Rhee S.J.; Simpson L.L. Fluidized Bed Polymerization Reactors. US 4,933,149, **1990**.

32. Jenkins J.M.; Jones R.L.; Jones T.M.; Beret S. Methods for Fluidized Bed Polymerization. US 4,588,790, **1986**.

33. Leclére, K.; Briens, C. L.; Bergougnou, M. A.; Bayle, J.; Gauthier, T.; Guigon, P. Experimental study of droplet vaporization in a fluidized bed. *Can. J. Chem. Eng.* **2001,** *79* (6), 866-873.

34. Yang, Y. R.; Yang, J. Q.; Chen, W.; Rong, S. X. Instability Analysis of the Fluidized Bed for Ethylene Polymerization with Condensed Mode Operation. *Ind. Eng. Chem. Res.* **2002,** *41* (10), 2579-2584.

35. Mirzaei, A.; Kiashemshaki, A.; Emami, M. Fluidized Bed Polyethylene Reactor Modeling in Condensed Mode Operation. *Macromol. Symp.* **2007,** *259* (1), 135-144.

36. Utikar, R. P.; Harshe, Y. M.; Mehra, A.; Ranade, V. V. Modeling of a fluidized bed propylene polymerization reactor operated in condensed mode. *J. Appl. Polym. Sci.* **2008,** *108* (4), 2067-2076.

37. Jiang, Y.; McAuley, K. B.; Hsu, J. C. C. Nonequilibrium modeling of condensed mode cooling of polyethylene reactors. *AIChE J.* **1997,** *43* (1), 13-24.

38. Jiang, Y.; McAuley, K. B.; Hsu, J. C. C. Heat Removal from Gas-Phase Polyethylene Reactors in the Supercondensed Mode. *Ind. Eng. Chem. Res.* **1997,** *36* (4), 1176-1180.

39. Jiang, Y.; McAuley, K. B.; Hsu, J. C. C. Effects of operating conditions on heat removal from polyethylene reactors. *AIChE J.* **1997,** *43* (8), 2073-2082.

40. Hutchinson, R. A.; Ray, W. H. Polymerization of olefins through heterogeneous catalysis: the effect of condensation cooling on particle ignition. *J. Appl. Polym. Sci.* **1991,** *43* (7), 1387-1390.

41. McKenna, T. F. L.; Di Martino, A.; Weickert, G.; Soares, J. B. P. Particle Growth During the Polymerisation of Olefins on Supported Catalysts, 1-Nascent Polymer Structures. *Macromolecular Reaction Engineering* **2010,** *4* (1), 40-64.

42. Kanellopoulos, V.; Mouratides, D.; Pladis, P.; Kiparissides, C. Prediction of Solubility of Olefins in Polyolefins Using a Combined Equation of State Molecular Dynamics Approach. *Ind. Eng. Chem. Res.* **2006,** *45* (17), 5870-5878.

43. Rogers, C. E.; Stannett, V.; Szwarc, M. The Sorption of Organic Vapors by Polyethylene. *J. Phys. Chem.* **1959,** *63* (9), 1406-1413.

44. Rogers, C. E.; Stannett, V.; Szwarc, M. The sorption, diffusion, and permeation of organic vapors in polyethylene. *J. Polym. Sci.* **1960,** *45* (145), 61-82.

45. Michaels, A. S.; Bixler, H. J. Solubility of gases in polyethylene. *J. Polym. Sci.* **1961,** *50* (154), 393-412.

46. Li, N. N.; Long, R. B. Permeation through plastic films. *AIChE J.* **1969,** *15* (1), 73-80.

47. Stern, S. A.; Mullhaupt, J. T.; Gareis, P. J. The effect of pressure on the permeation of gases and vapors through polyethylene. Usefulness of the corresponding states principle. *AIChE J.* **1969,** *15* (1), 64-73.

48. Kulkarni, S. S.; Stern, S. A. The diffusion of CO2, CH4, C2H4, and C3H8 in polyethylene at elevated pressures. *J. Polym. Sci. Polym. Phys. Ed.* **1983,** *21* (3), 441-465.

49. Castro, E. F.; Gonzo, E. E.; Gottifredi, J. C. Thermodynamics of the absorption of hydrocarbon vapors in polyethylene films. *Journal of Membrane Science* **1987,** *31* (2-3), 235-248.

50. Hutchinson, R. A.; Ray, W. H. Polymerization of olefins through heterogeneous catalysis. VIII. Monomer sorption effects. *J. Appl. Polym. Sci.* **1990,** *41* (1-2), 51-81.

51. Yoon, J. S.; Chung, C. Y.; Lee, I. H. Solubility and diffusion coefficient of gaseous ethylene and olefin in ethylene/olefin random copolymers. *European Polymer Journal* **1994,** *30* (11), 1209-1214.

52. Yoon, J. S.; Yoo, H. S.; Kang, K. S. Solubility of olefins in linear low density polyethylenes. *European Polymer Journal* **1996,** *32* (11), 1333-1336.

53. Jin, H. J.; Kim, S.; Yoon, J. S. Solubility of 1-hexene in LLDPE synthesized by (2-MeInd)2ZrCl2/MAO and by Mg(OEt)2/DIBP/TiCl4 TEA. *J. Appl. Polym. Sci.* **2002,** *84* (8), 1566-1571.

54. Moore, S. J.; Wanke, S. E. Solubility of ethylene, 1-butene and 1-hexene in polyethylenes. *Chemical Engineering Science* **2001,** *56* (13), 4121-4129.

55. Kiparissides, C.; Dimos, V.; Boultouka, T.; Anastasiadis, A.; Chasiotis, A. Experimental and theoretical investigation of solubility and diffusion of ethylene in semicrystalline PE at elevated pressures and temperatures. *J. Appl. Polym. Sci.* **2003,** *87* (6), 953-966.

56. Chien, J. C. W.; Nozaki, T. Ethylene-hexene copolymerization by heterogeneous and homogeneous Ziegler-Natta catalysts and the "comonomer" effect. *J. Polym. Sci. A Polym. Chem.* **1993,** *31* (1), 227-237.

57. Robeson, L. M.; Smith, T. G. Permeation of ethane-butane mixtures through polyethylene. *J. Appl. Polym. Sci.* **1968,** *12* (9), 2083-2095.

58. McKenna, T. F. Solubility and crystallinity data for ethylene/polyethylene systems. *European Polymer Journal* **1998,** *34* (9), 1255-1260.

59. Novak, A.; Bobak, M.; Kosek, J.; Banaszak, B. J.; Lo, D.; Widya, T.; Harmon Ray, W.; de Pablo, J. J. Ethylene and 1-hexene sorption in LLDPE under typical gas-phase reactor conditions: Experiments. *J. Appl. Polym. Sci.* **2006,** *100* (2), 1124-1136.

60. Yao, W.; Hu, X.; Yang, Y. Modeling the solubility of ternary mixtures of ethylene, iso-pentane, n-hexane in semicrystalline polyethylene. *J. Appl. Polym. Sci.* **2007,** *104* (6), 3654-3662.

61. Haslam, A. J.; von Solms, N.; Adjiman, C. S.; Galindo, A.; Jackson, G.; Paricaud, P.; Michelsen, M. L.; Kontogeorgis, G. M. Predicting enhanced absorption of light gases in polyethylene using simplified PC-SAFT and SAFT-VR. *Fluid Phase Equilibria* **2006,** *243* (1-2), 74-91.

62. Banaszak, B. J.; Lo, D.; Widya, T.; Ray, W. H.; de Pablo, J. J.; Novak, A.; Kosek, J. Ethylene and 1-Hexene Sorption in LLDPE under Typical Gas Phase Reactor Conditions: A Priori Simulation and Modeling for Prediction of Experimental Observations. *Macromolecules* **2004,** *37* (24), 9139-9150.

63. Nath, S. K.; Banaszak, B. J.; de Pablo, J. J. Simulation of Ternary Mixtures of Ethylene, 1-Hexene, and Polyethylene. *Macromolecules* **2001,** *34* (22), 7841-7848.

64. Banat Y.; Al-Obaidi F.; Malek A.K. Olefin Gas Phase Polymerisation. WO 2011/147539 A1, **2011**.

65. Moddox P.; Williams P. Polymerization Process. WO 98/30605, **1998**.

66. Lei, Z.; Chen, B.; Li, C.; Liu, H. Predictive Molecular Thermodynamic Models for Liquid Solvents, Solid Salts, Polymers, and Ionic Liquids. *Chem. Rev.* **2008,** *108* (4), 1419-1455.

67. Mueller, P. A.; Richards, J. R.; Congalidis, J. P. Polymerization Reactor Modeling in Industry. *Macromolecular Reaction Engineering* **2011,** *5* (7-8), 261-277.

68. Huang, S. H.; Radosz, M. Equation of state for small, large, polydisperse, and associating molecules: extension to fluid mixtures. *Ind. Eng. Chem. Res.* **1991,** *30* (8), 1994-2005.

69. Huang, S. H.; Radosz, M. Equation of state for small, large, polydisperse, and associating molecules. *Ind. Eng. Chem. Res.* **1990,** *29* (11), 2284-2294.

70. Chapman, W. G.; Gubbins, K. E.; Jackson, G.; Radosz, M. New reference equation of state for associating liquids. *Ind. Eng. Chem. Res.* **1990,** *29* (8), 1709-1721.

71. Chapman, W. G.; Gubbins, K. E.; Jackson, G.; Radosz, M. SAFT: Equation-of-state solution model for associating fluids. *Fluid Phase Equilibria* **1989,** *52* (0), 31-38.

72. Gross, J.; Sadowski, G. Modeling Polymer Systems Using the Perturbed-Chain Statistical Associating Fluid Theory Equation of State. *Ind. Eng. Chem. Res.* **2001,** *41* (5), 1084-1093.

73. Gross, J.; Sadowski, G. Perturbed-Chain SAFT: An Equation of State Based on a Perturbation Theory for Chain Molecules. *Ind. Eng. Chem. Res.* **2001,** *40* (4), 1244-1260.

74. Tumakaka, F.; Gross, J.; Sadowski, G. Modeling of polymer phase equilibria using Perturbed-Chain SAFT. *Fluid Phase Equilibria* **2002,** *194-197* (0), 541-551.

75. Chun Chan, A. K.; Radosz, M. Fluid-Liquid and Fluid-Solid Phase Behavior of Poly(ethylene-co-hexene-1) Solutions in Sub- and Supercritical Propane, Ethylene, and Ethylene + Hexene-1. *Macromolecules* **2000,** *33* (18), 6800-6807.

76. Adidharma, H.; Radosz, M. Inclusion and Exclusion Approximations of Copolymer Solids Applied to Calculation of Solid-Liquid Transitions. *Ind. Eng. Chem. Res.* **2002,** *41* (7), 1774-1779.

77. Ghosh, A.; Chapman, W. G. SAFT Modeling of the Effect of Various Carriers on the Operating Range of Slurry Reactors. *Ind. Eng. Chem. Res.* **2002,** *41* (22), 5529-5533.

78. Pan, C.; Radosz, M. Phase Behavior of Poly(ethylene-co-hexene-1) Solutions in Isobutane and Propane. *Ind. Eng. Chem. Res.* **1999,** *38* (7), 2842-2848.

79. McCabe, C.; Galindo, A.; Garcia-Lisbona, M. N.; Jackson, G. Examining the Adsorption (Vapor-Liquid Equilibria) of Short-Chain Hydrocarbons in Low-Density Polyethylene with the SAFT-VR Approach. *Ind. Eng. Chem. Res.* **2001,** *40* (17), 3835-3842.

80. Paricaud, P.; Galindo, A.; Jackson, G. Modeling the Cloud Curves and the Solubility of Gases in Amorphous and Semicrystalline Polyethylene with the SAFT-VR Approach and Flory Theory of Crystallization. *Ind. Eng. Chem. Res.* **2004,** *43* (21), 6871-6889.

81. Wei, Y. S.; Sadus, R. J. Equations of state for the calculation of fluid-phase equilibria. *AIChE J.* **2000,** *46* (1), 169-196.

82. Sadowski, G. Modeling of Polymer Phase Equilibria Using Equations of State. In *Polymer Thermodynamics*, Enders, S., Wolf, B. A., Eds.; Springer: Germany, **2011**; p 389.

83. Sanchez, I. C.; Lacombe, R. H. Statistical Thermodynamics of Polymer Solutions. *Macromolecules* **1978,** *11* (6), 1145-1156.

84. Lacombe, R. H.; Sanchez, I. C. Statistical thermodynamics of fluid mixtures. *J. Phys. Chem.* **1976,** *80* (23), 2568-2580.

85. Sanchez, I. C.; Lacombe, R. H. An elementary molecular theory of classical fluids. Pure fluids. *J. Phys. Chem.* **1976,** *80* (21), 2352-2362.

86. Inomata, H.; Honma, Y.; Imahori, M.; Arai, K. Fundamental study of de-solventing polymer solutions with supercritical CO2. *Fluid Phase Equilibria* **1999,** *158-160* (0), 857-867.

87. Dorr, H.; Kinzl, M.; Luft, G. The influence of inert gases on the high-pressure phase equilibria of EH-copolymer/1-hexene/ethylene-mixtures. *Fluid Phase Equilibria* **2001,** *178* (1-2), 191-201.

88. Gauter, K.; Heidemann, R. A. Modeling polyethylene-solvent mixtures with the Sanchez-Lacombe equation. *Fluid Phase Equilibria* **2001,** *183-184* (0), 87-97.

89. Koak, N.; Visser, R. M.; de Loos, T. High-pressure phase behavior of the systems polyethylene+ethylene and polybutene+1-butene. *Fluid Phase Equilibria* **1999,** *158-160* (0), 835-846.

90. Nagy, I.; de Loos, T.; Krenz, R. A.; Heidemann, R. A. High pressure phase equilibria in the systems linear low density polyethylene + n-hexane and linear low density polyethylene + n-hexane + ethylene: Experimental results and modelling with the Sanchez-Lacombe equation of state. *The Journal of Supercritical Fluids* **2006,** *37* (1), 115-124.

91. Haruki, M.; Mano, S.; Koga, Y.; Kihara, S. i.; Takishima, S. Phase behaviors for the supercritical ethylene + 1-hexene + hexane + polyethylene systems at elevated temperatures and pressures. *Fluid Phase Equilibria* **2010,** *295* (1), 137-147.

92. Chen, X.; Yasuda, K.; Sato, Y.; Takishima, S.; Masuoka, H. Measurement and correlation of phase equilibria of ethylene + n-hexane + metallocene polyethylene at temperatures between 373 and 473 K and at pressures up to 20 MPa. *Fluid Phase Equilibria* **2004,** *215* (1), 105-115.

93. Haruki, M.; Takakura, Y.; Sugiura, H.; Kihara, S. i.; Takishima, S. Phase behavior for the supercritical ethylene + hexane + polyethylene systems. *The Journal of Supercritical Fluids* **2008,** *44* (3), 284-293.

94. Neau, E. A consistent method for phase equilibrium calculation using the Sanchez-Lacombe lattice-fluid equation-of-state. *Fluid Phase Equilibria* **2002,** *203* (1-2), 133-140.

95. Xiong, Y.; Kiran, E. Prediction of high-pressure phase behaviour in polyethylene/n-pentane/carbon dioxide ternary system with the Sanchez-Lacombe model. *Polymer* **1994,** *35* (20), 4408-4415.

96. De Angelis, M. G.; Merkel, T. C.; Bondar, V. I.; Freeman, B. D.; Doghieri, F.; Sarti, G. C. Hydrocarbon and fluorocarbon solubility and dilation in poly(dimethylsiloxane): Comparison of experimental data with predictions of the Sanchez-Lacombe equation of state. *J. Polym. Sci. B Polym. Phys.* **1999,** *37* (21), 3011-3026.

97. Hariharan, R.; Freeman, B. D.; Carbonell, R. G.; Sarti, G. C. Equation of state predictions of sorption isotherms in polymeric materials. *J. Appl. Polym. Sci.* **1993,** *50* (10), 1781-1795.

98. Kanellopoulos, V.; Mouratides, D.; Tsiliopoulou, E.; Kiparissides, C. An Experimental and Theoretical Investigation into the Diffusion of Olefins in Semi-Crystalline Polymers: The Influence of Swelling in Polymer-Penetrant Systems. *Macromolecular Reaction Engineering* **2007,** *1* (1), 106-118.

99. Wu, J.; Pan, Q.; Rempel, G. L. High-pressure phase equilibria for a styrene/CO2/polystyrene ternary system. *J. Appl. Polym. Sci.* **2002,** *85* (9), 1938-1944.

100. Xiong, Y.; Kiran, E. Comparison of Sanchez-Lacombe and SAFT model in predicting solubility of polyethylene in high-pressure fluids. *J. Appl. Polym. Sci.* **1995,** *55* (13), 1805-1818.

101. Bashir, M. A.; Al-haj Ali, M.; Kanellopoulos, V.; Seppala, J. Modelling of multicomponent olefins solubility in polyolefins using Sanchez-Lacombe equation of state. *Fluid Phase Equilibria* **2013,** *358* (0), 83-90.

102. Soares, J. B. P.; McKenna, T. F. L. *Polyolefin Reaction Engineering;* 1st ed.; Wiley-VCH: **2012**.

103. Grolier, J.-P. E.; Boyer, S. A. E. Gas-Polymer Interactions: Key Thermodynamic Data and Thermophysical Properties. In *Polymer Thermodynamics*, Enders, S., Wolf, B. A., Eds.; Springer: Germany, **2011**; p 137.

Chapter 3

Liquid evaporation in condensed mode operation of gas phase ethylene polymerization on supported catalyst

Part of this chapter is published as:

Alizadeh, A.; McKenna, T. F. L. Condensed Mode Cooling in Ethylene Polymerisation: Droplet Evaporation. *Macromol. Symp.* **2013,** *333* (1), 242-247.

3. Liquid evaporation in condensed mode operation of gas phase ethylene polymerization on supported catalyst

3.1. Introduction

Introduction of liquid phase to the reactor after partial condensation of recycle gas is being practiced through different techniques in different patents discussed in Chapter 2. As a result, the reactor operating in condensed mode can be considered as a three phase system of gas phase, liquid phase, and solid particles coexisting simultaneously. Analysis of evaporation of liquid droplets in a system with this level of complexity is a demanding task which has not been addressed so far for the polyolefin fluidized bed reactors to the best of our knowledge. The purpose of this section is an effort to acquire a more clear insight about this process and to address some of the fundamental issues involved.

Fortunately, the vaporization of liquid droplets in hot environment is not limited to the condensed mode operation of polyolefin reactors; a liquid feed is sprayed into a hot fluidized catalyst in a Fluid Catalytic Cracking (FCC) riser reactor, where vaporization of this liquid feed is a key step determining performance of the FCC process. “Gasification” of liquid droplets is also an important part during combustion of hydrocarbons. Thanks to these well established technologies of FCC and fuel combustion, there are extensive studies on liquid droplet vaporization in the literature.[1-3] It is out of scope of the main discussion of the current study to review all the related researches performed on liquid droplet vaporization in the FCC process and combustion literature; however, the common aspects of liquid droplet vaporization in the condensed mode operation of polyethylene reactors and FCC and combustion process is investigated here and described phenomenologically. The models developed for liquid droplet vaporization will be briefly reviewed. The most widely accepted model appears to be well-adapted to the conditions encountered in condensed mode operation of gas phase polyethylene reactors. This will assist us to explore the effects of some of the influencing and determining parameters during the droplet vaporization and to ultimately be able to estimate the time scale required for complete vaporization of liquid droplets introduced to the reactor during the continuous operation of gas phase ethylene polymerization on supported catalyst in an FBR.

3.2. Phenomenological description of the process

While operating in condensed mode, the condensed part of the recycled gas is introduced to the bed with different techniques. Here, we focus on the two important techniques: the first method practiced in Union

Carbide patent, in which the liquid droplets are suspended in the gas phase stream and introduced to the reactor from the distributor plate at the bottom of the reactor and second BP patent, in which the liquid is injected into the fluidizing bed above the distributer plate through nozzles.

Different scenarios for the liquid droplets introduced to a "hot'' environment of fluidizing particles can be found in the literature. If the droplet is small enough there is a chance that it vaporizes "homogenously" before making any contact with the solid particles fluidizing in the bed. Otherwise, liquid-solid contact will be inevitable and we find "heterogeneous" evaporation. If the particles are much hotter than the liquid phase, an "elastic collision" between liquid droplet and solid particles is probable. In this case, the solid particle and liquid droplet are pushed away from each other once they collide because of local high vapour pressure generated from immediate vaporization of part of liquid droplet which contacts with hot solid surface. This phenomenon is known as the "Leidenfrost effect". The Leidenfrost temperature is the temperature of the solid surface at which wetting of the solid surface is prevented by insulating vapour generated by continuous vaporization of the liquid droplet. This parameter is not well understood yet but in context of our analysis we can use the simple correlation to estimate it[4] in order to assess the possibility of existence of such an effect in condensed mode operation of polyethylene reactors:

$$T_{Leid} = T_{sat} + 150\ (℃) \qquad (3.1)$$

where T_{Leid} and T_{sat} are the Leidenfrost temperature and the saturation temperature of the liquid phase, expressed in °C. Here, the Leidenfrost temperature is only a function of system pressure which determines saturation temperature of the liquid phase.

According to the data of patents, the gas phase and consequently the entrained liquid phase suspended in it are introduced to the bed at a temperature of approximately 50 °C. At the partial pressure of condensable components in the recycle gas equal to 4.5 and 2.3 bars for 1-butene and *iso*-pentane, respectively and assuming negligible pressure drop in the heat exchanger it is possible to estimate the gas phase dew point. This dew point can be treated as an estimation of the liquid saturation temperature in the reactor pressure. Note that, equation (3.1) is for pure materials, but considering it as dew point or bubble point for mixture of components does not make a difference in our final conclusion. It is in addition to difficulty to estimate the bubble point of the liquid phase because of lack of direct knowledge about its composition.

The dew point of gas phase of composition mentioned above is estimated with *K-value* method to be equal to 77 °C. The details of the method could be found in reference.[5] The same order of magnitude (50-70 °C) for dew point of recycle gas having different composition (*n*-hexane instead of *iso*-pentane, for

instance) is reported in literature and patents. As a result, it can be concluded that the Leidenfrost effect does not exist during liquid-solid contact in the condensed mode operation of polyethylene reactors simply because the surface temperature of solid particles are far lower than the Leidenfrost temperature for this system (200-220 °C).

Dismissing the possibility of elastic collision between liquid droplets and solid particles, the most probable scenario is that if solid particles collide with droplets, the droplets will be in the form of a liquid in contact with a solid particle, as schematically demonstrated in Figure 3.1. The liquid phase in contact with one particle may be distributed on two or more other particles before complete vaporization as they collide with each other during fluidization. Part of the liquid on one particle may also be separated from the particle because of shear force of gas flow resulting in another suspending droplet. This liquid droplet may collide again another particle before complete vaporization. Large droplets or "lumps" of liquid which will take longer time to evaporate may induce also agglomeration of particles and disturb the fluidization of the bed. This is one of the reasons that the conventional condensed mode operation is limited by the mole fraction of condensables that can be used in the gas phase composition.

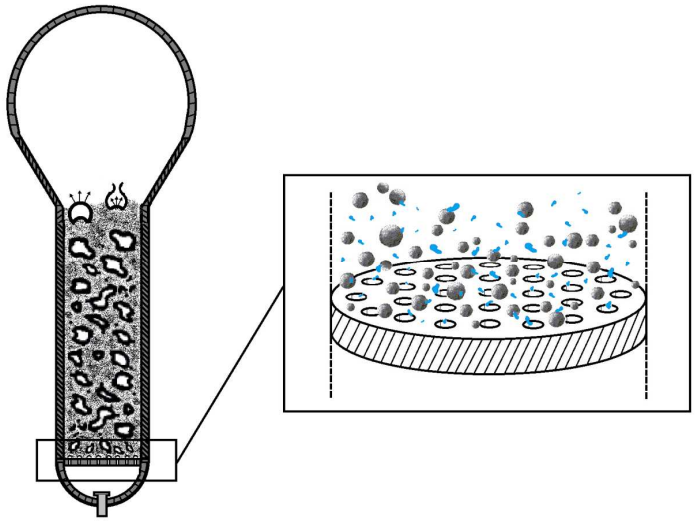

Figure 3.1. Schematic representation of vaporization process for liquefied portion of the recycle feed stream upon introduction into the gas phase polyethylene FBR during the condensed mode operation.

In terms of temperature evolution, it is believed[6] that when a cold "isolated" droplet is introduced to a hot environment, the temperature of the droplet will first rise quickly because of heat transferred from surrounding hot gas phase to the droplet. The rate of temperature rise will then decrease as the temperature of droplet and consequently the rate of vaporization increases. Finally, the droplet will reach a steady state temperature in which the heat transferred by convection of hot gas phase is consumed for

vaporization of the droplet. This temperature is known as the wet-bulb temperature. However, for the droplet evaporation in the presence of solid particles this steady state temperature may differ from the wet-bulb temperature because of heat transferred from particles to droplet as they collide.

3.3. Modeling droplet vaporization in presence of solid particles

It is generally accepted that the evaporation of the liquid droplets injected into the reactor accounts for a large portion of heat removal in the condensed mode. Therefore, we need to understand where/how this takes place inside the reactor. Obviously, parameters like droplet size, size distribution, heat of vaporization and properties of solid particle phase (like solid flux inside bed, size distribution, and heat capacity) as well as eventual contact between these two phases will control the overall vaporization process of the liquid droplet in the presence of fluidizing solid particles. The quality of contact between droplets and particles also depends on the fluidization pattern of the bed and the method by which the droplets are introduced. Despite extensive experimental and modeling studies in FCC and combustion literature, to the best of our knowledge, there is no single modeling approach which captures effect of all the parameters influencing the droplet vaporization in the fluidized bed with a phenomenological description.

There are interesting reviews such as Reference[1] on homogenous vaporization of liquid droplets (i.e. without presence of solid particles). The d^2-*Law* is the simplest modeling approach for vaporization of liquid droplets in a hot, stagnant environment. It can be shown that the droplet diameter, d, under this circumstance reduces by the following correlation

$$d^2 = d_0^2 - Kt \qquad (3.2)$$

where d_0 is the initial droplet diameter and K is a constant as discussed by Law.[1] Law has also provided an interesting discussion about how the shear stress exerted by the gas flow on the surface of droplet induces recirculation motion within droplet which enhances transport rates and consequently vaporization rate.

Nayak et al.[3] proposed an innovative model for evaporation of a droplet in the presence of solid particles which includes the effect of many of the parameters discussed above. However, it is based on the assumption that heat is transferred from a particle to a droplet during their contact, before they are pushed back because of generation of “specific volume” of vapour. According to our discussion about possibility of presence of such an effect (Leidenfrost effect), the applicability of this model for condensed mode operation of polyethylene reactors is dismissed.

Buchanan[2] has analyzed the vaporization of droplets in the presence of fluidizing particles to estimate the order of magnitude of time needed for droplet vaporization of different sizes. First the relative time scale for droplet heat up and vaporization is compared in case of homogenous vaporization of the droplet (i.e. without presence of solid particles). For the heterogeneous vaporization, two limiting cases have been considered: (a) fast heat transfer during "sticky" collision between droplet and particles; (b) elastic collisions between droplet and particles. As discussed previously, the elastic collision is not expected to occur in the condensed mode operation of ethylene polymerization. However, the vaporization time obtained in the case of elastic collision will be representative of upper limit of the vaporization time of droplet in presence of solid particles, while vaporization time assuming fast heat transfer between droplets and particles will be representative of lower limit of it. Here, the analysis of Buchanan is adapted for the condensed mode operation of polyethylene reactors. The predictive capabilities as well as limitation and drawbacks of this model will be discussed in more detail after model description and simulation results.

3.3.1. Homogenous droplet heat up and vaporization

In this method the lifetime of the cold droplet introduced to a hot environment is split to two overlapping periods. First, the droplet heats up rapidly with a small fraction of it being evaporated. In the second period, the droplet vaporizes at constant temperature, i.e. the wet-bulb temperature in our case. It is assumed that droplet composition is pure *iso*-pentane and gas phase is of composition given below at 80 °C and 20 bars:

Table 3-I. The gas phase composition in which *iso*-pentane droplet heats up and evaporates.

Component	mole fraction
ethylene	0.5
hydrogen	0.1
nitrogen	0.25
iso-pentane	0.15

The properties of gas phase at 80 °C and 20 bars and liquid phase at 80 °C are given in Table 3-II. The methods of estimation of these properties are provided in detail in Appendix D.

Table 3-II. Properties of gas phase of composition mentioned above at 80 °C and 20 bars and liquid *iso*-pentane and polymer particles at 80 °C.

Density			
Liquid	ρ_l	553.4	kg/m^3
Gas	ρ_g	21.8	kg/m^3
Particle	ρ_{pol}	900	kg/m^3
Heat capacity			
Liquid	$C_{p,l}$	2593.5	J/kg.K
Gas	$C_{p,g}$	1734.7	J/kg.K
Particle	$C_{p,pol}$	2000	J/kg.K
Kinematic viscosity of gas	v	6.2×10^{-7}	m^2/sec
Thermal conductivity of gas	$k_{c,g}$	3.1×10^{-2}	J/m.sec.K
Latent heat of	ΔH_v	292	kJ/kg
vaporization of liquid	$\Delta H_v'$	21076.6	kJ/kmol
Diffusivity of *iso*-pentane in the gas phase	$D_{i\text{-}C5}$	5×10^{-7}	m^2/sec
Vapor pressure of *iso*-pentane	P_{vap}	4.6	bar

It is essential to have a reasonable estimate of the relative velocity of liquid droplet and surrounding gas phase (as the gas-liquid slip velocity) during the course of heating up and evaporation in our calculations. The gas-liquid slip velocity for the injection devices are reported ranging from 7-30 m/sec in the literature.[2] By considering the fact that liquid droplets are introduced to a slow moving environment of fluidizing particles where superficial gas velocity is in the order of 1 m/sec, the gas-liquid slip velocity of $u_{slip}=10$ m/sec has been used through our analysis in this section, as a compromise. We could not find an indication about gas-liquid slip velocity in case of introduction of liquid droplets entrained in the gas phase in the literature nor patents. In order to avoid the possible confusion, it worth emphasizing that the droplet during its evaporation is most probable to experience different relative velocities with respect to gas phase. It will first be of relatively high slip velocity (30 m/sec typical for injection devices, and much higher in case of Union Carbide Patent in which the droplets are entrained and suspended in gas phase and introduced to bed through the holes. Considering the difference in "volumetric" size of two gas and liquid phases which pass through the holes, the relative gas-liquid (slip) velocity is expected to be much higher during its passage through the holes). However, it is logical to assume that droplets losing their momentum because of introduction to relatively dense fluidized bed environment will finally have relative gas-liquid (slip) velocity equal to superficial gas velocity in the bed of 1 m/sec. As a result, we use an averaged value of 10 m/sec during the course of its vaporization as a reasonable (but not accurate)

approximation. We will test the sensitivity of the calculations to the values of u_{slip} for the estimation of the heterogeneous vaporization time.

The droplet size distribution depends on the type of injection devices with average size being reported to be between 50-4000 μm.[10] On the other hand, in the case of introduction of liquid as entrained droplets in the gas phase, the holes of the distributor are of diameter of about one centimeter and maximum droplet size of diameter 5000 μm seems a reasonable approximation. As a result our analysis will cover droplet size distribution of 50-5000 μm.

3.3.1.1. Wet-Bulb temperature

In order to calculate the time scale for heat up and vaporization of droplet in the second step, it is essential to estimate the temperature of the droplet during the vaporization. In our analysis, it is estimated as the wet-bulb temperature. The wet-bulb temperature according to its definition is the steady state temperature reached by a liquid droplet evaporating into an unsaturated gas mixture. At this temperature the rate of heat transfer from the gas phase to the liquid will be equal to the rate of heat removal from droplet by evaporation:

$$h\left(T_g - T_w\right) = k_m\left(C_{eq} - C_b\right)\Delta H_v' \qquad (3.3)$$

where T_g and T_w are gas phase and wet-bulb temperature, respectively. C_{eq} and C_b are concentration of *iso*-pentane in gas phase in equilibrium with liquid *iso*-pentane and concentration of *iso*-pentane in bulk gas phase, respectively. C_{eq} can be obtained from *iso*-pentane vapour pressure by:

$$C_{eq} = \frac{P_{vap}}{R_g T} \qquad (3.4)$$

k_m, mass transfer coefficient for *iso*-pentane, and h, heat transfer coefficient, are obtained from the Ranz-Marshall correlations:

$$Sh = \frac{k_m d}{D} = 2 + 0.6\, Re^{1/2}\, Sc^{1/3} \qquad (3.5)$$

$$Nu = \frac{hd}{k_{c,g}} = 2 + 0.6\, Re^{1/2}\, Pr^{1/3} \qquad (3.6)$$

In equation (3.5), for estimation of mass transfer coefficient of *iso*-pentane, k_m, the dimensionless Sherwood number (*Sh*) is correlated to the dimensionless Reynolds number (*Re*) and dimensionless Schmidt number (*Sc*), in which d is the diameter of the droplet and D is the diffusivity of *iso*-pentane in the gas phase. Similarly, for estimation of heat transfer coefficient, h, in equation (3.6), the

dimensionless Nusselt number (*Nu*) is correlated to the dimensionless Reynolds number (*Re*) and the dimensionless Prandtl number (*Pr*), in which d is the diameter of the droplet and $k_{c,g}$ is the thermal conductivity of the gas phase.

Considering gas phase temperature of 80 °C, the wet-bulb temperature as the temperature of the droplet during vaporization step is estimated to be 61 °C.

3.3.1.2. Droplet heat up

It can be shown that the governing equation during the heat up period of an isolated droplet is given by

$$\tau \frac{dT}{dt} = T_g - T \qquad (3.7)$$

where

$$\tau = \left(\rho_l c_{p,l} d\right)/6h \qquad (3.8)$$

In this approach, a uniform temperature inside the droplet is assumed because of internal mixing effect of exerted shear stress applied by gas flow on the surface of the droplet. The heat transfer coefficient, *h*, can be estimated from conventional Ranz-Marshall correlation for heat transfer, equation (3.6).

The solution to equation (3.7) is:

$$t = -\tau \ln\left[\frac{T_g - T}{T_g - T_0}\right] \qquad (3.9)$$

T_g and T_0 are gas and initial droplet temperature, respectively.

For the droplet heat up step, the time needed for initial droplet temperature of 50 °C to reach wet-bulb temperature of 61°C is calculated. The results are summarized in Table 3-III.

Table 3-III. Estimation of time scale for *iso*-pentane droplets of slip liquid-gas velocity u_{slip}=10 m/sec to heat-up* and vaporize homogeneously.

Droplet size (μm)	50	100	300	1000	3000	5000
Heat-up time (sec)	5.0×10^{-4}	1.5×10^{-3}	7.8×10^{-3}	4.9×10^{-2}	2.6×10^{-1}	5.5×10^{-1}
Vaporization time (sec)	1.3×10^{-2}	3.9×10^{-2}	2.1×10^{-1}	1.4	7.1	15.4

(*) heat up time from 50 to 61°C as the wet-bulb temperature

3.3.1.3. Droplet vaporization

It is found empirically that the heat transfer coefficient from gas phase to a droplet decreases when there is a substantial vaporization from droplet. The physical explanation for this phenomenon is that "the vapors leaving the droplet tend to deflect the hot surrounding gases away from the droplet".[2]

As a result, in order to estimate the vaporization time, the heat transfer coefficient for vaporizing droplet as an effective heat transfer coefficient must be calculated as proposed by Renksizbulut:[7]

$$Nu^* = \frac{h^* d}{k_{c,g}} = \frac{Nu}{(1+B)^n} \qquad (3.10)$$

where Nu is the conventional Nusselt number obtained from Ranz-Marshall correlation, h^* and Nu^* are the effective heat transfer coefficient and Nusselt number for droplet in the presence of vaporization. n is constant equal to 0.7 and B is given by:

$$B = \frac{C_{p,g}(T_g - T)}{\Delta H_v}\left[1 + \frac{Q_R}{Q_C}\right] \qquad (3.11)$$

$C_{p,g}$ is heat capacity of gas phase, ΔH_v is the heat of vaporization of liquid. $\frac{Q_R}{Q_C}$ is the ratio of heat transferred to the droplet by radiation to convection which can be assumed to be equal to zero in operational conditions of condensed mode polyethylene reactors.

Assuming that all the heat transferred to the droplet is consumed for evaporation of the liquid from the droplet, it is possible to write the governing equation for evaporation as:

$$\Delta H_v \rho_l \frac{dV}{dt} = -h^* A (T_g - T) \qquad (3.12)$$

where V and A are droplet volume and surface area. T is the evaporation temperature of droplet which is estimated as wet-bulb temperature, as described before. Substituting V and A in terms of droplet diameter, it is possible to rewrite equation (3.12) as:

$$\frac{d(d)}{dt} = \frac{-2h^*(T_g - T)}{\Delta H_v \rho_l} \qquad (3.13)$$

Analytical solution for the equation (3.13) results in following correlation for vaporization time:

$$t_{vap} = -\frac{\Delta H_v \rho_l}{A'(T_g - T)}\left\{\frac{2}{B^4}\left[\frac{1}{3}(1 - v_0^3) - \frac{3}{2}(1 - v_0^2) + 3(1 - v_0) - \ln\left(\frac{1}{v_0}\right)\right]\right\} \qquad (3.14)$$

where *A'* and *B'* are clustered functions defined as:

$$A' = \frac{k_{c,g}}{\left[1 + \frac{C_{p,g(T_g - T)}}{\Delta H_v}\right]^{0.7}} \quad (3.15)$$

$$B' = 0.6\, Pr^{1/3} \left(\frac{u}{2v}\right)^{0.5} \quad (3.16)$$

and $v_0 = 1 + B' r_0^{0.5}$ in which r_o is the initial droplet radius.

The time needed for droplets of size between 50-5000 μm to vaporize homogeneously at slip gas-liquid velocity of $u_{slip} = 10$ m/sec are given in Table 3-III. By comparing the time scale for droplet heat up and vaporization, it can be concluded that the heat up time is negligible compared to vaporization step. As a result, in our discussion about heterogeneous droplet vaporization in the presence of solid particles we will focus on the vaporization step assuming that droplet reaches steady state temperature of vaporization instantaneously.

3.3.2. Heterogeneous droplet vaporization

In order to estimate the time scale for the vaporization of droplets in the presence of particles, Buchanan[2] considered two limit cases of heat transfer between droplets and particles. In the first limit, all of the heat possible from particles is transferred to droplet instantaneously. The formulation for this limit results in the following correlation for estimation of droplet vaporization time:

$$\frac{d(d)}{dt} = \frac{-u\rho_{pol}(1-\varepsilon)C_{p,pol}\left(T_{pol} - T\right)}{2\rho_l \Delta H_v} \quad (3.17)$$

where ε is the bed porosity and we use the value of bed porosity at minimum fluidization of 0.5 as an estimation. It is assumed that particles (T_{pol}) in bed are at the same temperature of the gas phase (T_g) and cooled down immediately to the droplet vaporization temperature as they are collided. The first assumption is not valid especially for the small active polymer particles. However, the correction for this will only result in even shorter time scales for vaporization of droplets in this extreme limit. Consequently, it is decided to keep this assumption despite its obvious imperfections. Similar to homogeneous vaporization, the vaporization temperature of the droplet is estimated as wet-bulb temperature. The results for this lower limit of vaporization time are given in the following Table.

Table 3-IV. Estimation of time scale for *iso*-pentane droplets to vaporize heterogeneously.

Slip liquid-gas velocity u_{slip}=*10* m/sec						
Droplet size (μm)	50	100	300	1000	3000	5000
Lower limit of vaporization time (sec)	9.5×10^{-5}	1.9×10^{-4}	5.7×10^{-4}	1.9×10^{-3}	5.7×10^{-3}	9.5×10^{-3}
Higher limit of vaporization time (sec)	2.4×10^{-3}	6.8×10^{-3}	3.6×10^{-2}	2.2×10^{-1}	1.1	2.4
Slip liquid-gas velocity u_{slip}=*1* m/sec						
Droplet size (μm)	50	100	300	1000	3000	5000
Lower limit of vaporization time (sec)	9.5×10^{-4}	1.9×10^{-3}	5.7×10^{-3}	1.9×10^{-2}	5.7×10^{-2}	9.5×10^{-2}
Higher limit of vaporization time (sec)	9.7×10^{-3}	2.8×10^{-2}	1.5×10^{-1}	9.5×10^{-1}	5.0	10.8

In the second limiting case, the collisions between droplet and particles are assumed to be elastic. This is intended to represent lower limit of heat transfer from particles to the droplets. Considering the observed trend[8,9] of decrease in heat transfer coefficient to immersed objects by dilution of fluidized bed, Buchanan proposed a correction for heat transfer coefficient for homogeneously vaporizing droplet (equation (3.14)). In this correction the gas phase density ρ_g in *Re* number is replaced by gas-solid density, $\rho_{pol}(1-\varepsilon)$. While not yet being validated, this correction is found to be consistent with the observed trends[8,9] in the literature.

Taking this correction into account will result in similar equation for estimation of droplet vaporization time as equation (3.14), except that the cluster parameter of *B'* (equation (3.16)) will be replaced by *B''* as:

$$B'' = B'\left(\frac{\rho_{pol}(1-\varepsilon)}{\rho_g}\right)^{1/2} \qquad (3.18)$$

This vaporization time is intended to be representative of higher limit of droplet vaporization time in the presence of solid particles. The results are provided in Table 3-IV.

Considering the uncertainties about the estimation of gas-liquid slip velocity, the sensitivity of the calculated heterogeneous vaporization time (in both limits) for the u_{slip} equal to 1 in addition to 10 m/sec has been calculated and provided in Table 3-IV for comparison purpose.

It should be noted that considering the uncertainties related to the heat transfer coefficients, estimation of slip velocity and actual droplet sizes in bed (as discussed before because of interactions between liquid droplets and solid particles), these time scales should be treated as a qualitative estimation. This approach also does not take into account the local hydrodynamics of the bed, the heat capacity of solid phase, possibility of distribution of liquid between particles and droplet surface deformation.

However, assuming the real vaporization time to be between two limits of the heat transfer in the heterogeneous vaporization, it seems logical to conclude that for a droplet of as large as 5000 μm, it takes in the order of a second to be vaporized completely assuming $u_{slip}=10\ m/sec$ and few seconds in case of $u_{slip}=1\ m/sec$.

This conclusion is in agreement with the patents claim about necessity of "immediate" vaporization of the droplets in the order to avoid the agglomeration and consequently disturbing the fluidization of bed. However, the droplets of order of several millimetres appear to be too large and the droplets in the order of few hundred microns are more in favour of "immediate" vaporization.

In other words, considering the lowest possible slip velocity of 1 m/sec equal to gas superficial velocity in the bed (obviously lower than the average slip gas-liquid velocity experienced by the droplets during the vaporization course) for the largest possible droplet, it takes few seconds for complete vaporization. This in turn implies that only the lower portion at the bottom of the FBR of 15 meters height becomes exposed to the introduced liquid. As a result, the latent heat of liquid evaporation enhances the rate of heat removal from the particles fluidizing only in this fraction of the bed. Consequently, it can be concluded that the vaporization of liquid droplets during the condensed mode operation will have only local effect on cooling the particles inside the fluidized bed reactor for gas phase ethylene polymerization on supported catalyst.

3.4. References

1. Law, C. K. Recent advances in droplet vaporization and combustion. *Progress in Energy and Combustion Science* **1982,** *8* (3), 171-201.

2. Buchanan, J. S. Analysis of Heating and Vaporization of Feed Droplets in Fluidized Catalytic Cracking Risers. *Ind. Eng. Chem. Res.* **1994,** *33* (12), 3104-3111.

3. Nayak, S. V.; Joshi, S. L.; Ranade, V. V. Modeling of vaporization and cracking of liquid oil injected in a gas-solid riser. *Chemical Engineering Science* **2005,** *60* (22), 6049-6066.

4. Le Corre, J. M.; Yao, S. C.; Amon, C. H. A mechanistic model of critical heat flux under subcooled flow boiling conditions for application to one- and three-dimensional computer codes. *Nuclear Engineering and Design* **2010,** *240* (2), 235-244.

5. Smith, J. M.; Van Ness, H. C.; Abbott, M. M. *Introduction to Chemical Engineering Thermodynamics;* 7th ed.; McGraw-Hill: **2005**.

6. Treybal, R. E. *Mass Transfer Operations;* 3rd ed.; McGraw-Hill: **1987**.

7. Renksizbulut, M.; Yuen, M. C. Experimental Study of Droplet Evaporation in a High-Temperature Air Stream. *Journal of Heat Transfer* **1983,** *105* (2), 384-388.

8. Vreedenberg, H. A. Heat transfer between a fluidized bed and a horizontal tube. *Chemical Engineering Science* **1958,** *9* (1), 52-60.

9. Kunii, D.; Levenspiel, O. *Fluidization Engineering;* R. E. Krieger Publishing Co.: **1977**.

10. Chinh J-C.; Filippelli M.C.H; Newton D.; Power M.B. Polymerization Process. US 5,541,270, **1996**.

Chapter 4

Thermodynamics of sorption equilibrium

4. Thermodynamics of sorption equilibrium

In the bibliography chapter, we briefly discussed the condensed mode operation of gas phase ethylene polymerization reactors and the fact that it allows one to achieve higher polymer production yield for the same reactor set-up than in dry mode. In the condensed mode, in addition to containing ethylene, nitrogen, hydrogen and eventually a comonomer (which can also be condensable), the gas phase feed stream of the FBR also contains an inert condensing agent (ICA) such as *iso*-pentane or *n*-hexane. In the most common configurations for condensed mode operation, the feed stream is partially liquefied in an external heat exchanger by cooling it below the dew point of the heavier components and the liquefied portion of the feed stream is injected into the reactor in the form of small droplets. The droplets of liquid then heat up and vaporize in the reactor. In this manner the latent heat of vaporization is used to absorb a significant portion of the heat of reaction in the bottom part of the reactor, thereby making it possible to polymerize at higher rates than would be possible with a completely dry feed stream.

While it is clear that evaporation of condensable components will ultimately help to control the temperature in the zones where these components are injected, it was shown in Chapter 3 that the evaporation process will be relatively fast so it is unlikely that these components remain in the liquid state much more than few seconds. In the previous chapter, we showed that the lifetime of a reasonably sized droplet of *iso*-pentane as ICA would be on the order of a second in the reactor environment, whereas it can take on the order of 15 to 30 seconds or more for the gas phase to leave the reactor. This means that the ICAs are present in the vapor phase of FBR for a much longer time than they are in the liquid phase. Thus, in order to develop a sound understanding about the condensed mode operation, we need to ask whether or not the presence of ICAs in the gas phase has any additional influence on the quality of polymerization.

In order to answer this question, one needs to think about how the reaction proceeds on the supported catalysts used in this type of reaction. At the risk of oversimplifying the situation, the catalytic sites are deposited inside the pores of a highly porous solid. The particles are injected into the reactor, where ethylene rapidly polymerizes in the pores. The stress created in the confined space of the pores by this initial polymerization causes the initial structure of the support to fragment and the particle is transformed into a polymer particle where the semi-crystalline polyethylene forms the continuous phase with the fragments of the support dispersed therein. The reaction continues as monomer diffuses into the pores of the particle, sorbs in the polymer layer covering the active sites, and then diffuses once more toward the

active centers where it reacts. The continuous formation of polymer causes the particle to expand as the reaction proceeds. As the polymer layer that immediately covers the active sites is essentially made of amorphous material, the rate of reaction will be determined by the concentration of monomer in the amorphous phase of the semi-crystalline PE and the rate at which the monomer diffuses through the polymer. As a result, one needs to be able to quantify the solubility of ethylene in the amorphous phase of the polymer with an appropriate thermodynamic model in order to be able to develop a comprehensive understanding about the effect of process conditions on product quality and rate of polymerization.

As discussed in the bibliography chapter, the importance of the sorption process during the gas phase polymerization has motivated many experimental studies that focus on measuring the solubility of the different species present in the gas phase composition. However, as discussed in Chapter 2 most of these measurements were conducted for the sorption of a single solute like ethylene in a polymer like polyethylene in the form of a binary system. On the other hand, the feed stream to a real process will contain more than one component (upwards of 5 or 6 is not uncommon), and as discussed in the Chapter 2, the presence of a heavier component in the gas phase composition is believed to enhance the solubility of lighter component of ethylene monomer in the polymer phase. This is referred to as the "cosolubility" effect. A non-negligible cosolubility effect would in turn result in higher rate of polymerization thanks to the higher availability of ethylene at the active sites even if the heavier solvent was in principle chemically inert.

In the current chapter, the effect of *n*-hexane as the inert condensing agent (ICA) on the solubility and more importantly concentration of ethylene in amorphous phase of polyethylene is explored using the equilibrium solubility data for the binary systems of ethylene-PE and *n*-hexane-PE, and the ternary system of ethylene-*n*-hexane-PE which are measured by implementing pressure-decay technique in the group of Yang in a series of papers.[1,2]

As underlined in Chapter 2, the Sanchez-Lacombe EOS is one of the most commonly used thermodynamic models in the simulation of polymerization processes due to its excellent predictive capabilities, and also to its relative mathematical simplicity compared to the other classes of thermodynamic models for the systems including polymer component. In the current chapter, the application of Sanchez-Lacombe EOS is extended from the binary system of ethylene-PE to the ternary system of ethylene-*n*-hexane-PE, in order to describe the change in concentration of ethylene in the amorphous phase of polyethylene in the absence and presence of *n*-hexane in the gas phase composition, respectively. The predictive performance of Sanchez-Lacombe EOS in describing the solubility of

ethylene and *n*-hexane in the ternary system of ethylene-*n*-hexane-PE is evaluated against the solubility data obtained experimentally. Finally, a method is proposed to have the best fitting of Sanchez-Lacombe EOS prediction for the ethylene and *n*-hexane solubility to the experimental data simultaneously which would eventually lead to a more accurate estimation of ethylene concentration in the amorphous phase of PE.

4.1. Sanchez-Lacombe equation of state

The Sanchez-Lacombe (SL) EOS is

$$\bar{\rho}^2 + \bar{P} + \bar{T}\left[ln(1-\bar{\rho}) + \left(1 - \frac{1}{r}\right)\bar{\rho}\right] = 0 \qquad (4.1)$$

where $\bar{T}, \bar{P}, \bar{V}$, and $\bar{\rho}$ are the reduced temperature, pressure, volume, and density respectively which are defined as follows

$$\bar{T} = T/T^*, \qquad T^* = \varepsilon^*/R_g \qquad (4.2)$$

$$\bar{P} = P/P^*, \qquad P^* = \varepsilon^*/v^* \qquad (4.3)$$

$$\bar{\rho} = \rho/\rho^* = 1/\bar{V} = V^*/V, \qquad V^* = N(rv^*) \text{ and } \rho^* = MW/(rv^*) \qquad (4.4)$$

ε^* is the mer-mer interaction energy, v^*, is the closed packed molar volume of a mer, *MW* is molecular weight, *N* is number of molecules, *r* is the number of sites (mers) a molecule occupies in the lattice, and R_g is the universal gas constant. The parameters ε^*,v^*, and *r* are used to define T^*, P^*, and ρ^* which are the characteristic temperature, pressure, and close-packed mass density.

With a mixture of components, it is necessary to define combining rules for estimation of ε^*_{mix}, v^*_{mix}, and r_{mix} to be able to use the equation of state to calculate the properties of mixture. The *"van der Waals"* mixing rule is chosen and applied in our study.

For characteristic closed-packed molar volume of a "mer" of the mixture, v^*_{mix}, the so called *"van der Waals"* mixing rule is defined as

$$v^*_{mix} = \sum_i \sum_j \phi_i \phi_j v^*_{ij} \qquad (4.5)$$

with

$$v^*_{ij} = \frac{v^*_{ii} + v^*_{jj}}{2}\left(1 - n_{ij}\right) \qquad (4.6)$$

where n_{ij} corrects the deviation from the arithmetic mean and subscripts *i* and *j* are the components in the solution. The closed-packed volume fraction of the *i*th component at the limit of zero temperature or incompressible state, ϕ_i is defined as

$$\phi_i = \frac{\omega_i}{\rho_i^* v_i^*} \Big/ \sum_j \left(\frac{\omega_j}{\rho_j^* v_j^*} \right) \qquad (4.7)$$

where ω_i is the mass fraction of the component *i* in the mixture.

The mixing rule for the characteristic interaction energy for the mixture is defined as

$$\varepsilon_{mix}^* = \frac{1}{v_{mix}^*} \sum_i \sum_j \phi_i \phi_j \varepsilon_{ij}^* v_{ij}^* \qquad (4.8)$$

with

$$\varepsilon_{ij}^* = \left(\varepsilon_{ii}^* \varepsilon_{jj}^* \right)^{0.5} (1 - k_{ij}) \qquad (4.9)$$

where ε_{ii} and ε_{jj} are the characteristic mer-mer interaction energies for components *i* and *j*, and k_{ij} is a mixture parameter that accounts for specific binary interactions between components *i* and *j*. Finally, the mixing rule for the number of sites (mers) occupied by a molecule of the mixture, r_{mix}, is given by

$$\frac{1}{r_{mix}} = \sum_j \frac{\phi_j}{r_j} \qquad (4.10)$$

where r_j is the number of sites occupied by molecule *j* in the lattice.

In most of the applications used for Sanchez-Lacombe model, the only binary interaction parameter used for fitting the mixture experimental data to model is k_{ij} while n_{ij} assumed to be equal to zero. It will be the same for all of our related calculations and it is assumed $n_{ij}=0$ while k_{ij} will be the experimentally adjusted parameter describing the interaction of two components.

For calculation of sorption equilibrium for polymer-solvent system, the expression for chemical potential of component *i* in each phase of the mixture is also required given by following equation in SL EOS

$$\mu_i = R_g T \left[\ln \phi_i + \left(1 - \frac{r_i}{r} \right) \right] + \qquad (4.11)$$
$$r_i \left\{ -\bar{\rho} \left[\frac{2}{v^*} \left(\sum_j \phi_j \upsilon_{ij}^* \varepsilon_{ij}^* - \varepsilon^* \sum_j \phi_j \upsilon_{ij}^* \right) + \varepsilon^* \right] + \frac{R_g T}{\bar{\rho}} \left[(1 - \bar{\rho}) ln(1 - \bar{\rho}) + \frac{\bar{\rho}}{r_i} ln\bar{\rho} \right] + \frac{P}{\bar{\rho}} \left(2 \sum_j \phi_j \upsilon_{ij}^* - \upsilon^* \right) \right\}$$

A brief overview about the procedure in order to derive the solubility and other properties of interest from Sanchez-Lacombe EOS is provided hereunder for the both binary and ternary systems. The detailed calculation steps for the calculation of the solubility and other properties of interest, for the both binary system of solute-polymer, and ternary system of solute(*1*)-solute(*2*)-polymer, are provided in Appendix A. For the sake of brevity, the reader is directly referred to this Appendix for detailed explanations.

In order to derive the solubility of a single solute in polymer in binary system of solute-polymer, two non-linear equations must be solved simultaneously. The first equation is the Sanchez-Lacombe EOS for the polymer phase, equation (4.1), and the second is the definition of thermodynamic equilibrium condition, i.e. that the chemical potential of each component is equal in all phases at the equilibrium state ($\mu_1^{pol} = \mu_1^{gas}$). The simultaneous solution of these two non-linear equations allows us to obtain the two unknowns of these equations, i.e. the closed-packed volume fraction of solute in the polymer phase, ϕ_1^{pol}, and the reduced density of polymer phase, $\bar{\rho}^{pol}$. The solubility of solute in polymer phase, the extent of swelling of the polymer phase, and the solute concentration in polymer phase are consequently derived from ϕ_1^{pol} and $\bar{\rho}^{pol}$.

Similarly, in the ternary system of solute(*1*)-solute(*2*)-polymer, three non-linear equations are required to be solved simultaneously; the Sanchez-Lacombe EOS for the polymer phase, and the equilibrium condition for two solute components $\mu_1^{pol} = \mu_1^{gas}$ and $\mu_2^{pol} = \mu_2^{gas}$. The simultaneous solution of these three non-linear equations, allows us to obtain the closed-packed volume fractions of solute (*1*) and solute (*2*) in the polymer phase, ϕ_1^{pol} and ϕ_2^{pol} and the reduced density of polymer phase, $\bar{\rho}^{pol}$. Once again, the solubility of solutes in polymer phase, the extent of swelling of the polymer phase, and the solute concentration in polymer phase is consequently derived from ϕ_1^{pol}, ϕ_2^{pol}, and $\bar{\rho}^{pol}$.

4.2. Application of Sanchez-Lacombe EOS to binary systems

In an initial step, we will identify the binary interaction parameters of k_{ij} of the Sanchez-Lacombe EOS required to describe the solubility of gaseous solute species of interest in the current study (i.e. ethylene and *n*-hexane) in *binary* systems of solute-polymer. The characteristic parameters used for the pure components in the current study are provided in Table 4-I.

Table 4-I. The characteristic parameters of Sanchez-Lacombe model for pure components.

Component	$T^*(K)$	$P^*(bar)$	$\rho^*(kg/m^3)$	Reference
Ethylene	283	3395	680	[3]
n-Hexane	476	2979.1	775	[4]
LLDPE	653	4360	903	[3]

The related sorption equilibrium data are extracted from the solubility measurements made using the pressure decay method presented by the group of Yang.[1] In the pressure decay method, the pressure decrease of solute(s) in a constant volume vessel containing the gas and polymer sample is continuously measured during the sorption process. The details of principles and operational aspects to acquire the solubility data using pressure decay method can be found elsewhere[5] and are not presented here.

The measurement temperature and solute pressures of Yang's data are in the range of typical gas phase ethylene polymerization in fluidized bed reactor. The measurement temperatures are in the range of 60-90 °C, with ethylene pressures up to 20 bars and *n*-hexane pressures up to around 1 bar. The polyethylene sample used in the measurements with commercial grade name of DGM1820 is assumed to be LLDPE since its density was 920 kg/m^3 and crystallinity on the order of 49%.[1] The same polymer grade of DGM1820 is used as the polyethylene sample in the cosolubility measurements in the ternary system of ethylene, *n*-hexane, and PE.

The software of Plot Digitizer was used to extract the related solubility data from the associated figures in which the solubility of species in polymer are presented versus their pressure in the gas phase at specific temperatures in the paper.[1] In order to evaluate and minimize the possible generation of errors due to extraction of the data from the figures, the procedure of extracting the data was repeated twice. The mean absolute percentage of difference between two consecutive readings of solubility points from the figures i.e. $\left|\frac{S_{R_1}-S_{R_2}}{S_{R_1}}\right| \times 100$ in which R_1 and R_2 represents first and second reading of solubility values for a specific point in the figure was calculated to be 0.16% and 0.17% for ethylene and *n*-hexane solubility data in polyethylene, respectively. This in turn indicates that the errors generated at the step of extraction of solubility data from figures are negligible and assures the reliability of acquired set of data.

Once the solubility data were extracted, the Sanchez-Lacombe model was fitted to the data set by adjusting the binary interaction parameter, k_{ij}. This is done for solubility values at each temperature by minimizing the following objective function (*O.F.*) through adjustment of interaction parameter of k_{ij}

$$O.F. = \frac{1}{N}\sum_{i=1}^{N}\left(\frac{S_{calc_i} - S_{exp_i}}{S_{exp_i}}\right)^2 \qquad (4.12)$$

in which S_{calc} and S_{exp} are the solubility values calculated from binary Sanchez-Lacombe model and experimental solubility values extracted, respectively. N is the number of solubility data points at each temperature.

Figure 4.1 demonstrates the ethylene solubility as a function of its pressure at different temperatures. The solubility values are expressed in terms of gram of solute per gram of amorphous polymer while assuming the crystalline phase of polymer to be impenetrable to the solute species.[6,7]

As expected, SL model can predict and describe the temperature and pressure dependency of ethylene in LLDPE very well. The average of absolute deviation percentage of model prediction from experimental data i.e. $\left|\frac{S_{calc}-S_{exp}}{S_{exp}}\right| \times 100$ is calculated to be 0.59%, 0.65%, 0.66%, and 0.46% at 60, 70, 80, and 90 °C, respectively. However, the ethylene-LLDPE binary interaction parameter calculated to provide the best fit of model prediction to experimental data is temperature-dependent. As provided in Figure 4.1, the k_{ij} value to give the best fitting is calculated to be $k_{ij} = -0.004, -0.014, -0.022, and -0.032$ at 60, 70, 80, and 90 °C, respectively.

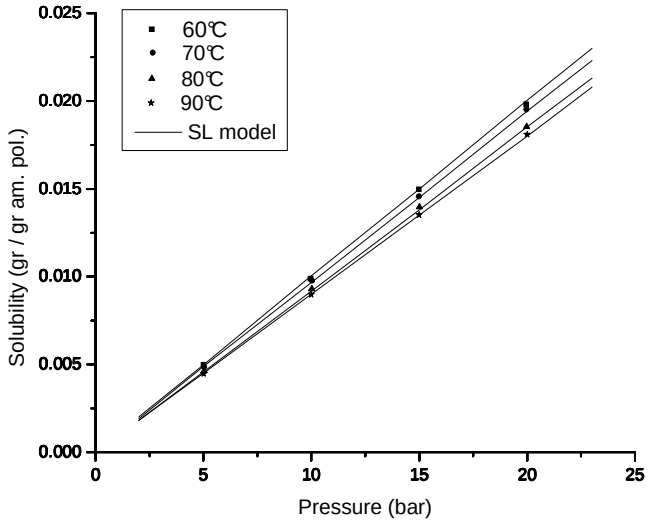

Figure 4.1. Ethylene solubility in LLDPE with the solid lines representing the SL model prediction with binary interaction parameter of $k_{ij} = -0.004, -0.014, -0.022, and -0.032$ at 60, 70, 80, and 90 °C, respectively.

The solubility of *n*-hexane as a function of pressure at different temperatures is provided in Figure 4.2. Following the same procedure described for fitting the SL model to the experimental data, the SL model prediction is provided as the solid lines in the figure.

As can be seen from the figure, the quality of fitting the SL model prediction to experimental data is not as good as for ethylene. The general pattern in all the measurement temperatures is that the SL model overestimates the solubility of *n*-hexane at lower pressures while underestimating the solubility values at higher pressures. The average of absolute deviation percentage of model prediction from experimental data, i.e. $\left|\frac{S_{calc}-S_{exp}}{S_{exp}}\right| \times 100$ is calculated to be 16.6%, 29.0%, 23.9%, and 33.7% at 70, 80, 85, and 90 °C, respectively. The *n*-hexane-LLDPE binary interaction parameter calculated to provide the best fit of model prediction to experimental data is also temperature-dependent. As provided in Figure 4.2, the k_{ij} value to give the best fitting is calculated to be $k_{ij} = 0.010,\ 0.020,\ 0.028, and\ 0.038$ at 70, 80, 85, and 90 °C, respectively.

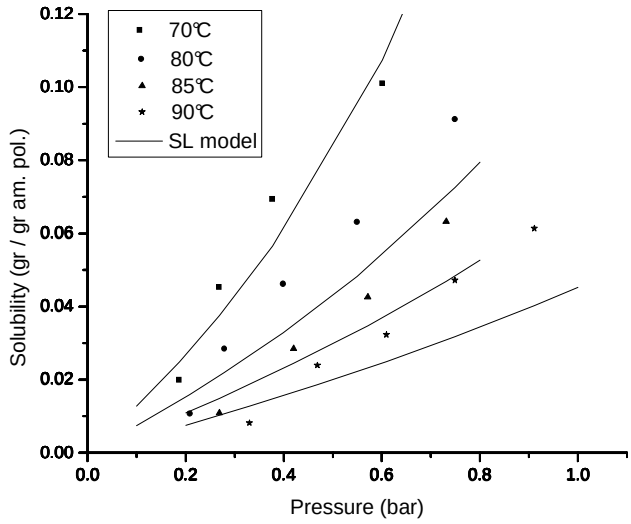

Figure 4.2. *n*-Hexane solubility in LLDPE with the solid lines representing the SL model prediction with binary interaction parameter of $k_{ij} = 0.010,\ 0.020,\ 0.028, and\ 0.038$ at 70, 80, 85, and 90 °C, respectively.

While the errors in prediction of *n*-hexane solubility in LLDPE by Sanchez-Lacombe model cannot be considered to be negligible, the adjusted binary interaction parameters calculated to give the best fitting of SL model to the experimental data at each temperature will be used in the upcoming sections in order to analyze the sorption behavior of the solutes in polymer in the ternary system of ethylene-*n*-hexane-

LLDPE. This is due to the fact that this is the only available data set which we could find in the open literature for solubility of ethylene in a constant specific grade of PE in the absence and presence of an ICA like *n*-hexane in corresponding binary and ternary systems, respectively.

4.3. Application of Sanchez-Lacombe EOS to ternary systems

In this section, the predictive capability of Sanchez-Lacombe EOS in order to describe the sorption behavior of solutes (ethylene and *n*-hexane) in polymer in the ternary system of ethylene-*n*-hexane-PE will be explored.

Despite extensive experimental and modeling studies of the solubility of different species and corresponding polymer swelling due to the sorption, the impact of the cosolubility effect on the rate of polymerization of ethylene has not been addressed in the open literature, either in modeling or in experimental studies.

Since the rate of ethylene polymerization is considered[8] to be of first order with respect to the ethylene concentration at the active sites, the "local" rate of polymerization inside the particle can be expressed as:

$$R_{pol.}^{loc.} = k_p C^* [M]_{amorph.pol.}^{loc.} \qquad (4.13)$$

in which, k_p, is the propagation rate constant and C^* is the local concentration of the active sites on the specific catalyst fragment. More importantly, $[M]_{amorph.pol.}^{loc.}$, is the local concentration of ethylene in the amorphous phase of polymer surrounding the catalyst fragment, while the crystalline phase of polymer is considered to be impenetrable to the solute species as shown schematically in Figure 4.3.

This in turn implies that in order to have a more realistic description of phenomena related to the sorption in the ternary system, one must be able to predict not only the ethylene mass sorbed to the polymer but also the increase in the volume of the polymer phase (polymer swelling) in the presence of the heavier component of *n*-hexane. This would provide a more accurate estimation of the change in the ethylene concentration in amorphous polymer surrounding the active sites and consequently the rate of polymerization.

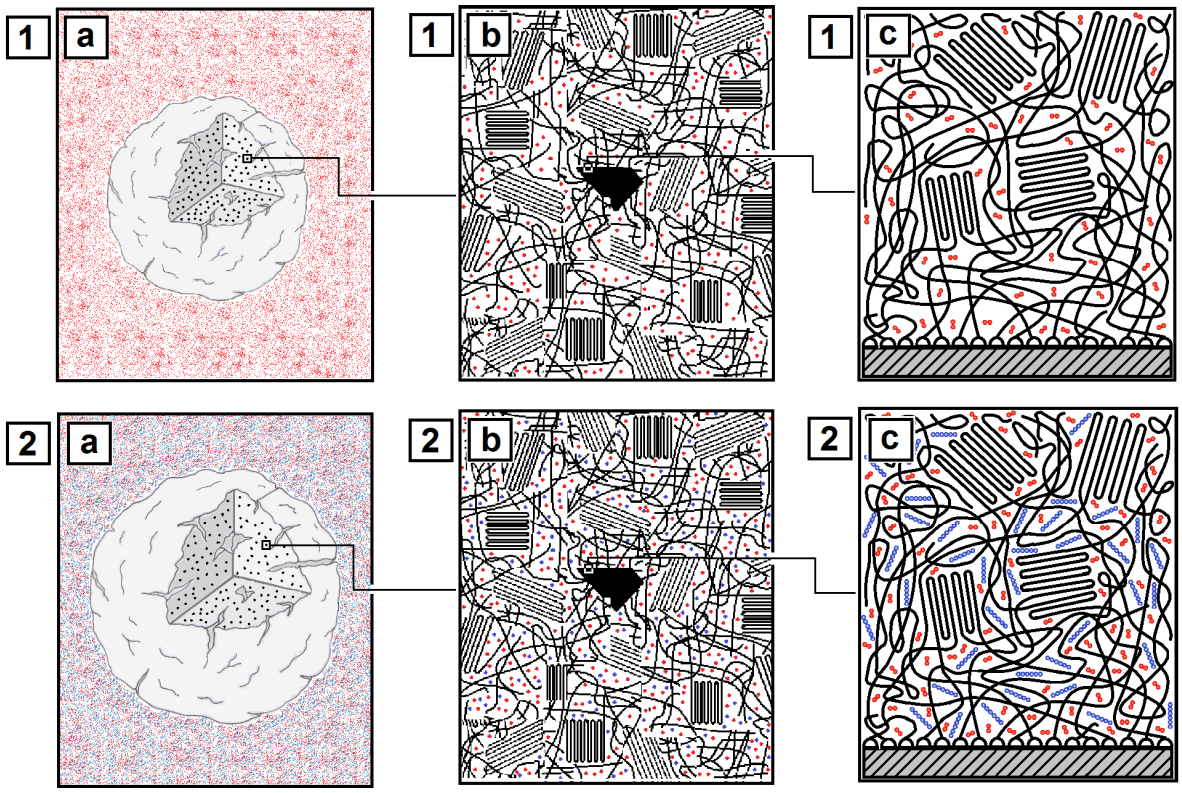

Figure 4.3. Schematic representation of ethylene-polyethylene binary system (1) and ethylene-*n*-hexane-polyethylene ternary system (2) at the size scale corresponding to (a) particle level, (b) catalyst fragment surrounded by produced semi-crystalline polyethylene at sub-particle level, and (c) polymer chains being initiated from active sites immobilized on the surface of catalyst fragment.

Fitting the Sanchez-Lacombe EOS to a ternary system can be challenging, especially in the face of a lack of extensive data for the system of interest. Therefore, before fitting the model to the data that we have found, we will perform a study in order to identify which parameters are the most important in terms of model sensitivity, and that require careful estimation (and conversely which parameters can be treated as being of secondary importance).

Following the parametric study, we will examine the predictive capability of Sanchez-Lacombe EOS using a set of experimentally obtained solubility data of ethylene and *n*-hexane in the ternary system of ethylene-*n*-hexane-PE provided by group of Yang.[2]

4.4. Parametric study of Sanchez-Lacombe EOS

In the following parametric studies, the primary objective is to explore the performance of Sanchez-Lacombe model in describing the ternary systems which are generated by addition of the third component

of a solute (*j*) to the "known" binary system of solute (*i*)-polymer. In the ternary systems discussed below, component (*1*) and (*2*) represent the solute molecules of ethylene and *n*-hexane, respectively, while component (*3*) refers to the LLDPE polymer.

In simple words, let us consider the "known" ethylene-LLDPE binary system in which the solubility of ethylene in LLDPE at specific equilibrium temperature and pressure is determined experimentally and described by Sanchez-Lacombe model through adjustment of binary interaction parameter of k_{13}. It is our intention here to explore how Sanchez-Lacombe EOS predicts the evolution of ethylene solubility, polymer swelling, and concentration of ethylene in amorphous polymer upon addition of *n*-hexane in the created ternary system of ethylene-*n*-hexane-LLDPE.

This analysis will be performed first on the effect of *n*-hexane on the ethylene solubility, having ethylene-LLDPE as the "known" system and then followed by similar analysis on the effect of ethylene on the *n*-hexane solubility, having *n*-hexane-LLDPE as the "known" system.

Before moving on to these set of parametric studies, it must be emphasized that in these series of "idealistic" simulations, we will neglect the effect of polymer crystalline phase[9,10] on model predictions of the solubility of solutes in amorphous phase, the extent of swelling of amorphous polymer phase and consequently the ethylene concentration in the amorphous polymer phase. In fact, the crystalline phase is observed to play a more pronounced role at higher pressure of the solutes.[10] This is due to the fact that at the higher pressures, the crystalline phases dispersed in the polymer start to act as physical crosslinks that limit the swelling of amorphous polymer phase. As a result, neglecting the effect of crystalline phase would lead to over-prediction of solubility at high-pressure limits of solutes. However, under the conditions typical of most gas phase polymerization reactions, the model retains its validity. This point will be elucidated further in the related section.

4.4.1. Effect of *n*-hexane on ethylene-LLDPE as the "known" system

In this section, first a parametric study is performed in the typical conditions for the gas phase ethylene polymerization. This is followed by a series of parametric studies investigating the effect of partial pressure of ethylene, gas-polymer equilibrium temperature, and more importantly the effect of *n*-hexane-LLDPE binary interaction parameter of k_{23}, on the trends predicted by Sanchez-Lacombe model.

In the all of the following modeling analysis of the ternary systems, and as appears to have been done in the other ternary modeling studies available in literature,[11] the ethylene-*n*-hexane binary interaction parameter of k_{12} is assumed to be equal to zero. This indicates that the ethylene-*n*-hexane mixture is expected to behave as an ideal mixture. The validity of this assumption has been demonstrated in an

experimental vapor-liquid equilibrium study of a system of ethylene and 4-methyl-1-pentene, so it appears that for the ethylene-*n*-hexane binary system considered here this assumption is reasonable.[12]

The ethylene-LLDPE interaction parameter of k_{13} was determined by fitting the SL model to the experimental data in the previous section. This will provide us with the ethylene solubility in amorphous polyethylene, $\left(S_{1,am}\right)^{binary}$, expressed in $\frac{gr\ sol.1}{gr\ am.pol}$, extent of volume change of amorphous polymer, $(1+SW_{am})^{binary}$, expressed in $\frac{lit\ (am.pol+sol.1)}{lit\ (am.pol)}$, and concentration of ethylene in amorphous polymer, $\left(C_{1,am}\right)^{binary}$, expressed in $\frac{mol\ sol.1}{lit\ (am.pol+sol.1)}$ in the absence of *n*-hexane as the "base" case.

Without any a priori knowledge about *n*-hexane solubility in PE and as a result *n*-hexane-LLDPE binary interaction parameter of k_{23}, it is assumed to be equal to zero, while the effect of k_{23} on the trends predicted by model will be explored through parametric study.

4.4.1.1. Parametric study at the typical condition for gas phase ethylene polymerization on supported catalyst

Here, the effect of *n*-hexane on the ethylene solubility, amorphous polymer swelling, and ethylene concentration is investigated upon addition to the system containing 10 bars of ethylene in equilibrium with LLDPE at 80 °C (typical conditions for the gas phase ethylene polymerization on supported catalyst).

In order to understand the sensitivity of the predictions of ethylene solubility and the other properties mentioned above to the presence of *n*-hexane, the following normalized functions are defined below.

Normalized solubility, $S_{1,am}^{norm.}$:

$$S_{1,am}^{norm.}=\frac{\left(S_{1,am}\right)^{ternary}}{\left(S_{1,am}\right)^{binary}}[=]\frac{\left(\frac{gr\ sol.1}{gr\ am.pol}\right)^{ternary}}{\left(\frac{gr\ sol.1}{gr\ am.pol}\right)^{binary}} \qquad (4.14)$$

in which $\left(S_{1,am}\right)^{ternary}$ is the ethylene solubility in the ternary system of ethylene-*n*-hexane-LLDPE while $\left(S_{1,am}\right)^{binary}$ is the ethylene solubility in the "known" binary system of ethylene-LLDPE.

Normalized volume, $V^{norm.}$:

$$V^{norm.} = \frac{\left(1 + SW_{12,am}\right)^{ternary}}{(1 + SW_{am})^{binary}} [=] \frac{\left(\frac{lit\ (am.pol + sol.1 + sol.2)}{lit\ (am.pol)}\right)^{ternary}}{\left(\frac{lit\ (am.pol + sol.1)}{lit\ (am.pol)}\right)^{binary}} \quad (4.15)$$

in which $\left(1 + SW_{12,am}\right)^{ternary}$ represents the volume change of the amorphous phase of polymer due to sorption of ethylene and *n*-hexane solutes in the ternary system of ethylene-*n*-hexane-LLDPE, while $(1 + SW_{am})^{binary}$ represents the volume change of the amorphous phase of polymer due to sorption of ethylene in the "known" binary system of ethylene-LLDPE.

Normalized concentration of ethylene in amorphous phase of polymer, $C_{1,am}^{norm.}$:

$$C_{1,am}^{norm.} = \frac{\left(C_{1,am}\right)^{ternary}}{\left(C_{1,am}\right)^{binary}} [=] \frac{\left(\frac{mol\ sol.1}{lit\ (am.pol + sol.1 + sol.2)}\right)^{ternary}}{\left(\frac{mol\ sol.1}{lit\ (am.pol + sol.1)}\right)^{binary}} \quad (4.16)$$

in which $\left(C_{1,am}\right)^{ternary}$ is the concentration of ethylene in amorphous phase of polymer in the ternary system of ethylene-*n*-hexane-LLDPE, while $\left(C_{1,am}\right)^{binary}$ is the concentration of ethylene in amorphous phase of polymer in the "known" binary system of ethylene-LLDPE.

Normalized pressure of *n*-hexane, $P^{norm.}$:

$$P^{norm.} = \frac{P}{P_{vap}} \quad (4.17)$$

in which P is *n*-hexane pressure and P_{vap} is the vapor pressure of the *n*-hexane in the equilibrium temperature at which the ternary system is being studied. The vapor pressures of *n*-hexane at different temperatures of interest in the current study are summarized in Table 4-II.

Table 4-II. The vapor pressure of *n*-hexane in the temperature range of interest.

Temperature (°C)	70	80	90
Vapor Pressure (bar)	1.05	1.42	1.89

Figure 4.4 demonstrates the effect of the normalized partial pressure of *n*-hexane in the ternary system of ethylene-*n*-hexane-LLDPE, on the normalized solubility of ethylene in the amorphous phase of polymer (referred to as "normalized solubility" from now on), the normalized volume of the amorphous polymer

phase (referred to as “normalized volume” from now on), and the normalized concentration of ethylene in the amorphous phase of polymer (referred to as “normalized concentration” from now on).

In this set of simulations, the ethylene-*n*-hexane interaction parameter is assumed to be $k_{12} = 0.0$, as previously explained. The ethylene-LLDPE interaction parameter, k_{13}, found by fitting SL model to the ethylene solubility data at 80 °C is $k_{13} = -0.022$, and for now we will assume $k_{23} = 0.0$ without considering any a priori experimental knowledge about solubility of *n*-hexane.

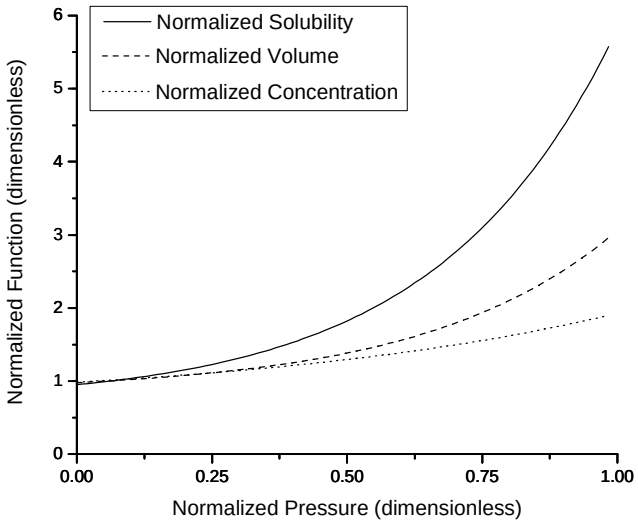

Figure 4.4. A priori simulation on effect of *n*-hexane on the ethylene solubility, swelling of amorphous phase of LLDPE, and ethylene concentration in the amorphous phase of LLDPE at typical polymerization condition of 80 °C temperature and 10 bars of ethylene partial pressure.

As can be seen from this figure, under these conditions the normalized solubility, normalized volume, and normalized concentration start to increase as a function of normalized partial pressure of *n*-hexane. In other words, according to the SL model, a higher partial pressure of *n*-hexane in the ternary system of ethylene-*n*-hexane-LLDPE is expected to result in higher solubility of ethylene in amorphous polyethylene, higher swelling of polymer’s amorphous phase, and eventually higher concentration of ethylene in the amorphous phase of polyethylene.

The important aspect of the trend predicted by Sanchez-Lacombe model which needs to be emphasized here is that at each specific normalized pressure, the extent of increase in the normalized solubility of ethylene is higher than the extent of the increase in the normalized volume due to the sorption of *n*-hexane which results in a prediction of the increase in the normalized concentration, and as a result an

enhancement of the concentration of ethylene in the amorphous phase of polyethylene in the presence of *n*-hexane. However, since the normalized concentration is proportional to the ratio of normalized solubility to normalized volume ($C_{1,am}^{norm.} \alpha \frac{S_{1,am}^{norm.}}{V^{norm.}}$), the extent of increase in the normalized concentration is much lower than the extent of increase in the normalized solubility due to presence of *n*-hexane.

4.4.1.2. Parametric study of effect of partial pressure of ethylene

In this section, the effect of partial pressure of ethylene at 80 °C on the magnitude of the predicted enhancement trend by Sanchez-Lacombe EOS in ethylene solubility, amorphous polyethylene swelling, and ethylene concentration in amorphous polyethylene in the ternary system of ethylene-*n*-hexane-LLDPE is presented. As described in the previous section, the defined normalized functions of normalized solubility, normalized volume, and normalized concentration are used as the "measure of enhancement" in ethylene solubility, volume of amorphous polymer, and concentration of ethylene in amorphous polymer in the ternary system of ethylene-*n*-hexane-LLDPE, respectively. In these set of simulations, the partial pressure of ethylene is varied between the possible operational range of 5 to 15 bars. As in the previous set of simulations, the ethylene-*n*-hexane interaction parameter is assumed to be $k_{12} = 0.0$. The ethylene-LLDPE interaction parameter, k_{13}, which is determined by fitting SL model to the ethylene solubility data at 80 °C is used as $k_{13} = -0.022$ while assuming $k_{23} = 0.0$ without considering any a priori experimental knowledge about solubility of *n*-hexane.

In addition, the solubility of ethylene in amorphous polyethylene, $\left(S_{1,am}\right)^{binary}$, the extent of change in volume of amorphous polyethylene due to sorption, $(1 + SW_{am})^{binary}$, and the concentration of ethylene in the amorphous phase of PE, $\left(C_{1,am}\right)^{binary}$, at each pressure of ethylene at 80 °C which are predicted by Sanchez-Lacombe model for the "known" binary system of ethylene-LLDPE having the corresponding binary interaction parameter are summarized in Table 4-III.

Table 4-III. Predicted solubility of ethylene, volume change of amorphous polymer, and concentration of ethylene in the amorphous phase of polyethylene by SL model at 80 °C and different ethylene pressures for the "known" ethylene-LLDPE system with k_{ij} = -0.022.

Ethylene Pressure	5	10	15	bar
$\left(S_{1,am}\right)^{binary}$	0.0046	0.0092	0.0138	$\left(\frac{gr\ sol.1}{gr\ am.pol}\right)^{binary}$
$(1 + SW_{am})^{binary}$	1.0076	1.0153	1.0230	$\left(\frac{lit\ (am.pol + sol.1)}{lit\ (am.pol)}\right)^{binary}$
$\left(C_{1,am}\right)^{binary}$	0.1343	0.2671	0.3982	$\left(\frac{mol\ sol.1}{lit\ (am.pol + sol.1)}\right)^{binary}$

Figure 4.5, Figure 4.6, and Figure 4.7 demonstrate the predicted effect of partial pressure of ethylene on normalized solubility, normalized volume, and normalized concentration as a function of normalized pressure of *n*-hexane at 80 °C, respectively. An interesting pattern predicted by Sanchez-Lacombe model is revealed by comparing these three graphs. In all of these figures, the partial pressure of ethylene does not have any effect on the predicted magnitude of increase in normalized solubility, normalized volume, and normalized concentration due to presence of *n*-hexane, in the lower limit of normalized partial pressure of *n*-hexane up to about $P^{norm.} = 0.5$. This in turn implies that in the lower limit of normalized partial pressure of *n*-hexane, the "level of enhancement" in ethylene solubility in the amorphous polymer, volume of amorphous phase, and concentration of ethylene in amorphous polyethylene due to presence of *n*-hexane is independent of the partial pressure of ethylene.

As explained above, some caution must be taken in interpreting these simulation results for a normalized function as a measure to represent the level of change (here, enhancement) of a specific function while moving from binary to ternary system. According to equations (4.14) to (4.16), in order to calculate the absolute values of ethylene solubility, change of amorphous phase's volume, and concentration of ethylene in amorphous phase in the ternary system of ethylene-*n*-hexane-LLDPE, the calculated normalized functions are needed to be multiplied by the corresponding values obtained experimentally for "known" binary system of ethylene-LLDPE, summarized in Table 4-III.

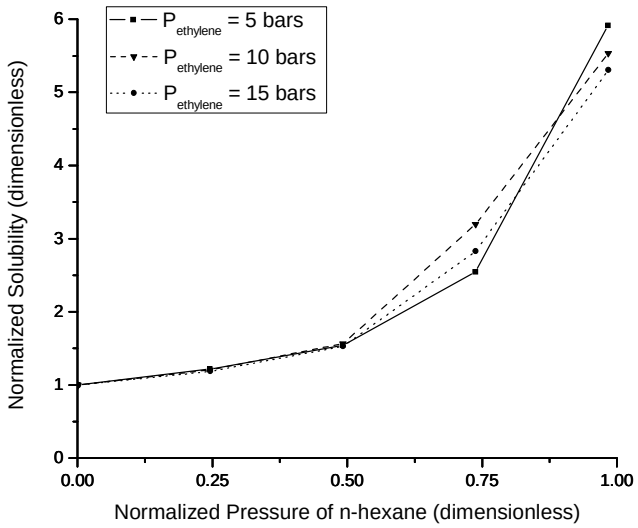

Figure 4.5. The prediction of Sanchez-Lacombe model on the effect of partial pressure of ethylene on the normalized solubility presented as a function of normalized pressure of *n*-hexane at 80 °C. The lines on the graph are to guide the eye.

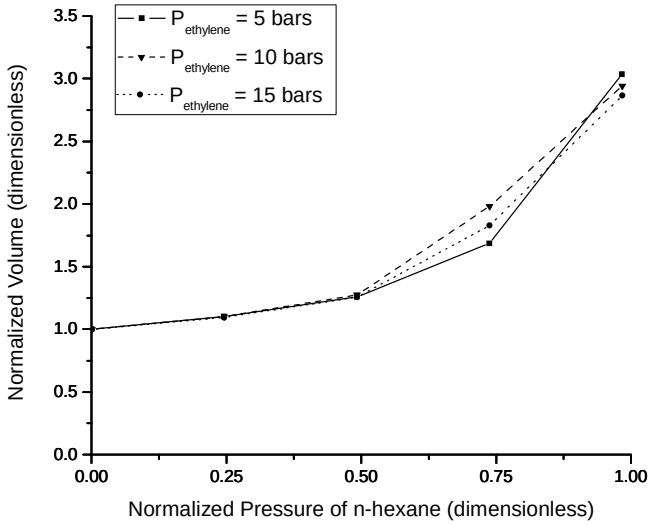

Figure 4.6. The prediction of Sanchez-Lacombe model on the effect of partial pressure of ethylene on the normalized volume presented as a function of normalized pressure of *n*-hexane at 80 °C. The lines on the graph are to guide the eye.

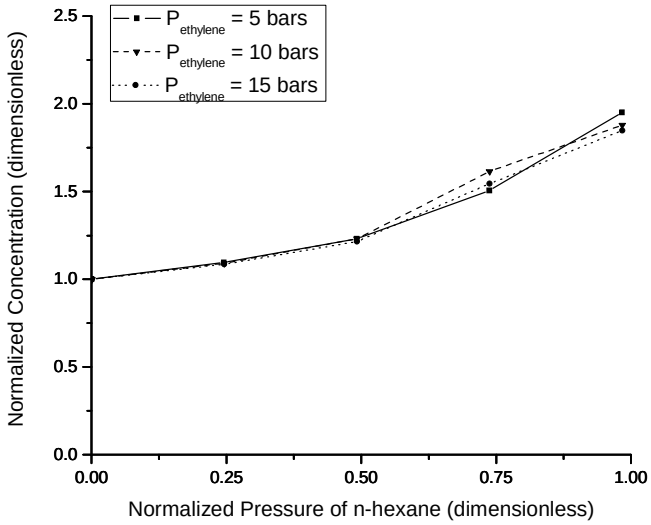

Figure 4.7. The prediction of Sanchez-Lacombe model on the effect of partial pressure of ethylene on the normalized concentration presented as a function of normalized pressure of *n*-hexane at 80 °C. The lines on the graph are to guide the eye.

However, at the higher limit of normalized pressure of *n*-hexane (above $P^{norm.} = 0.5$), the normalized solubility and normalized volume predicted at each partial pressure of ethylene start to diverge one from the other. The maximum divergence of predicted normalized solubility at higher ethylene pressures of 10

and 15 bars with respect to the predicted normalized solubility at 5 bars ethylene is calculated to be about 26% while the maximum divergence of predicted normalized volume at higher ethylene pressures of 10 and 15 bars with respect to the predicted normalized volume at 5 bars ethylene is calculated to be about 17%.

By comparing Figure 4.5 and Figure 4.6, one can notice that the pattern of divergence of predicted normalized solubility and normalized volume at different partial pressures of ethylene are similar. It is because the change in the volume of the amorphous phase is directly related to the mass of solutes sorbed into it. For this reason, and since the normalized concentration is proportional to the ratio of normalized solubility to normalized volume ($C_{1,am}^{norm.} \alpha \frac{S_{1,am}^{norm.}}{V^{norm.}}$), it can be seen in Figure 4.7 that the magnitude of increase in dimensionless concentration as a function of dimensionless pressure of *n*-hexane still remains approximately independent of partial pressure of ethylene in higher limit of normalized pressure of *n*-hexane. The maximum divergence of predicted normalized concentration at higher ethylene pressures of 10 and 15 bars with respect to the predicted normalized concentration at 5 bars ethylene is calculated to be about 7%, which can be considered to be negligible.

Similar trends are predicted by Sanchez-Lacombe model for the effect of partial pressure of ethylene on normalized solubility, normalized volume, and normalized concentration at 70 and 90 °C and are not presented here for the purpose of brevity.

This set of parametric study on the effect of partial pressure of ethylene on the predicted level of enhancement in ethylene solubility, change in volume of amorphous phase and most importantly concentration of ethylene in amorphous polymer highlights the potential attractiveness of this category of equations of state from a practical point of view. Let us consider a gas phase fluidized bed reactor for ethylene polymerization at specific temperature (typically 80 °C) with specific catalytic system. Having an appropriate set of equilibrium data for solubility in binary and ternary system of interest, Sanchez-Lacombe model can predict the level of enhancement in concentration of ethylene in the amorphous polyethylene surrounding the immobilized active sites (demonstrated in Figure 4.3) and consequently the enhancement in the reactor productivity upon introduction of *n*-hexane (or other ICA) to the reaction environment independent of the partial pressure of ethylene at which the reactor is operating. This claim of course is valid if we can neglect the potential effect of *n*-hexane on the morphology of particle, crystallinity degree of produced polyethylene and in short the mass transfer resistance through a growing particle. These points will be elucidated further in upcoming discussions in the next chapter, while it was intended here to provide a hint about the importance and necessity of current set of parametric study simulations in a larger context.

4.4.1.3. Parametric study of effect of equilibrium temperature

In this section, the effect of equilibrium temperature on the magnitude of predicted enhancement trend by Sanchez-Lacombe EOS in ethylene solubility, amorphous polyethylene swelling, and ethylene concentration in amorphous polyethylene in the ternary system of ethylene-*n*-hexane-LLDPE is presented. In this set of simulations, the partial pressure of ethylene is 10 bars while the equilibrium temperature of gas-polymer system is varied between 70 to 90 °C, in a temperature range close to the typical operating condition of the gas phase ethylene polymerization on supported catalyst. Similar to previous parametric studies presented, ethylene-*n*-hexane mixture is assumed to behave ideally i.e. $k_{12} = 0.0$ and no a priori knowledge about *n*-hexane solubility in polyethylene is considered by assuming $k_{23} = 0.0$. However, the ethylene-LLDPE interaction parameter, k_{13}, which has been determined by fitting the SL model to the experimental data in binary system, is used to be $k_{13} = -0.014, -0.022, and -0.032$ at each equilibrium temperature of 70, 80, and 90 °C, respectively.

In addition, the solubility of ethylene in amorphous polyethylene, $\left(S_{1,am}\right)^{binary}$, the extent of change in volume of amorphous polyethylene due to sorption, $(1 + SW_{am})^{binary}$, and the concentration of ethylene in the amorphous phase of PE, $\left(C_{1,am}\right)^{binary}$, at each equilibrium temperature which are predicted by Sanchez-Lacombe model for the "known" binary system of ethylene-LLDPE in which pressure of ethylene is 10 bars are summarized in Table 4-IV having the corresponding binary interaction parameters at each temperature.

Table 4-IV. Predicted solubility of ethylene, volume change of amorphous polymer, and concentration of ethylene in the amorphous phase of polyethylene by SL model at 10 bars of ethylene and different equilibrium temperatures of 70, 80, 90 °C for the "known" ethylene-LLDPE system with k_{ij} = -0.014, -0.022, -0.032 respectively.

Temperature	70	80	90	°C
$\left(S_{1,am}\right)^{binary}$	0.0097	0.0092	0.0090	$\left(\frac{gr\ sol.1}{gr\ am.pol}\right)^{binary}$
$(1 + SW_{am})^{binary}$	1.0159	1.0153	1.0151	$\left(\frac{lit\ (am.pol + sol.1)}{lit\ (am.pol)}\right)^{binary}$
$\left(C_{1,am}\right)^{binary}$	0.282	0.2671	0.2591	$\left(\frac{mol\ sol.1}{lit\ (am.pol + sol.1)}\right)^{binary}$

Figure 4.8, Figure 4.9, and Figure 4.10 demonstrate the predicted effect of gas-polymer equilibrium temperature on the normalized solubility, normalized volume, and normalized concentration as a function of normalized pressure of *n*-hexane, respectively, with partial pressure of ethylene equal to 10 bars in the ternary system of ethylene-*n*-hexane-LLDPE.

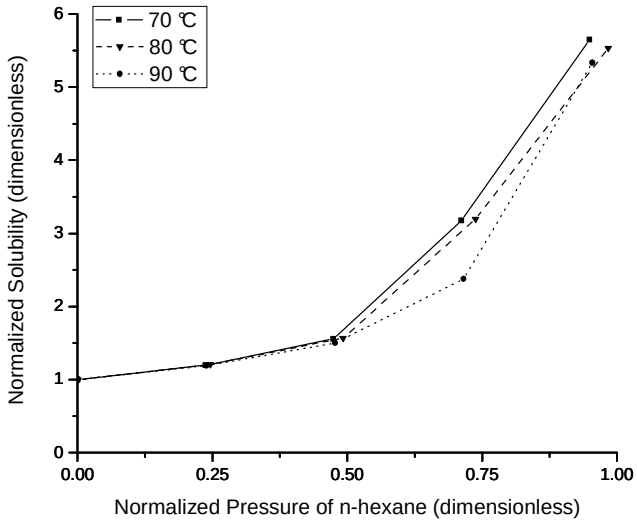

Figure 4.8. The prediction of Sanchez-Lacombe model on the effect of gas-polymer equilibrium temperature on the normalized solubility presented as a function of normalized pressure of *n*-hexane with partial pressure of ethylene equal to 10 bars in the ternary system of ethylene-*n*-hexane-LLDPE. The lines on the graph are to guide the eye.

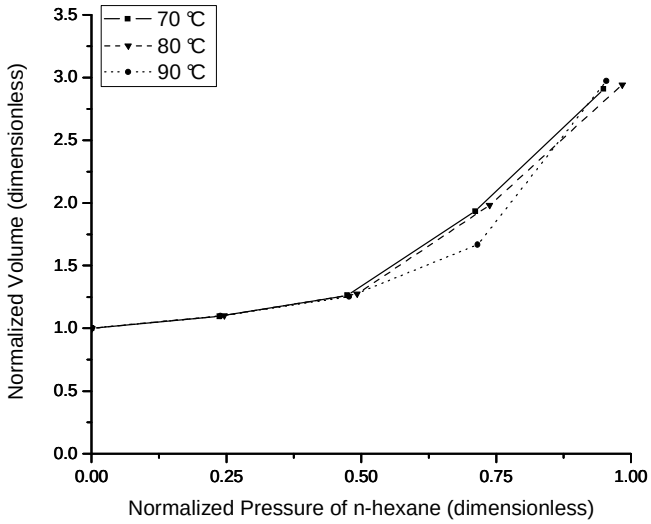

Figure 4.9. The prediction of Sanchez-Lacombe model on the effect of gas-polymer equilibrium temperature on the normalized volume presented as a function of normalized pressure of *n*-hexane with partial pressure of ethylene equal to 10 bars in the ternary system of ethylene-*n*-hexane-LLDPE. The lines on the graph are to guide the eye.

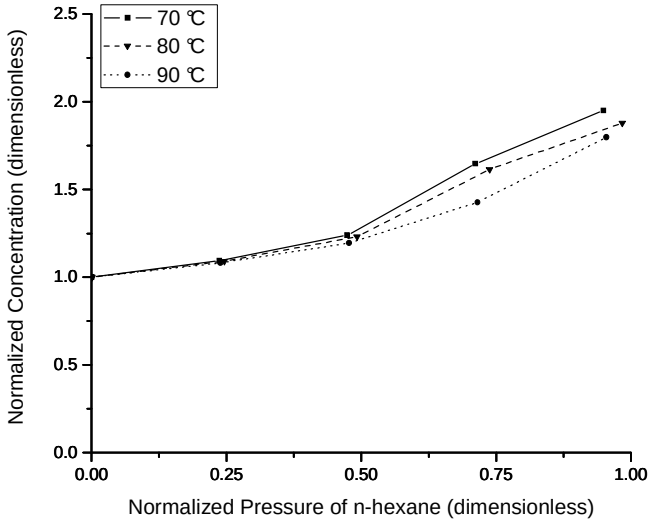

Figure 4.10. The prediction of Sanchez-Lacombe model on the effect of gas-polymer equilibrium temperature on the normalized concentration presented as a function of normalized pressure of *n*-hexane with partial pressure of ethylene equal to 10 bars in the ternary system of ethylene-*n*-hexane-LLDPE. The lines on the graph are to guide the eye.

These last three Figures suggest that the temperature at which the gas-polymer system is in equilibrium does not affect the magnitude of enhancement in normalized solubility, normalized volume, and normalized concentration as a function of normalized pressure of *n*-hexane upon addition of this third component of *n*-hexane to the "known" binary system in the lower limit of normalized pressure of *n*-hexane up to about $P^{norm.} = 0.5$. However, at higher limit of normalized pressure of *n*-hexane (above $P^{norm.} = 0.5$), the Sanchez-Lacombe model predicts that the magnitude of enhancement in normalized solubility, normalized volume, and normalized concentration would decrease by increasing the temperature at which the gas-polymer system is in equilibrium.

Similar trends are predicted with Sanchez-Lacombe model for the effect of equilibrium temperature for the ternary system of ethylene-*n*-hexane-LLDPE with partial pressure of ethylene equal to 5 and 15 bars and are not presented here for the brevity purpose.

4.4.1.4. Parametric study of effect of *n*-hexane-LLDPE binary interaction parameter, k_{23}

In this section, the effect of *n*-hexane-LLDPE binary interaction parameter, k_{23}, on the normalized solubility of ethylene in amorphous PE, normalized volume of amorphous phase of PE, and normalized concentration of ethylene in the amorphous polyethylene will be explored in the ternary system of ethylene-*n*-hexane-LLDPE. This set of simulations is performed at the equilibrium temperature of 80 °C with 10 bars of ethylene partial pressure. Similar to previous simulations, the ethylene-*n*-hexane

interaction parameter is assumed $k_{12}=0.0$, while the ethylene-LLDPE interaction parameter obtained from fitting SL model to the experimental data at 80 °C is used $k_{13}=-0.022$.

While the binary interaction parameter, k_{ij}, between a solute (*i*) and a polymer (*j*) component in a binary or ternary system is generally perceived and used as the adjustable parameter in order to fit the Sanchez-Lacombe model prediction to the experimental solubility data in a binary or ternary system (and it will be the same in our upcoming discussions), however, it would be useful here to briefly take a closer look on the conceptual meaning of this parameter in the context of Sanchez-Lacombe EOS.

According to its definition, k_{ij}, represents the deviation of cross mer-mer interaction energy of component (*i*) and (*j*), ε_{ij}^*, from the geometric mean of mer-mer interaction energy of component (*i*), ε_{ii}^*, and component (*j*), ε_{jj}^*. While positive interaction parameter, k_{ij}, implies that ε_{ij}^* is lower than the geometric mean of ε_{ii}^* and ε_{jj}^*. Due to this weaker interaction energy with positive binary interaction parameter, the predicted solubility of solute (*i*) in polymer (*j*) will be lower than the case where the binary interaction parameter is equal to zero i.e. the system following the SL model ideally. On the other hand, negative interaction parameter implies that ε_{ij}^* is higher than geometric mean of ε_{ii}^* and ε_{jj}^* and because of this stronger interaction energy with negative binary interaction parameter, the predicted solubility of solute (*i*) in polymer (*j*) will be higher than the case where the binary interaction parameter is equal to zero.

It is intended in this section to explore the effect of *n*-hexane-LLDPE binary interaction parameter, k_{23}, as a measure determining the solubility of *n*-hexane in the amorphous PE on the enhancement trend predicted for ethylene solubility in amorphous PE, volume of amorphous PE, and concentration of ethylene in amorphous PE in the ternary system of ethylene-*n*-hexane-LLDPE. The magnitude of the range in which the *n*-hexane-LLDPE binary interaction parameter, k_{23}, is altered in these simulations is in the order of maximum magnitude required for fitting the SL model to the experimental solubility data of *n*-hexane in LLDPE in the previous section. As a result, the k_{23} is altered between -0.04 and +0.04. Figure 4.11, Figure 4.12, and Figure 4.13 demonstrate the predicted effect of *n*-hexane-LLDPE binary interaction parameter, k_{23}, on the normalized solubility of ethylene, normalized volume of amorphous phase, and normalized concentration of ethylene in amorphous PE presented as a function of normalized pressure of *n*-hexane in the ternary system of ethylene-*n*-hexane-LLDPE, respectively.

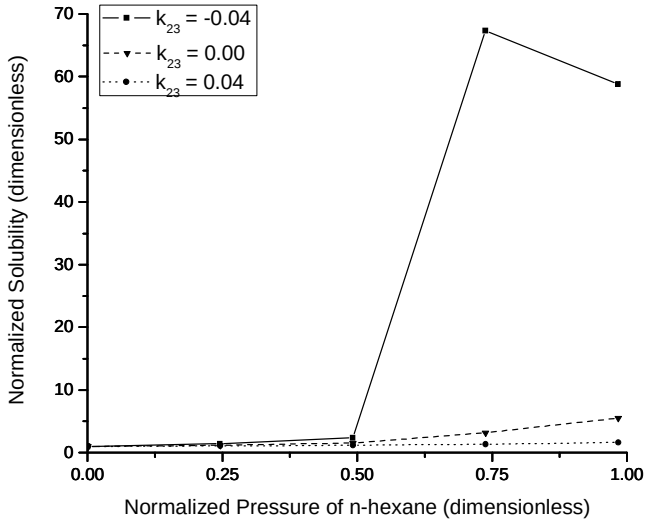

Figure 4.11. The prediction of Sanchez-Lacombe model on the effect of *n*-hexane-LLDPE binary interaction parameter, k_{23}, on the normalized solubility of ethylene presented as a function of normalized pressure of *n*-hexane for the ternary system of ethylene-*n*-hexane-LLDPE at equilibrium temperature of 80 °C having 10 bars of partial pressure of ethylene.

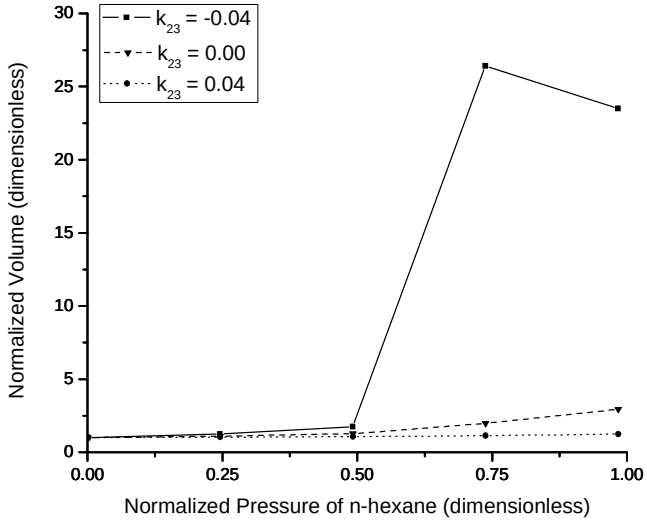

Figure 4.12. The prediction of Sanchez-Lacombe model on the effect of *n*-hexane-LLDPE binary interaction parameter, k_{23}, on the normalized volume of amorphous phase presented as a function of normalized pressure of *n*-hexane for the ternary system of ethylene-*n*-hexane-LLDPE at equilibrium temperature of 80 °C having 10 bars of pressure of ethylene.

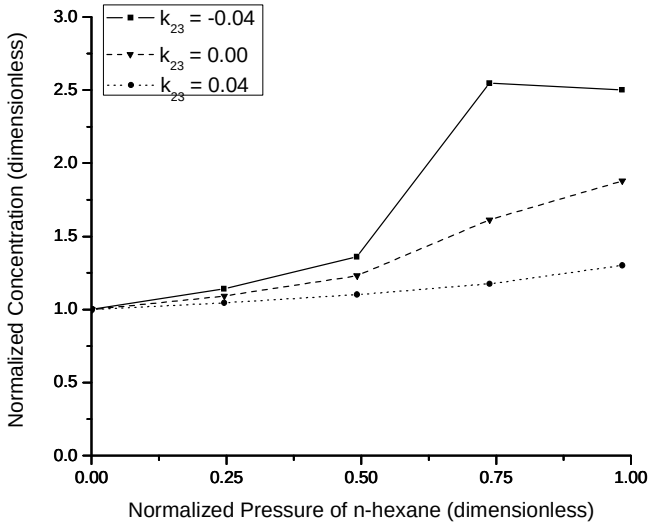

Figure 4.13. The prediction of Sanchez-Lacombe model on the effect of *n*-hexane-LLDPE binary interaction parameter, k_{23}, on the normalized concentration of ethylene presented as a function of normalized pressure of *n*-hexane for the ternary system of ethylene-*n*-hexane-LLDPE at equilibrium temperature of 80 °C having 10 bars of pressure of ethylene.

Regarding these figures and according to the Sanchez-Lacombe model predictions, as the *n*-hexane-LLDPE binary interaction parameter, k_{23}, decreases (i.e. as "assumed" solubility of *n*-hexane in amorphous phase of LLDPE increases) in the ternary system of ethylene-*n*-hexane-LLDPE, the solubility of ethylene in amorphous phase, volume of amorphous phase, and ethylene concentration in the amorphous phase also increase.

In all of these three figures and at the binary interaction parameter k_{23}=*-0.04*, we see an unexpected drop in normalized solubility, normalized volume , and normalized concentration when increasing the normalized partial pressure of *n*-hexane from 0.75 to 1. We do not have any explanation for this unexpected predicted trend by model.

The important aspect of this set of simulations is that while regarding Figure 4.11 and Figure 4.12, the normalized solubility and normalized volume are very sensitive to the *n*-hexane-LLDPE binary interaction parameter, k_{23}, the normalized concentration of ethylene shows much less sensitivity to this parameter. This is due to the fact that the normalized concentration of ethylene is proportional to the ratio of normalized solubility of ethylene to normalized volume ($C_{1,am}^{norm.} \alpha \frac{S_{1,am}^{norm.}}{V^{norm.}}$).

In short, this series of simulations help us to see that in the ternary system of ethylene-*n*-hexane-LLDPE, the solubility of ethylene in LLDPE is sensitive to the *n*-hexane-LLDPE binary interaction parameter

while the ethylene concentration shows less sensitivity to k_{23} compared to ethylene solubility. The importance of this finding will be highlighted again and emphasized later in the section related to the fitting the Sanchez-Lacombe model to the experimental solubility data of ethylene and *n*-hexane in LLDPE for the ternary system of ethylene-*n*-hexane-LLDPE.

The same trends are predicted for ethylene-*n*-hexane-LLDPE ternary system at equilibrium temperature of 80 °C having ethylene partial pressure of 5 and 15 bars. In addition, another series of simulations are performed for this ternary system at equilibrium temperature of 70 and 90 °C with 10 bars of ethylene partial pressure which also lead to similar trends. The aforementioned series of simulation analyses are not presented here for the brevity purpose.

4.4.2. Effect of ethylene on *n*-hexane-LLDPE as the "known" system

In this section, first, the effect of addition of ethylene to *n*-hexane-LLDPE as the "known" binary system is explored through a parametric study of Sanchez-Lacombe model at the equilibrium temperature of 80 °C as the typical temperature for the gas phase ethylene polymerization reactors. Then, this is followed by series of parametric studies on the effect of equilibrium temperature, and also ethylene-LLDPE binary interaction parameter of k_{13}, on the trends predicted by Sanchez-Lacombe model.

Similar to the previous set of simulations, the ethylene-*n*-hexane binary interaction parameter of k_{12} is assumed to be equal to zero. The *n*-hexane-LLDPE binary interaction parameter of k_{23} has been already determined through fitting the SL model to the experimental data in the previous section. This will provide us with *n*-hexane solubility in amorphous polyethylene, $\left(S_{2,am}\right)^{binary}$, expressed in $\frac{gr\ sol.2}{gr\ am.pol}$ in absence of ethylene as the "base" case. Without any a priori knowledge about ethylene solubility in PE and as a result ethylene-LLDPE binary interaction parameter of k_{13}, it is assumed to be equal to zero, while the effect of k_{13} on the trends predicted by model will be explored through parametric study.

4.4.2.1. Parametric study at the typical conditions for the gas phase ethylene polymerization on supported catalyst

Here, the effect of addition of up to 20 bars of ethylene to the "known" *n*-hexane-LLDPE system with three different normalized partial pressure of *n*-hexane $P^{norm.} = 0.25, 0.50, and\ 0.75$ is explored at 80 °C as the typical condition for the gas phase ethylene polymerization on supported catalyst.

In order to develop a better picture and as a result understanding of the predicted effect of ethylene on the solubility of *n*-hexane in LLDPE while transiting from *n*-hexane-LLDPE binary system to ethylene-*n*-hexane-LLDPE ternary system, the following normalized function is defined below.

Normalized solubility of *n*-hexane, $S_{2,am}^{norm.}$:

$$S_{2,am}^{norm.} = \frac{\left(S_{2,am}\right)^{ternary}}{\left(S_{2,am}\right)^{binary}} [=] \frac{\left(\frac{gr\ sol.2}{gr\ am.pol}\right)^{ternary}}{\left(\frac{gr\ sol.2}{gr\ am.pol}\right)^{binary}} \quad (4.18)$$

in which $\left(S_{2,am}\right)^{ternary}$ is the *n*-hexane solubility in the ternary system of ethylene-*n*-hexane-LLDPE while $\left(S_{2,am}\right)^{binary}$ is the *n*-hexane solubility in the "known" binary system of *n*-hexane-LLDPE.

In this set of simulation, as mentioned earlier, ethylene-*n*-hexane binary interaction parameter, k_{12} and ethylene-LLDPE binary interaction parameter, k_{13} is assumed to be equal to zero while the *n*-hexane-LLDPE binary interaction parameter obtained from fitting SL model to *n*-hexane solubility data at 80 °C is used as $k_{23} = 0.020$.

Table 4-V summarizes the predicted solubility of *n*-hexane in LLDPE for the binary system of *n*-hexane-LLDPE at 80 °C using SL model with binary interaction parameter of $k_{23} = 0.020$.

Table 4-V. The predicted solubility of *n*-hexane in LLDPE for the binary system of *n*-hexane-LLDPE at 80 °C using SL model with binary interaction parameter of k_{23} =0.020.

$P^{norm.}$	0.25	0.5	0.75	dimensionless
$\left(S_{2,am}\right)^{binary}$	0.0281	0.0657	0.1214	$\left(\frac{gr\ sol.2}{gr\ am.pol}\right)^{binary}$

Figure 4.14 demonstrates the predicted effect of addition of ethylene on the solubility of *n*-hexane by Sanchez-Lacombe EOS. The general trend is that the solubility of *n*-hexane starts to increase with partial pressure of ethylene (as unexpected co-solvency effect of ethylene) until it reaches a maxima in solubility of *n*-hexane. After this point, the solubility of *n*-hexane decreases by increasing the partial pressure of ethylene (anti-solvent effect of ethylene). The rate of initial increase and subsequent decrease in normalized solubility of *n*-hexane as a function of ethylene partial pressure slightly increases with the normalized partial pressure of *n*-hexane in the ternary system.

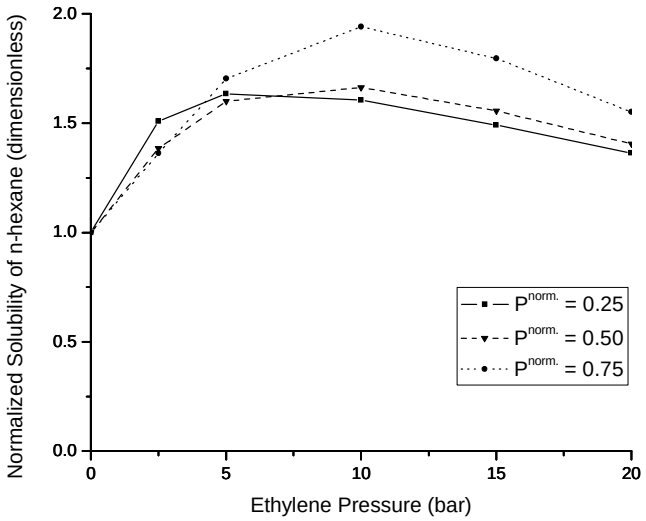

Figure 4.14. The predicted effect of addition of ethylene on the solubility of *n*-hexane by Sanchez-Lacombe EOS. The lines on the graph are to guide the eye.

This set of predictions are obviously in contradiction with the experimental findings of Novak et al.[13] for the ternary system of ethylene-hexene-LLDPE and group of Yang[2] for the ternary system of ethylene-*n*-hexane-LLDPE. The aforementioned experimental investigations have reported an anti-solvent effect of ethylene on the solubility of heavier solute component independent of partial pressure of ethylene in the ternary system. This in turn highlights the necessity for adjusting the binary interaction parameters of Sanchez-Lacombe EOS in order to be able to describe the solubility set of data acquired experimentally in the ternary system. We will explore this point in the upcoming section where the predictive capability of SL model is evaluated against experimental solubility data in the ternary system.

4.4.2.2. Parametric study of effect of equilibrium temperature

In this section, the effect of equilibrium temperature on the trends predicted by Sanchez-Lacombe model on the influence of partial pressure of ethylene on the solubility of *n*-hexane in LLDPE in the ternary system of ethylene-*n*-hexane-LLDPE is explored.

In this set of simulations, the equilibrium temperature is varied between 70 to 90 °C, in a range close to the operational condition of gas phase ethylene polymerization reactors. The normalized partial pressure of *n*-hexane at each equilibrium temperature is assumed to be equal to 0.5 in the studied ternary system. Similar to the previous section, ethylene-*n*-hexane binary interaction parameter, k_{12} and ethylene-LLDPE binary interaction parameter, k_{13} is assumed to be equal to zero while the *n*-hexane-LLDPE binary

interaction parameter which has been obtained by fitting SL model to the experimental data is used as $k_{23} = 0.010, 0.020, and\ 0.038$ at each equilibrium temperature of 70, 80, and 90 °C, respectively.

Table 4-VI summarizes the predicted solubility of *n*-hexane in LLDPE for the binary system of *n*-hexane-LLDPE with *n*-hexane normalized pressure of 0.5 at 70, 80, and 90 °C using SL model with corresponding binary interaction parameter at each temperature.

Table 4-VI. The predicted solubility of *n*-hexane in LLDPE for the binary system of *n*-hexane-LLDPE with *n*-hexane normalized pressure of 0.5 at 70, 80, and 90 °C using Sanchez-Lacombe model with binary interaction parameter k_{23} = 0.010, 0.020, and 0.038, respectively.

Temperature	70	80	90	°C
$(S_{2,am})^{binary}$	0.0815	0.0657	0.0394	$\left(\frac{gr\ sol.2}{gr\ am.pol}\right)^{binary}$

Figure 4.15 demonstrates the effect of equilibrium temperature on the trend predicted by SL model on the influence of partial pressure of ethylene on the solubility of *n*-hexane in LLDPE in the ternary system of ethylene-*n*-hexane-LLDPE.

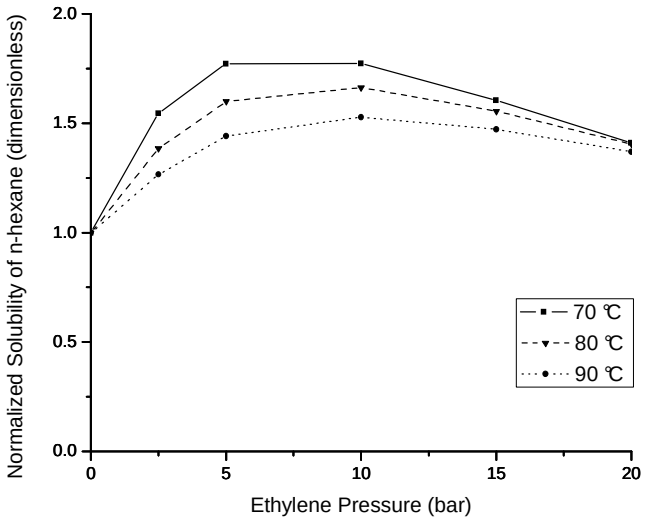

Figure 4.15. The predicted effect of equilibrium temperature on the influence of partial pressure of ethylene on the solubility of *n*-hexane in LLDPE in the ternary system of ethylene-*n*-hexane-LLDPE.
The lines on the graph are to guide the eye.

It can be seen that as the temperature in which the ternary system is in equilibrium increases, the effect of ethylene on the solubility of *n*-hexane is attenuated. However, the trend for the dependency of *n*-hexane solubility to the partial pressure of ethylene remains the same; the solubility of *n*-hexane starts to increase with partial pressure of ethylene until it reaches a maxima in solubility of *n*-hexane. After this point the solubility of *n*-hexane decreases by increasing the partial pressure of ethylene. Similar trends are predicted for the effect of equilibrium temperature for the ternary system of ethylene-*n*-hexane-LLDPE in which the normalized partial pressure of *n*-hexane is equal to 0.25 and 0.75. The associated results of these simulations are not presented here for the brevity purpose.

4.4.2.3. Parametric study of effect of ethylene-LLDPE binary interaction parameter, k_{13}

In this section, the predicted effect of ethylene-LLDPE binary interaction parameter, k_{13} on the solubility of *n*-hexane in LLDPE presented as a function of partial pressure of ethylene in the ternary system of ethylene-*n*-hexane-LLDPE is explored. This set of simulations with SL model is performed at the equilibrium temperature of 80 °C with normalized partial pressure of *n*-hexane equal to 0.5 in the ternary system. Similar to the previous set of simulations, the ethylene-*n*-hexane binary interaction parameter, k_{12} is assumed to be equal to zero. The *n*-hexane-LLDPE binary interaction parameter, k_{23} which has been determined by fitting the SL model to the experimental data at 80 °C is used as $k_{23} = 0.020$.

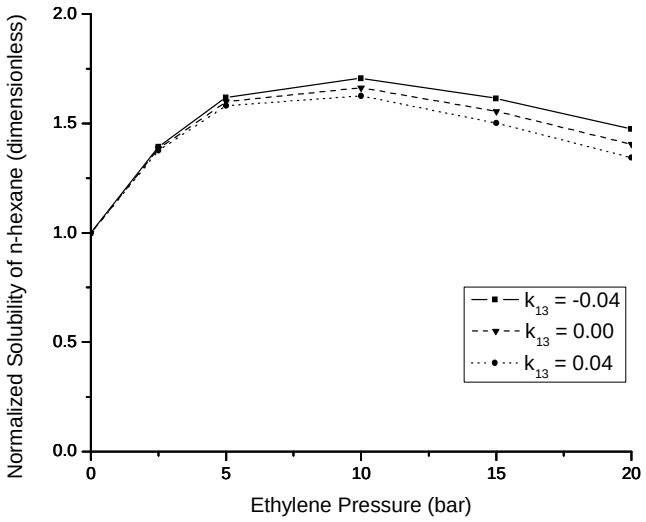

Figure 4.16. The predicted effect of ethylene-LLDPE binary interaction parameter, k_{13}, on the normalized solubility of *n*-hexane in LLDPE presented as a function of partial pressure of ethylene in the ternary system of ethylene-*n*-hexane-LLDPE. The lines on the graph are to guide the eye.

The magnitude of the range in which ethylene-LLDPE binary interaction parameter, k_{13}, is altered in these simulations is in the order of maximum magnitude required for fitting the SL model to the experimental solubility data of ethylene in LLDPE in the previous section. As a result, the k_{13} is altered between -0.04 and +0.04.

Figure 4.16 demonstrates the predicted effect of ethylene-LLDPE binary interaction parameter, k_{13}, on the normalized solubility of *n*-hexane in LLDPE presented as a function of partial pressure of ethylene in the ternary system of ethylene-*n*-hexane-LLDPE. As one can see from this figure, as the ethylene-LLDPE binary interaction parameter, k_{13}, decreases or alternatively, as the "assumed" solubility of ethylene in LLDPE increases in the ternary system of ethylene-*n*-hexane-LLDPE, the normalized solubility of *n*-hexane in LLDPE also increases.

However, the magnitude of the effect of changing the ethylene-LLDPE binary interaction parameter, k_{13}, on the normalized solubility of *n*-hexane is very small and can be considered almost negligible in comparison with the predicted effect of *n*-hexane-LLDPE binary interaction parameter, k_{23}, on the normalized solubility of ethylene provided in Figure 4.11 in the previous section. As a result, in the next section, where the predictive capability of Sanchez-Lacombe EOS is evaluated against experimental solubility data of ethylene and *n*-hexane in the ternary system of ethylene-*n*-hexane-LLDPE, the binary interaction of *n*-hexane-LLDPE, k_{23}, is used as the adjustable parameter in order to obtain the best fitting of Sanchez-Lacombe model prediction to the experimental solubility values of both ethylene and *n*-hexane which will lead to best estimation of ethylene concentration in the amorphous phase of PE using SL model. This is because as shown in our parametric study, in the ternary system of ethylene-*n*-hexane-LLDPE, while the ethylene solubility is very sensitive to the *n*-hexane-LLDPE binary interaction parameter, k_{23}, however, the *n*-hexane solubility shows much less (almost negligible) sensitivity to the ethylene-LLDPE binary interaction parameter, k_{13}. This point will be elucidated and clarified further in the upcoming related section.

Similar trends for the effect of ethylene-LLDPE binary interaction parameter, k_{13}, on the normalized solubility of *n*-hexane in the ternary system of ethylene-*n*-hexane-LLDPE at different equilibrium temperature of 70 and 90 °C and with different normalized partial pressure of *n*-hexane equal to 0.25 and 0.75 are predicted with Sanchez-Lacombe EOS and are not presented here for the sake of brevity.

4.5. Performance of Sanchez-Lacombe EOS in the ternary system

In this section, first, the performance of the Sanchez-Lacombe EOS in describing the solubility of ethylene and *n*-hexane in the ternary system of ethylene-*n*-hexane-LLDPE is evaluated against the solubility set of data obtained experimentally using the pressure decay method.[2] This is followed by the discussion of a method to fit the SL EOS for the ternary system of ethylene-*n*-hexane-PE to the experimental solubility data through adjustment of *n*-hexane-LLDPE binary interaction parameter, k_{23}. The optimized fitting of the SL model to the experimental data of both ethylene and *n*-hexane solubility in LLDPE simultaneously is of profound importance, as it will lead to a more accurate estimation of ethylene concentration in the amorphous phase of LLDPE. As highlighted earlier, the concentration of ethylene in the amorphous phase of polyethylene (not the solubility) controls the rate of gas phase ethylene polymerization on the supported catalyst. Using the available set of equilibrium solubility data for ethylene and *n*-hexane in LLDPE in ternary system, the performance of Sanchez-Lacombe EOS in prediction of enhancement in the ethylene concentration in the amorphous phase of polyethylene in presence of *n*-hexane, and as a result the rate of polymerization will be evaluated under reactive conditions (in Chapter 5). This is the first time such a thermodynamic model has been tested in reactive conditions in the open literature.

4.5.1. Evaluation of predictive capability of Sanchez-Lacombe EOS against experimental solubility data in the ternary system

The binary interaction parameters of ethylene-LLDPE, k_{13}, and *n*-hexane-LLDPE, k_{23}, were determined in the previous section by fitting the SL EOS for binary systems of solute-polymer to the experimental data at different equilibrium temperatures. In this section, we will extend the model to a ternary system. We will first test the quality of model predictions by implementing the obtained binary interaction parameter of k_{13} and k_{23} into Sanchez-Lacombe model for ternary systems of solute(*1*)-solute(*2*)-polymer, and comparing the results to the experimental solubility data of ethylene and *n*-hexane in the ternary system of ethylene-*n*-hexane-LLDPE (still assuming that $k_{12} = 0.0$).

The procedure for evaluating the predictive capability of Sanchez-Lacombe EOS in the ternary system is illustrated schematically in Figure 4.17.

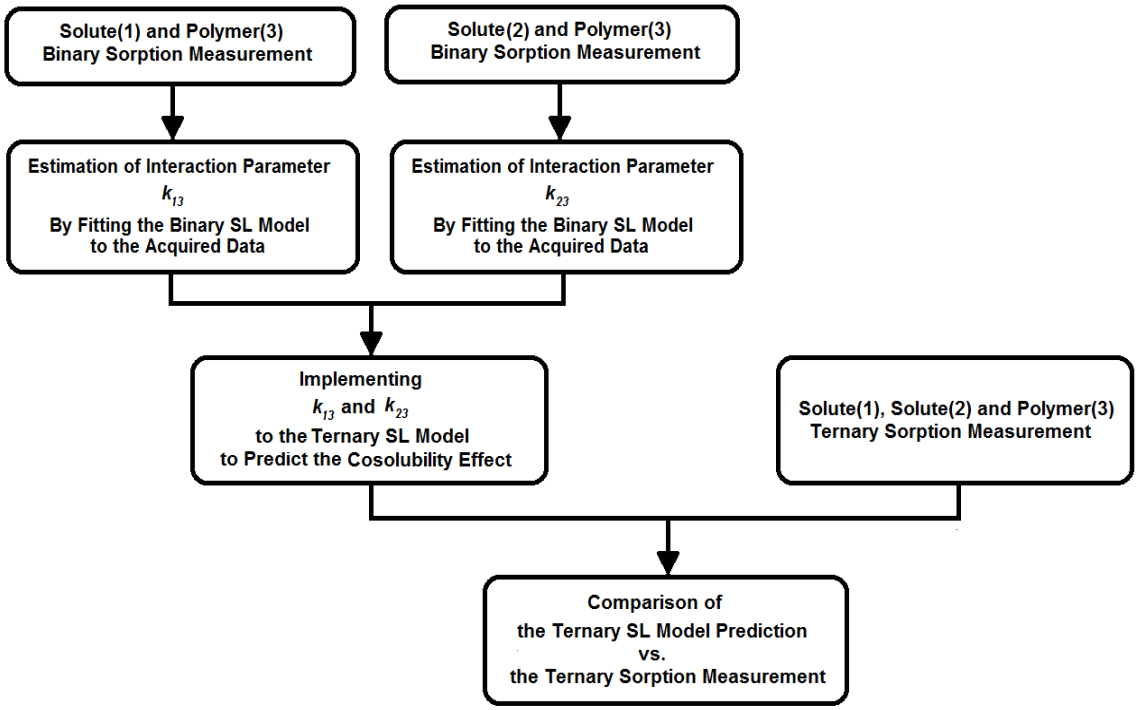

Figure 4.17. The schematic representation of the procedure for evaluation of predictive capability of Sanchez-Lacombe model in describing the solubility of the solutes in ternary system.

The sorption equilibrium data for ethylene and *n*-hexane in the ternary system of ethylene-*n*-hexane-LLDPE is extracted from the paper by group of Yang[2] in which the related sorption measurements are performed using the pressure-decay method.

The solubility measurements were performed at three equilibrium temperature of 70, 80, and 90 °C in a range close to the operational temperature of gas phase ethylene polymerization reactors. At each equilibrium temperature, four series of solubility measurements were performed for total gas phase pressures (as a mixture of ethylene and *n*-hexane with different compositions) of 5, 10, 15, and 20 bars. The maximum partial pressure of *n*-hexane in the gas phase composition is about 0.9 bar in all of these sets of experiments. The polyethylene sample used in the solubility measurements of ternary system is the same as the one used previously in the binary systems with the commercial grade name of DGM1820. This is assumed to be LLDPE according to its density of 920 kg/m^3 and crystallinity of 49%.

The software of Plot Digitizer is used in order to extract the related solubility data from the associated figures in which the solubility of species in polymer are presented versus their partial pressure in the gas phase at specific temperatures in the paper.[2] In order to evaluate and minimize the possible generation of

errors due to extraction of the data from the figures, the procedure of extracting the data is repeated for the two times. The mean absolute percentage of difference between two consecutive readings of solubility points from the figures i.e. $\left|\frac{S_{R_1}-S_{R_2}}{S_{R_1}}\right| \times 100$ in which R_1 and R_2 represents first and second reading of solubility values for a specific point in the figure is calculated to be 0.08% and 0.49% for ethylene and *n*-hexane solubility data in polyethylene, respectively. This in turn indicates that the errors generated at the step of extraction of solubility data from the figures are negligible and assures the reliability of acquired set of data.

Figure 4.18, Figure 4.19, and Figure 4.20 demonstrate the predictive capability of ternary Sanchez-Lacombe model in order to describe the solubility of ethylene and *n*-hexane in LLDPE in the ternary system of ethylene-*n*-hexane-LLDPE at three measurement equilibrium temperatures of 70, 80, and 90 °C, respectively. As previously mentioned, in the ternary Sanchez-Lacombe model, the ethylene-LLDPE binary interaction parameter, k_{13}, and the *n*-hexane-LLDPE binary interaction parameter, k_{23}, are obtained by fitting the binary Sanchez-Lacombe model to the experimental solubility data in the corresponding binary system of solute-polymer at each measurement equilibrium temperature, while k_{12} is assumed to be equal to zero.

A short explanation about the observed solubility behavior of ethylene as a function of its partial pressure in the mixture might be useful here. Since the sorption measurements are performed at a constant pressure of gas phase at each equilibrium temperature, as the partial pressure of ethylene in the mixture decreases, the partial pressure of *n*-hexane was increased in order to keep the pressure of gas phase constant. The higher partial pressure of *n*-hexane, in turn, results in a greater enhancement of ethylene solubility in the polymer (see the parametric study above). As a result, we can see that as the partial pressure of ethylene in the gas phase mixture decreases, its solubility in LLDPE remains more or less the same or even slightly increases.

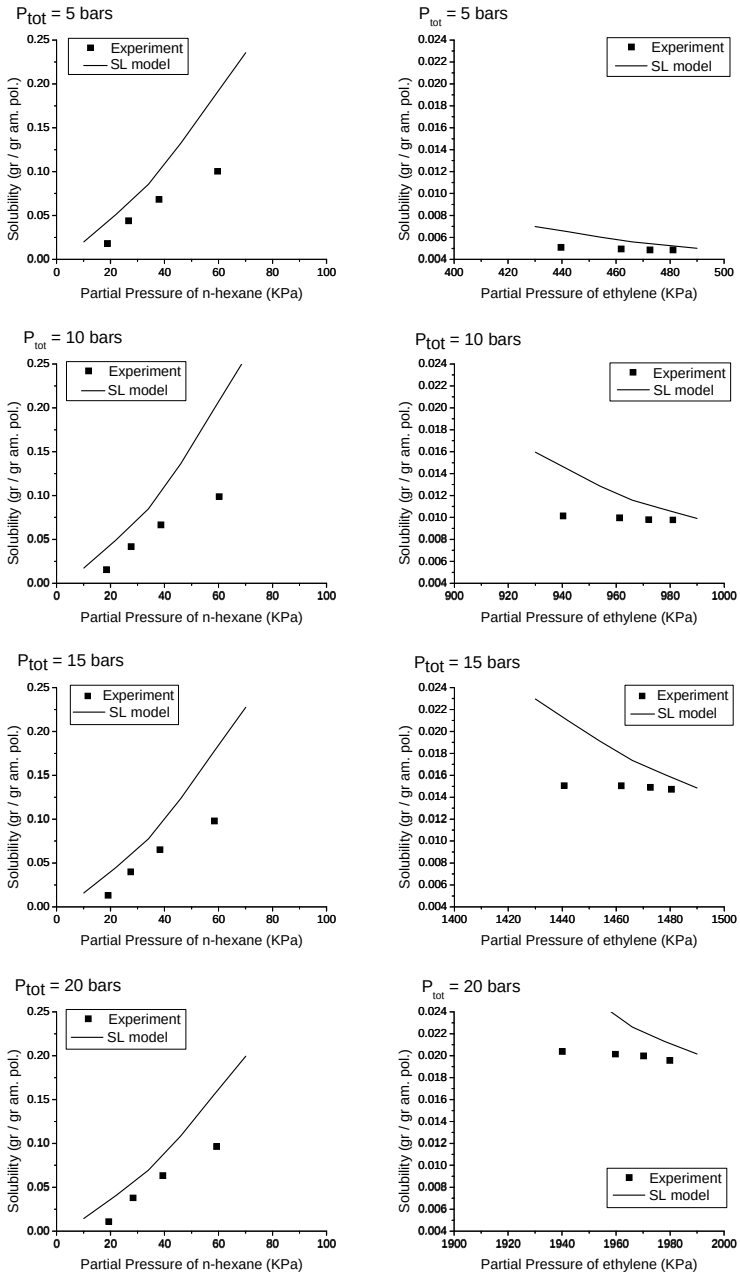

Figure 4.18. The solubility of *n*-hexane and ethylene in LLDPE in the ternary system of ethylene-*n*-hexane-LLDPE at 70 °C with P_{tot} = *5, 10, 15, and 20* bars and its comparison with the prediction of the ternary Sanchez-Lacombe model with the corresponding binary interaction parameters of k_{12} = *0.00*, k_{13} = *-0.014*, k_{23} = *0.010* at 70 °C.

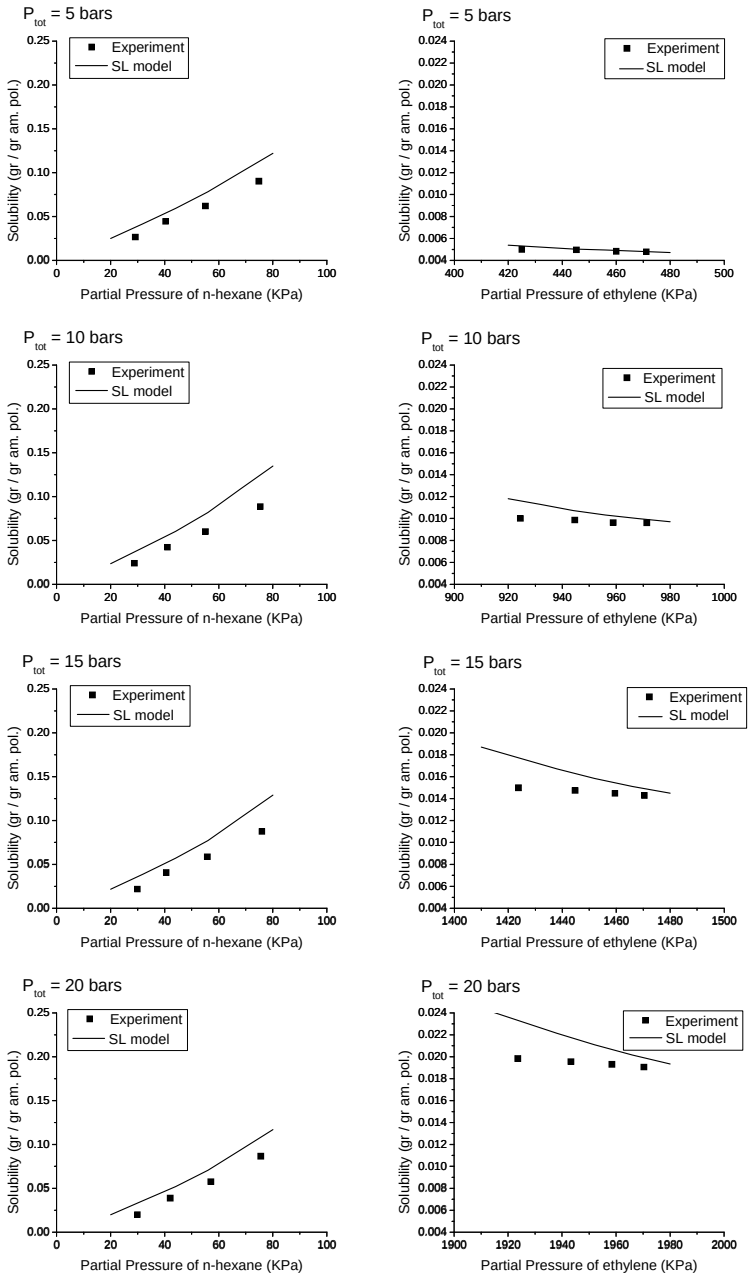

Figure 4.19. The solubility of *n*-hexane and ethylene in LLDPE in the ternary system of ethylene-*n*-hexane-LLDPE at 80 °C with P_{tot} = *5, 10, 15, and 20* bars and its comparison with the prediction of the ternary Sanchez-Lacombe model with the corresponding binary interaction parameters of k_{12} = *0.00*, k_{13} = *-0.022*, k_{23} = *0.020* at 80 °C.

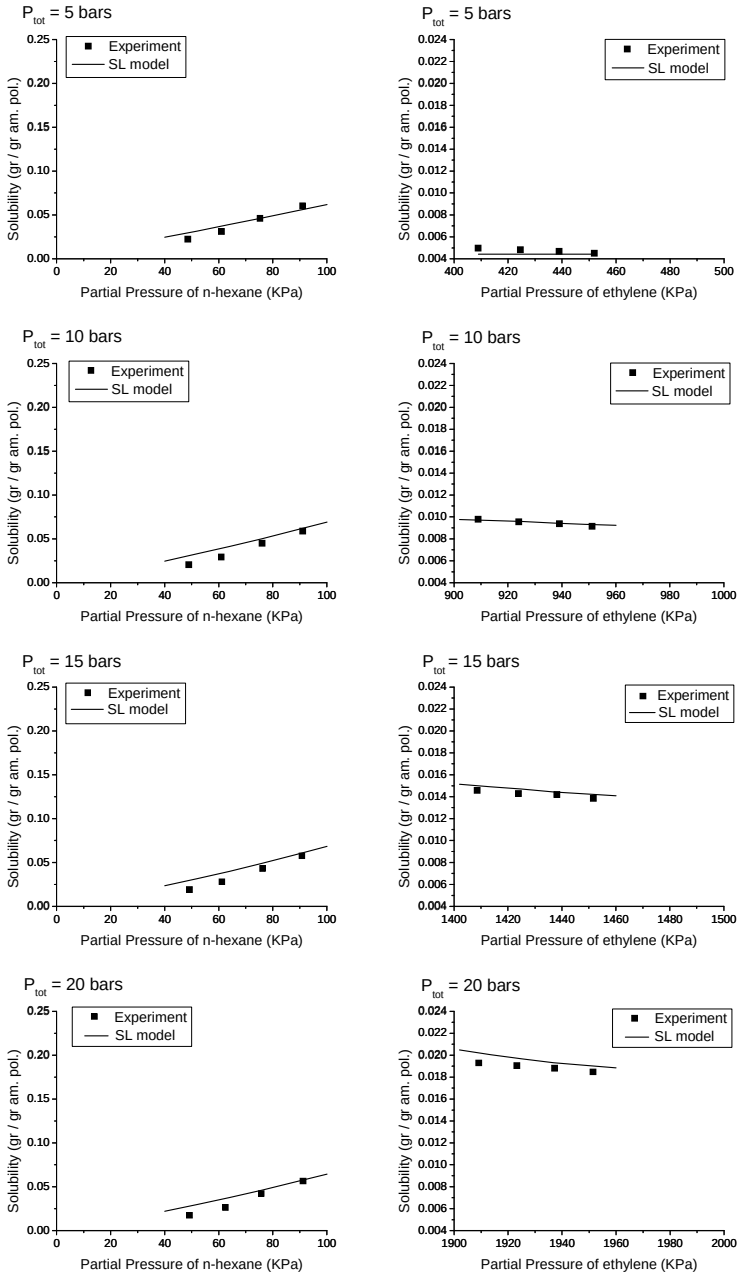

Figure 4.20. The solubility of *n*-hexane and ethylene in LLDPE in the ternary system of ethylene-*n*-hexane-LLDPE at 90 °C with P_{tot} = *5, 10, 15, and 20* bars and its comparison with the prediction of the ternary Sanchez-Lacombe model with the corresponding binary interaction parameters of k_{12} = *0.00*, k_{13} = *-0.032*, k_{23} = *0.038* at 90 °C.

As can be seen from Figure 4.18 to Figure 4.20, the prediction of ternary Sanchez-Lacombe model overestimates the solubility of both ethylene and *n*-hexane in comparison with the experimentally obtained solubility data in the ternary system of ethylene-*n*-hexane-LLDPE (except for ethylene solubility at 90 °C and P_{tot} = 5 bars). However, as the temperature at which the system is in equilibrium increases, the quality of the model predictions increases for both ethylene and *n*-hexane compared to experimental data.

4.5.2. Fitting the prediction of Sanchez-Lacombe EOS to the solubility of ethylene and *n*-hexane in the ternary system of ethylene-*n*-hexane-LLDPE

As was demonstrated above, model predictions are very sensitive to the *n*-hexane-LLDPE binary interaction parameter, k_{23}, but not at all to the value of the ethylene-LLDPE binary interaction parameter, k_{13}. We therefore propose to use k_{23} as an adjustable parameter in order to fit the prediction of the ternary Sanchez-Lacombe model to the experimentally obtained solubility of ethylene and *n*-hexane in LLDPE, while keeping k_{13} constant at the value estimated for the binary system.

It is important to note once again that having an accurate estimation of solubility of both ethylene and *n*-hexane in the ternary system of ethylene-*n*-hexane-LLDPE is crucial in order to have an accurate estimation of ethylene concentration in the amorphous phase of polyethylene. This is because while the solubility of ethylene provide us with the mass (or number of moles) of ethylene sorbed in the amorphous phase of polyethylene, it is the solubility of *n*-hexane that controls the extent of swelling and consequently the volume of amorphous phase.

Similar to fitting the binary SL model to the experimental data, it has been attempted to fit the ternary SL model to the experimentally obtained solubility data of both ethylene and *n*-hexane. This was done at each equilibrium temperature by minimizing the following objective function (*O.F.*) for solubility values of ethylene and *n*-hexane, through adjustment of *n*-hexane-LLDPE binary interaction parameter, k_{23}, as previously explained.

$$O.F. = \frac{1}{N}\sum_{i=1}^{N}\left(\frac{S_{calc_i} - S_{exp_i}}{S_{exp_i}}\right)^2 \qquad (4.19)$$

in which S_{calc} and S_{exp} are the solubility values calculated from ternary Sanchez-Lacombe model and experimental solubility values extracted, respectively. N is the number of solubility data points at each temperature.

However, the objective functions defined for ethylene and *n*-hexane are not minimized at the same value for binary interaction parameter of k_{23}. As a result, another criterion is required to be defined in order to determine the binary interaction parameter of k_{23} at each measurement equilibrium temperature which leads to an "optimized" estimation of both ethylene and *n*-hexane solubility and consequently the ethylene concentration in the amorphous phase of PE by the ternary SL model.

This "optimized" simultaneous fitting of the ternary SL model to the experimentally obtained solubility values of ethylene and *n*-hexane is achieved by adjusting the *n*-hexane-LLDPE binary interaction parameter, k_{23}, in a manner that it minimizes the objective function (*O.F.*) for *n*-hexane as defined in equation (4.19), while keeping the maximum error in estimation of ethylene solubility for all of the solubility points at each equilibrium temperature below 15%, in other words $Max \left|\frac{S_{calc_i} - S_{exp_i}}{S_{exp_i}}\right| \times 100 < 15\%$.

In order to meet the criterion defined to have the "optimized" fitting of the ternary SL model to the experimental data and as a result, more accurate estimation of ethylene concentration in the amorphous phase of PE, the *n*-hexane-LLDPE binary interaction parameter, k_{23}, is needed to be adjusted from 0.010 to 0.034 at 70 °C, from 0.020 to 0.030 at 80 °C, and from 0.038 to 0.046 at 90 °C. According to the better predictive capability of ternary Sanchez-Lacombe model at higher equilibrium temperatures which has been observed in the previous section, it is not surprising to find that the magnitude of required adjustment in the *n*-hexane-LLDPE binary interaction parameter, k_{23}, in order to meet the defined criterion decreases by increasing the equilibrium temperature.

Figure 4.21, Figure 4.22, and Figure 4.23 demonstrate the "optimized" fitting of the ternary Sanchez-Lacombe model to the experimentally obtained solubility values of ethylene and *n*-hexane in the ternary system of ethylene-*n*-hexane-LLDPE at 70, 80, and 90 °C, respectively with the corresponding adjusted *n*-hexane-LLDPE binary interaction parameter, k_{23}, at each measurement equilibrium temperature.

The average of absolute deviation percentage of the ternary SL model prediction from experimental data i.e. $\left|\frac{S_{calc} - S_{exp}}{S_{exp}}\right| \times 100$ is calculated to be 6.5%, 4.4%, and 3.2% for ethylene and 30.5%, 8.5%, and 15.6% for *n*-hexane at each measurement equilibrium temperature of 70, 80, and 90 °C, respectively. This in turn indicates that except for lowest measurement equilibrium temperature of 70 °C in which the prediction of ternary SL model for *n*-hexane deviates considerably from the experimental values, the proposed method for "optimized" simultaneous fitting of the ternary SL model to the experimentally obtained solubility values of both ethylene and *n*-hexane provides an acceptable estimation for solubility of both solutes in polymer at equilibrium temperatures of 80 and 90 °C. As highlighted earlier, the ternary Sanchez-

Lacombe model implementing the adjusted binary interaction parameter of k_{23} to provide optimized fitting of model to the available equilibrium solubility data of ethylene and *n*-hexane in LLDPE in the ternary system of ethylene-*n*-hexane-LLDPE will be used in order to estimate the effect of *n*-hexane on the magnitude of enhancement of ethylene concentration in the amorphous phase of polymer surrounding the catalyst active sites and consequently the rate of ethylene polymerization. This will be eventually compared with the observed effect of *n*-hexane on the rate of gas phase ethylene polymerization on supported catalyst performed with stirred-bed gas phase reactor, in the next chapter.

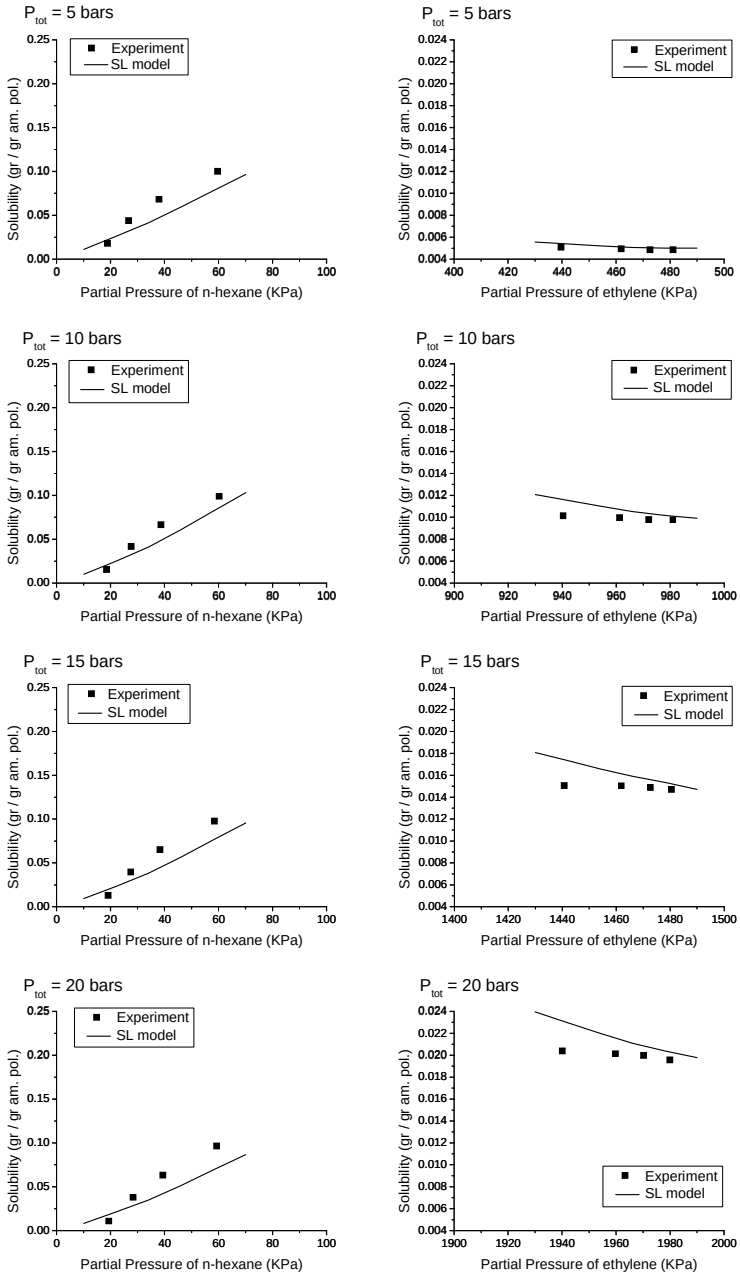

Figure 4.21. The solubility of *n*-hexane and ethylene in LLDPE in the ternary system of ethylene-*n*-hexane-LLDPE at 70 °C with P_{tot} = *5, 10, 15, and 20* bars and its comparison with the prediction of the ternary Sanchez-Lacombe model with the corresponding binary interaction parameters of k_{12} = *0.00*, k_{13} = *-0.014*, and adjusted k_{23} = *0.034* at 70 °C.

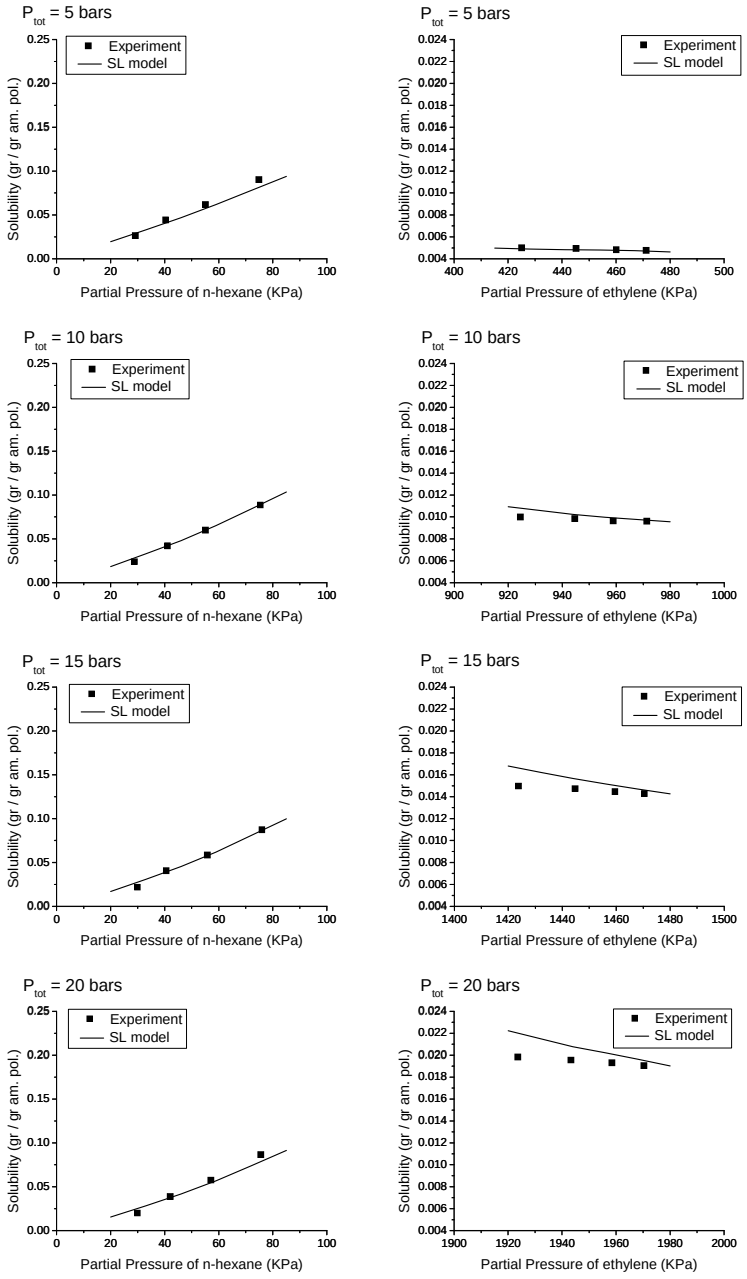

Figure 4.22. The solubility of *n*-hexane and ethylene in LLDPE in the ternary system of ethylene-*n*-hexane-LLDPE at 80 °C with P_{tot} = *5, 10, 15, and 20* bars and its comparison with the prediction of the ternary Sanchez-Lacombe model with the corresponding binary interaction parameters of k_{12} = *0.00*, k_{13} = *-0.022*, and adjusted k_{23} = *0.030* at 80 °C.

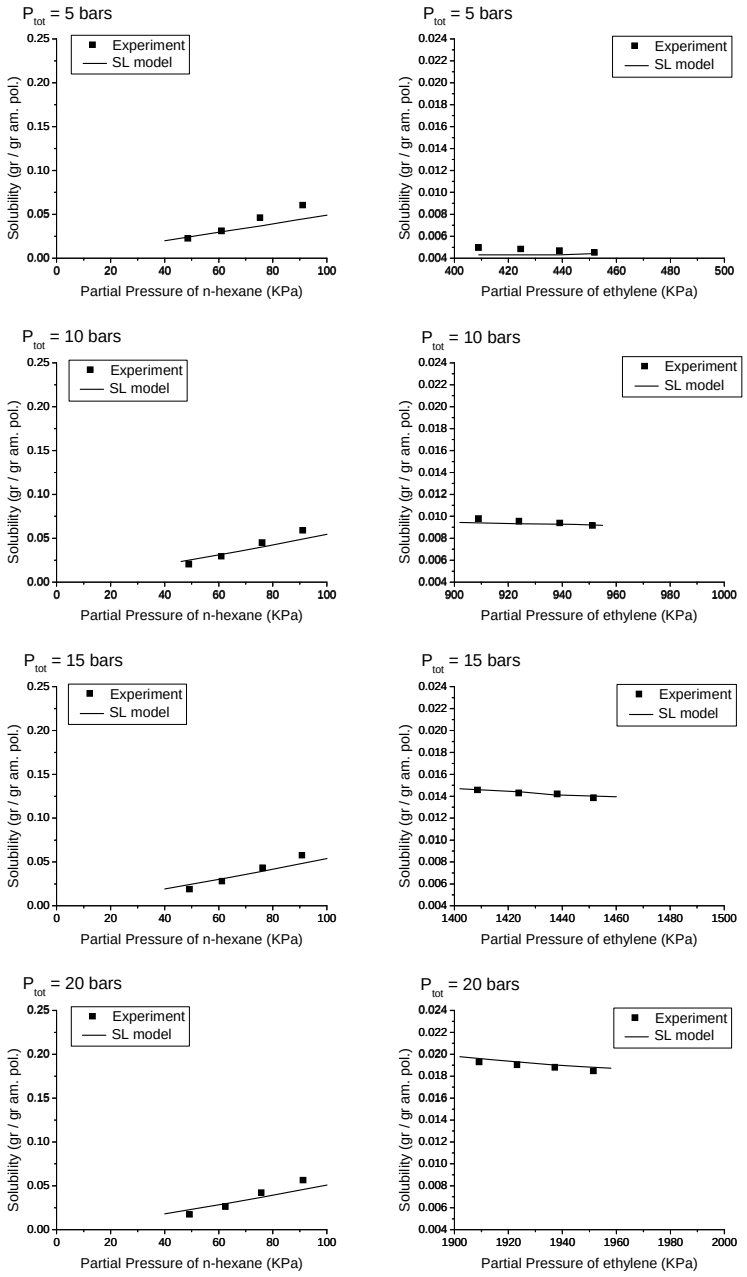

Figure 4.23. The solubility of *n*-hexane and ethylene in LLDPE in the ternary system of ethylene-*n*-hexane-LLDPE at 90 °C with P_{tot} = *5, 10, 15, and 20* bars and its comparison with the prediction of the ternary Sanchez-Lacombe model with the corresponding binary interaction parameters of k_{12} = *0.00*, k_{13} = *-0.032*, and adjusted k_{23} = *0.046* at 90 °C.

4.6. Conclusion

The Sanchez-Lacombe EOS, one of the most commonly used thermodynamic models in the polymer field, was used to predict the solubility of ethylene, of *n*-hexane and of mixtures of the two in LLDPE.

In an initial step, we looked at the capability of Sanchez-Lacombe EOS to describe the solubility of gaseous ethylene and *n*-hexane in polyethylene in binary solute-polymer systems through adjustment of the binary interaction parameter of model, k_{ij}. It is found that while the binary SL model can predict and describe the temperature and pressure dependency of ethylene in PE in an excellent manner, the quality of best fitting of the binary SL model prediction to the available set of experimental solubility data of *n*-hexane was less satisfactory.

Moving on to the ternary system and using a set of parametric studies, it is found that the ternary SL model predicts that the solubility of ethylene in PE, volume of amorphous phase of PE, and more importantly the concentration of ethylene in the amorphous phase of PE increase by increasing the partial pressure of *n*-hexane in the created ternary system of ethylene-*n*-hexane-PE. However, since the concentration of ethylene in the amorphous phase of polymer is proportional to the ratio of solubility of ethylene to volume of amorphous phase of PE, the extent of predicted enhancement in the ethylene concentration is much lower than the one for ethylene solubility.

In addition, parametric studies revealed that according to the predictions of ternary Sanchez-Lacombe model and in the lower limit of normalized partial pressure of *n*-hexane up to about $P^{norm.} = 0.5$, the "level of enhancement" predicted for ethylene solubility in the amorphous polyethylene, volume of amorphous phase, and concentration of ethylene in the amorphous polyethylene due to presence of *n*-hexane is independent of partial pressure of ethylene and also the temperature at which the ternary system is in equilibrium.

More importantly, the parametric study also showed that in the ternary system of ethylene-*n*-hexane-LLDPE, while the ethylene solubility is very sensitive to the *n*-hexane-LLDPE binary interaction parameter, k_{23}, the *n*-hexane solubility shows much less (almost negligible) sensitivity to the ethylene-LLDPE binary interaction parameter, k_{13}. As a result, the binary interaction of *n*-hexane-LLDPE, k_{23}, can be used as the adjustable parameter in order to obtain the best fitting of the ternary Sanchez-Lacombe model prediction to the experimental solubility values of both ethylene and *n*-hexane in the ternary system of ethylene-*n*-hexane-PE which will lead to the most accurate estimation of ethylene concentration in the amorphous phase of PE using SL model.

Following the set of parametric studies, the predictive capability of the ternary Sanchez-Lacombe EOS in describing the solubility of solutes in the ternary system from their available solubility data in the corresponding binary system was evaluated. It was shown that the prediction of the ternary Sanchez-Lacombe model overestimates the solubility of both ethylene and *n*-hexane in comparison with the experimentally obtained solubility data in the ternary system of ethylene-*n*-hexane-LLDPE if the binary interaction parameters obtained from binary solubility data were used directly in the ternary model. A method was therefore proposed to have better fitting of the Sanchez-Lacombe EOS to the experimental data through adjustment of the *n*-hexane-LLDPE binary interaction parameter, k_{23}. A comparison of the predicted and measured solubilities revealed that the proposed method allows us to obtain reasonable values.

The results from this chapter show that the optimized fitting of the SL model to the experimental data of both ethylene and *n*-hexane solubility in LLDPE simultaneously can be extremely important, as it will lead to a more accurate estimation of ethylene concentration in the amorphous phase of LLDPE using SL EOS. As highlighted earlier, the concentration of ethylene in the amorphous phase of polyethylene (not the solubility) controls the rate of gas phase ethylene polymerization on the supported catalyst. Using the available set of equilibrium solubility data for ethylene and *n*-hexane in LLDPE in ternary system, the performance of Sanchez-Lacombe EOS in prediction of enhancement in the ethylene concentration in the amorphous phase of polyethylene in presence of *n*-hexane and as a result the rate of polymerization will be eventually evaluated under reactive condition, for the first time in this field, against the set of heterogeneous ethylene polymerization experiments performed using stirred-bed gas phase reactor which will be presented in the following chapter.

4.7. References

1. Yao, W.; Hu, X.; Yang, Y. Modeling solubility of gases in semicrystalline polyethylene. *J. Appl. Polym. Sci.* **2007,** *103* (3), 1737-1744.

2. Yao, W.; Hu, X.; Yang, Y. Modeling the solubility of ternary mixtures of ethylene, iso-pentane, n-hexane in semicrystalline polyethylene. *J. Appl. Polym. Sci.* **2007,** *104* (6), 3654-3662.

3. Kanellopoulos, V.; Mouratides, D.; Pladis, P.; Kiparissides, C. Prediction of Solubility of Olefins in Polyolefins Using a Combined Equation of State Molecular Dynamics Approach. *Ind. Eng. Chem. Res.* **2006,** *45* (17), 5870-5878.

4. Sanchez, I. C.; Lacombe, R. H. An elementary molecular theory of classical fluids. Pure fluids. *J. Phys. Chem.* **1976,** *80* (21), 2352-2362.

5. Grolier, J.-P. E.; Boyer, S. A. E. Gas-Polymer Interactions: Key Thermodynamic Data and Thermophysical Properties. In *Polymer Thermodynamics*, Enders, S., Wolf, B. A., Eds.; Springer: Germany, **2011**; p 137.

6. Rogers, C. E.; Stannett, V.; Szwarc, M. The Sorption of Organic Vapors by Polyethylene. *J. Phys. Chem.* **1959,** *63* (9), 1406-1413.

7. Michaels, A. S.; Bixler, H. J. Solubility of gases in polyethylene. *J. Polym. Sci.* **1961,** *50* (154), 393-412.

8. Floyd, S.; Choi, K. Y.; Taylor, T. W.; Ray, W. H. Polymerization of olefins through heterogeneous catalysis. III. Polymer particle modelling with an analysis of intraparticle heat and mass transfer effects. *J. Appl. Polym. Sci.* **1986,** *32* (1), 2935-2960.

9. Moore, S. J.; Wanke, S. E. Solubility of ethylene, 1-butene and 1-hexene in polyethylenes. *Chemical Engineering Science* **2001,** *56* (13), 4121-4129.

10. Kiparissides, C.; Dimos, V.; Boultouka, T.; Anastasiadis, A.; Chasiotis, A. Experimental and theoretical investigation of solubility and diffusion of ethylene in semicrystalline PE at elevated pressures and temperatures. *J. Appl. Polym. Sci.* **2003,** *87* (6), 953-966.

11. Bashir, M. A.; Al-haj Ali, M.; Kanellopoulos, V.; Seppala, J. Modelling of multicomponent olefins solubility in polyolefins using Sanchez-Lacombe equation of state. *Fluid Phase Equilibria* **2013,** *358* (0), 83-90.

12. Laugier, S.; Richon, D. High-Pressure Vapor-Liquid Equilibria for Ethylene + 4-Methyl-1-pentene and 1-Butene + 1-Hexene. *J. Chem. Eng. Data* **1996,** *41* (2), 282-284.

13. Novak, A.; Bobak, M.; Kosek, J.; Banaszak, B. J.; Lo, D.; Widya, T.; Harmon Ray, W.; de Pablo, J. J. Ethylene and 1-hexene sorption in LLDPE under typical gas-phase reactor conditions: Experiments. *J. Appl. Polym. Sci.* **2006,** *100* (2), 1124-1136.

Chapter 5

Modeling effect of *n*-hexane as ICA on the gas phase ethylene polymerization on supported catalyst

Part of this chapter is published as:

Namkajorn, M.; Alizadeh, A.; Somsook, E.; McKenna, T. F. L. Condensed-Mode Cooling for Ethylene Polymerization: The Influence of Inert Condensing Agent on the Polymerization Rate. *Macromol. Chem. Phys.* **2014,** *215* (9), 873-878.

5. Modeling effect of *n*-hexane as ICA on the gas phase ethylene polymerization on supported catalyst

In the previous chapter, we looked at the thermodynamics of sorption in binary systems (ethylene-PE and *n*-hexane-PE) and ternary systems (ethylene-*n*-hexane-PE) of interest representative of the condensed mode of operation of gas phase ethylene polymerizations, at equilibrium and under non-reactive conditions. In addition, the Sanchez-Lacombe EOS was used in order to describe experimental solubility data from the literature in binary and ternary systems through adjustment of the binary interaction parameters between components (*i*) and (*j*), k_{ij}. It was found that the model parameters obtained in this manner allowed us to predict the solubility values in the available set of experimental data. Furthermore, it was found that the ternary Sanchez-Lacombe model could also be used to predict the increase in the concentration of ethylene in the amorphous phase of PE as a function of the partial pressure of *n*-hexane in the gas phase composition.

In the current chapter we will present an experimental study to quantify the effect of presence of *n*-hexane in the gas phase composition during the gas phase ethylene polymerization on the supported catalyst. The experimental study will then be followed by a comprehensive modeling analysis, in order to enhance our understanding and ultimately being able to predict the experimentally observed trends for the polymerization rate in presence of *n*-hexane.

5.1. Experimental section

5.1.1. Materials

Ethylene with a minimum purity of 99.5% was obtained from Air Liquide (Paris, France) and was passed over purifying columns of zeolite and active carbon before use. Argon with a minimum purity of 99.5% (used to keep the reaction environment free of oxygen and other impurities) was obtained from Air Liquide and used as received. Triethylaluminium (TEA) co-catalyst was obtained from Witco (Germany). An in-house Zeigler-Natta catalyst ($TiCl_4$ supported on $MgCl_2$) was used as the catalytic system for the series of gas phase polymerizations in the current study. This catalyst was synthesized using a procedure developed in our laboratories and published elsewhere.[1] NaCl with a range of particle size between 250 and 500 µm was obtained from Laurylab (France) and used as seedbed to disperse the catalyst particles. The salt was dried under vacuum four times, each time for 4 hours at 400 °C before use in order to eliminate all traces of water.

5.1.2. Experimental set-up and procedure

The experimental set-up used in this study is demonstrated schematically in Figure 5.1. It consisted of a 2.5 litre spherical stirred-bed gas phase reactor heated by circulating water in a jacket covering the external surface of the reactor. A pressure regulator controlled the pressure of ethylene in the reactor. The gas phase reactor was conditioned at 80 °C for at least 1 hour by 5 cycles of vacuum and consequent introduction of argon to the reactor. This was followed by introduction of 1 cm^3 of 1M solution of TEA in heptane into the reactor for scavenging all the remaining traces of water while also acting as the co-catalyst. The catalyst was introduced into the reactor with a catalyst injection cartridge having an inner volume of 100 cm^3. The cartridge was filled with the catalyst diluted in the dried NaCl, and was pressurized with 10 bars of hydrogen as an agent to control the molecular weight of produced polymer chains and optionally chosen to push all the catalyst/salt mixture into the reaction environment. Finally, the reaction was started by feeding the ethylene gas to the reactor while maintaining its pressure at the desired level of 7 or 12 bars during the polymerization reaction for 2 hours at the reaction temperature of 80 °C. It must be mentioned that in all of the polymerization reactions, in addition to ethylene, 1 bar of argon as the inert and less than 0.4 bar of hydrogen (estimated from relative volume of reactor and catalyst injection cartridge) were present in the reaction environment. In order to stop the reaction, the reactor was degassed from ethylene while being cooled down by circulation of cold water in the external jacket.

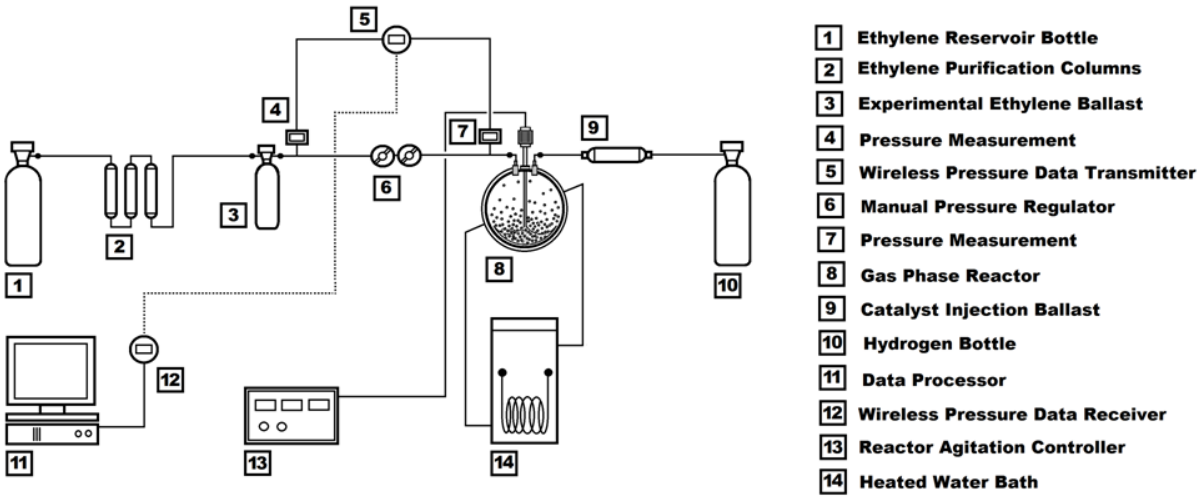

Figure 5.1. Schematic representation of the experimental set-up used to study gas phase ethylene polymerization on supported catalyst.

In order to study the effect of *n*-hexane as ICA, after conditioning the reactor, first, at room temperature of 25 °C, a specific amount of liquid *n*-hexane was injected to bed. Then the reactor temperature was

raised to 80 °C assuring all *n*-hexane inside the reactor was vaporized. This was followed by catalyst injection and ethylene introduction, respectively.

5.1.3. Experimental results

Figure 5.2 demonstrates the effect of presence of *n*-hexane in the gas phase composition having partial pressure of 0.0 bar (R_{p1}), 0.3 bar (R_{p2}), 0.6 bar (R_{p3}), and 0.8 bar (R_{p4}) on the instantaneous rate of ethylene polymerization at 80 °C using supported catalyst with partial pressure of ethylene in the reactor environment, equal to (a)7 and (b)12 bars. Each polymerization reaction with 0.0, 0.3, 0.6, and 0.8 bar of *n*-hexane partial pressure was repeated at least three times. These levels of *n*-hexane were chosen based on the range of quantities typically used in condensed mode operation. As can be seen in this figure, the instantaneous rate of ethylene polymerization increases in the presence of *n*-hexane, thus supporting the initial speculation of the effect of *n*-hexane on the enhancement of the ethylene solubility in polymer.

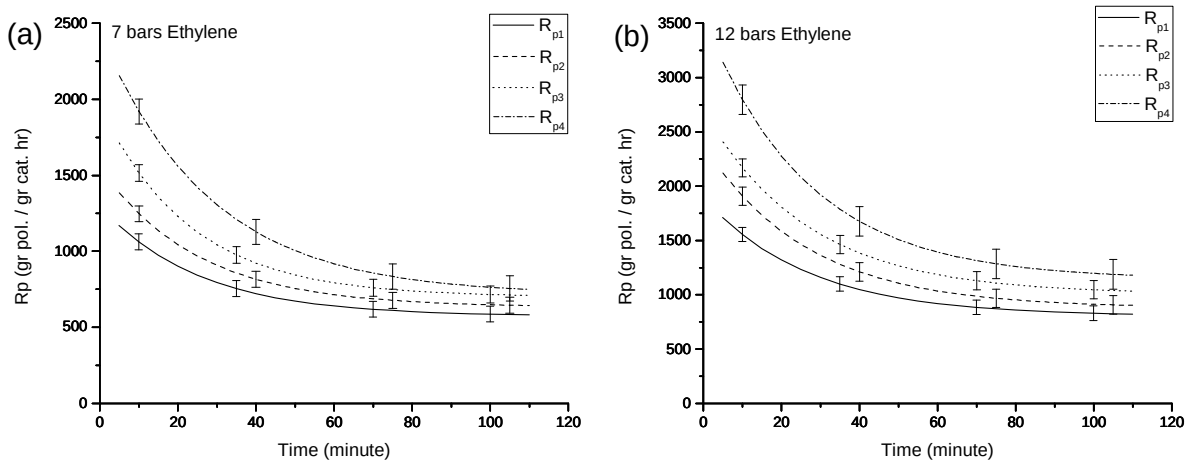

Figure 5.2. Instantaneous rate of ethylene polymerization at 80 °C in presence of 0.0, 0.3, 0.6, and 0.8 bar of partial pressure of *n*-hexane in the reaction environment corresponding to R_{p1}, R_{p2}, R_{p3}, and R_{p4} with partial pressure of ethylene in the reactor environment, equal to (a)7 and (b)12 bars.

In order to have a better picture and understanding, the averaged instantaneous rate of polymerization in the presence of *n*-hexane is normalized with the one without any *n*-hexane and presented in Figure 5.3. Consequently, this helps us to see that while the effect of *n*-hexane increases proportionally to its partial pressure in the gas phase composition, this effect is more pronounced at the initial steps during the course of polymerization.

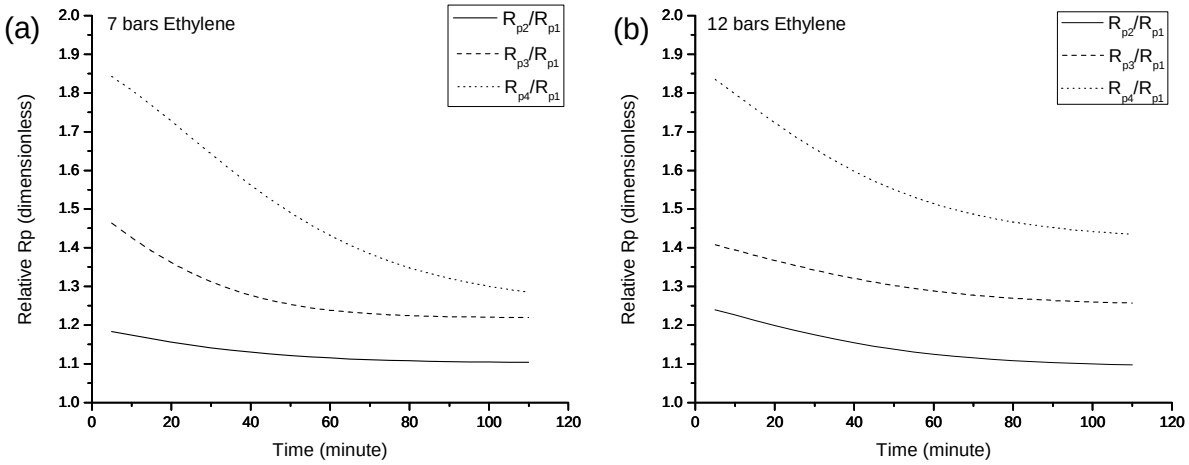

Figure 5.3. The averaged instantaneous rate of polymerization in presence of *n*-hexane normalized with the one without any *n*-hexane with partial pressure of ethylene in the reactor, equal to (a)7 and (b)12 bars.

In addition, by comparing Figure 5.3 (a) and (b) for the effect of partial pressure of ethylene on the observed "enhancement" of the instantaneous rate of ethylene polymerization on supported catalyst in presence of *n*-hexane, it can be concluded that while the magnitude of the acceleration of the instantaneous rate of polymerization in presence of *n*-hexane is almost the same during the initial steps of polymerization with both of the partial pressures of ethylene equal to 7 and 12 bars, this influence (clearly due to cosolubility effect of *n*-hexane) appears to fade out more rapidly as a function of time during the polymerization with 7 bars of ethylene partial pressure in comparison with the polymerization by 12 bars of reactant ethylene.

We have clearly shown here that the cosolubility effect of the heavier ICA (*n*-hexane) on the solubility, concentration, and consequently the rate of polymerization of lighter reactant ethylene can be quite significant. To the best of our knowledge this is the first time this effect has been quantified under reactive conditions in an academic study.

In the following section, we will present a more comprehensive description of the experimentally observed trends of the effect of *n*-hexane on the instantaneous rate of ethylene polymerization. This is achieved by providing a phenomenological description of the imposed change to the operational condition of the gas phase ethylene polymerization process on supported catalyst due to addition of *n*-hexane as ICA to the gas phase composition. Finally, the capability of the developed phenomenological modeling approach to describe and predict the effect of imposed change on the process condition of the polymerization reaction by addition of *n*-hexane will be evaluated against the effect of *n*-hexane on the instantaneous rate of ethylene polymerization which has been observed experimentally under the reactive conditions.

5.2. Polymer Flow Model (PFM)

Generally speaking, the local rate of ethylene polymerization inside a growing particle (Figure 5.4) is considered to be of first order with respect to the local ethylene concentration in the amorphous phase of polyethylene surrounding the active sites immobilized on the fragments of initial catalyst particle.

$$R_{pol.}^{loc.} = k_p C^* [M]_{amorph.pol.}^{loc.} \qquad (5.1)$$

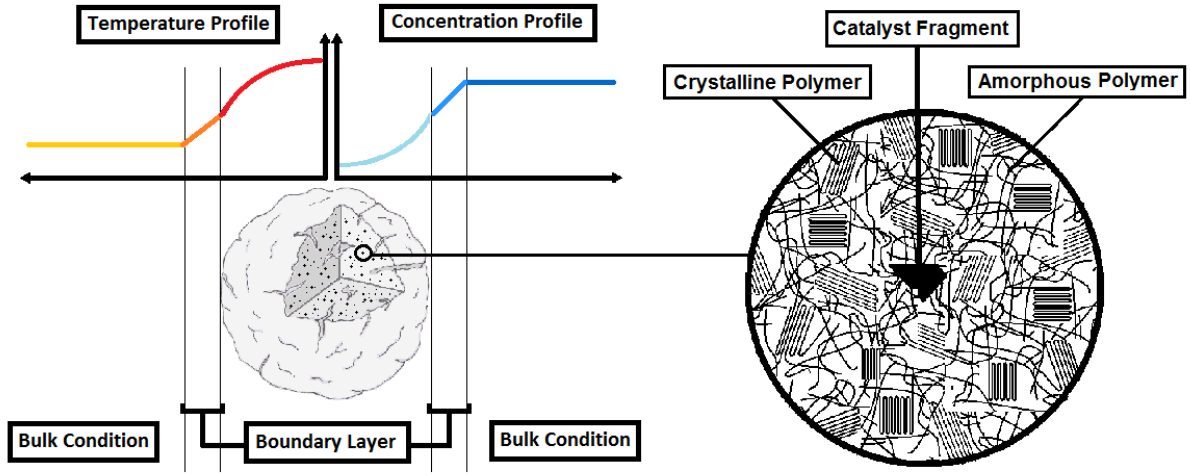

Figure 5.4. Schematic presentation of concept of local monomer concentration and local temperature inside a growing polymer particle.

While the local concentration of ethylene is primarily determined by the equilibrium of sorption of monomer solutes from the gas phase to the polymer phase, it also depends on the effective (or overall) diffusivity of ethylene through the polymer particle as a measure indicating the rate of monomer supply for the polymerization reaction at the active sites. The effective monomer diffusivity through the particle would in turn depend on morphology of the polymer particle. For instance, this effective diffusivity is expected to be much larger in a porous polymer particle with large cracks compared to a non-porous compact polymer particle.

In addition to the local concentration of reactant at the active sites, the instantaneous rate of polymerization obviously will also depend on the chemistry and kinetic behavior of catalytic system being used. While the kinetic behavior of the catalytic system is primarily designed and established during the preparation step of the catalyst, the activity of the polymerization active sites immobilized on the catalyst fragments will depend on the local temperature through the particle. For instance, for a

conventional catalyst system of Ziegler-Natta, while the propagation rate constant, k_p, increases as a function of temperature, the concentration of active sites, C^*, would decrease.

As a result, in order to be able to predict the effect of change in the process condition (here, addition of *n*-hexane as ICA to the gas phase composition) on the quality and rate of gas phase ethylene polymerization utilizing a specific type of supported catalyst system, not only it is necessary to be able to describe the change in the solubility behaviour of ethylene in the polymer, but it is also necessary to consider the change in the effective diffusivity of ethylene through the growing particle and also local temperature at the polymerization active sites dispersed inside the particle.

In simple terms, the effect of changing the process operating condition from condition (*1*) to condition (*2*) on the instantaneous local rate of gas phase ethylene polymerization using a specific type of supported catalyst system, without affecting the chemical nature and functionality of polymerization active sites during this applied transition in the process condition can be described by

$$\frac{\left(R_{pol.}^{loc.}\right)_2}{\left(R_{pol.}^{loc.}\right)_1} = \frac{f\left(S_2, D_2, T_2^{loc.}\right)}{f\left(S_1, D_1, T_1^{loc.}\right)} \qquad (5.2)$$

in which $\left(R_{pol.}^{loc.}\right)_2$ and $\left(R_{pol.}^{loc.}\right)_1$ are the instantaneous local rate of ethylene polymerization in the process operating condition (*2*) and (*1*), respectively, while *S*, *D*, and $T^{loc.}$ representing the solubility of ethylene in polyethylene, the effective diffusivity of ethylene through the growing polymer particle, and the local temperature of the active site in the corresponding operating condition of the process, respectively.

f is a function which correlates the local rate of ethylene polymerization at each instant during the course of polymerization reaction to the solubility of ethylene, the effective diffusivity of ethylene, and the local temperature at the polymerization active sites for the gas phase ethylene polymerization process utilizing a specific type of heterogeneous catalytic system.This in turn highlights the importance of adapting a single particle model in this study in order to be able to define such a function (*f*) which could properly reflect the effect of parameters dependent on the process condition i.e. *S*, *D*, and *T* on the instantaneous rate of gas phase ethylene polymerization in a growing polymer particle in a fluidized bed reactor.

In Chapter 2, a brief overview of different classes of single particle models developed for processes of polyolefin's production using heterogeneous catalyst was presented. In the current study, the Polymer Flow Model (PFM) has been adapted and used to serve for the aforementioned purpose. While relatively simplistic, the polymer flow model framework is the easiest to adapt for single particle models in this

field and will be presented in detail in the following section. For further discussions about the available single particle models developed in this field with their associated functionalities, advantages, and limitations, the reader is referred to the bibliography chapter and other references available in the literature.

In order to be able to provide a better description of Polymer Flow Model (PFM) and the assumptions made implicitly during its development, it would be helpful to take a brief closer look on the evolution of a real catalyst/polymer particle during its residence time inside the reactor, i.e. from introduction of fresh catalyst (or prepolymer) to the reaction environment to its withdrawal from the reactor as a fully grown particle, as provided in Figure 5.5. As discussed earlier, in this type of polymerization, the catalytic sites are deposited inside the pores of a highly porous mineral solid. The particles are injected into the reactor, where ethylene rapidly polymerizes in the pores. The stress created by this initial polymerisation causes the initial structure of the support to fragment and the particle is transformed into a polymer particle where the semi-crystalline polyethylene forms the continuous phase with the fragments of the support dispersed therein. The reaction continuous as monomer diffuses into the pores of the particle, sorbs in the polymer layer covering the active sites, and then diffuses once more toward the active centres where it reacts. The continuous formation of polymer causes the particle to expand as the reaction proceeds. Without intending to go into further detail, it can be seen that in reality, a growing polymer particle at each moment after start of polymerization reaction can be considered to be constituted of at least three distinguished phases of catalyst fragments, produced polymer, and pores. The polymer phase, in turn, is composed of amorphous and crystalline phases.

In the PFM model, the process of fragmentation of initial catalyst particle is considered to take place and be completed immediately after its exposure to the reaction environment. In addition, the growing polymer particle at each instant during the course of polymerization is assumed to constitute a spherical pseudo-homogeneous medium, through which the polymerization active sites are dispersed uniformly.

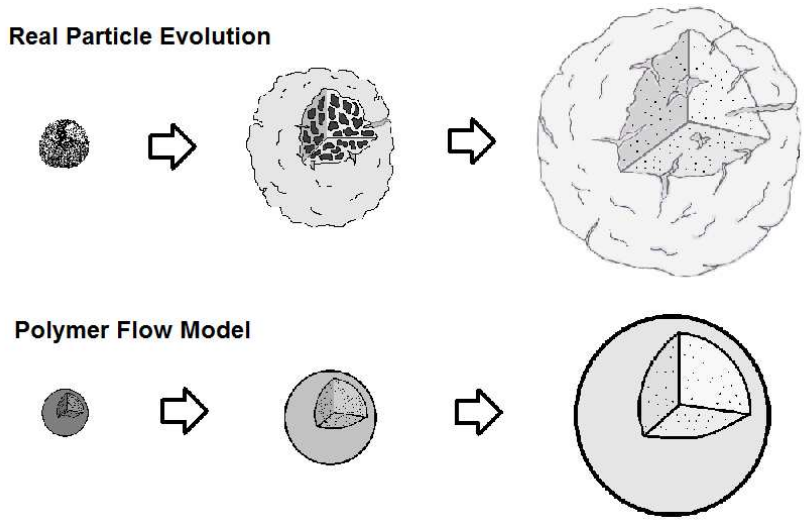

Figure 5.5. Comparative schematic representation of morphological evolution of a real catalyst/polymer particle during gas phase ethylene polymerization on supported catalyst with the one assumed by PFM.

In order to describe the polymer particle growth during gas phase ethylene polymerization in presence of *n*-hexane as an ICA by PFM model, the two sets of mass balance equations for reactant ethylene and *n*-hexane need to be solved simultaneously along with an energy balance equation for the growing polymer particle. The balances with the corresponding boundary and initial conditions in the spherical coordinates are provided below:

5.2.1. Mass and energy balance equations

5.2.1.1. Mass balance equation for ethylene as the reactant

$$\frac{\partial [M]_{ov.1}}{\partial t} = \frac{1}{r_l^2}\frac{\partial}{\partial r_l}\left(D_{ov.1} r_l^2 \frac{\partial [M]_{ov.1}}{\partial r_l}\right) - R_v \qquad (5.3)$$

Boundary conditions

$$[M]_{ov.1} = [M]_{ov.eq.1} \quad @ \quad r_l = R_l \qquad (5.4)$$

$$\frac{\partial [M]_{ov.1}}{\partial r_l} = 0 \qquad @ \quad r_l = 0 \qquad (5.5)$$

Initial condition

$$[M]_{ov.1} = 0 \qquad @ \quad t = 0 \quad and \quad 0 \le r_l \le R_l \qquad (5.6)$$

where $[M]_{ov.1}$ is overall ethylene concentration through the particle, $[M]_{ov.eq.1}$ is the overall equilibrium concentration of ethylene in the particle, $D_{ov.1}$ is the overall ethylene diffusivity through the particle, and R_v is the volumetric rate of ethylene monomer consumption.

In all of the balance equations, t represents the time, r_l is radial position in the pseudo-homogeneous polymer particle and R_l is the radius of the pseudo-homogeneous polymer particle at each time step during its growth.

$[M]_{ov.eq.1}$ is calculated by the following equation

$$[M]_{ov.eq.1} = [M]_{eq.1}(1-\epsilon) \qquad (5.7)$$

$[M]_{eq.1}$ is the equilibrium concentration of ethylene in the total volume of polymer phase being constituted of amorphous and crystalline phases, while $[M]_{ov.eq.1}$ is the overall equilibrium concentration of ethylene in whole pseudo-homogenous particle considering its porosity, ϵ.

By considering the first boundary condition, the resistance to mass transfer through the boundary layer of the growing polymer particle is implicitly assumed to be negligible. This is found to be valid for catalyst systems having low to medium activity (as is the case in our study) with particles being fluidized in circumstances close to the ideal mixing in typical fluidized bed or stirred bed reactors.[2]

The volumetric rate of ethylene polymerization, R_v, is calculated by

$$R_v = R_{pol}\left(\frac{(1-\epsilon)}{\phi^3}\right) \qquad (5.8)$$

in which, ϵ, is the particle porosity and ϕ is the overall growth factor defined as

$$\phi = \frac{R_p}{r_{cat}} \qquad (5.9)$$

with R_p representing the equivalent radius of "polymer-only" particle at each time step without considering the existing particle porosity. r_{cat} is the radius of initial catalyst particle.

R_{pol} is the local rate of ethylene polymerization at the surface of catalyst fragment

$$R_{pol} = k_p C^* [M]_{ov.1} \qquad (5.10)$$

with k_p representing the propagation constant at the local particle temperature and C^* being the local concentration of polymerization active sites.

The temperature dependency of the propagation constant is described here by Arrhenius-type of correlation

$$k_p = k_{p,ref} e^{-\frac{E_a}{R_g}\left(\frac{1}{T}-\frac{1}{T_{ref}}\right)} \quad (5.11)$$

in which $k_{p,ref}$ is the propagation constant at the reference temperature, T_{ref}. E_a is the activation energy for propagation and R_g is the universal gas constant. T represents the local temperature of active site in the polymer particle.

The deactivation of catalyst active sites during the course of polymerization is considered in the model by

$$C^* = C_1^* e^{-k_d t} + C_2^* \quad (5.12)$$

where C_1^* and C_2^* are the constants determining the concentration of actives sites at the beginning of the reaction and asymptotic value of the concentration of the polymerization sites which remain active by time, respectively. k_d is the deactivation constant which determines the rate of deactivation of catalyst active sites and its temperature dependency is also described by Arrhenius-type of correlation

$$k_d = k_{d,ref} e^{-\frac{E_d}{R_g}\left(\frac{1}{T}-\frac{1}{T_{ref}}\right)} \quad (5.13)$$

in which $k_{d,ref}$ is the deactivation constant at the reference temperature, T_{ref}. E_d is the activation energy for the catalyst deactivation.

k_p, C_1^*, C_2^*, and k_d are the characteristic parameters determining the intrinsic activity and evolution of the kinetic behavior of active sites by time for specific catalyst system being studied.

5.2.1.2. Mass balance equation for *n*-hexane as the inert condensing agent (ICA)

$$\frac{\partial [M]_{ov.2}}{\partial t} = \frac{1}{r_l^2}\frac{\partial}{\partial r_l}\left(D_{ov.2} r_l^2 \frac{\partial [M]_{ov.2}}{\partial r_l}\right) \quad (5.14)$$

Boundary conditions

$$[M]_{ov.2} = [M]_{ov.eq.2} \quad @ \quad r_l = R_l \quad (5.15)$$

$$\frac{\partial [M]_{ov.2}}{\partial r_l} = 0 \qquad @ \quad r_l = 0 \tag{5.16}$$

Initial condition

$$[M]_{ov.2} = 0 \qquad @ \quad t = 0 \quad and \quad 0 \le r_l \le R_l \tag{5.17}$$

where $[M]_{ov.2}$ is overall ICA concentration through the particle, $[M]_{ov.eq.2}$ is the overall equilibrium concentration of ICA in the particle, and $D_{ov.2}$ is the overall ICA diffusivity through the particle.

$[M]_{ov.eq.2}$ is calculated by the following equation

$$[M]_{ov.eq.2} = [M]_{eq.2}(1 - \epsilon) \tag{5.18}$$

$[M]_{eq.2}$ is the equilibrium concentration of the ICA in the total volume of polymer phase being constituted of amorphous and crystalline phases, while $[M]_{ov.eq.2}$ is the overall equilibrium concentration of the ICA in whole pseudo-homogenous particle considering its porosity, ϵ.

5.2.1.3. Energy balance equation

$$\frac{\partial T}{\partial t} = \alpha_{ov} \frac{1}{r_l^2} \frac{\partial}{\partial r_l} \left(r_l^2 \left(\frac{\partial T}{\partial r_l} \right) \right) + \left(\frac{-\Delta H_{\text{pol}}}{\rho_{ov} C_{p,pol}} \right) R_v \tag{5.19}$$

Boundary conditions

$$-k_{c,p} \frac{\partial T}{\partial r_l} \Big|_{R_l} = h\left(T \Big|_{R_l} - T_b\right) \quad @ \quad r_l = R_l \tag{5.20}$$

$$\frac{\partial T}{\partial r_l} = 0 \qquad @ \quad r_l = 0 \tag{5.21}$$

Initial condition

$$T = T_b \qquad @ \quad t = 0 \quad and \quad 0 \le r_l \le R_l \tag{5.22}$$

where T, α_{ov}, ΔH_{pol}, ρ_{ov}, and $C_{p,pol}$ representing the temperature, overall thermal diffusivity of the particle, enthalpy of ethylene polymerization, overall particle density, and heat capacity of polymer in the energy balance equation, while $k_{c,p}$, h, and T_b representing thermal conductivity of polymer, heat transfer coefficient, and reactor bulk temperature in the boundary and initial conditions.

The overall thermal diffusivity of the particle is given by

$$\alpha_{ov} = \frac{k_{c,p}}{\rho_{ov} C_{p,pol}} \quad (5.23)$$

and the overall particle density can be calculated from

$$\rho_{ov} = \rho_{pol}(1 - \epsilon) \quad (5.24)$$

with ρ_{pol} representing the polymer phase density.

The heat transfer coefficient, *h*, for the spherical polymer particle is calculated by Ranz-Marshall correlation given as

$$Nu = 2 + 0.6 Re^{1/2} Pr^{1/3} \quad (5.25)$$

in which

$$Nu = \frac{h d_p}{k_{c,g}} \quad (5.26)$$

$$Re = \frac{\rho_g u d_p}{\mu} \quad (5.27)$$

$$Pr = \frac{\mu C_{p,g}}{k_{c,g}} \quad (5.28)$$

with

$$d_p = 2R_l \quad (5.29)$$

In these correlations, Nu is Nusselt number, Re is Reynolds number, and Pr is Prandtl number. $k_{c,g}$, ρ_g, μ, $C_{p,g}$ represents thermal conductivity, density, viscosity, and heat capacity of gas phase and finally u is the superficial gas-particle velocity.

At this point it should be noted that the effect of heat of sorption of heavy ICA component is not included in the energy balance equation presented here. In the Appendix C, the energy balance equation including the heat of sorption of ICA is developed and presented. The simulation results of PFM model for the growing particle under appropriate fluidization with ideal mixing reveal that the effect of heat of sorption

during the normal condition of the polymerization process is negligible and can be safely neglected. However, we will nevertheless take a closer look on the potential effect of heat of sorption of heavy components like ICAs on the thermal behavior of an active growing particle during its temporary exposition to the defluidized regions inside the FBR with poor heat transfer in Chapter 6.

5.2.2. Numerical solution method for balance equations in PFM

In order to be able to calculate the local concentration of solutes and the local temperature inside the growing particle at each moment during the course of polymerization, the set of mass and energy balance equations provided in the previous section must be solved simultaneously. This in turn imposes a problem of dynamic mass and heat transfer in the spherical coordinate with moving boundary condition which needs to be solved by applying an appropriate numerical method.

The Nonstandard Finite Difference scheme (NSFD) is applied in the current study in order to solve the set of partial differential equations (PDE) obtained from mass and energy balances to calculate the evolution of solutes' concentration and temperature as a function of time and radial position inside a growing particle.

The concept of dynamic consistency constitutes the core underlying principle of this methodology. Letting a differential equation and/or its solutions have property *P*, the discretized form of equation is considered as dynamically consistent with the original differential equation, if it and/or its solutions also have property *P*. For many systems in engineering science, the dependent variables represent physical variables that cannot take negative values. For example, they may be concentration or absolute temperature. For such systems the property *P* is referred to "positivity". As a result, in the dynamically consistent schemes with positivity condition, the nonnegative initial and/or boundary data will evolve into nonnegative solutions at later times.

The main issue regarding the numerical solution for differential equations is the possibility of encountering numerical instabilities. Generally speaking, numerical instabilities are indicative of solutions to the discrete equations that do not correspond to any solution of the corresponding differential equation. One possible reason for this to occur is to have the finite difference scheme that does not satisfy some physical principal e.g. positivity on the solutions of PDEs. In simple words, if the solutions of the PDEs are restricted to have nonnegative values, numerical instabilities would exist if the finite difference method allows negative values as its solution for nonnegative initial and/or boundary condition.

As a result, the main purpose of Nonstandard Finite Difference (NSFD) method is to construct a "dynamically consistent" scheme in order to avoid such numerical instabilities. In this method, the finite difference scheme for the studied model must be "designed" in a manner that it meets the requirement to be dynamically consistent to avoid the instability problems. This in turn implies that each differential equation has to be treated as a unique mathematical structure and as a result, must be discretized in a unique manner in this method. For instance, if one is dealing with a system model in which the positivity condition is valid for the dependent variable (i.e. negative value for this variable is physically meaningless), the finite difference scheme should be designed in a way that preserves this condition.
A comprehensive presentation of this method is provided in Appendix B, where the applicability of Nonstandard Finite Difference scheme (NSFD) is extended for solving reaction-diffusion type of problem in spherical coordinates as the main interest of this project and the interested readers are referred to this appendix for further discussions about this methodology.

In summary, by implementing the Nonstandard Finite Difference method (NSFD), the partial differential equations obtained from mass and energy balances for a growing particle can be solved numerically at each time step during the course of polymerization. This methodology leads to explicit solution schemes for concentration and temperature by applying the positivity preserving condition while providing a functional relationship between the time-step sizes and space-step sizes which ensures the scheme to be numerically stable.

5.2.3. Computational steps of PFM

The details of computational steps of Polymer Flow Model (PFM) in order to describe the growth of polymer particle during the course of polymerization are provided in Appendix C. An overview of these computational steps is provided in the following section hereunder, while referring to Appendix C for the detailed related discussions about each of these computational steps.

In the notation used here, the superscript refers to time step while subscript refers to the number of the grid to which the physical property belongs to. For instance, T_i^j represents the temperature of *i*th grid at the *j*th time step.

5.2.3.1. Grid generation

At the beginning of each time step, *j*, including the beginning of the reaction at *t=0*, the particle is discretized into *N* radial shells having the same thickness as provided in Figure 5.6.

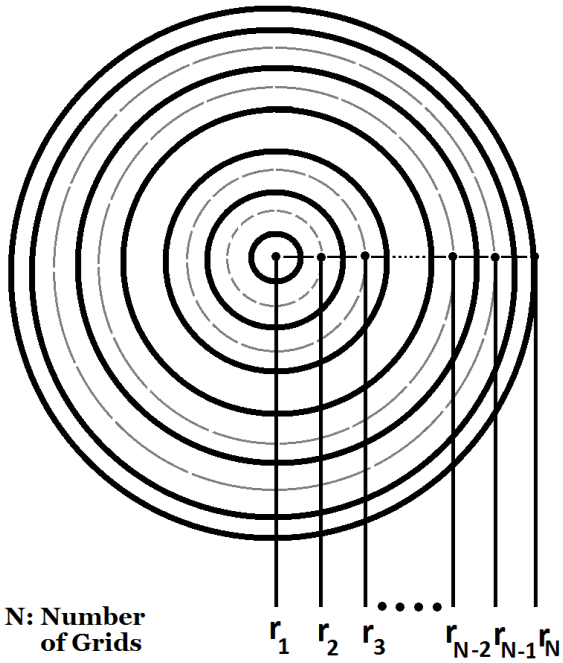

Figure 5.6. The discretization of normalized particle radius into *N* shells.

The radius of the particle is normalized at each time step, by dividing the particle radius at that time step, R_l^j, to itself. In other words

$$r_N = \frac{R_l^j}{R_l^j} = 1 \qquad (5.30)$$

This is followed by calculation of radial position and volume of each grid in the normalized particle. By assuming homogeneous distribution of polymerization active sites through the growing polymer particle and, consequently in the normalized particle at each moment, the volume of catalyst dispersed in each grid is calculated accordingly.

5.2.3.2. Grid growth

In order to calculate the solute concentration and temperature in each grid *i*, at each time step *j*, the two mass balance equations and the energy balance equation are transformed into their dimensionless forms and then discretized according to the Nonstandard Finite Difference scheme (NSFD). This in turn leads to explicit expressions to calculate the concentration of solutes and temperature of each grid *i*, at each time step *j*.

After calculation of ethylene concentration and temperature at each grid of *i* inside the normalized polymer particle at the time step *j* from their values at the previous time step *j-1*, it is now possible to calculate the mass of polymer produced at *i*th grid, the total mass of polymer produced in the particle and as a result the instantaneous rate of ethylene polymerization during the *j*th time interval. In this manner, the radius of particle at the end of *j*th time step or beginning of *j+1*th time step can be calculated while capturing the particle growth.

5.2.3.3. Grid update and normalization

After calculation of the particle radius at the end of time step *j*, R_l^{j+1}, the particle radius is normalized similar to the equation (5.30) as

$$r_N = \frac{R_l^{j+1}}{R_l^{j+1}} = 1 \qquad (5.31)$$

The normalized particle is discretized afterwards with the same method as previously explained.

In order to calculate the dimensionless concentration and temperature gradients in the normalized particle during the next time step of *j+1*, and consequently to be able to estimate the instantaneous polymerization rate and the mass and volume of the polymer produced during the next time interval, the dimensionless mass and energy balance equations are updated, accordingly.

After calculation of dimensionless concentration and temperature at each grid *i* and time step of *j+1*, the mass and volume of polymer produced during the next time interval and consequently the new particle radius is calculated as explained for the previous time step of *j*.

The computational loop for grid normalization, growth, and update is schematically demonstrated in Figure 5.7.

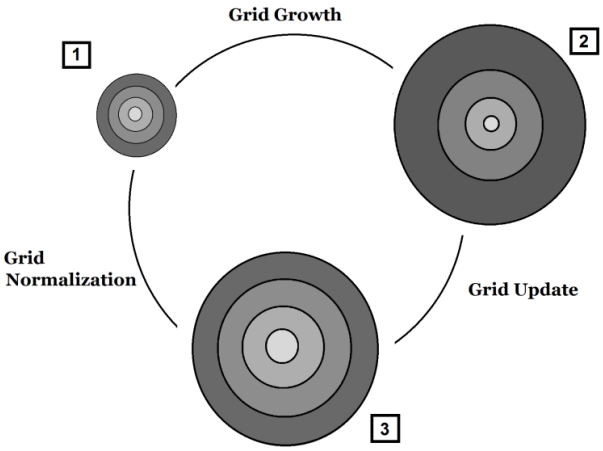

Figure 5.7. The schematic representation of computational loop for grid normalization, growth, and update.

The computational loop is repeated until the time reaches the residence time of the catalyst particle in the polymerization reaction environment, from the time of its exposure to the reactor until the time of its withdrawal from the reactor in the form of a fully grown polymer particle.

The standard procedure to determine the appropriate number of grids, *N*, required in order to provide the most accurate estimation of concentration and temperature gradients through the assumed spherical particle is as follows: in a series of simulations, the number of grids are needed to be increased while calculating the concentration and temperature gradients inside the particle. The number of grids of *N*, in which the values of the calculated concentration and temperature gradients differ negligibly compared to the values obtained by simulation with *N-1* grids, is chosen for the series of simulations. Because of lack of access to higher computational power than normal PC, the maximum number of grids that could be applied in our study was limited by the related required computational time as one simulation per day with number of grids *N=5*. The required computational time for the developed algorithm increased exponentially with the number of grids. As a result, the obtained concentration and temperature gradients with these series of simulations must be regarded as an approximation of real gradients. This issue can be obviously solved by utilizing a more powerful computational system which would allow implementing a higher number of grids with lower associated computational time.

5.2.4. Parameters of PFM: Estimation methods with associated assumptions

In this section, the methodologies used to estimate the parameters of Polymer Flow Model have been introduced and described. In addition, the assumptions which have been made explicitly or implicitly during the estimation of these model parameters have been elucidated while the accuracy and potential effect of these assumptions in the performance of PFM model being discussed.

5.2.4.1. Solubility

In the previous chapter, the Sanchez-Lacombe EOS was developed to describe the solubility of gaseous solutes in the polymer for binary systems of solute-polymer and ternary systems of solute(*1*)-solute(*2*)-polymer. The predictions of the Sanchez-Lacombe model are fitted to the available experimentally obtained solubility data of ethylene in the amorphous phase of LLDPE in the binary system of ethylene-LLDPE and solubility of ethylene and *n*-hexane in the amorphous phase of LLDPE in the ternary system of ethylene-*n*-hexane-LLDPE, by adjusting the binary interaction parameters (k_{ij}) of model.

By utilizing the fitted Sanchez-Lacombe model, it is then possible to estimate concentration of ethylene in the amorphous phase of polyethylene in the absence and presence of *n*-hexane in the gas phase composition in the corresponding binary and ternary systems, respectively, while the crystalline phase of polyethylene is considered to be impenetrable to the solute species.

In order to be able to apply the experimentally obtained solubility data and the Sanchez-Lacombe model developed for binary and ternary systems and fitted to describe these set of available solubility data, the following set of assumptions and considerations are needed to be taken into account:

- It has already been demonstrated phenomenologically and clarified that the local rate of polymerization inside a particle is determined by concentration of reactant ethylene in the amorphous phase of semi-crystalline polyethylene surrounding the active sites immobilized on the fragments of initial catalyst. However, the PFM considers the particle as a pseudo-homogeneous medium and as a result, at the first step, it is needed to transform the equilibrium concentration of ethylene in the amorphous phase of polymer into the equilibrium concentration of ethylene in entire polymer phase including the crystalline phase of polyethylene. The calculation steps in order to transform the equilibrium concentration of ethylene in the amorphous phase into the equilibrium concentration of ethylene in the total polymer volume including its crystalline phase in the binary and ternary systems, $[M]_{eq.1}$, are provided in the details in the Appendix A and skipped here for the sake of brevity.

At the next step and in order to calculate the overall equilibrium concentration of ethylene in the pseudo-homogeneous particle, $[M]_{ov.eq.1}$, which in reality it is constituted of polymer phase and pore phase (and negligible catalyst fragments dispersed within) with a porosity of ϵ, the equilibrium concentration of ethylene in polymer phase is transformed into overall equilibrium concentration of ethylene in the pseudo-homogeneous particle including its porosity according to the previously given equation of (5.7).

All the discussion made here in order to be able to estimate the overall equilibrium concentration of ethylene in the pseudo-homogenous polymer particle assumed in the Polymer Flow Model is also valid for the other solute of *n*-hexane as the inert condensing agent.

- The crystallinity of the produced HDPE polymer particle in all of the reaction conditions simulated is assumed to be constant, with the weight-based crystallinity equal to $\chi = \%60$. In other words, it is assumed that the effect of the presence of *n*-hexane in the gas phase composition on the crystallinity of produced HDPE is not significant and can be considered to be negligible for the purpose of this modeling study.

  In addition to the fact that the value chosen for the weight-base crystallinity of HDPE is in the range of typical degree of crystallinity for the industrial HDPE grade of polyethylenes, it also represents the measured value for the crystallinity of HDPE polymer particles with DSC analysis that have been obtained from the gas phase ethylene polymerizations presented above, in the absence of any *n*-hexane as the base case of our modeling analysis.

- As discussed earlier in Chapter 4, according to the provided crystallinity and density for the polymer sample on which the binary and ternary sorption measurements were performed by the group of Yang,[3,4] it was assumed that the polyethylene sample is LLDPE. Consequently, the experimentally obtained solubility of solutes of ethylene and *n*-hexane in the amorphous phase of polyethylene in the corresponding binary and ternary systems were described by Sanchez-Lacombe EOS utilizing the characteristic SL model parameters (T^*, P^*, and ρ^*) for LLDPE resulting in the acquired set of binary interaction parameters in order to have the best fitting of model prediction to the available experimental data.

  As a result, in all of the PFM simulations implementing the Sanchez-Lacombe model in order to describe the thermodynamics of sorption in the binary and ternary systems, it was assumed that the amorphous phase of HDPE polymer particles obtained in our set of polymerization experiments would exhibit thermodynamic behavior that is the same as that of the amorphous phase of LLDPE for which the model parameters have been estimated. In other words, the effect

of presence short chain branches due to the insertion of comonomer into the backbone of polymer chains is assumed to have a negligible effect on the solubility behavior of studied solutes in the amorphous phase of LLDPE (as the polymer for which the experimental solubility data is available) compared to HDPE with no short chain branches along its backbone structure (as the polymer being produced in our polymerization experiments).

- The effect of polymer crystalline phase[5,6] on the solubility of solutes in the amorphous phase, the extent of swelling of the amorphous phase, and consequently the ethylene concentration in the amorphous polymer phase is neglected. In fact, the crystalline phase is observed to play a more pronounced role at higher pressure of the solutes than one finds in a typical FBR gas phase process.[6] It is due to the fact that at the higher pressures, the crystalline phases dispersed in the polymer would start to act as physical crosslinks that limit the swelling of amorphous polymer phase and consequently the amount of sorbed solutes in it. However, under the conditions considered here the model retains its validity.

- In the solubility analysis, the role of other components present in the reaction environment i.e. argon and hydrogen are neglected. This is due to their low partial pressure and very low order of magnitude of solubility in polyethylene compared to ethylene.

Following the procedure explained above, the overall equilibrium concentration of reactant ethylene and inert *n*-hexane in the pseudo-homogeneous particle of PFM model is estimated by Sanchez-Lacombe EOS in the binary system of ethylene-PE and ternary system of ethylene-*n*-hexane-PE at the equilibrium temperature of 80 °C (as the polymerization reaction temperature) with the corresponding binary interaction parameters of model in order to provide the best fitting of model prediction to the experimentally obtained solubility data in the binary and ternary systems at this temperature, as provided in the previous chapter.

5.2.4.2. Diffusivity

Estimation of the overall (or effective) diffusivity coefficient that could describe the process of diffusion of reactant ethylene through pseudo-homogeneous particle assumed by PFM model is of crucial importance in predicting the significance of mass transfer resistance through a growing polymer during the course of its polymerization.

In reality, the diffusion of ethylene takes place concurrently through two different mechanisms in the growing polyethylene particle; in the first mechanism, ethylene diffuses through the macro-pores of

polymer particle. This diffusion in the gas phase continues through the network of available pores in the structure of the particle depending on its morphology at each instant during the course of polymerization. In the second mechanism, the ethylene has already been sorbed from the gas phase into the polymer phase and its diffusion takes place through the amorphous phase of polyethylene until it reaches the active sites immobilized on the surface of initial catalyst fragments where the polymerization reaction finally takes place. Knudsen diffusion, which takes place in very small pores on the order of tens of nanometers or less, is neglected in the current study. It is expected to make only a minor contribution to the overall diffusivity of pseudo-homogeneous particle after initial steps during the course of polymerization and by completion of fragmentation step which is assumed to take place instantaneously in PFM model.

By considering a random distribution of pore phase in the structure of polymer particle, and despite its obvious discrepancy with the morphology of most of the real polymer particles obtained experimentally from different industrial processes, Kanellopoulos et al. suggested[7] the following correlation in order to estimate the overall diffusivity of ethylene, $D_{ov.1}$, through the pseudo-homogeneous particle assumed by PFM model:

$$D_{ov.1} = \left(\frac{\epsilon}{\tau_f^2}\right) D_{1,g} + (1-\epsilon)(1+3\epsilon) D_{1,pol} \qquad (5.32)$$

in which $D_{1,g}$ and $D_{1,pol}$ are the diffusivity of ethylene in the bulk gas phase and polymer phase, respectively. ϵ, the porosity, and τ_f, the tortuosity factor represent the morphological aspects of the particle in this proposed model.

It must be mentioned that the first term on the right-hand side of equation (5.32) accounts for ethylene diffusion in the gas phase through pore phase of the particle while second term represents the ethylene diffusion through the polymer phase, as previously explained.

Since the diffusivity of ethylene in the bulk of gas phase is about 3-4 orders of magnitude higher than its diffusivity through the semi-crystalline polyethylene, according to equation (5.32) and as expected logically, one needs to have a reasonable estimation of the porosity and morphological aspects of polymer particle and their evolution as a function of the reaction time in order to be able to have a precise prediction about the overall diffusivity of any penetrants, and consequently of the significance of mass transfer resistance through the polymer particle.

The porosity of HDPE powder obtained from the set of gas phase ethylene polymerization experiments in the absence and presence of *n*-hexane was examined using the nitrogen adsorption porosimetry. The

results of this set of analysis reveal that the HDPE polymer particles produced both in the absence and presence of *n*-hexane have negligible porosity of less than 1%.

In order to validate the compact morphology of the HDPE particles having negligible porosity, a set of polymer particles were cut and SEM analysis was performed on the obtained cross-section area of the polymer particles as provided in Figure 5.8.

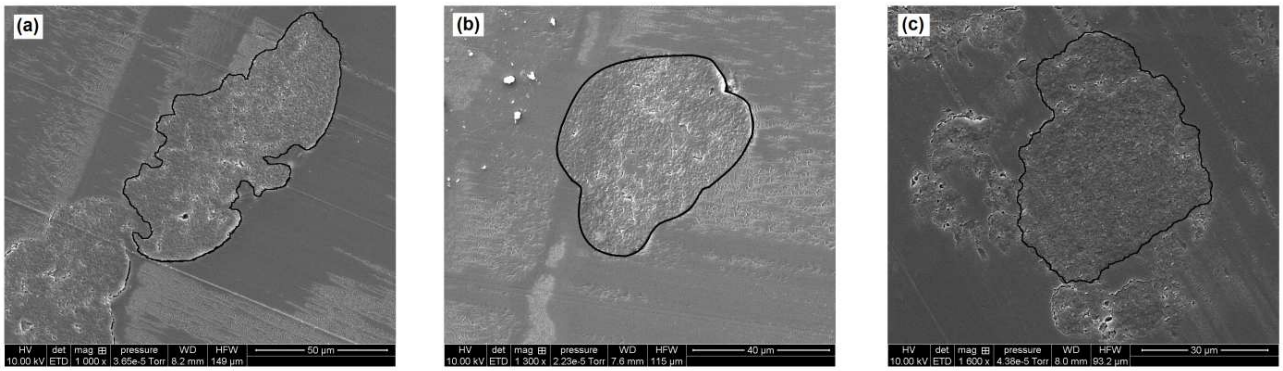

Figure 5.8. The morphology of cross-section area of HDPE particles produced in the presence of (a) 0.0, (b) 0.3, and (c) 0.6 bar of partial pressure of *n*-hexane.

As can be seen from this figure, the HDPE polymer particles obtained in the absence and presence of *n*-hexane demonstrate a very compact structure with negligible porosity, either as cracks on the surface of the particle or as a network of pore phase distributed through the volume of the particle (at the end of the experiments). While only individual particles are shown in these images, it has been verified that they are representative of the different powders.

As a result, the porosity of the polymer particle was assumed to be zero, $\epsilon = 0$, as the characteristic of the catalyst system and the operating condition of gas phase process in which the polymer particle is being produced. Note that this simplification might lead to an underestimation of the diffusivity of ethylene during the early stages of the polymerization before the porosity is lost. This is turn might produce an underestimation of the rate of polymerization. Nevertheless, if we invoke the hypothesis of negligible porosity, the overall diffusivity of ethylene in the pseudo-homogeneous particle presented in equation (5.32) is simplified to

$$D_{ov.1} = D_{1,pol} \qquad (5.33)$$

Ideally we would have a description of the evolution of the porosity, but time and experimental constraints on withdrawing samples from the reactor make this difficult. Nevertheless, in the larger context of our modeling analysis using this simplification will still allow us to describe the effect of the addition of *n*-hexane as an ICA to the gas phase composition on rate of polymerization. As a result, it does not impose any kind of restrictions for the application of the general modeling approach proposed and developed here in order to explore the effect of change in the operating condition of the polymerization process.

Diffusion through semi-crystalline polyethylene

The diffusion through semi-crystalline polymers is a very complex process which depends on many factors including the crystallinity of polymer, solubility of penetrant, mass fraction of absorbed penetrant, temperature, and as a result the extent of plasticization of polymer chains and swelling of polymer phase. An interesting review article targeting this subject is written by Hedenqvist and Gedde[8] and interested readers are referred to this reference for comprehensive related discussions.

As mentioned earlier, the diffusion of solutes in semi-crystalline polymer takes place through its amorphous phase while the crystalline phase is impenetrable to almost all of the solutes. The presence of the crystalline phase dispersed throughout the semi-crystalline polymer would in turn lead to a reduced level of diffusivity of penetrants compared to the fully amorphous polymer for at least two reasons. First, it is due to the necessity for the penetrant molecules to bypass the crystallites through the amorphous phase which would result in the lengthening the diffusive pathway and second, it is because of considerable constraints imposed by the crystalline phase on the segmental mobility of the polymer chains and consequently the mobility of the penetrant molecules in the amorphous phase of the semi-crystalline polymer.

Most of the diffusion models developed to describe the mass transfer have been developed first for fully amorphous polymers. These models have been applied subsequently to the semi-crystalline polymers with considering some correction factors. The same approach is adapted in the current analysis in order to estimate the diffusivity of ethylene in the semi-crystalline polyethylene and the effect of *n*-hexane on it. First, the diffusivity of ethylene in the fully permeable medium being composed of (a) amorphous polyethylene in the binary system of ethylene-polyethylene, and (b) amorphous polyethylene plus *n*-hexane acting as local solvent in the ternary system of ethylene-*n*-hexane-polyethylene is calculated. The values obtained for diffusivity of ethylene in the "fully permeable" medium is subsequently corrected in order to reflect the semi-crystalline nature of HDPE, as discussed above.

In the current study, the diffusivity of ethylene through the semi-crystalline polyethylene is estimated by the correlation suggested by Michaels and Bixler:[9]

$$D_{1,pol} = \frac{D_{1,am.pol}{\alpha_v}^n}{\beta} \quad (5.34)$$

in which $D_{1,pol}$ and $D_{1,am.pol}$ represent the diffusivity of ethylene in the semi-crystalline polymer and the diffusivity of ethylene in the amorphous phase of polymer, respectively. α_v is the volume fraction of amorphous phase in the polymer; this parameter is calculated by the previously given assumption of weight-based crystallinity of $\chi = \%60$ for the HDPE produced polymers. Please see Appendix A for the details of related calculations. β is the chain immobilization factor for the penetrant molecules of ethylene and finally n is a constant which for the HDPE polymer, Michaels and Bixler suggested the use of $n = 1.5$ in the equation (5.34).

Michaels and Bixler relate the diffusivity of ethylene in the amorphous phase, $D_{1,am.pol}$, and the immobilization factor, β, to a parameter termed the reduced molecular diameter of penetrant (d) which can be calculated from the true molecular diameter of penetrant (σ) by the following equation:

$$d = \sigma - \sqrt{\phi}/2 \quad (5.35)$$

in which ϕ is the free volume per unit –CH_2– along the polymer chain axis, while $\sqrt{\phi}/2$ representing the mean unoccupied space between two polymer chain segments. A value of 0.9 Å is recommended for $\sqrt{\phi}/2$ in the reference.[9] The values for σ are taken from Transport Phenomena by Bird et al.[10]

The parameter of reduced diameter is used in the estimation of the parameters of interest as follows:

$$ln\left(\frac{10^7 D_{1,am.pol}^{25}}{\sigma^2}\right) = 3.66 - 1.32d \quad (5.36)$$

$$ln(\beta) = 0.079d^2 \qquad \alpha_v \leq 0.8 \quad (5.37)$$

In equation (5.36), $D_{1,am.pol}^{25}$ represents the diffusivity of ethylene in the amorphous polyethylene at 25 °C having the units of (cm^2/sec) while σ and d having the unit of Å. The effect of the temperature on diffusivity through the amorphous polyethylene is expressed through an Arrhenius type of correlation

$$D_{1,am.pol} = D_{1,am.pol}^0 exp\left(-E_D/R_g T\right) \quad (5.38)$$

with

$$E_D = 2.6 + 2.2d \qquad (5.39)$$

in which E_D has the unit of (kcal/mol).

The diffusivity of ethylene in the binary system of ethylene-PE is estimated with the correlation of Michaels and Bixler, as presented. While it is found that this correlation provides a reasonable estimate of diffusivity in semi-crystalline polymer as a function of penetrant size, polymer crystallinity, and temperature, it is not capable of predicting the enhancement in the diffusivity of ethylene resulting from polymer swelling or mixture effects in the ternary system of ethylene-*n*-hexane-PE.

In the case of ethylene polymerization in the presence of *n*-hexane and regarding higher solubility of *n*-hexane with respect to ethylene (more than two orders of magnitude), ethylene must diffuse through the amorphous polymer "phase" of polyethylene which is basically constituted of two "component"s: the component of amorphous polymer chains and the component of *n*-hexane solute acting also as local solvent.

While the diffusion of both of the solutes of reactant ethylene and inert *n*-hexane takes place simultaneously during the continuous production of polymer in the particle, however, after initial steps of polymerization, the polymer particle becomes saturated with *n*-hexane due to its inert nature with respect to polymerization reaction. The accuracy of this assumption is validated with the PFM model. As a result, one can assume that ethylene is diffusing through a medium which is constituted of amorphous PE chains swollen and in equilibrium with *n*-hexane in the ternary system of ethylene-*n*-hexane-PE.

Since the ethylene diffusivity in the liquid *n*-hexane as a solvent is found to be one order of magnitude higher than its diffusion in the amorphous polyethylene, it is entirely reasonable to expect that the order of magnitude for ethylene diffusivity in the amorphous polyethylene swollen by *n*-hexane to be in the range between its diffusivity through the medium composed of liquid *n*-hexane and the medium composed of amorphous polyethylene chains, as schematically demonstrated in Figure 5.9. The diffusivity of ethylene in this case will depend on the relative portion of each of the aforementioned components in constituting the fully permeable medium of solvent-swollen amorphous polymer.

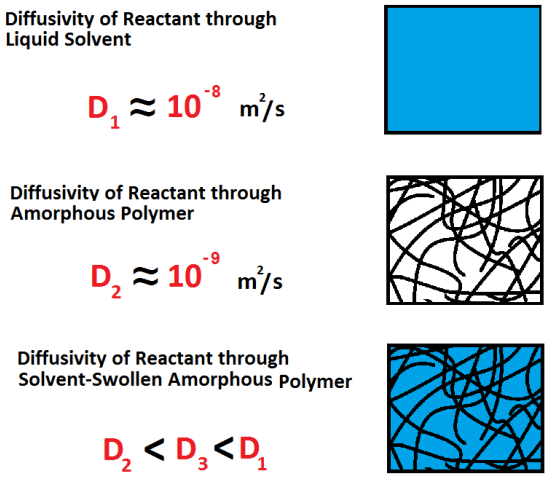

Figure 5.9. Phenomenological description of expected diffusivity of ethylene through amorphous phase of polyethylene swollen by *n*-hexane.

Regarding the complex nature of concurrent diffusion phenomenon of different solutes through semi-crystalline polymer and in the absence of a reliable theoretical approach to accurately describe it, the simplified correlation suggested[11] for diffusion of component (*1*) in the mixture of components (*1*), (*2*), and (*3*) is adapted here as follows:

For X_1 small:

$$D_{1,am.pol} = \frac{1}{\frac{X_2}{D_{12}} + \frac{X_3}{D_{13}}} \qquad (5.40)$$

in which component (*1*), (*2*), and (*3*) represent ethylene, *n*-hexane, and amorphous phase of polyethylene, respectively. X_i is the mole fraction of component *i* in the mixture.

$D_{1,am.pol}$ is the diffusivity of ethylene in amorphous phase of polyethylene swollen by *n*-hexane, D_{12} is the diffusivity of ethylene through liquid *n*-hexane, and finally D_{13} is the diffusion of ethylene through amorphous polyethylene chains in the absence of *n*-hexane. The condition of small X_1 holds true for application this correlation to our system regarding low solubility of ethylene.

X_i in the equation (5.40) is estimated by the Sanchez-Lacombe EOS, as the mole fraction of mers of component (*i*) occupying total mers (sites) of the model lattice in closed-packed state for the amorphous phase of polyethylene at each equilibrium condition. The details of related calculations are provided in Appendix A. D_{13} as the ethylene diffusivity in the amorphous polyethylene in the absence of *n*-hexane is calculated by the previously given equations of (5.36) and (5.38) and in the same manner.

D_{12} as the diffusivity of ethylene in the liquid *n*-hexane as solvent is estimated by the Wilke-Chang method:[12]

$$D_{12} = \frac{7.4 \times 10^{-8} (\phi MW_2)^{1/2} T}{\mu_2 V_1^{0.6}} \qquad (5.41)$$

in which MW_2 is the molecular weight of solvent *2* (gr/mol), T is the temperature (K), μ_2 is the viscosity of solvent *2* (cP), and V_1 is the molar of solute *1* at its normal boiling temperature (cm^3/mol). ϕ represents a dimensionless association factor for solvent *2* which is equal to 1 for the unassociated solvents like *n*-hexane. This correlation provides the diffusivity of ethylene in *n*-hexane, D_{12}, in the unit of (cm^2/sec).

After calculation of $D_{1,am.pol}$, it is implemented in equation (5.34) in order to estimate the diffusivity of ethylene in the semi-crystalline polyethylene swollen by *n*-hexane in the ternary system of ethylene-*n*-hexane-polyethylene. The diffusivity of *n*-hexane through the semi-crystalline HDPE in the ternary system of ethylene-*n*-hexane-PE is estimated by the Michaels and Bixler's method as described through the equations (5.34) to (5.39), while assuming that the concurrent diffusion of ethylene has negligible effect on the diffusivity of *n*-hexane through the polymer.

5.2.4.3. Catalytic system

Characteristic size of initial catalyst particles

Figure 5.10 demonstrates a SEM image of initial powder of Ziegler-Natta catalyst supported on $MgCl_2$. As expected, the catalyst particles show a size distribution ranging from less than 10 µm up to more than 100 µm.

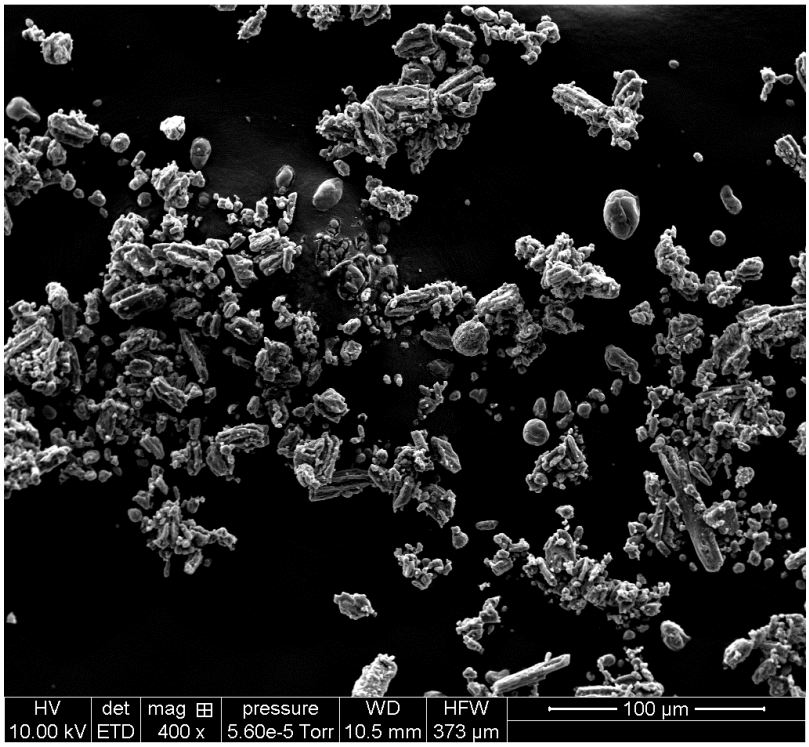

Figure 5.10. SEM image of powder of Ziegler-Natta catalyst supported on $MgCl_2$.

In order to obtain an accurate distribution of catalyst particle size and as a result to have a more precise estimation about the characteristic size of the heterogeneous catalyst particles used in the process, the powder needs to be characterized with an advanced particle size analyzer device. In the lack of possibility to have access to such an analyzer and regarding the different SEM images of the catalyst powder like the one presented in Figure 5.10, the characteristic radius of 35 µm is considered as the approximate size for the average catalyst particle representing the catalyst powder being used in the gas phase polymerization of ethylene.

While exploring the effect of different initial catalyst particle sizes on the significance of mass and heat transfer through the growing catalyst/polymer particle and consequently local and overall rate of polymerization would provide additional useful information about thermal and activity behavior of the catalytic system in general, however this is out of scope of the current study. Here it is intended to investigate the effect of change in the process condition (here, by addition of *n*-hexane to the gas phase composition) on the quality and rate of gas phase ethylene polymerization utilizing a specific catalyst system with known kinetic and geometric characteristics. As a result, a reasonable approximation of the average diameter of catalyst particles as the characteristic size representing the catalyst powder being used in the polymerization reaction is sufficient for the aforementioned purpose in current analysis.

Kinetic parameters

The kinetic parameters of $k_{p,ref}$, $k_{d,ref}$, C_1^*, and C_2^* are obtained by fitting the PFM model to the experimentally obtained instantaneous rate of polymerization as a function of time in the base cases of ethylene polymerization in the absence of *n*-hexane with partial pressure of ethylene equal to 7 and 12 bars, respectively. These parameters are considered as the characteristic kinetic parameters of the catalytic system being used and as a result will remain the same in the following simulated reactions in order to explore the effect of *n*-hexane on the instantaneous rate of polymerization. Both of the activation energies of E_a and E_d are assumed to be equal to 10 (kcal/mol) as the typical values reported in the literature for these parameters.[7]

5.2.4.4. Polymer particle

As discussed earlier, the polymer particle is assumed to have no porosity. The density of semi-crystalline polyethylene is calculated by Sanchez-Lacombe EOS (as provided in Appendix A) and is found to change slightly by the partial pressure of *n*-hexane in the gas phase composition. The thermal conductivity, $k_{c,p}$, and heat capacity of semi-crystalline polyethylene, $C_{p,pol}$, is assumed to be constant while considering the effect of solubilized *n*-hexane on these parameters to be negligible.

5.2.4.5. Gas phase

The gas phase is assumed to be composed of ethylene, *n*-hexane, and argon while neglecting the presence of hydrogen due to its negligible partial pressure compared to other components and total operating pressure. The methods used to estimate the gas phase properties of interest (i.e. viscosity, thermal conductivity, heat capacity, and density) as a function of gas phase composition are provided in details in Appendix D. An overview about the estimation methods of gas phase properties is provided in this section, hereunder.

Viscosity of gas phase

The viscosity of each component present in the gas phase composition is first calculated at its low pressure limit by an estimation method using the Lennard-Jones parameters.[10] The effect of pressure is then applied by the Reichenberg method[12] in order to estimate the viscosity of each component at the pressure corresponding to its partial pressure in the reactor. The gas phase viscosity as a mixture of pure components is finally calculated by the semi-empirical correlation suggested by Wilke.[10]

Thermal conductivity of gas phase

First, the Roy and Thodos estimation technique[12] is employed in order to estimate the thermal conductivity of each component at its low pressure limit. The thermal conductivity of each component at the pressure corresponding to its partial pressure in the reactor is then calculated by the Stiel and Thodos method.[12] The thermal conductivity of gas phase as a mixture of pure components is calculated by an analogous method proposed by Wilke.[10]

Heat capacity of gas phase

The heat capacity of each component is first calculated by a correlation which is only a function of temperature.[12] The heat capacity of gas phase as a mixture of components is then calculated by considering the mole fraction of each component present in the gas phase composition.

Density of gas phase

Regarding that ethylene and argon constitute the major portion of the gas phase composition, the density of gas phase is estimated by safely assuming it to behave as the ideal gas.

Relative velocity of gas-particle

The spherical stirred-bed reactor, in which the gas phase ethylene polymerization reactions were performed, was operated with an agitation speed that provides the same order of magnitude for the relative velocity of gas-particles as the one for the fluidized bed reactors. As a result, the relative gas-particle velocity is assumed to be $u = 1\ (m/sec)$, which is in the typical range for relative gas-particle velocities in the industrial FBRs.

5.2.4.6. Summary of parameters of PFM model

All of the parameters described above and used in the PFM model in order to predict the effect of change in the operating condition of gas phase ethylene polymerization process on supported catalyst by addition of *n*-hexane as an inert condensing agent (ICA) are summarized in Table 5-I.

Table 5-I. Summary of parameters of PFM model.

Process independent parameters					unit
T_b	353.15	K	ϵ	0.0	dimensionless
T_{ref}	313.15	K	$k_{c,p}$	0.20	J/m.sec.K
$D_{ov,2}$	1.74×10^{-11}	m^2/sec	$C_{p,pol}$	2000	J/kg.K
C^*_1	0.52	mol site/m^3 cat	$-\Delta H_{pol}$	107.6×10^3	J/mol
C^*_2	0.41	mol site/m^3 cat	$-\Delta H_{sorp,2}$	29.12×10^3	J/mol
$k_{d,ref}$	1.0×10^{-4}	1/sec	ρ_{cat}	2300	kg/m^3
E_a	4.2×10^4	J/mol	r_{cat}	35×10^{-6}	m
E_d	4.2×10^4	J/mol	u	1.0	m/sec

Process dependent parameters during polymerization by 7 bars ethylene

$k_{p,ref}$ 180 m^3 tot/mol site.sec

	7 bar Ethylene 1 bar Argon	7 bar Ethylene 1 bar Argon 0.3 bar n-Hexane	7 bar Ethylene 1 bar Argon 0.6 bar n-Hexane	7 bar Ethylene 1 bar Argon 0.8 bar n-Hexane	unit
$D_{ov.1}$	1.45×10^{-10}	1.53×10^{-10}	1.59×10^{-10}	1.63×10^{-10}	m^2/sec
ρ_{pol}	920.4	915.7	910.2	905.7	kg/m^3
$[M]_{eq.1}$	84.26	90.17	97.41	103.49	mol/m^3 pol
$[M]_{eq.2}$	0.00	125.16	269.27	386.49	mol/m^3 pol
μ	1.29×10^{-5}	1.25×10^{-5}	1.21×10^{-5}	1.19×10^{-5}	kg/m.sec
$k_{c,g}$	2.59×10^{-2}	2.53×10^{-2}	2.48×10^{-2}	2.45×10^{-2}	J/m.sec.K
$C_{p,g}$	1553.4	1589.1	1618.4	1635.2	J/kg.K
ρ_g	8.0	8.9	9.8	10.4	kg/m^3

Process dependent parameters during polymerization by 12 bars ethylene

$k_{p,ref}$ 150 m^3 tot/mol site.sec

	12 bar Ethylene 1 bar Argon	12 bar Ethylene 1 bar Argon 0.3 bar n-Hexane	12 bar Ethylene 1 bar Argon 0.6 bar n-Hexane	12 bar Ethylene 1 bar Argon 0.8 bar n-Hexane	unit
$D_{ov.1}$	1.45×10^{-10}	1.56×10^{-10}	1.62×10^{-10}	1.67×10^{-10}	m^2/sec
ρ_{pol}	919.1	914.5	908.9	904.1	kg/m^3
$[M]_{eq.1}$	144.17	153.73	165.78	176.22	mol/m^3 pol
$[M]_{eq.2}$	0.00	119.19	263.56	384.84	mol/m^3 pol
μ	1.25×10^{-5}	1.23×10^{-5}	1.21×10^{-5}	1.19×10^{-5}	kg/m.sec
$k_{c,g}$	2.66×10^{-2}	2.62×10^{-2}	2.58×10^{-2}	2.56×10^{-2}	J/m.sec.K
$C_{p,g}$	1631.6	1649.8	1665.9	1675.5	J/kg.K
ρ_g	12.8	13.7	14.6	15.2	kg/m^3

5.2.5. PFM simulation results and discussion

In this section, the predictive capability of the Polymer Flow Model developed based on the phenomenological description of the associated physical effects due to addition of *n*-hexane to the gas phase composition is evaluated against the experimental instantaneous rates of ethylene polymerization in the absence and presence of *n*-hexane, presented in the experimental section.

As mentioned earlier, the kinetic parameters of the supported catalytic system i.e. $k_{p,ref}$, $k_{d,ref}$, C_1^*, and C_2^* are fitted to the instantaneous rate of polymerization for the base cases of gas phase ethylene polymerization with 7 and 12 bars of ethylene in the absence of *n*-hexane in the gas phase composition. These kinetic parameters, provided in Table 5-I, are considered as the characteristic of the catalytic system being used in the polymerization reactions and consequently remain constant during the PFM simulations in order to predict the effect of the presence of *n*-hexane on the instantaneous rate of ethylene polymerization.

To the best of our knowledge, there are currently no papers in the open literature where one studies the effect of change in the process conditions of this type on rate of polymerization. Thus, the quality of the performance of this modeling analysis in predicting the effect of process condition can be regarded as an indicator of the reliability of this methodology while demonstrating the potential capability of the current general approach in order to be adapted and improved to serve as a process simulator for the gas phase ethylene polymerization reactors, in the absence of such a commercial software in this field.

Figure 5.11 and Figure 5.12 demonstrate the prediction of PFM model for the effect of presence of *n*-hexane in the gas phase composition on the instantaneous rate of gas phase ethylene polymerization with 7 and 12 bars of ethylene partial pressure, respectively. R_{p1}, R_{p2}, R_{p3}, and R_{p4} represent the instantaneous rate of ethylene polymerization in presence 0.0, 0.3, 0.6, and 0.8 bar of partial pressure of *n*-hexane in the gas phase composition.

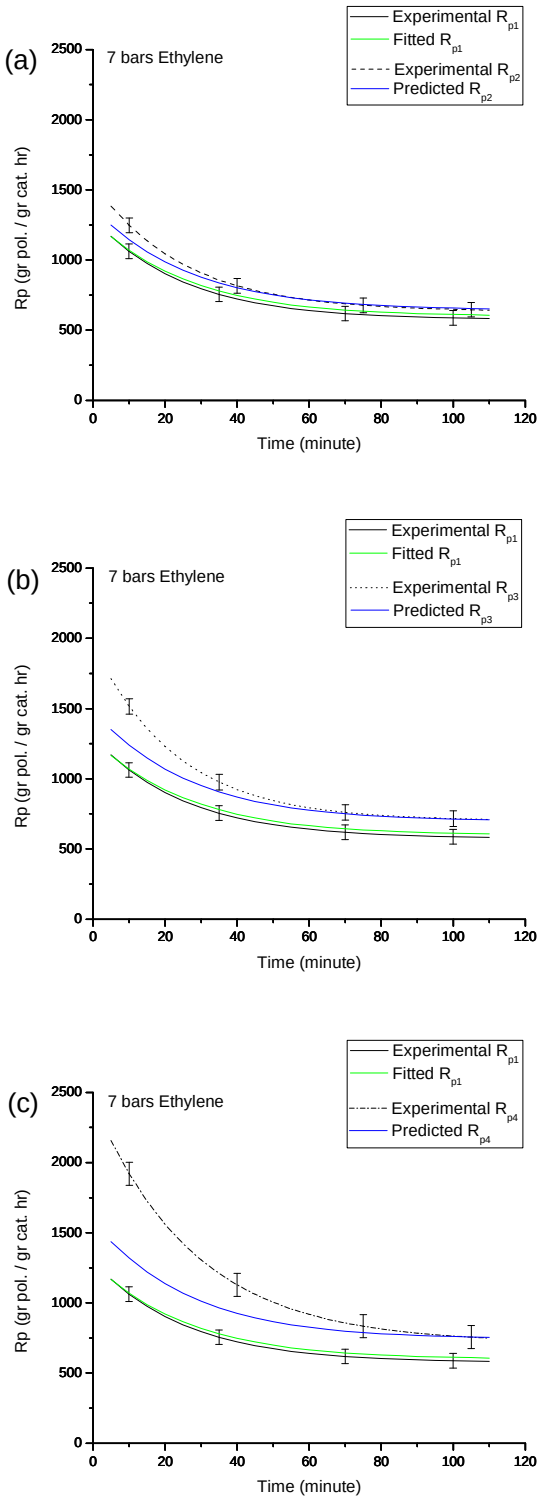

Figure 5.11. Evaluation of predictive capability of PFM model for the effect of presence of *n*-hexane in the gas phase composition on the instantaneous rate of gas phase ethylene polymerization with 7 bars of ethylene partial pressure.

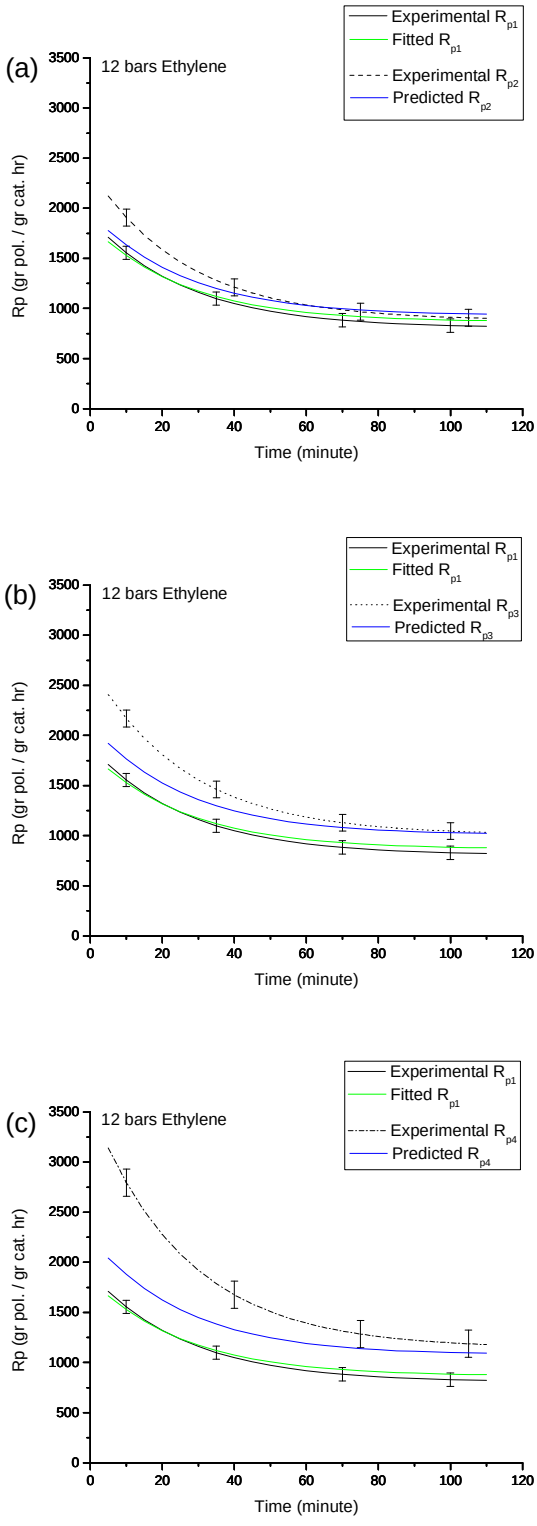

Figure 5.12. Evaluation of predictive capability of PFM model for the effect of presence of *n*-hexane in the gas phase composition on the instantaneous rate of gas phase ethylene polymerization with 12 bars of ethylene partial pressure.

As can be seen from both of these figures, the prediction of PFM model is in better agreement with the experimental rates of polymerization at a lower partial pressure of *n*-hexane in the gas phase. As the partial pressure of *n*-hexane increases, the prediction of PFM model and experimental rates of polymerization start to converge later during the polymerization, and the model underpredicts the effect of *n*-hexane during the early phase of the reaction. However, one could notice that at later steps of polymerization, in which the growing polymer particle has reached to its thermal stability and the solubility of solutes in the polymer phase are closer to the equilibrium condition, the prediction of PFM model matches with the experimental rates of polymerization in an excellent manner of almost perfect fit.

On the other hand, the model underestimates the observed boost in the rate of polymerization during the initial steps of polymerization. The reason for this discrepancy between model prediction and experimental observation can be attributed to the some of assumptions made during the development of PFM model, but most importantly to the assumption made about the porosity of polymer particle. Regarding the morphology of obtained HDPE particles and the porosimetry analysis performed on them, the porosity of growing catalyst/polymer particle is assumed to be zero during the whole time period of polymerization reaction. Since during the polymerization reaction, the initial porous catalyst particle undergoes through the fragmentation process and the final morphology of polymer particle is established by time during the course of polymerization, the assumption of zero porosity of particle does not seem to appropriately reflect the reality of the polymerization process. In a more porous catalyst/polymer particle during the initial steps of polymerization, less concentration gradient of ethylene would be expected resulting in higher rate of polymerization due to both higher local concentration of reactant and local temperature through the growing particle. This, in turn, can explain the higher boost observed during the initial steps of polymerization in the experimental results compared to the prediction of PFM model.

As a result, in order to be able to have a more accurate prediction about the effect of operating condition of the polymerization process, one not only needs to be able to describe the morphology of the obtained polymer particles but also requires to have a reasonable estimation about the evolution of morphology and porosity of the growing catalyst/polymer particle during the course of polymerization. The exact determination of evolution of the catalyst/polymer particle morphology by time as the characteristic of the catalyst system and the process of polymerization can be quite challenging and would require advanced characterization techniques such as video-microscopy and micro-tomography. However, one could estimate the porosity evolution of the catalyst/polymer particle during the course of polymerization with ethylene only (as the base case), by stopping the reaction at certain time intervals during the course of polymerization and analyzing the porosity of acquired polymer powder.

Figure 5.13 (a) and (b), demonstrate the significance of predicted mass transfer resistance through the growing polymer particle assumed by PFM model and the effect of *n*-hexane as the ICA with partial pressure of 0.6 bar on it during polymerization with 7 and 12 bars of ethylene, respectively.

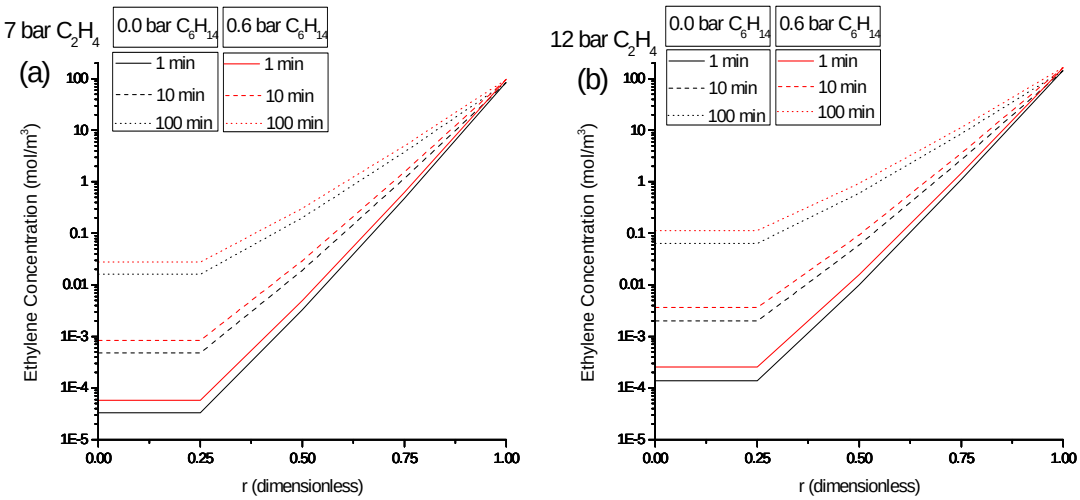

Figure 5.13. The predicted concentration gradient through the growing polymer particle and the effect of *n*-hexane as the ICA on it during polymerization with (a)7 and (b)12 bars of ethylene, respectively.

The concentration gradient of reactant ethylene is provided at 1, 10, and 100 minutes from beginning of the polymerization reaction. As expected, considering the polymer particle as a fully compact medium without any porosity has resulted in a significant mass transfer resistance through the particle. As the polymerization reaction proceeds, the active sites becomes dispersed and diluted in the produced polyethylene and consequently the volumetric rate of ethylene consumption in the particle decreases. This, in turn, results in the predicted attenuation in the significance of the concentration gradient of the reactant through the growing particle by time, as demonstrated in Figure 5.13. However, this figure allows us to visualize the concept of local ethylene concentration inside the growing polymer particle during the course of polymerization and demonstrates how the presence of *n*-hexane results in the enhancement of local ethylene concentration due to induced increase in both solubility and diffusivity of ethylene in the polymer particle.

As explained in the section 5.2.3, in the standard procedure, the minimum number of grids required for numerical solution of the mass and energy balance equations in order to obtain accurate concentration and temperature gradients is determined by increasing the number of grids in solution; once the numerical solution becomes independent of the number of grids used, the corresponding number of grids can be considered as the minimum required number of grids. However, in the case of access to the limited computational power, the number of grids used in the current study is $N=5$, and as a result the

concentration and the temperature gradients predicted by PFM model must be considered as approximation of real gradients. Figure 5.14 demonstrates the effect of number of grids on the calculated concentration gradient through the particle after 1 minute from start of the polymerization reaction with 7 bars of ethylene. As it can be seen from this figure, more significant concentration gradients are predicted by increasing the number of grids. However, considering that the concentration gradients are provided in a logarithmic scale, one can notice that by increasing the grid numbers the difference between calculated concentration gradients decreases and as expected the numerical solution is converging to a value which is independent of grid numbers, as explained previously.

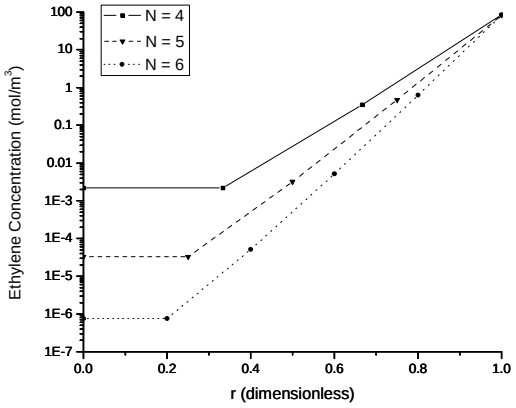

Figure 5.14. The effect of number of grids on the calculated concentration gradient through the particle after 1 minute from start of the polymerization reaction with 7 bars of ethylene.

Because of the significant predicted resistance to the reactant transfer in the compact polymer particle, the concentration of ethylene in radial positions inside the particle closer to the center is much lower compared to the surface. Consequently, the local rate of polymerization and associated heat generation is negligible in the center of particle compared to the particle surface. As a result, while the heat of polymerization is being removed from the particle surface by surrounding gas phase with the convective mechanism, however, simultaneously almost no heat is being generated in radial positions close to the center of particle. This has resulted in prediction of no temperature gradient with PFM model through the polymer particle under all the simulated circumstances for the mass transfer presented in Figure 5.13. With the local particle temperature in all radial positions being equal to 80.5 °C (slightly higher than the reactor bulk temperature) in all simulations, the related figure of local temperature inside the particle is skipped here for brevity and also lack of its necessity.

5.3. Conclusion

In conclusion, we can evaluate the performance of the developed general approach in order to be able to predict the effect of change in the process condition, here by addition of *n*-hexane as the ICA, on the quality and rate of gas phase ethylene polymerization on supported catalyst. In fact, as has been discussed earlier, the local instantaneous rate of ethylene polymerization using a specific supported catalytic system, would depend on the local monomer concentration and local temperature at the active sites inside the growing particle. The local monomer concentration at the active sites, as a measure of monomer availability for the polymerization reaction, would in turn depend on its solubility in the polymer phase and diffusivity through the particle. In the current methodology, the PFM model is utilized to act as the platform in order to estimate the local concentration of monomer and local temperature at the active sites at each instant during the course of polymerization. This eventually has enabled us to predict the effect of change in the process condition by addition of *n*-hexane on the local and consequently the overall rate of gas phase ethylene polymerization using a supported catalytic system with known kinetic behavior in the absence of *n*-hexane.

By comparing the PFM model prediction with the experimental results on the effect of *n*-hexane on the instantaneous rate of gas phase ethylene polymerization, it can be concluded that the current approach provides an excellent predictive capability on the effect of *n*-hexane on the instantaneous rate of ethylene polymerization during the later steps of polymerization. This is when the solubility of solutes can be considered to be very close to the equilibrium condition and the growing catalyst/polymer particle has reached its thermal stability. This remarkably good predictive capability originates from the reasonable estimation of the local concentration of reactant and local temperature inside the particle by the PFM model. In the case of local concentration, in combination with the adapted simplified diffusivity model, it demonstrates the outstanding predictive capability of the Sanchez-Lacombe model which has been developed and fitted to the experimentally obtained set of solubility data in the ternary system of ethylene-*n*-hexane-PE in order to describe the effect of *n*-hexane on the concentration of ethylene in the amorphous phase of polyethylene.

Direct application of solubility data obtained experimentally under equilibrium condition for the binary system of ethylene-PE and the ternary system of ethylene-*n*-hexane-PE by implementing into the Sanchez-Lacombe EOS in order to describe the observed enhancement in the rate of ethylene polymerization in the presence of *n*-hexane under the reactive conditions during which the polymer particle is closer to the equilibrium state (both in terms of solubility and thermally) is a novel approach. This methodology is proposed, developed and applied successfully in the current study for the first time in this field while demonstrating the universal potential of this approach to be extended for description of

different process operational conditions, for instance, for predicting the effect of other commonly used ICAs on the polymerization rate. An overview of the systematic development of the phenomenological approach which is designed in order to be able to predict the effect of change in the process condition by addition of ICA of *n*-hexane on the rate of gas phase ethylene polymerization on supported catalyst is provided orderly in Figure 5.15 with the corresponding experimental and modeling steps. However, this general modeling approach at its current development state appears to underestimate the rate of gas phase ethylene polymerization in presence of *n*-hexane at initial steps during the course of polymerization. This discrepancy between the model prediction and experimentally obtained rates of polymerization on the effect of *n*-hexane is an indicator of some phenomena that are not captured appropriately in the developed model. These phenomena may include (but are not limited to) the evolution of morphology of the particle during the polymerization, and the quality and exact mechanism of processes of reactant sorption and diffusion in the absence and presence of ICA during the initial moments of polymerization in which the catalyst/polymer particle rapidly evolves in terms of its size, structure, and thermal behavior. This, in turn, implies the necessity for the improvement of current state of the general modeling approach proposed in order to have a more precise prediction of the effect of change in process condition by including a more accurate description of the evolution of the particle morphology and also quality of reactant diffusion and sorption in the catalyst/polymer particle by time during the course of polymerization.

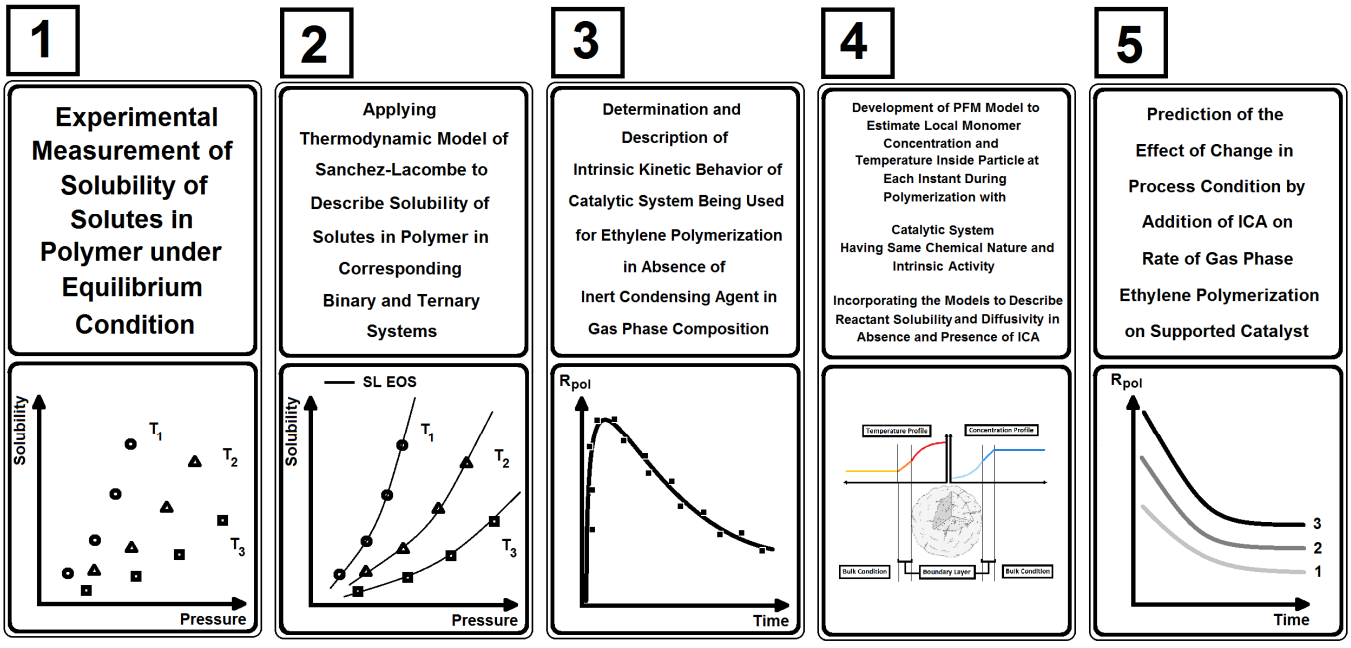

Figure 5.15. An overview of the phenomenological approach designed to predict the effect of change in the process condition by addition of ICA on the rate of gas phase ethylene polymerization.

5.4. References

1. Dupuy, J.; Spitz, R. Modification of Ziegler-Natta catalysts by cyclopentiadienyl-type ligands: Activation of titanium-based catalysts. *J. Appl. Polym. Sci.* **1997,** *65* (12), 2281-2288.

2. Floyd, S.; Choi, K. Y.; Taylor, T. W.; Ray, W. H. Polymerization of olefines through heterogeneous catalysis IV. Modeling of heat and mass transfer resistance in the polymer particle boundary layer. *J. Appl. Polym. Sci.* **1986,** *31* (7), 2231-2265.

3. Yao, W.; Hu, X.; Yang, Y. Modeling solubility of gases in semicrystalline polyethylene. *J. Appl. Polym. Sci.* **2007,** *103* (3), 1737-1744.

4. Yao, W.; Hu, X.; Yang, Y. Modeling the solubility of ternary mixtures of ethylene, iso-pentane, n-hexane in semicrystalline polyethylene. *J. Appl. Polym. Sci.* **2007,** *104* (6), 3654-3662.

5. Moore, S. J.; Wanke, S. E. Solubility of ethylene, 1-butene and 1-hexene in polyethylenes. *Chemical Engineering Science* **2001,** *56* (13), 4121-4129.

6. Kiparissides, C.; Dimos, V.; Boultouka, T.; Anastasiadis, A.; Chasiotis, A. Experimental and theoretical investigation of solubility and diffusion of ethylene in semicrystalline PE at elevated pressures and temperatures. *J. Appl. Polym. Sci.* **2003,** *87* (6), 953-966.

7. Kanellopoulos, V.; Dompazis, G.; Gustafsson, B.; Kiparissides, C. Comprehensive Analysis of Single-Particle Growth in Heterogeneous Olefin Polymerization: The Random-Pore Polymeric Flow Model. *Ind. Eng. Chem. Res.* **2004,** *43* (17), 5166-5180.

8. Hedenqvist, M.; Gedde, U. W. Diffusion of small-molecule penetrants in semicrystalline polymers. *Progress in Polymer Science* **1996,** *21* (2), 299-333.

9. Michaels, A. S.; Bixler, H. J. Flow of gases through polyethylene. *J. Polym. Sci.* **1961,** *50* (154), 413-439.

10. Bird, R. B.; Stewart, W. E.; Lightfoot, E. N. *Transport Phenomena;* 2nd ed.; John Wiley & Sons, Inc.: **2007**.

11. Treybal, R. E. *Mass Transfer Operations;* 3rd ed.; McGraw-Hill: **1987**.

12. Reid, R. C.; Prausnitz, J. M.; Poling, B. E. *The Properties of Gases and Liquids;* 4th ed.; McGraw-Hill: **1987**.

Chapter 6

The influence of the heat of sorption

Part of this chapter is published as:

Alizadeh, A.; McKenna, T. F. L. Condensed Mode Cooling for Ethylene Polymerization: The Influence of the Heat of Sorption. *Macromolecular Reaction Engineering* **2014,** *8* (5), 419-433.

6. The influence of the heat of sorption

6.1. Inroduction

In the present chapter, it is intended to demonstrate how the thermal effect associated with the heat of sorption of ICAs can have a positive effect in terms of avoiding particle over-heating under certain circumstances like its temporary exposition to the defluidized regions inside a FBR as a possible undesirable operating condition for this type of reactor set-up. The Sanchez-Lacombe model will be used to describe the temperature dependency of the solubility of heavy condensable solute in the polyethylene at different pressures using a reliable set of thermodynamic data. Subsequently, this will be included in an energy balance for a simplified representation of a polymerizing particle in order to investigate the impact of absorbed ICA on the evolution of particle temperature in a FBR.

6.2. Model development

6.2.1. Heat of sorption

The sorption process of a condensable solute in a polymer can be considered as a combination of two thermodynamic steps[1]: (1) condensation of the solute vapour to the liquid state occurs. This is the opposite of the liquid vaporization process; (2) the dissolution of the liquefied solute in the polymer which involves enthalpy of mixing for a polymer-solute system. As a result, one can estimate the heat of sorption of a condensable solute in a polymer as summation of enthalpy of condensation of the solute and the enthalpy of solute-polymer mixing. For the system of condensable alkanes or alkenes and the polyolefins, the heat of mixing is smaller and negligible compared to the heat of condensation. Consequently, the heat release associated with sorption of condensable solute of a longer hydrocarbon molecule in a polyolefin is approximately equal to the heat of condensation.

Different experimental techniques are available to measure the associated interaction heat for a solvent-polymer system, including recently developed scanning transitiometry and titration calorimetry.[2,3] The sorption heat can also be indirectly interpreted from the inverse gas chromatography method, and Tian et al.[4] have reported the sorption heat for a wide range of common solvent-polymer systems implementing this method. While the transitiometry and titration calorimetric method are promising methods, no data

relevant to the current study are available, so the values of the heat of sorption reported herein were those obtained using the inverse gas chromatography method.[4]

6.2.2. Solubility data

Experimental studies in this field have shown that the solubility of alkanes or α-olefins in polyolefins decreases as the temperature increases. In other words, as the temperature of a particle circulating in a reactor increases, the solute becomes more volatile and starts to desorb. The phenomenon of mass transfer of solute out of/into the polymer phase by increasing/decreasing the temperature at which the system is in equilibrium is referred to as desorption/resorption, respectively in this chapter.

In order to investigate the relative importance of sorption heat of condensable components on the thermal behavior of growing polymer particles, *n*-hexane is chosen as the inert condensing agent for two reasons: (1) it has a higher solubility than shorter chain alkanes; and (2) it has a higher enthalpy of sorption per mole compared to the lighter condensable components such as 1-butene or *n*-pentane. Thus, if there is a potential impact of the desorption/resorption process on particle temperature it will be most demonstrable with *n*-hexane.

In the Chapter 4, it was demonstrated that the Sanchez-Lacombe EOS does provide a mediocre prediction for the set of solubility data for *n*-hexane as ICA presented by group of Yang.[5,6] However, it was shown that the prediction of SL model about the effect of *n*-hexane on the ethylene concentration in the amorphous phase of polymer is much less sensitive than ethylene solubility and polymer swelling to the "assumed" solubility of *n*-hexane or in other words the *n*-hexane-PE binary interaction parameter. This resulted in satisfactory predictions of enhancement in the rate of gas phase ethylene polymerization on supported catalyst in presence of *n*-hexane, presented in Chapter 5.

It should be mentioned here that the role of commonly used α-olefin comonomers such as 1-butene and 1-hexene have been extensively studied given their importance in the production of linear low density polyethylene (LLDPE). Thus, more reliable solubility data reported in the literature for α-olefins in polyethylene is much more easily found than it is for saturated alkanes of the same length.[7-9] Meanwhile, it is reasonable to suppose that *n*-hexane and 1-hexene have a similar nature of interaction with segments of non-polar polyethylene chains. They are both constituted of linear hydrocarbon molecules of the same number of carbons with almost the same degree of non-polarity. This in turn implies that regarding the similar size, shape, and polarity of these solutes, it is possible to safely approximate the solubility of *n*-hexane with available and more reliable set of data for solubility of 1-hexene for the purposes of this analysis. An experimental evidence to support further the validity of this assumption can be found in the

earlier sorption studies of Michaels et al.,[10] in which the solubility constant of Henry's law for sorption of propane in polyethylene is reported to be about only 10% higher than the one for propene at 25 °C. As a result, regarding the mediocre fitting of SL model to the available solubility data of *n*-hexane, in the current modeling analysis the solubility of *n*-hexane in LLDPE and its temperature dependency is approximated with the more reliable set of data for 1-hexene in the literature.[7-9] While this assumption will slightly underestimate the *n*-hexane solubility in polyethylene (similar to the case of propane and propene), this induced error is neglected in the current modeling study in order to investigate ''the order of magnitude'' of the effect related to the sorption heat of ICA of *n*-hexane on the thermal behavior of growing particles.

The Sanchez-Lacombe model is applied here in order to describe the temperature dependency of the solubility of 1-hexene in linear low density polyethylene at different pressures. The characteristic model parameters for each component of the system, taken from reference[7] are provided in Table 6-I. This parameter set was established using experimental data available in the literature[8,9] for the solubility of different olefinic solutes in polyolefins through adjustment of the binary interaction parameter.

Table 6-I. Sanchez-Lacombe characteristic parameters for pure components.[7]

Component	$T^*(K)$	$P^*(bar)$	$\rho^*(kg/m^3)$
Ethylene	283	3395	680
1-hexene	450	3252	814
LLDPE	653	4360	903

Figure 6.1 illustrates the temperature dependency of 1-hexene solubility in LLDPE as predicted by the Sanchez-Lacombe model. The variation of solubility with temperature is provided for two different pressures of 1-hexene (0.5 and 1 bar), and up to 130 °C (we will not simulate situations above this temperature as this is the approximate melting temperature for PE). It is important to note here that in the extension of the Sanchez-Lacombe model for prediction of 1-hexene solubility at the higher pressure of 1 bar, the potential effect of the crystalline phase on the extent of polymer swelling and consequently the solubility has been neglected.

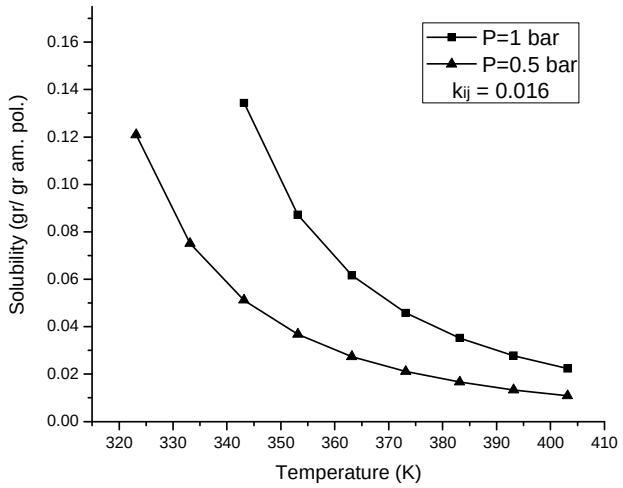

Figure 6.1. Temperature dependency of solubility of 1-hexene in LLDPE.

For the needs of our simplified particle model (developed below) a rapid correlation of solubility as a function of temperature will suffice. The method of least squares was used to fit the SL curves with the following type of function:

$$S_{2,am} = Ae^{-BT} \qquad (6.1)$$

in which $S_{2,am}$ is the solubility of 1-hexene in the amorphous phase of the LLDPE polymer and T is the temperature at which the gas-polymer system is in equilibrium. A and B are the pressure-dependent constants and are provided in Table 6-II with the corresponding r^2-values for quality of the fitting. This correlation will be used in order to describe the temperature dependency of the solubility of the *n*-hexane in the following section in the development of energy balance model for simulating thermal behavior of active particles under different physical circumstances.

Table 6-II. Fitted model parameters and corresponding r^2-values for describing temperature dependency of 1-hexene solubility in LLDPE at different pressures.

Pressure(bar)	*A(gr/ gr am. pol)*	*B(1/K)*	r^2
0.5	1342	0.029	0.9818
1	2826.3	0.029	0.9853

6.2.3. Energy balance model for a single polymer particle

The energy balance around a reacting polymer particle can be written:

$$\rho_{pol} V_{pol} C_{p,pol} \left(\frac{dT_{pol}}{dt}\right) = k_p C^* [M]_1 V_{cat} \left(-\Delta H_{pol}\right) + V_{pol} \left(-\Delta H_{sorp,2}\right) \frac{d[M]_2}{dt} - hA_{pol} \left(T_{pol} - T_b\right) \quad (6.2)$$

The left side of the equation represents the rate of energy accumulation in the polymer particle. The terms on the right hand side are (in order): the rate of energy generation due to polymerization; the rate of heat release associated with the sorption of the condensable component in the polymer particle; and the rate of heat removal from the particle to the surrounding gas phase by convection.

Since we are focusing on the relative importance of heat of sorption of the condensable component on the thermal behavior of polymer particles, the following simplifying assumptions are considered through the development of the current model:

- The polymer particle is treated as a spherical non-porous object.
- Mass and heat transfer resistances through the particle are neglected.
- The particle size is assumed to be constant during the simulated transition periods (on the order of several seconds).
- The effect of cosolubility phenomenon on the rate of polymerization is neglected and as a result its associated thermal effect is not included in the energy balance of the particle system.
- The ethylene solubility in the amorphous phase of LLDPE for 10 bars of ethylene pressure and at 80 °C is estimated using Sanchez-Lacombe EOS. In the energy balance, the term related to the ethylene sorption heat is neglected due to its lower solubility and lower sorption heat per mole compared to the heavier condensable component. Preliminary simulations (not shown here for the sake of brevity) revealed that the effect of the heat of sorption of ethylene on the thermal behavior of the particle is negligible and can be dismissed. In addition, in the term for heat generation due to ethylene polymerization, the temperature dependency of ethylene solubility is also neglected since it will not affect the model validity in exploring the influence of sorption heat of *n*-hexane on the thermal behavior of the polymer particles.

The temperature dependency of the propagation constant is described here by an Arrhenius-type of correlation

$$k_p = k_{p,ref} e^{-\frac{E_a}{R_g}\left(\frac{1}{T_{pol}} - \frac{1}{T_{ref}}\right)} \quad (6.3)$$

in which $k_{p,ref}$ is the propagation constant at the reference temperature, T_{ref}. E_a is the activation energy for propagation and R_g is the universal gas constant.

The solubility values of the solutes in the amorphous polymer (gr/gr am. pol) were obtained using the Sanchez-Lacombe EOS and are translated to an average concentration over the entire polymer particle volume (mol/ m^3 pol) by the following expressions:

$$[M]_1 = \frac{1000(1-\chi)\rho_{pol}}{MW_1} S_{1,am} \quad (6.4)$$

$$[M]_2 = \frac{1000(1-\chi)\rho_{pol}}{MW_2} S_{2,am} \quad (6.5)$$

where χ is the weight-based crystallinity of the polymer particle.

Equation (6.1) can be substituted into equation (6.5) in order to describe the temperature dependency of concentration of condensable component of *n*-hexane in the polymer particle:

$$[M]_2 = \frac{1000(1-\chi)\rho_{pol}}{MW_2} Ae^{-BT_{pol}} \quad (6.6)$$

And consequently

$$\frac{d[M]_2}{dt} = -\frac{1000(1-\chi)\rho_{pol}AB}{MW_2} e^{-BT_{pol}} \left(\frac{dT_{pol}}{dt}\right) \quad (6.7)$$

It is important to underline the significance of the assumption implicitly made when we use equation (6.1) to describe the temperature dependency of the *n*-hexane concentration in the polymer particle, and the way this will influence the simulation results. Recall that equation (6.1) is obtained from fitting the available reliable set of equilibrium solubility data. However, this correlation is being applied here in order to describe the solubility of the condensable in the particle which undergoes through thermal transition in non-equilibrium conditions. As a result, it is implicitly assumed that the solubility of *n*-hexane in the polymer particle immediately reaches the equilibrium value corresponding to the particle temperature during each step of this thermal transition. In other words, the desorption/resorption of the condensable component is assumed to take place promptly by increasing/decreasing the particle temperature while the dynamic of the associated thermal-induced mass transfer through the particle is being neglected. Hence, while the magnitude of the effect of sorption heat on the thermal behaviour of a growing particle can be considered to be reliable in slow transitions in which the particle is closer to its equilibrium state, caution must be taken in interpreting the simulated thermal behaviour under fast

transitions. Considering this point, the time scale involved in our simulations is in the order of several seconds to fractions of a minute while intending to avoid extremely fast impulsive transitions.

By substituting equation (6.3) and (6.7) in equation (6.2), the energy balance of the particle system can be rewritten in the following form

$$\beta_1\left(\frac{dT_{pol}}{dt}\right) = \beta_2 e^{-\frac{E_a}{R_g}\left(\frac{1}{T_{pol}}-\frac{1}{T_{ref}}\right)} - \beta_3 e^{-BT_{pol}}\left(\frac{dT_{pol}}{dt}\right) - \beta_4\left(T_{pol}-T_b\right) \quad (6.8)$$

in which β_1, β_2, β_3, and β_4 are clustered function defined as

$$\beta_1 = \rho_{pol} V_{pol} C_{p,pol} \quad (6.9)$$

$$\beta_2 = k_{p,ref} C^* [M]_1 V_{cat}\left(-\Delta H_{pol}\right) \quad (6.10)$$

$$\beta_3 = \frac{1000 V_{pol}\left(-\Delta H_{sorp,2}\right) AB(1-\chi)\rho_{pol}}{MW_2} \quad (6.11)$$

$$\beta_4 = hA_{pol} \quad (6.12)$$

Finally, in order to be able to numerically solve equation (6.8) to obtain the temperature evolution of the particle under different transition circumstances, it is rewritten as

$$\frac{dT_{pol}}{dt} = \frac{\beta_2 e^{-\frac{E_a}{R_g}\left(\frac{1}{T_{pol}}-\frac{1}{T_{ref}}\right)} - \beta_4\left(T_{pol}-T_b\right)}{\beta_1 + \beta_3 e^{-BT_{pol}}} \quad (6.13)$$

A fourth-order Runge-Kutta method is applied here in order to solve the equation (6.13).

A plethora of correlations for gas-solid mass and heat transfer coefficients can be found in the literature. Based on the earlier studies of Floyd et al.[11] we have chosen to use the Ranz-Marshall correlation for a single sphere in a fluid medium:

$$Nu = 2 + 0.6 Re^{1/2} Pr^{1/3} \quad (6.14)$$

where

$$Nu = \frac{h d_p}{k_{c,g}} \quad (6.15)$$

$$Re = \frac{u d_p}{\nu} \quad (6.16)$$

$$Pr = \frac{\mu C_{p,g}}{k_{c,g}} \qquad (6.17)$$

The gas phase properties with the other physical, kinetics, and thermal parameters used in this modeling study are summarized in Table 6-III.

Table 6-III. The physical properties and model parameters used in describing thermal behavior of single polymer particle.

Polymer properties			
	ρ_{pol}	900	kg/m^3
	$C_{p,pol}$	2000	J/kg.K
	χ	0.4	dimensionless
Catalyst and kinetic parameters			
	$k_{p,ref}$	2.5-10	m^3/mol sit.sec
	T_{ref}	330	K
	E_a	42	kJ/mol
	C^*	54	mol sit/m^{3}cat
	r_{cat}	15-35×10^{-6}	m
	ρ_{cat}	2800	kg/m^3
Gas phase properties			
	Pr	0.763	dimensionless
	v	1.22×10^{-6}	m^2/sec
	$k_{c,g}$	2.69×10^{-2}	J/m.s.K
	T_b	353.15	K
	MW_1	28.05	gr/mol
	MW_2	86.16	gr/mol
Enthalpy			
	$-\Delta H_{pol}$	107.6	kJ/mol
	$-\Delta H_{sorp,2}$	29.12	kJ/mol

6.3. Simulation results and discussion

6.3.1. Thermal behaviour of the particle by its exposure to the defluidized region inside FBR

In the normal operation of the fluidized bed reactors, particles are suspended by the fluid and are continuously in motion relative to the other particles. However, under certain undesirable circumstances, localized non-uniform distribution of the gas can be observed in a part of the bed (due e.g. to channeling or dead spots), the flow may become insufficient to fluidize the particles, resulting in local defluidization. In this case, defluidization is defined here as the status of particles having substantially no motion relative to the other neighboring particles. Regardless of the exact cause, a defluidized particle evolving in a zone with low particle-gas velocity will undergo heat-up since the energy generated from the polymerization cannot be removed appropriately by convection. If the particles overheat and melt, this will lead to local formation of polymer agglomerates, and an in extreme case would result in the bed collapse and reactor shut-down.

Here we will simulate the thermal behavior of active growing particle which becomes exposed to the defluidized region in the bed. At $t = 0$, it is assumed the heat of polymerization is continuously removed from the particle by convection so its temperature is at steady state, i.e. $\left(\frac{dT_{pol}}{dt}\right) = 0$. Applying the steady-state condition to the equation (6.13), the particle temperature at the initial condition is obtained by solving the resultant non-linear equation for T_{pol}.

The exposure of the particle to the defluidized region is taken into account in the model by defining an arbitrary function, provided in equation (6.18), for the relative gas-particle velocity in which the velocity fluctuates by time.

$$u = 1 - \sin(t/2) \qquad (6.18)$$

Under these conditions, the relative gas-polymer velocity cycles from 1 *m/s* to 0 in about 3 seconds indicating the time period in which the particle becomes exposed to the defluidized region. In the next 3 seconds, the relative velocity rises back from 0 to 1 *m/s* which implies the particle leaving the defluidized region and being in the region of having appropriate fluidization regime.

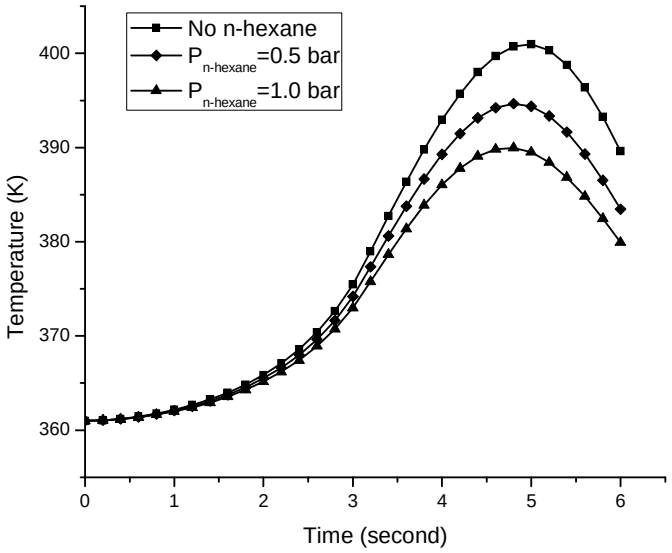

Figure 6.2. Simulated thermal behaviour of active polymer particle of the size r_p=500 μm during its temporary exposition to the defluidized region inside the FBR.

Figure 6.2 demonstrates the simulated thermal behavior of active particle of the size r_p=500 μm originated from initial catalyst size of r_{cat}=35 μm during the defined transition period of 6 seconds. This can be considered as the size of a fully grown particle in the FBR in typical industrial gas phase processes. The kinetic parameters of polymerization used in this modeling study correspond to the productivity of 16 (kg PE/gr cat.h) which is also in the typical range for the productivity of industrial gas phase FBRs (see Table 6-III).

As can be seen in this Figure, the particle starts to heat-up by its exposure to the defluidized region due to the accumulation of the released polymerization energy. The temperature rise continues until the particle starts to leave the defluidized region and the heat of polymerization starts to be removed from the particle by convection mechanism due to the relative movement of the particle with respect to its surrounding gas phase. The rate of increase in the particle temperature is lower in the presence of *n*-hexane; as the particle starts to heat up due to the accumulation of polymerization energy, part of this energy is consumed in order to partially desorb *n*-hexane solubilized in the particle leading to lower rate of particle temperature rise. At higher pressure of the condensable, the amount of solute solubilized in the polymer particle is higher. As demonstrated in Figure 6.1, this in turn implies that higher amount of condensable can be desorbed from the particle at higher pressure by increasing the equilibrium temperature of the system. As a result, the effect associated with the desorption of condensable solute on the thermal behavior of the

particle is stronger at higher pressure simply due to higher amount of solute available in the particle to be desorbed.

Simulated thermal behavior of the particle during transition period of its temporary exposition to the defluidized region demonstrates that in the absence of *n*-hexane, the particle temperature reaches the approximate fusion temperature of the polyethylene (130 °C) due to its higher rate of heat-up, while for instance in the presence of 1 bar of *n*-hexane and under the same transition, the particle temperature remains at least 10 °*C* below the polymer fusion temperature. As a result, it can be concluded that the probability of the particle temperature to reach its fusion temperature and consequently the probability of the resultant polymer agglomerate formation due to the local defluidization inside the FBR becomes lower in the presence of inert condensing agent of *n*-hexane.

In this set of illustrative simulations, it was intended to demonstrate how the lower fluctuation in the particle temperature resulting from partial desorption of *n*-hexane as ICA would reduce the probability of particle melting and local agglomerate formation due to local defluidization inside the FBR. In the following part, we will take a closer look on the influence of different parameters like particle size, time scale for transition cycle and rate of polymerization on the induced effect of *n*-hexane on the thermal behavior of the growing particles.

However, before moving on to these parametric studies and for the clarification purpose, it must be noted here that the size of initial catalyst particle dispersed in the polymer particle is different and smaller in most of upcoming parametric studies than the one presented in the demonstrative simulation of Figure 6.2. There were two main reasons which obliged us to make the choice of going with smaller initial catalyst particle size and consequently lower rate of heat generation in the polymer particle in the series of parametric studies below: (1) non-convergence of solution in order to estimate the initial particle temperature from the resultant non-linear equation by imposing the steady state condition, i.e. $\left(\frac{dT_{pol}}{dt}\right) = 0$ to equation (6.13), for large catalyst particles (r_{cat}=*35* μm, for instance) dispersed in small polymer particles (r_p=*150* μm, for instance); and (2) rapid rise of particle temperature during the transition period which would lead to unrealistically large values for the particle temperature in the case of large catalyst particles dispersed in the polymer particles. As a result, while having smaller initial catalyst particle size in the following section will decrease the rate of heat generation inside the growing particles and consequently attenuate the temperature fluctuation of the particles during the transition period, however, it will allow us to systematically analysis the influence of aforementioned parameters on the induced effect of *n*-hexane on the thermal behavior of the growing particles and to be able to track the related predicted trends during the transition period.

6.3.1.1. Size of polymer particle

In this part, the thermal behavior of a polymer particle originating from initial catalyst size of $r_{cat}=15\ \mu m$ upon its temporary exposition to the defluidized region during different steps of polymerization course which correspond to different polymer particle sizes will be investigated. Three particle sizes (r_p) of 150, 300, and 500 µm have been considered in this study in order to represent the polymer particle during initial steps of polymerization, average polymer particle size, and fully grown particle size, respectively. Similar to the previous example, the activity of the catalyst corresponds to 16 (kg PE/ gr cat.h) and the transition cycle takes place during 6 seconds.

The simulation results provided in Figure 6.3, reveal that, as expected, the heat of (de)sorption plays a stronger role in keeping the temperature lower for the smallest polymer particles. The difference between maximum temperature reached by the particle without *n*-hexane and in presence of 1 bar of *n*-hexane during the transition is about 1.3, 0.3, and 0.1 °C for the particle size (r_p) of 150, 300, and 500 µm, respectively.

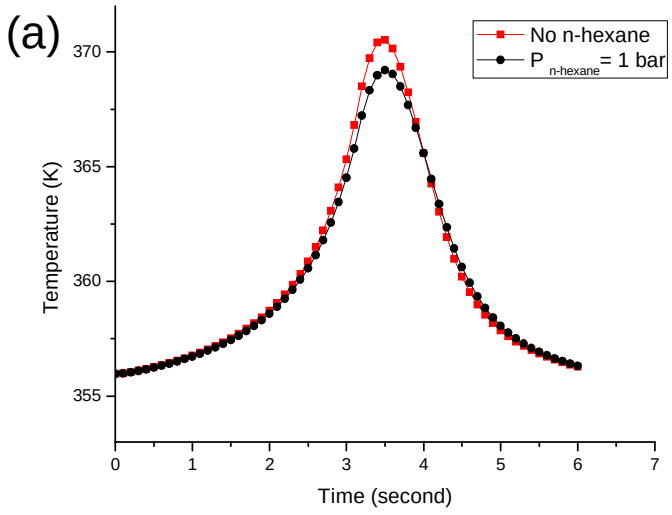

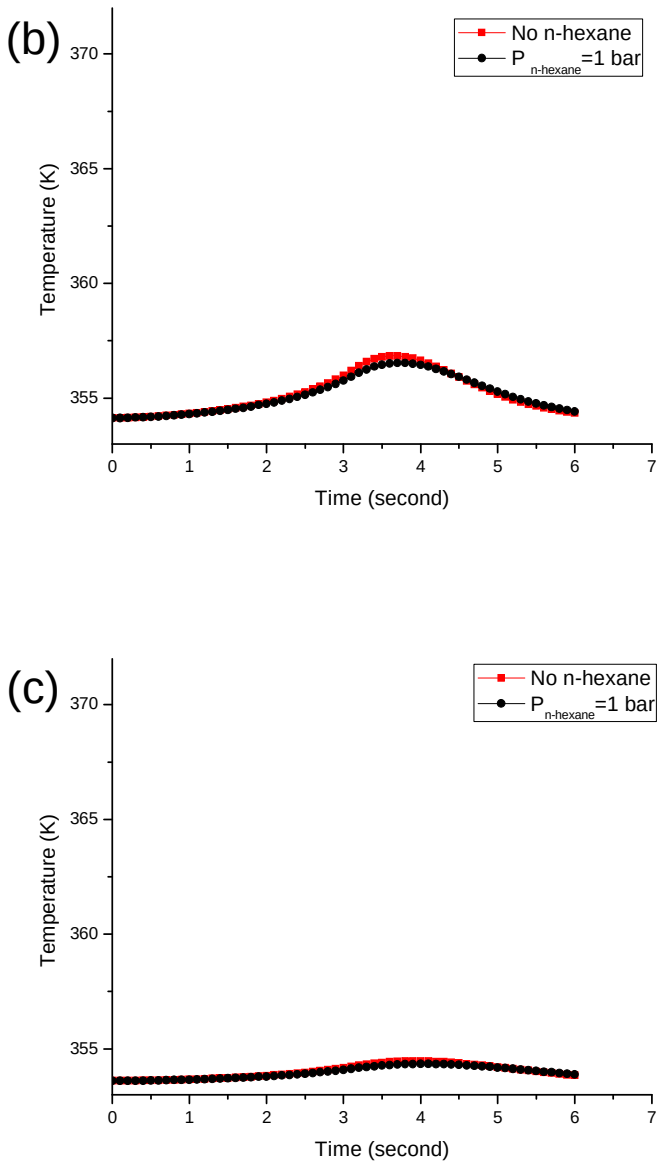

Figure 6.3. Simulated thermal behaviour of polymer particle during its temporary exposition to the defluidized region with size of r_p equal to (a) 150, (b) 300, and (c) 500 µm.

This is due to the fact that during the initial steps of polymerization, the concentration of polymerization active site per volume of the particle and as a result the volumetric rate of heat generation inside the particle is higher. As a result, the smaller particles are more sensitive to degradation in the heat transfer conditions in the bed, meaning the probability of particle overheating is higher under these circumstances for the smaller particles. Regarding higher thermal sensitivity of the smaller particles, these simulations

predict that the partial desorption of condensable *n*-hexane solved in polymer phase surrounding the active sites have more pronounced effect on the temperature fluctuation of the smaller particles during insufficient heat removal inside the FBR.

This strongest potential effect of heat of sorption of *n*-hexane as ICA in decreasing the rate of overheating for smaller polymer particles upon insufficient heat removal inside the FBR during the initial steps of polymerization is of industrially profound importance. As mentioned earlier, these small active particles are more vulnerable to overheating which result in polymer melting, creating fouling and local polymer agglomerates inside the reactor.

6.3.1.2. Activity of polymerization process

In order to explore the effect of heat of sorption of *n*-hexane on the thermal behavior of polymer particles having different activities, a series of comparative simulations for polymer particle size of $r_p=500\ \mu m$ originated from initial catalyst particle size of $r_{cat}=35\ \mu m$ are performed for three polymerization activities corresponding to production of 16, 8, and 4 (kg PE/ gr cat.h) and are provided in Figure 6.4. These simulation results show that, as one would expect, the heat of sorption has a more pronounced effect on the thermal behavior of polymer particle having higher activity; the difference between maximum temperature reached by the particle without *n*-hexane and in presence of 1 bar of *n*-hexane during the transition cycle of 6 seconds as described before is about 11.0, 1.2, and 0.5 °C for the activity of 16, 8, and 4 (kg PE/ gr cat.h), respectively.

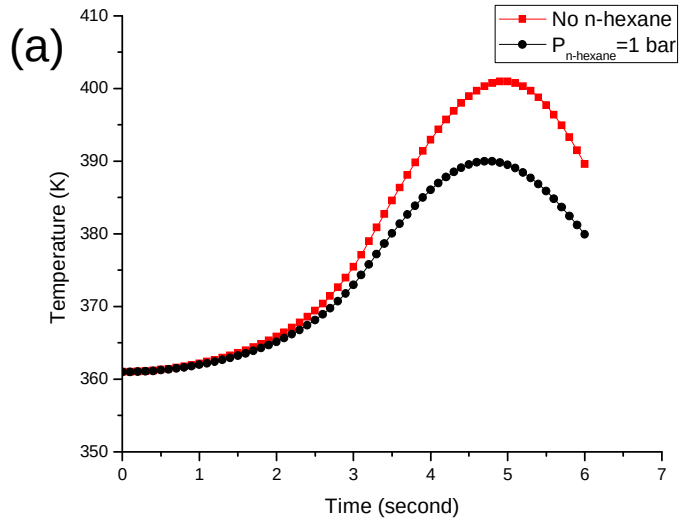

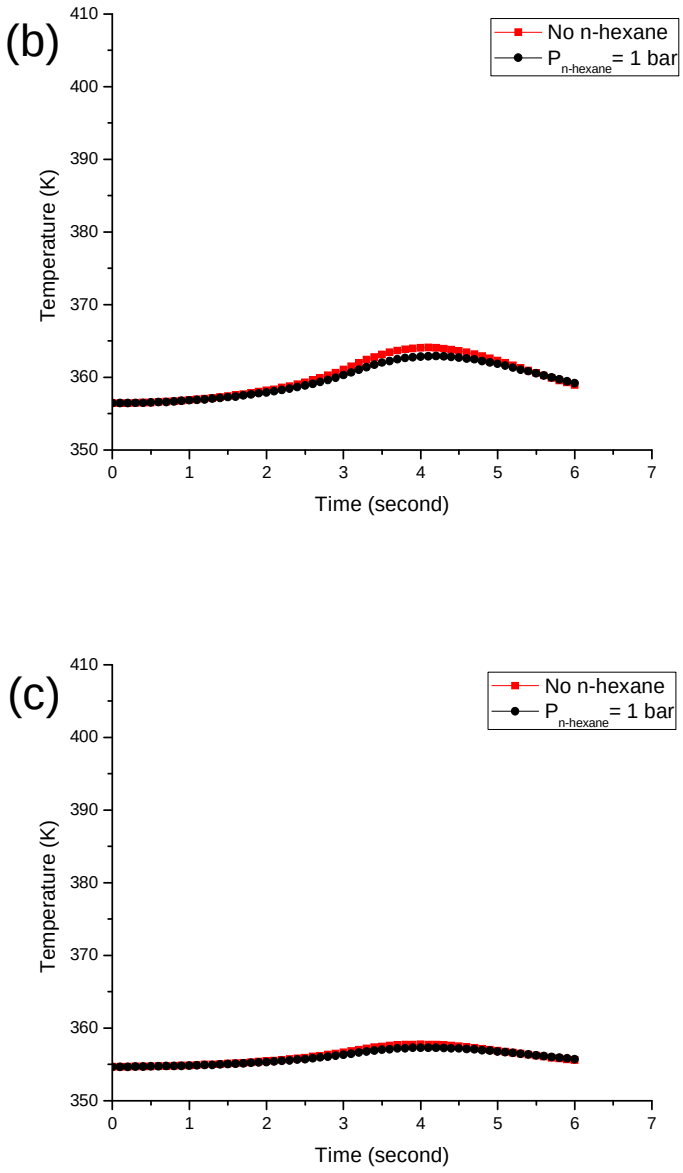

Figure 6.4. Simulated thermal behavior of particle size of r_p=500 μm with activity corresponding to production of (a) 16, (b) 8, and (c) 4 (kg PE/ gr cat.h).

This predicted trend can be explained by the fact that the rate of energy accumulation inside the polymer particle with higher activity is faster during its temporary exposition to the defluidized region in bed with insufficient capability for heat removal. This in turn implies that the temperature of the more active particle rises faster while desorbing larger amount of condensable *n*-hexane solubilized in itself. This leads to a more pronounced effect of heat of sorption for more active particle.

6.3.1.3. Time scale for temporary exposition of the particle to the defluidized region

The thermal behavior of the particle size of $r_p=500\ \mu m$ originating from initial catalyst size of $r_{cat}=30\ \mu m$ during three different times scales of 3, 6, and 12 seconds for cycle of its temporary exposition to the defluidized region in bed are provided in Figure 6.5.

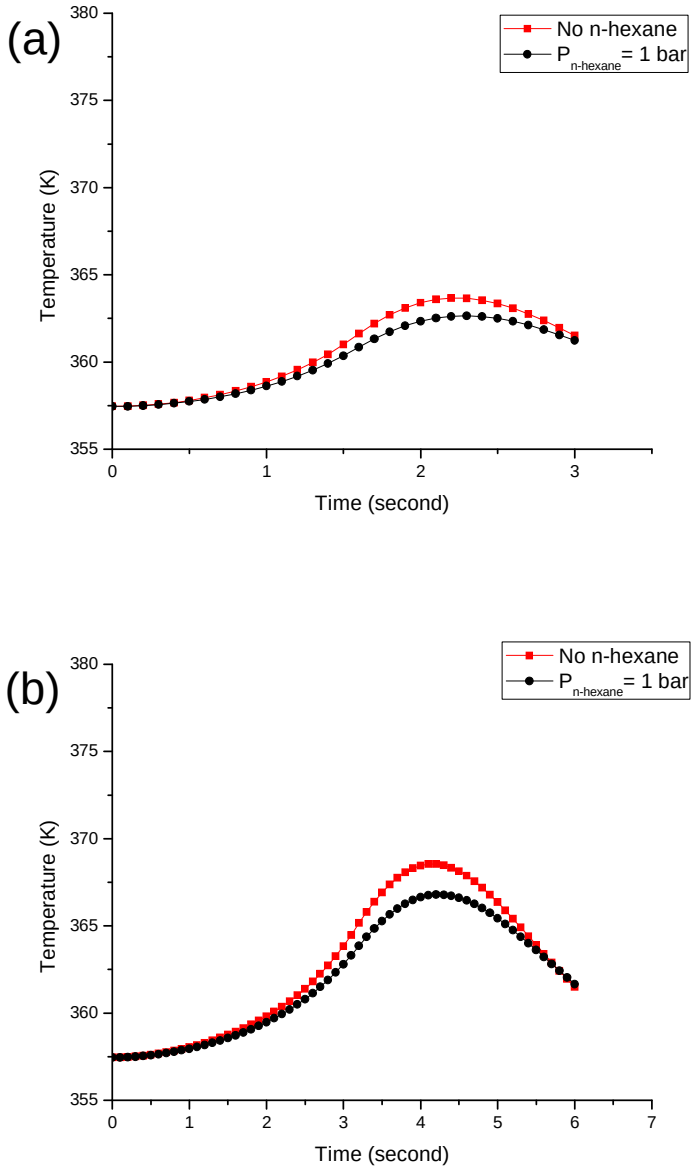

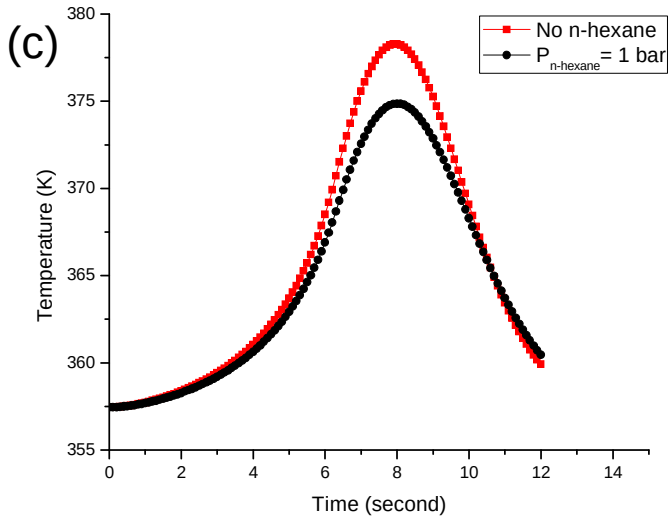

Figure 6.5. Simulated thermal behavior of the particle size of r_p=500 μm during three different time scales of (a) 3, (b) 6, and (c) 12 seconds.

The heat of sorption has a more pronounced effect at longer time scales of being exposed to the defluidized region and insufficient heat removal; the difference between maximum temperature reached by the particle without *n*-hexane and in the presence of 1 bar of *n*-hexane is about 3.4, 1.7, and 1.0 °C during the transition cycle times of 12, 6, and 3 seconds, respectively.

Insufficient heat removal from the growing particle during longer period of time would result in a higher rise in particle temperature, causing more *n*-hexane to desorb.

6.3.2. Thermal behaviour of the particle by its exposure to different temperature of surrounding bulk gas phase

A common practice in industry in order to keep the reactor temperature at desirable operation condition, is to cool the reactor feed stream in an external heat exchanger prior to its introduction to the bed. As a result, the heat of polymerization is removed from the reactor in the form of sensible heat of fluidizing gas phase stream which leaves the reaction environment from top of the reactor. Introduction of colder feed stream to the reactor will induce a temperature gradient through the height of the fluidized bed reactor. Using the thermocouples in different locations on the internal wall of the reactor, it is found that the gas phase temperature reaches to the desired operational bulk temperature of the reactor in less than 1 meter above the distributor plate, resulting in the temperature profile as demonstrated in Figure 6.6.

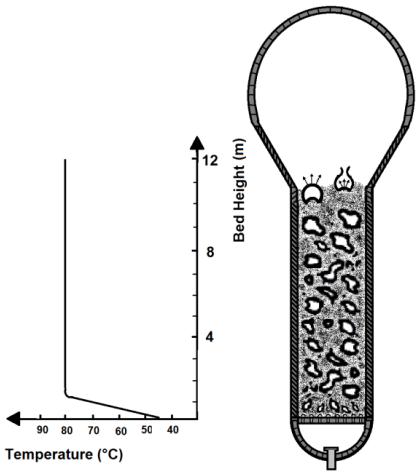

Figure 6.6. The temperature profile within a typical fluidized bed reactor of the gas phase ethylene polymerization.[12]

Consequently, a single growing particle which is fluidizing inside the reactor will spend a certain portion of its total residence time in the colder region at the bottom of the reactor. The exposure of the particle to the region with lower bulk temperature of surrounding gas phase will in turn affect its instantaneous rate of polymerization, quality of crystallization of the generated polymer chains and in short the consistency of the final polymer product. In fact, the velocity profile of the individual polymer particles in the fluidized bed reactor has been measured by a positron emission tracking technique.[12] In agreement with the related theoretical CFD studies, the results of these measurements demonstrate that there is an intense circulation loop of solid particles inside the reactor with an upstream flow in the center and a downstream flow at the periphery of the reactor, as schematically depicted in Figure 6.7. This circulation loop is generally considered as a single loop with a circulation velocity which is proportional to the fluidization velocity.

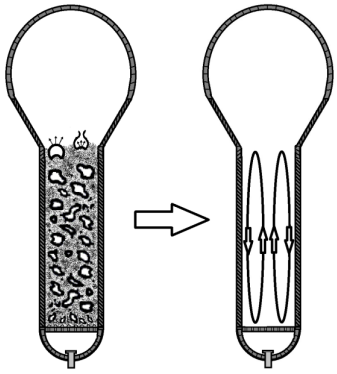

Figure 6.7. Schematic representation of the circulation loop of polymer particles fluidizing inside the FBR.

Considering a single polymer particle fluidizing which is in continuous movement in the reactor and inside the aforementioned circulation loop, the bulk gas phase temperature experienced by this particle during its circulation can be considered to be as provided in Figure 6.8.

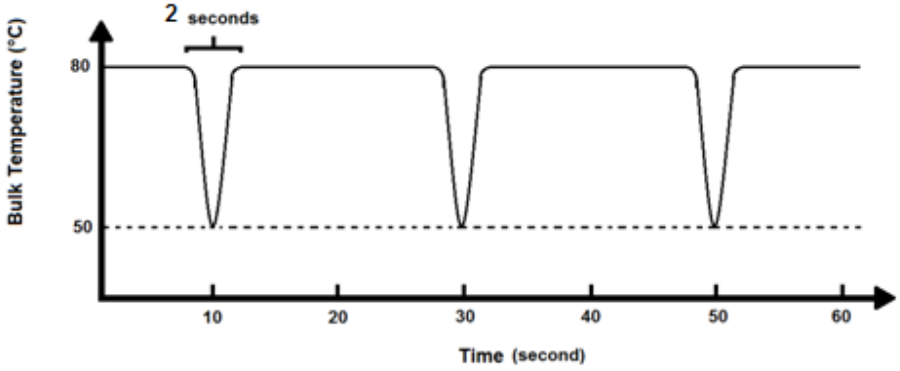

Figure 6.8.The bulk gas phase temperature experienced by a single particle during its circulation inside the reactor.

Obviously, the frequency at which the particle will meet the bottom of the reactor and the colder surrounding bulk gas phase will depend on the circulation velocity and consequently the reactor fluidization velocity. While advanced CFD studies and experimental analysis will be required for the accurate estimation of the time scale needed for a specific particle to complete a single circulation loop inside the reactor, however, in the current modeling analysis and in order to explore the effect of condensable component on the thermal behavior of a polymer particle during its exposure to the different bulk temperature of surrounding gas phase, the time scale required for the particle to do a single circulation inside the reactor is considered to be in the order of 20 seconds. The bed height of a commercial scale fluidized bed reactor can be on the order of 12 m, and the gas superficial velocity inside the reactor can be considered to be on the order of 1 m/sec. It should take approximately 10 seconds for the particle to go up through the centre at constant temperature, and 10 seconds for its peripheral descent. The time during which the particle becomes exposed to the cold region at the bottom of the reactor can be estimated to be on the order of 2 seconds (see Figure 6.8). While attempting to provide a relatively realistic picture, it must be noted that the assumption about the rate of particle circulation inside the reactor will not affect the validity of current model in exploring the significance of the effect of sorption heat of condensable component on the particle thermal behavior as exposed to the different surrounding bulk temperatures. In addition, it is worth mentioning that the partial pressure of *n*-hexane in these series of simulations is considered to be 0.5 bar. This is in order to avoid the possibility of partial condensation

of *n*-hexane at the higher pressure of 1 bar (as the other choice) at the bottom of the reactor having local temperature close to 50 °C.

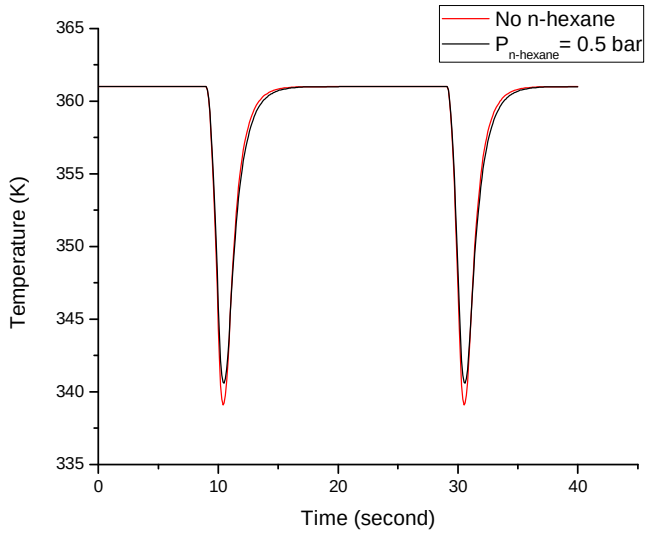

Figure 6.9. Simulated thermal behaviour of the polymer particle of the size r_p=500 μm during its circulation inside FBR.

Figure 6.9 demonstrates the simulated thermal behavior of the polymer particle of the size r_p=500 μm during its circulation inside the bed. As can be seen in this figure, for the same extent of fluctuation in the surrounding bulk temperature, the magnitude of temperature fluctuation is smaller in the presence of 0.5 bar of condensable *n*-hexane. By exposure of the particle to the colder environment, higher amount of *n*-hexane can be sorbed into the polymer. Consequently, the heat released due to the sorption of the *n*-hexane will reduce the rate at which particle temperature decreases (very slightly) when it is exposed to colder surrounding environment. Similarly, as the particle becomes surrounded by hotter bulk temperature, it starts to desorb part of condensable *n*-hexane which results in lower rate of increase in particle temperature. However, as can be seen in Figure 6.9, this effect does not appear to be significant and for the imposed fluctuation of 30 °C for the bulk temperature, the particle temperature fluctuates around 21.9 °C without any *n*-hexane while in presence of 0.5 bar of *n*-hexane it fluctuates around 20.4 °C.

In order to explore the effect of other parameters (like size of polymer particle, polymerization activity, and the time scale in which the particle becomes exposed to the colder region at the bottom of the reactor) on the significance of effect of heat of sorption, a parametric study is performed and summarized in Table 6-IV.

Table 6-IV. Summary of parametric study on the effect of heat of sorption of *n*-hexane on the thermal behavior of particles during its temporary exposition to the colder region inside the FBR.

Effect of Particle Size			
r_{cat}	15	µm	
Activity	16	kg PE/ gr cat.h	
Time scale	2	second	
r_p (µm)	Temperature fluctuation with no *n*-hexane (°C)	Temperature fluctuation with 0.5 bar *n*-hexane (°C)	Difference in fluctuation of particle temperature due to presence of *n*-hexane (°C)
150	29.81	29.38	0.43
300	24.76	23.52	1.24
500	19.08	17.71	1.37
Effect of Activity			
r_{cat}	35	µm	
r_p	500	µm	
Time scale	2	second	
Activity (kg PE/ gr cat.h)	Temperature fluctuation with no *n*-hexane (°C)	Temperature fluctuation with 0.5 bar *n*-hexane (°C)	Difference in fluctuation of particle temperature due to presence of *n*-hexane (°C)
16	21.89	20.41	1.48
8	20.12	18.68	1.44
4	19.47	18.07	1.4
Effect of Time Scale			
r_{cat}	30	µm	
r_p	500	µm	
Activity	16	kg PE/ gr cat.h	
Time scale (second)	Temperature fluctuation with no *n*-hexane (°C)	Temperature fluctuation with 0.5 bar *n*-hexane (°C)	Difference in fluctuation of particle temperature due to presence of *n*-hexane (°C)
2	20.51	19.04	1.47
4	25.95	24.64	1.31
8	29.58	28.67	0.91

As can be seen in this Table, the difference between fluctuation of particle temperature without *n*-hexane and in the presence of *n*-hexane under the aforementioned transition increases with the size of the particle. This can be explained by the solubilization of larger amount of *n*-hexane in larger particle upon its exposure to the colder region. In addition, the effect of heat of sorption on the fluctuation of particle temperature under the defined transition increases slightly by its activity. Finally, with longer time scale of being exposed to the colder region, the particle temperature fluctuation becomes closer to the imposed fluctuation in the bulk temperature while the effect of heat of sorption decreasing.

Based on these results, it is reasonable to conclude that sorption heat of *n*-hexane has a minor effect in fluctuation of the particle temperature during its circulation inside FBR, which is induced from the fluctuation in the bulk gas phase temperature.

6.4. Conclusion

In the current study, the effect of the heat of sorption of *n*-hexane on the thermal behavior of growing polymer particles under different physical circumstances has been investigated. *n*-Hexane is an inert condensing agent that is present in the gas phase during condensed mode operation of gas phase ethylene polymerization. Simulated thermal behavior of the particle during transition period of its temporary exposition to the defluidized region demonstrated that the rate of increase in the particle temperature is lower in the presence of *n*-hexane; as the particle starts to heat up due to the accumulation of polymerization energy, part of this energy is consumed in order to partially desorb the condensable *n*-hexane solubilized in the particle leading to lower rate of particle temperature rise. As a result, it is concluded that the probability of the particle temperature to reach its fusion temperature and consequently the probability of the resultant polymer agglomerate formation due to the local defluidization inside the FBR becomes lower in the presence of condensable *n*-hexane. In addition, using a parametric analysis, it is demonstrated that the effect of heat of sorption becomes more pronounced for polymer particles with higher activity during the initial steps of polymerization. On the other hand, it is observed that the heat of sorption of *n*-hexane has at most a minor effect on fluctuation of the particle temperature during its circulation inside FBR which has been induced from the fluctuation in the surrounding bulk gas phase temperature.

6.5. References

1. Huang, J. C. Estimation of solubility parameter components of solutes and polymers using heat of vaporization and heat of sorption of solutes. *J. Appl. Polym. Sci.* **2009,** *112* (4), 2027-2032.

2. Grolier, J.-P. E.; Boyer, S. A. E. Gas-Polymer Interactions: Key Thermodynamic Data and Thermophysical Properties. In *Polymer Thermodynamics*, Enders, S., Wolf, B. A., Eds.; Springer: Germany, **2011**; p 137.

3. Grolier, J. P. E.; Dan, F.; Boyer, S. A. E.; Orlowska, M.; Randzio, S. L. The Use of Scanning Transitiometry to Investigate Thermodynamic Properties of Polymeric Systems over Extended T and p Ranges. *International Journal of Thermophysics* **2004,** *25* (2), 297-319.

4. Tian, M.; Munk, P. Characterization of Polymer-Solvent Interactions and Their Temperature Dependence Using Inverse Gas Chromatography. *J. Chem. Eng. Data* **1994,** *39* (4), 742-755.

5. Yao, W.; Hu, X.; Yang, Y. Modeling solubility of gases in semicrystalline polyethylene. *J. Appl. Polym. Sci.* **2007,** *103* (3), 1737-1744.

6. Yao, W.; Hu, X.; Yang, Y. Modeling the solubility of ternary mixtures of ethylene, iso-pentane, n-hexane in semicrystalline polyethylene. *J. Appl. Polym. Sci.* **2007,** *104* (6), 3654-3662.

7. Kanellopoulos, V.; Mouratides, D.; Pladis, P.; Kiparissides, C. Prediction of Solubility of Olefins in Polyolefins Using a Combined Equation of State Molecular Dynamics Approach. *Ind. Eng. Chem. Res.* **2006,** *45* (17), 5870-5878.

8. Jin, H. J.; Kim, S.; Yoon, J. S. Solubility of 1-hexene in LLDPE synthesized by (2-MeInd)2ZrCl2/MAO and by Mg(OEt)2/DIBP/TiCl4 TEA. *J. Appl. Polym. Sci.* **2002,** *84* (8), 1566-1571.

9. Moore, S. J.; Wanke, S. E. Solubility of ethylene, 1-butene and 1-hexene in polyethylenes. *Chemical Engineering Science* **2001,** *56* (13), 4121-4129.

10. Michaels, A. S.; Bixler, H. J. Solubility of gases in polyethylene. *J. Polym. Sci.* **1961,** *50* (154), 393-412.

11. Floyd, S.; Choi, K. Y.; Taylor, T. W.; Ray, W. H. Polymerization of olefines through heterogeneous catalysis IV. Modeling of heat and mass transfer resistance in the polymer particle boundary layer. *J. Appl. Polym. Sci.* **1986,** *31* (7), 2231-2265.

12. Chamayou, J. L.; Marissal, D. Polymerisation Control Process. WO 2012/072417 A1, **2012**.

Chapter 7

Significant contributions and perspectives

7. Significant contributions and perspectives

7.1. Major contributions

In the current thesis study, it was intended to investigate the potential effect of the inert condensing agent of *n*-hexane used in condensed mode operation on the solubility of ethylene in produced polyethylene and consequently the quality and rate of gas phase ethylene polymerization on supported catalyst under reactive conditions, for the first time in this field. Performing the set of designed polymerization reaction experiments using a lab-scale stirred-bed gas phase reactor, it is observed that the instantaneous rate of ethylene polymerization increases in the presence of *n*-hexane, thus supporting the initial speculation of the effect of *n*-hexane on the enhancement of the ethylene solubility in polymer. In order to have a better picture and understanding, the averaged instantaneous rate of polymerization in presence of *n*-hexane is normalized with the one without any *n*-hexane. Consequently, this helped to demonstrate that while the effect of *n*-hexane increases proportionally to its partial pressure in the gas phase composition, this effect is more pronounced at the initial steps during the course of polymerization. In addition, by comparing the effect of partial pressure of ethylene on the observed "enhancement" of the instantaneous rate of ethylene polymerization on supported catalyst in presence of *n*-hexane, it is concluded that while the magnitude of promotion in the instantaneous rate of polymerization in presence of *n*-hexane is almost the same during the initial steps of polymerization with both of the partial pressures of ethylene used equal to 7 and 12 bars. However, this enhancement in rate of polymerization due to cosolubility effect of *n*-hexane appears to fade out more rapidly by time during the polymerization with 7 bars of ethylene partial pressure in comparison with the polymerization by 12 bars of reactant ethylene.

The experimental studies in the lab-scale reactors to investigate the effect of changes in the process operating conditions for instance here by varying the gas phase composition during the ethylene polymerization on supported catalyst provide extremely valuable insight and understanding about the expected kinetic and thermal behavior of the studied catalytic system in the commercial scale fluidized bed reactors while experiencing similar imposed changes in the operating condition of the process. However, the reliable experimental studies of gas phase ethylene polymerization process with different gas phase compositions which induce different operating conditions are found to be very time consuming. As a result, being capable to predict how the quality and rate of gas phase ethylene polymerization would evolve upon imposing a change in the process operating condition, here by addition of an ICA to the gas phase composition, appears to be of profound importance and interest from practical point of view during the operation of a FBR.

In order to achieve this level of predictive capability, at the first step, one needs to be able to describe the solubility behavior of ethylene in PE in the presence of the additional solute component of ICA by implementing the related experimental solubility data under equilibrium condition into an appropriate thermodynamic model which is capable to properly capture the speculated cosolubility phenomenon. In the current thesis study for the first time, the Sanchez-Lacombe EOS as one of the most widely applied thermodynamic models in polymer industry is adapted and developed in order to study not only the solubility but also concentration of ethylene in polyethylene in the absence and presence of an inert condensing agent in order to quantify the speculated cosorption phenomenon under the reactive polymerization condition. By incorporating this thermodynamic model to describe the solubility of ethylene in polymer into a single particle model like PFM model to estimate the concentration and temperature gradient through a growing polymer particle, it is ultimately attempted to predict the effect of change in the process operating condition by addition of *n*-hexane as the ICA to the gas phase composition.

Direct application of solubility data obtained experimentally under equilibrium condition for the binary system of ethylene-PE and the ternary system of ethylene-*n*-hexane-PE by implementing into the Sanchez-Lacombe EOS in order to describe the observed enhancement in the rate of ethylene polymerization in the presence of *n*-hexane under the reactive conditions is a novel approach. This methodology is proposed, developed and applied successfully in the current study for the first time in this field while demonstrating the universal potential of this approach to be extended for description of different process operational conditions, for instance, for predicting the effect of other commonly used ICAs on the polymerization rate. It is found that at the later steps of polymerization, in which the growing polymer particle has reached to its thermal stability and the solubility of solutes in the polymer phase are closer to the equilibrium condition, the prediction of the approach developed in the current study matches with the experimental rates of polymerization in an excellent manner of almost perfect fit. This remarkably good predictive capability is in fact originated from the reasonable estimation of the local concentration of reactant ethylene and local temperature inside the particle by the PFM model. In the case of local concentration, in combination with the adapted simplified diffusivity model, it demonstrates the outstanding predictive capability of the Sanchez-Lacombe model which has been developed and fitted to the experimentally obtained set of solubility data in the ternary system of ethylene-*n*-hexane-PE in order to describe the effect of *n*-hexane on the concentration of ethylene in the amorphous phase of polyethylene. However, the general modeling approach at its current development state appears to underestimate the rate of gas phase ethylene polymerization in presence of *n*-hexane at initial steps during the course of polymerization. This discrepancy between the model prediction and experimentally obtained

rates of polymerization on the effect of *n*-hexane is an indicator of some phenomena which are not captured appropriately in the developed model. These phenomena may include (but are not limited to) the evolution of morphology and porosity of catalyst/polymer particle during the polymerization reaction, and the quality and exact mechanism of processes of reactant sorption and diffusion in the absence and presence of ICA during the initial moments of polymerization in which the catalyst/polymer particle rapidly evolves in terms of its size, structure, and thermal behavior.

Finally in the current thesis study, it is demonstrated how the thermal effect associated with the heat of sorption of ICAs can have a positive effect in terms of avoiding particle over-heating under certain circumstances like its temporary exposition to the defluidized regions inside a FBR as a possible undesirable operating condition for this type of reactor set-ups. Simulated thermal behavior of the particle during transition period of its temporary exposition to the defluidized region demonstrated that the rate of increase in the particle temperature is lower in the presence of *n*-hexane; as the particle starts to heat up due to the accumulation of polymerization energy, part of this energy is consumed in order to partially desorb the condensable *n*-hexane solubilized in the particle leading to lower rate of particle temperature rise. As a result, it is concluded that the probability of the particle temperature to reach its fusion temperature and consequently the probability of the resultant polymer agglomerate formation due to the local defluidization inside the FBR becomes lower in the presence of condensable *n*-hexane.

7.2. Perspectives and future works

The observed enhancement in the rate of gas phase ethylene polymerization on supported catalyst in presence of gaseous condensable component of *n*-hexane which is considered to be inert to the polymerization active sites is of profound importance in acquiring a more comprehensive understanding of the "comonomer" effect of α-olefins, in this case 1-hexene. Further polymerization reaction experiments can be designed in order to enhance our perception of the comonomer effect and the relative importance of physical effects (i.e. increase in solubility and diffusivity of ethylene in presence of heavier 1-hexene comonomer) and chemical effects (i.e. modifications in the chemical nature of polymerization active sites) in boosting the rate of ethylene polymerization. This will be achieved by comparing the magnitude of enhancement in the rate of ethylene polymerization in presence of *n*-hexane and 1-hexene, respectively.

In addition, the effect of other inert condensing agents applied in industry (like *iso*-pentane) on the rate of polymerization and properties of produced polymer can be explored in order to provide a better insight on the practical aspects related to the condensed mode operation of gas phase ethylene polymerization.

From modeling perspective, the level of complexity of physical and chemical phenomena which occur simultaneously during the ethylene polymerization on supported catalyst has already been highlighted. However, the general modeling approach which is developed for the first time in the current thesis study can be considered as the first step in moving toward simulator software for polyolefin processes in general and gas phase polyethylene process in particular with real practical functionalities. Such software can be applied in order to predict the change in process operating conditions on the quality and rate of polymerization and consequently the thermal behavior of growing polymer particles and the overall reactor. In order to reach to such a predictive capability for the simulator software, the general modeling approach developed here needs to be improved in two major aspects:

(a) physical aspects:

1. Since after the initial moments during the polymerization, the active sites are surrounded by the produced polymer, as a result an accurate description of solubility of all the species present in the reactor in the polymer is required. This can be achieved by implementing an appropriate thermodynamic model to describe the solubility of the gas phase as a mixture of two or more solute components which has been fitted to the corresponding solubility data in the equilibrium condition.
2. A more precise description of the evolution of morphology and porosity of catalyst/polymer particle would be needed, especially during the initial steps of the polymerization in which the catalyst/polymer particle rapidly evolves in terms of its size, structure, and thermal behavior.

(b) chemical aspects:

A more accurate and comprehensive understanding of the effect of different active species present in the reactor environment on the intrinsic kinetic behavior at the active sites of catalytic system being used would also be of great importance in order to enhance the quality of the predicted trend upon imposing a change in process condition.

Appendix A

Sanchez-Lacombe EOS

Model Development

A. Sanchez-Lacombe EOS

In this Appendix, using Sanchez-Lacombe equation of state, the details of mathematical formulation to derive the interested properties related to the sorption phenomenon is presented. The formulations for both of the binary and ternary systems are provided.

Here, first we briefly describe the Sanchez-Lacombe equation of state and its parameters. After, the details of the calculations for binary and ternary systems are provided to derive the properties of interest.

A.1. Description of Sanchez-Lacombe model

The Sanchez-Lacombe (SL) EOS is

$$\bar{\rho}^2 + \bar{P} + \bar{T}\left[ln(1-\bar{\rho}) + \left(1-\frac{1}{r}\right)\bar{\rho}\right] = 0 \qquad (A.1)$$

where $\bar{T}, \bar{P}, \bar{V}$, and $\bar{\rho}$ are the reduced temperature, pressure, volume, and density respectively which are defined as follows

$$\bar{T} = T/T^*, \qquad T^* = \varepsilon^*/R_g \qquad (A.2)$$

$$\bar{P} = P/P^*, \qquad P^* = \varepsilon^*/v^* \qquad (A.3)$$

$$\bar{\rho} = \rho/\rho^* = 1/\bar{V} = V^*/V, \qquad V^* = N(rv^*) \text{ and } \rho^* = MW/(rv^*) \qquad (A.4)$$

where ε^* is the mer-mer interaction energy, v^*, is the closed packed molar volume of a mer, *MW* is molecular weight, *N* is number of molecules, *r* is the number of sites (mers) a molecule occupies in the lattice, and R_g is the universal gas constant. The parameters ε^*,v^*, and *r* are used to define T^*, P^*, and ρ^* which are the characteristic temperature, pressure, and close-packed mass density.

With a mixture of components, it is necessary to define combining rules for estimation of ε^*_{mix}, v^*_{mix}, and r_{mix} to be able to use the equation of state to calculate the properties of mixture. The *"van der Waals"* mixing rule is chosen and applied in our study.

For characteristic closed-packed molar volume of a "mer" of the mixture, v^*_{mix}, the so called *"van der Waals"* mixing rule is defined as

$$v^*_{mix} = \sum_i \sum_j \phi_i \phi_j v^*_{ij} \qquad (A.5)$$

with

$$v_{ij}^{*} = \frac{v_{ii}^{*} + v_{jj}^{*}}{2}\left(1 - n_{ij}\right) \qquad (A.6)$$

where n_{ij} corrects the deviation from the arithmetic mean and subscripts *i* and *j* are the components in the solution. The closed-packed volume fraction of the *i*th component at the limit of zero temperature or incompressible state, ϕ_i is defined as

$$\phi_i = \frac{\omega_i}{\rho_i^{*} v_i^{*}} \Big/ \sum_j \left(\frac{\omega_j}{\rho_j^{*} v_j^{*}}\right) \qquad (A.7)$$

where ω_i is the mass fraction of the component *i* in the mixture.

The mixing rule for the characteristic interaction energy for the mixture is defined as

$$\varepsilon_{mix}^{*} = \frac{1}{v_{mix}^{*}} \sum_i \sum_j \phi_i \phi_j \varepsilon_{ij}^{*} v_{ij}^{*} \qquad (A.8)$$

with

$$\varepsilon_{ij}^{*} = \left(\varepsilon_{ii}^{*} \varepsilon_{jj}^{*}\right)^{0.5} (1 - k_{ij}) \qquad (A.9)$$

where ε_{ii} and ε_{jj} are the characteristic mer-mer interaction energies for components *i* and *j*, and k_{ij} is a mixture parameter that accounts for specific binary interactions between components *i* and *j*. Finally, the mixing rule for the number of sites (mers) occupied by a molecule of the mixture, r_{mix}, is given by

$$\frac{1}{r_{mix}} = \sum_j \frac{\phi_j}{r_j} \qquad (A.10)$$

where r_j is the number of sites occupied by molecule *j* in the lattice.

In most of the applications used for Sanchez-Lacombe model, the only binary interaction parameter used for fitting the mixture experimental data to model is k_{ij} while n_{ij} assumed to be equal to zero. It will be the same for all of our related calculations and it is assumed $n_{ij}=0$ while k_{ij} will be the experimentally adjusted parameter describing the interaction of two components.

For calculation of sorption equilibrium for polymer-solvent system, the expression for chemical potential of component *i* in each phase of the mixture is also required given by following equation in SL EOS

$$\mu_i = R_g T \left[\ln \phi_i + \left(1 - \frac{r_i}{r}\right)\right] + \qquad (A.11)$$

$$r_i\left\{-\bar{\rho}\left[\frac{2}{v^*}\left(\sum_j \phi_j \upsilon_{ij}^* \varepsilon_{ij}^* - \varepsilon^* \sum_j \phi_j \upsilon_{ij}^*\right) + \varepsilon^*\right] + \frac{R_g T}{\bar{\rho}}\left[(1-\bar{\rho})ln(1-\bar{\rho}) + \frac{\bar{\rho}}{r_i} ln\bar{\rho}\right] + \frac{P}{\bar{\rho}}\left(2\sum_j \phi_j \upsilon_{ij}^* - \upsilon^*\right)\right\}$$

To avoid the possible confusion, it is useful here to give an explanation about the usage of the terms "component" and "phase". Let's consider a gas "phase" which is in contact and equilibrium with a polymer "phase". It is possible for each of the "phases" to be constituted of different "components". In the simple case of a binary mixture of volatile solute and polymer "components", we will have two phases in equilibrium; gas "phase" which is constituted of only volatile solute component and polymer "phase" which is constituted of both polymer and solute "components".

In the notation used here, the superscript refers to the phase of property while subscript refers to the component which the property belongs to. For example, μ_i^{pol}, refers to the chemical potential of *i*th *component* in the polymer *phase*.

The other point which needs clarification is that the sorption of solute species is assumed to take place only in the amorphous phase of the polymer, while the crystalline phase is assumed to be impenetrable to the solute species.

A.2. Binary systems

In the binary system described below, the subscript *1* refers to the solute component and subscript *2* refers to the polymer component. The first objective is to calculate the extent of sorption of specific solute in equilibrium with the polymer at specific temperature and pressure (*T*, *P*). The solute and polymer characteristic parameters are T^*_1, P^*_1, ρ^*_1 and T^*_2, P^*_2, and ρ^*_2 , respectively. The interaction parameter of k_{12} is taken from the available literature in which it is experimentally determined. The rest of the properties of interest are consequently determined from the extent of sorption, as described hereunder.

At first step the reduced density of the gas phase, $\bar{\rho}^{gas}$, is calculated. It is assumed that no polymer exists in the gas phase. As a result, the reduced density of gas phase will be equal to the reduced density of "pure" volatile component existing in the gas phase or in other words$\bar{\rho}^{gas} = \bar{\rho}_1{}^{gas}$.

The reduced density of gas phase is found by solving the equation (A.12), which can easily be obtained by rewriting equation (4.1).

$$\bar{\rho}_1{}^{gas} = 1 - \exp\left(-\frac{(\bar{\rho}_1{}^{gas})^2}{\bar{T}_1} - \frac{\overline{P_1}}{\overline{T_1}} - \left(1 - \frac{1}{r_1}\right)\bar{\rho}_1{}^{gas}\right) \qquad (A.12)$$

Next, the chemical potential of component *1* in the gas phase is determined. The chemical potential of a pure component in a phase can be easily calculated from equation (4.11) to be equal to:

$$\mu_1^{gas} = r_1\left\{-\bar{\rho}_1{}^{gas}\varepsilon_1^* + \frac{R_gT}{\bar{\rho}_1{}^{gas}}\left[(1-\bar{\rho}_1{}^{gas})ln(1-\bar{\rho}_1{}^{gas}) + \frac{\bar{\rho}_1{}^{gas}}{r_1}ln\bar{\rho}_1{}^{gas}\right] + \frac{Pv_1^*}{\bar{\rho}_1{}^{gas}}\right\} \qquad (A.13)$$

The closed-packed volume fraction of solute in the polymer phase, $\phi_1{}^{pol}$, and the reduced density of polymer phase, $\bar{\rho}^{\,pol}$, are consequently obtained by simultaneous solution of the two following non-linear equations. First equation is the Sanchez-Lacombe EOS for the polymer phase (4.1), and the second equation is obtained from the thermodynamic principle that the chemical potential of each components are equal in all phases at the equilibrium state. In other words, $\mu_1^{pol} = \mu_1^{gas}$.

In order to write the Sanchez-Lacombe EOS for polymer phase, being constituted of two components, it is necessary to apply the mixing rules, as described before.

For characteristic closed-packed molar volume of a "mer" of the polymer phase as a mixture of solute and polymer molecules, it is possible derive equation (A.14), considering $\phi_1^{pol} + \phi_2^{pol} = 1$ and by expanding the equation (4.5)

$$v_{mix}^*{}^{pol} = \alpha\phi_1^{pol} + \beta \qquad (A.14)$$

in which α and β are defined as

$$\alpha = v_1^* - v_2^* \qquad (A.14.1)$$
$$\beta = v_2^* \qquad (A.14.2)$$

Similarly it is possible to derive equation (A.15) for interaction energy of mixture "mer"s, starting from equation (4.8).

$$\varepsilon_{mix}^*{}^{pol} = \frac{A\phi_1^{pol\,2} + B\phi_1^{pol} + C}{\alpha\phi_1^{pol} + \beta} \qquad (A.15)$$

in which *A*, *B*, and *C* are clustered functions defined as

$$A = \varepsilon_1^* v_1^* + \varepsilon_2^* v_2^* - \varepsilon_{12}^*(v_1^* + v_2^*) \qquad (A.15.1)$$
$$B = \varepsilon_{12}^*(v_1^* + v_2^*) - 2\varepsilon_2^* v_2^* \qquad (A.15.2)$$
$$C = \varepsilon_2^* v_2^* \qquad (A.15.3)$$

Finally using equation (4.10) and considering that $r_2 >> r_1$, it is possible to derive the equation (A.16) for number of sites (mers) occupied by a molecule of the mixture

$$\frac{1}{r_{mix}{}^{pol}} = \frac{\phi_1^{pol}}{r_1} \qquad \text{(A.16)}$$

By combining equations (A.14), (A.15), and (A.16) with (4.2) and (4.3), and substituting them into equation (4.1), the Sanchez-Lacombe EOS for polymer phase as a mixture of polymer and solute molecules are obtained, as equation (A.17). The only unknown parameters in this equation are reduced density of polymer phase, $\bar{\rho}^{\,pol}$, and closed-packed volume fraction of solute molecules in the polymer phase, $\phi_1{}^{pol}$.

$$\bar{\rho}^{pol\,2} + P\frac{\left(\alpha\phi_1^{pol}+\beta\right)^2}{A\phi_1^{pol\,2}+B\phi_1^{pol}+C} + R_gT\frac{\alpha\phi_1^{pol}+\beta}{A\phi_1^{pol\,2}+B\phi_1^{pol}+C}\left[\ln\left(1-\bar{\rho}^{pol}\right)+\left(1-\frac{\phi_1^{pol}}{r_1}\right)\bar{\rho}^{pol}\right]=0 \qquad \text{(A.17)}$$

Similarly by combining (A.14), (A.15), and (A.16) with (4.2) and (4.3) and substituting them into equation (4.11), the chemical potential of component *1* in the polymer phase is obtained which is equal to its chemical potential in the gas phase. As a result the second equation of (A.18) is obtained in which $\bar{\rho}^{\,pol}$ and $\phi_1{}^{pol}$ are only unknowns.

$$R_gT\left[ln\phi_1^{pol}+1-\phi_1^{pol}\right]+ \qquad \text{(A.18)}$$
$$r_1\left\{-\bar{\rho}^{pol}\left[\frac{2}{\alpha\phi_1^{pol}+\beta}\left(\left(M'\phi_1^{pol}+N'\right)-\left(\frac{A\phi_1^{pol\,2}+B\phi_1^{pol}+C}{\alpha\phi_1^{pol}+\beta}\right)\left(M''\phi_1^{pol}+N''\right)\right)+\left(\frac{A\phi_1^{pol\,2}+B\phi_1^{pol}+C}{\alpha\phi_1^{pol}+\beta}\right)\right]+\right.$$
$$\left.\frac{R_gT}{\bar{\rho}^{pol}}\left[\left(1-\bar{\rho}^{pol}\right)\ln\left(1-\bar{\rho}^{pol}\right)+\frac{\bar{\rho}^{pol}}{r_1}ln\bar{\rho}^{pol}\right]+\frac{P}{\bar{\rho}^{pol}}\left(2\left(M''\phi_1^{pol}+N''\right)-\left(\alpha\phi_1^{pol}+\beta\right)\right)\right\}-\mu_1^{gas}=0$$

in which,

$$M' = v_1^*\varepsilon_1^* - v_{12}^*\varepsilon_{12}^* \qquad \text{(A.18.1)}$$
$$N' = v_{12}^*\varepsilon_{12}^* \qquad \text{(A.18.2)}$$
$$M'' = v_1^* - v_{12}^* \qquad \text{(A.18.3)}$$
$$N'' = v_{12}^* \qquad \text{(A.18.4)}$$

By simultaneous solution of equations (A.17) and (A.18), the reduced polymer phase density, $\bar{\rho}^{\,pol}$, and closed-packed volume fraction of solute molecules in the polymer phase, ϕ_1^{pol} are obtained. All of the properties of interest related to the sorption phenomenon are calculated consequently from $\bar{\rho}^{\,pol}$ and ϕ_1^{pol} as explained below.

A.2.1. Solubility in polymer

According to equation (4.7), the mass fraction of solute in the amorphous polymer phase is calculated from

$$\omega_{1,am} = \frac{\left(\frac{\phi_1^{pol}}{1-\phi_1^{pol}}\right)}{\left(\frac{\rho_2^* v_2^*}{\rho_1^* v_1^*}\right) + \left(\frac{\phi_1^{pol}}{1-\phi_1^{pol}}\right)} [=] \frac{gr\ sol.1}{gr\ (sol.1 + am.pol)} \qquad (A.19)$$

The solubility of the solute species in the amorphous polymer phase can be calculated from

$$S_{1,am} = \frac{\omega_{1,am}}{1-\omega_{1,am}} [=] \frac{gr\ sol.1}{gr\ am.pol} \qquad (A.20)$$

The extent of solubility in the total polymer (including amorphous and crystalline phases) can be calculated from

$$S_{1,tot} = S_{1,am}(1-\chi) [=] \frac{gr\ sol.1}{gr\ (am.pol+crys.pol)} \qquad (A.21)$$

in which, χ, is the weight-based crystallinity of the polymer particle.

A.2.2. Swelling of polymer

In order to estimate the extent of swelling of amorphous polymer phase because of sorption of solute species, firstly, the initial density of the amorphous polymer at the same temperature and pressure is needed to be calculated. This is done by solving equation (A.22) for reduced density of pure amorphous polymer similar to the equation (A.12).

$$\overline{\rho_2} = 1 - \exp\left(-\frac{\overline{\rho_2}^2}{\overline{T_2}} - \frac{\overline{P_2}}{\overline{T_2}} - \overline{\rho_2}\right) \qquad (A.22)$$

where, $\overline{\rho_2}$, is the reduced amorphous polymer density. According to its definition, the amorphous polymer density will be equal to $\overline{\rho_2}\rho_2^*$.

On the other hand, in order to estimate the density of the polymer phase at equilibrium sorption (including solute and polymer components), the characteristic density of the polymer phase is defined as

$$\rho^* = \frac{1}{\left(\frac{\omega_{1,am}}{\rho_1^*}\right) + \left(\frac{1-\omega_{1,am}}{\rho_2^*}\right)} \quad \text{(A.23)}$$

and consequently the density of the amorphous polymer phase will be equal to $\rho^*\bar{\rho}^{\,pol}$.

The extent of swelling of polymer amorphous phase can be obtained by simple mathematical manipulations to be equal to

$$SW_{am} = \frac{\rho_2^*\overline{\rho_2}\left(1+S_{1,am}\right)}{\rho^*\bar{\rho}^{\,pol}} - 1 \quad \text{(A.24)}$$

$$\frac{\rho_2^*\overline{\rho_2}\left(1+S_{1,am}\right)}{\rho^*\bar{\rho}^{\,pol}}[=]\frac{lit\ (am.pol + sol.1)}{lit\ (am.pol)} \quad \text{(A.24.1)}$$

The extent of total polymer swelling considering no solubility in the crystalline phase can be calculated to be equal to

$$SW_{tot} = \frac{\chi v_c + \frac{(1-\chi)\left(1+S_{1,am}\right)}{\rho^*\bar{\rho}^{\,pol}}}{\chi v_c + \frac{(1-\chi)}{\rho_2^*\overline{\rho_2}}} - 1 \quad \text{(A.25)}$$

$$\frac{\chi v_c + \frac{(1-\chi)\left(1+S_{1,am}\right)}{\rho^*\bar{\rho}^{\,pol}}}{\chi v_c + \frac{(1-\chi)}{\rho_2^*\overline{\rho_2}}}[=]\frac{lit\ (am.pol + crys.pol + sol.1)}{lit\ (am.pol + crys.pol)} \quad \text{(A.25.1)}$$

in which, v_c, is the specific volume of fully crystalline polymer phase. For fully crystalline polyethylene $v_c = 0.001\ m^3/kg$.

A.2.3. Concentration of solute species in the polymer phase

The concentration of solute species in the amorphous phase of polymer can be easily calculated from

$$C_{1,am} = \frac{\omega_{1,am}\,\rho^*\bar{\rho}^{\,pol}}{MW_1}[=]\frac{mol\ sol.1}{lit\ (am.pol+sol.1)} \quad \text{(A.26)}$$

in which, MW_1, is molecular weight of solute species *1* having unite of *gr/mol*.

In order to estimate the concentration of species *1* in the whole polymer including amorphous and crystalline phase, first the volume-based crystallinity of polymer is calculated

$$\chi_v = \frac{\chi v_c}{\chi v_c + \frac{(1-\chi)}{\rho_2^* \overline{\rho_2}}} [=] \frac{lit\ crys.pol}{lit\ (crys.pol + am.pol)} \qquad (A.27)$$

And the concentration of component *1* in total polymer phase can be estimated by

$$C_{1,tot} = C_{1,am} \frac{(1+SW_{am})}{(1+SW_{tot})} (1-\chi_v)[=] \frac{mol\ sol.1}{lit\ (am.pol + crys.pol + sol.1)} \qquad (A.28)$$

A.2.4. The density change in the polymer particle due to the sorption

According to the equation (A.21), the ratio of mass of polymer particles after and before sorption is given by

$$\frac{m_{\substack{swollen \\ polymer}}}{m_{\substack{non-swollen \\ polymer}}} = 1 + S_{1,tot}[=] \frac{gr\ (sol. + am.pol + crys.pol)}{gr\ (am.pol + crys.pol)} \qquad (A.29)$$

and according to the equation (A.25), the ratio between volumes of swollen and non-swollen polymer particles will be given by

$$\frac{V_{\substack{swollen \\ polymer}}}{V_{\substack{non-swollen \\ polymer}}} = 1 + SW_{tot}[=] \frac{lit\ (sol. + am.pol + crys.pol)}{lit\ (am.pol + crys.pol)} \qquad (A.30)$$

The change in the density of polymer particles (including amorphous and crystalline phases) due to the sorption is

$$\rho_{change} = \frac{\rho_{\substack{swollen \\ polymer}}}{\rho_{\substack{non-swollen \\ polymer}}} - 1 = \frac{\frac{m_{\substack{swollen \\ polymer}}}{V_{\substack{swollen \\ polymer}}}}{\frac{m_{\substack{non-swollen \\ polymer}}}{V_{\substack{non-swollen \\ polymer}}}} - 1 = \frac{\frac{m_{\substack{swollen \\ polymer}}}{m_{\substack{non-swollen \\ polymer}}}}{\frac{V_{\substack{swollen \\ polymer}}}{V_{\substack{non-swollen \\ polymer}}}} - 1 \qquad (A.31)$$

By substituting equation (A.29) and (A.30) into equation (A.31), the change in the density of polymer particles (including amorphous and crystalline phases) due to the sorption will be given by

$$\rho_{change} = \frac{1 + S_{1,tot}}{1 + SW_{tot}} - 1 \qquad (A.32)$$

A.3. Ternary systems

In the ternary system described below, the subscript *1* and *2* refers to the solute molecules; component *1* is the lighter one in the gas phase. Subscript *3* refers to the polymer component. Here, the primary objective is to calculate the extent of solubility of solute components in the polymer phase, knowing the partial pressure of solute components (P_1, P_2) and total pressure of $P = P_1+P_2$ at specific temperature (T). All of the other properties of interest are calculated from the extent of solubility for solute components afterwards.

The characteristic parameters of the solutes (*1, 2*) are T^*_1, P^*_1, ρ^*_1 and T^*_2, P^*_2, ρ^*_2, respectively and for polymer component (*3*), the characteristic parameters are T^*_3, P^*_3, ρ^*_3. The pair interaction parameters of k_{12}, k_{13}, and k_{23} are taken from the available literature, in which they are determined experimentally.

At first step, it is necessary to calculate the chemical potential of solutes *1* and *2* in the gas phase. These values will later be used in the equilibrium condition, in which the chemical potential of each of the components are equal in all phases. In other words, $\mu_1^{gas} = \mu_1^{pol}$ and $\mu_2^{gas} = \mu_2^{pol}$.

Knowing the partial pressure of component *1* and *2* in the gas phase at the specific temperature, the reduced density of each component in the gas phase is calculated by solving equation (A.33) and (A.34), respectively.

$$\bar{\rho}_1{}^{gas} = 1 - \exp\left(-\frac{(\bar{\rho}_1{}^{gas})^2}{\overline{T_1}} - \frac{\overline{P_1}}{\overline{T_1}} - \left(1 - \frac{1}{r_1}\right)\bar{\rho}_1{}^{gas}\right) \qquad (A.33)$$

$$\bar{\rho}_2{}^{gas} = 1 - \exp\left(-\frac{(\bar{\rho}_2{}^{gas})^2}{\overline{T_2}} - \frac{\overline{P_2}}{\overline{T_2}} - \left(1 - \frac{1}{r_2}\right)\bar{\rho}_2{}^{gas}\right) \qquad (A.34)$$

The density of component *1* and *2* in the gas phase will be equal to

$$\rho_1{}^{gas} = \rho_1^* \bar{\rho}_1{}^{gas} \qquad (A.35)$$

$$\rho_2^{gas} = \rho_2^* \bar{\rho}_2{}^{gas} \qquad (A.36)$$

At given volume of the gas phase mixture, the mass fraction of component *1* and *2* in the gas phase is given by

$$\omega_1^{gas} = \frac{\rho_1^{gas}}{\rho_1^{gas} + \rho_2^{gas}} \quad (A.37)$$

$$\omega_2^{gas} = \frac{\rho_2^{gas}}{\rho_1^{gas} + \rho_2^{gas}} \quad (A.38)$$

As a result, according to the equation (4.7), the closed packed volume fraction of components in the gas phase can be found by

$$\phi_1^{\text{gas}} = \frac{\frac{\left(\rho_1{}^{gas}/\rho_1^{gas} + \rho_2^{gas}\right)}{\rho_1^* v_1^*}}{\frac{\left(\rho_1{}^{gas}/\rho_1^{gas} + \rho_2^{gas}\right)}{\rho_1^* v_1^*} + \frac{\left(\rho_2{}^{gas}/\rho_1^{gas} + \rho_2^{gas}\right)}{\rho_2^* v_2^*}} \quad (A.39)$$

Assuming no polymer molecules in the gas phase, $\phi_2^{\text{gas}} = 1 - \phi_1^{\text{gas}}$.

The reduced gas phase density, $\bar{\rho}^{gas}$, is calculated by solving equation (A.40)

$$\bar{\rho}^{gas} = 1 - \exp\left(-\frac{\bar{\rho}^{gas2}}{\bar{T}^{gas}} - \frac{\bar{P}^{gas}}{\bar{T}^{gas}} - \left(1 - \frac{1}{r^{gas}{}_{mix}}\right)\bar{\rho}^{gas}\right) \quad (A.40)$$

in which

$$\bar{T}^{gas} = R_g T \frac{\alpha\phi_1^{gas} + \beta}{A\phi_1^{gas2} + B\phi_1^{gas} + C} \quad (A.40.1)$$

$$\bar{P}^{gas} = P \frac{\left(\alpha\phi_1^{gas} + \beta\right)^2}{A\phi_1^{gas2} + B\phi_1^{gas} + C} \quad (A.40.2)$$

$$\frac{1}{r^{gas}{}_{mix}} = \frac{\phi_1^{gas}}{r_1} + \frac{\left(1 - \phi_1^{gas}\right)}{r_2} \quad (A.40.3)$$

The clustered function of *α*, *β*, *A*, *B*, and *C* are defined according to the equations (A.14) and (A.15).

After calculation of closed-packed volume fraction of components in the gas phase ($\phi_1^{\text{gas}}$and ϕ_2^{gas}) and the reduced gas phase density ($\bar{\rho}^{gas}$), it is possible to calculate chemical potential of components *1* and *2* in the gas phase from equations (A.41) and (A.42), respectively.

$$\mu_1^{gas} = R_g T\left[ln\phi_1^{gas} + 1 - \frac{r_1}{r^{gas}{}_{mix}}\right] \quad (A.41)$$

$$+ r_1 \left\{ \begin{array}{l} -\bar{\rho}^{gas}\left[\frac{2}{{v^*}^{gas}{}_{mix}}\left(\left(\phi_1^{gas} v_1^* \varepsilon_1^* + \phi_2^{gas} v_{12}^* \varepsilon_{12}^*\right) - {\varepsilon^*}^{gas}{}_{mix}\left(\phi_1^{gas} v_1^* + \phi_2^{gas} v_{12}^*\right)\right) + {\varepsilon^*}^{gas}{}_{mix}\right] + \\ \frac{R_g T}{\bar{\rho}^{gas}}\left[(1-\bar{\rho}^{gas})\ln(1-\bar{\rho}^{gas}) + \frac{\bar{\rho}^{gas}}{r_1} ln\bar{\rho}^{gas}\right] + \frac{P}{\bar{\rho}^{gas}}\left[2\left(\phi_1^{gas} v_1^* + \phi_2^{gas} v_{12}^*\right) - {v^*}^{gas}{}_{mix}\right] \end{array} \right\}$$

$$\mu_2^{gas} = R_g T\left[ln\phi_2^{gas} + 1 - \frac{r_2}{{r^{gas}}_{mix}}\right] \qquad (A.42)$$

$$+ r_2 \left\{ \begin{array}{l} -\bar{\rho}^{gas}\left[\frac{2}{{v^*}^{gas}{}_{mix}}\left(\left(\phi_1^{gas} v_{12}^* \varepsilon_{12}^* + \phi_2^{gas} v_2^* \varepsilon_2^*\right) - {\varepsilon^*}^{gas}{}_{mix}\left(\phi_1^{gas} v_{12}^* + \phi_2^{gas} v_2^*\right)\right) + {\varepsilon^*}^{gas}{}_{mix}\right] + \\ \frac{R_g T}{\bar{\rho}^{gas}}\left[(1-\bar{\rho}^{gas})\ln(1-\bar{\rho}^{gas}) + \frac{\bar{\rho}^{gas}}{r_2} ln\bar{\rho}^{gas}\right] + \frac{P}{\bar{\rho}^{gas}}\left[2\left(\phi_1^{gas} v_{12}^* + \phi_2^{gas} v_2^*\right) - {v^*}^{gas}{}_{mix}\right] \end{array} \right\}$$

in which ${v^*}^{gas}{}_{mix}$ and ${\varepsilon^*}^{gas}{}_{mix}$ are defined as

$${v^*}^{gas}{}_{mix} = \alpha\phi_1^{gas} + \beta \qquad (A.43)$$

$${\varepsilon^*}^{gas}{}_{mix} = \frac{A\phi_1^{gas\,2} + B\phi_1^{gas} + C}{\alpha\phi_1^{gas} + \beta} \qquad (A.44)$$

The clustered function of α, β, A, B, and C are defined according to the equations (A.14) and (A.15).

Similar to binary system described before, it is necessary to define the characteristic parameters for the polymer phase as the mixture of solute (*1, 2*) and polymer (*3*) components. By expanding equation (4.5) and considering $\phi_1^{pol} + \phi_2^{pol} + \phi_3^{pol} = 1$, the characteristic closed-packed molar volume of "mer" of polymer phase mixture can be written as

$${v_{mix}^*}^{pol} = \sigma_1\phi_1^{pol} + \sigma_2\phi_2^{pol} + \sigma_3 \qquad (A.45)$$

in which,

$$\sigma_1 = v_1^* - v_3^* \qquad (A.45.1)$$

$$\sigma_2 = v_2^* - v_3^* \qquad (A.45.2)$$

$$\sigma_3 = v_3^* \qquad (A.45.3)$$

Similarly, for the characteristic mer-mer interaction energy of polymer phase mixture, it is possible to obtain equation (A.46) by expanding equation (4.8)

$${\varepsilon_{mix}^*}^{pol} = \frac{A_1\phi_1^{pol\,2} + A_2\phi_2^{pol\,2} + A_{12}\phi_1^{pol}\phi_2^{pol} + B_1\phi_1^{pol} + B_2\phi_2^{pol} + C_1}{\sigma_1\phi_1^{pol} + \sigma_2\phi_2^{pol} + \sigma_3} \qquad (A.46)$$

in which,

$$A_1 = \varepsilon_1^* v_1^* + \varepsilon_3^* v_3^* - 2\varepsilon_{13}^* v_{13}^* \quad (A.46.1)$$

$$A_2 = \varepsilon_2^* v_2^* + \varepsilon_3^* v_3^* - 2\varepsilon_{23}^* v_{23}^* \quad (A.46.2)$$

$$A_{12} = 2(\varepsilon_{12}^* v_{12}^* - \varepsilon_{13}^* v_{13}^* - \varepsilon_{23}^* v_{23}^* + \varepsilon_3^* v_3^*) \quad (A.46.3)$$

$$B_1 = 2\varepsilon_{13}^* v_{13}^* - 2\varepsilon_3^* v_3^* \quad (A.46.4)$$

$$B_2 = 2\varepsilon_{23}^* v_{23}^* - 2\varepsilon_3^* v_3^* \quad (A.46.5)$$

$$C_1 = \varepsilon_3^* v_3^* \quad (A.46.6)$$

Finally the number of sites (mers) occupied in the lattice by a molecule of polymer phase mixture will be given by equation (A.47) assuming $r_3 >> r_1, r_2$.

$$\frac{1}{r_{mix}^{pol}} = \frac{\phi_1^{pol}}{r_1} + \frac{\phi_2^{pol}}{r_2} \quad (A.47)$$

The Sanchez-Lacombe EOS for polymer phase is obtained by substituting equations (A.45), (A.46), and (A.47) into the equation (4.1) as given by equation (A.48)

$$\bar{\rho}^{pol\,2} + P\frac{\left(\sigma_1\phi_1^{pol} + \sigma_2\phi_2^{pol} + \sigma_3\right)^2}{A_1\phi_1^{pol\,2} + A_2\phi_2^{pol\,2} + A_{12}\phi_1^{pol}\phi_2^{pol} + B_1\phi_1^{pol} + B_2\phi_2^{pol} + C_1} + R_gT\frac{\sigma_1\phi_1^{pol} + \sigma_2\phi_2^{pol} + \sigma_3}{A_1\phi_1^{pol\,2} + A_2\phi_2^{pol\,2} + A_{12}\phi_1^{pol}\phi_2^{pol} + B_1\phi_1^{pol} + B_2\phi_2^{pol} + C_1}\left[ln\left(1-\bar{\rho}^{pol}\right) + \left(1 - \frac{\phi_1^{pol}}{r_1} - \frac{\phi_2^{pol}}{r_2}\right)\bar{\rho}^{pol}\right] = 0 \quad (A.48)$$

in which, reduced polymer phase density, $\bar{\rho}^{pol}$, and closed packed volume fractions of solute components in the polymer phase, $\phi_1^{pol}$and ϕ_2^{pol} are the only unknowns.

The other two equations needed are provided by the thermodynamic rule for the equilibrium condition as mentioned earlier; i.e. $\mu_1^{gas} = \mu_1^{pol}$ and $\mu_2^{gas} = \mu_2^{pol}$. These equations are obtained by substituting equations (A.45), (A.46), and (A.47) into equation (4.11).

For component *1*, the equilibrium condition is given by

$$R_gT\left[ln\phi_1^{pol} + 1 - r_1\left(\frac{\phi_1^{pol}}{r_1} + \frac{\phi_2^{pol}}{r_2}\right)\right] + r_1\left\{-\bar{\rho}^{pol}\left[\frac{2}{\sigma_1\phi_1^{pol} + \sigma_2\phi_2^{pol} + \sigma_3}\left(\left(G_1\phi_1^{pol} + G_2\phi_2^{pol} + G_3\right) - \left(\frac{A_1\phi_1^{pol\,2} + A_2\phi_2^{pol\,2} + A_{12}\phi_1^{pol}\phi_2^{pol} + B_1\phi_1^{pol} + B_2\phi_2^{pol} + C_1}{\sigma_1\phi_1^{pol} + \sigma_2\phi_2^{pol} + \sigma_3}\right)\left(g_1\phi_1^{pol} + g_2\phi_2^{pol} + g_3\right)\right) + \right. \quad (A.49)$$

$$\left(\frac{A_1\phi_1^{pol^2}+A_2\phi_2^{pol^2}+A_{12}\phi_1^{pol}\phi_2^{pol}+B_1\phi_1^{pol}+B_2\phi_2^{pol}+C_1}{\sigma_1\phi_1^{pol}+\sigma_2\phi_2^{pol}+\sigma_3}\right)\Bigg] + \frac{R_gT}{\bar{\rho}^{pol}}\left[\left(1-\bar{\rho}^{pol}\right)\ln\left(1-\bar{\rho}^{pol}\right)+\frac{\bar{\rho}^{pol}}{r_1}ln\bar{\rho}^{pol}\right]+$$

$$\frac{P}{\bar{\rho}^{pol}}\left[2\left(g_1\phi_1^{pol}+g_2\phi_2^{pol}+g_3\right)-\left(\sigma_1\phi_1^{pol}+\sigma_2\phi_2^{pol}+\sigma_3\right)\right]\Bigg\}-\mu_1^{gas}=0$$

in which G_1, G_2, G_3, g_1, g_2, and g_3 are clustered functions given by

$$G_1 = v_1^*\varepsilon_1^* - v_{13}^*\varepsilon_{13}^* \quad (A.49.1)$$

$$G_2 = v_{12}^*\varepsilon_{12}^* - v_{13}^*\varepsilon_{13}^* \quad (A.49.2)$$

$$G_3 = v_{13}^*\varepsilon_{13}^* \quad (A.49.3)$$

$$g_1 = v_1^* - v_{13}^* \quad (A.49.4)$$

$$g_2 = v_{12}^* - v_{13}^* \quad (A.49.5)$$

$$g_3 = v_{13}^* \quad (A.49.6)$$

and for component *2*, the equilibrium condition is given by

$$R_gT\left[ln\phi_2^{pol}+1-r_2\left(\frac{\phi_1^{pol}}{r_1}+\frac{\phi_2^{pol}}{r_2}\right)\right] \quad (A.50)$$

$$+r_2\Bigg\{-\bar{\rho}^{pol}\Bigg[\frac{2}{\sigma_1\phi_1^{pol}+\sigma_2\phi_2^{pol}+\sigma_3}\Bigg(\left(H_1\phi_1^{pol}+H_2\phi_2^{pol}+H_3\right)-$$

$$\left(\frac{A_1\phi_1^{pol^2}+A_2\phi_2^{pol^2}+A_{12}\phi_1^{pol}\phi_2^{pol}+B_1\phi_1^{pol}+B_2\phi_2^{pol}+C_1}{\sigma_1\phi_1^{pol}+\sigma_2\phi_2^{pol}+\sigma_3}\right)\left(h_1\phi_1^{pol}+h_2\phi_2^{pol}+h_3\right)\Bigg)+$$

$$\left(\frac{A_1\phi_1^{pol^2}+A_2\phi_2^{pol^2}+A_{12}\phi_1^{pol}\phi_2^{pol}+B_1\phi_1^{pol}+B_2\phi_2^{pol}+C_1}{\sigma_1\phi_1^{pol}+\sigma_2\phi_2^{pol}+\sigma_3}\right)\Bigg] + \frac{R_gT}{\bar{\rho}^{pol}}\left[\left(1-\bar{\rho}^{pol}\right)\ln\left(1-\bar{\rho}^{pol}\right)+\frac{\bar{\rho}^{pol}}{r_2}ln\bar{\rho}^{pol}\right]+$$

$$\frac{P}{\bar{\rho}^{pol}}\left[2\left(h_1\phi_1^{pol}+h_2\phi_2^{pol}+h_3\right)-\left(\sigma_1\phi_1^{pol}+\sigma_2\phi_2^{pol}+\sigma_3\right)\right]\Bigg\}-\mu_2^{gas}=0$$

in which H_1, H_2, H_3, h_1, h_2, and h_3 are clustered functions given by

$$H_1 = v_{12}^*\varepsilon_{12}^* - v_{23}^*\varepsilon_{23}^* \quad (A.50.1)$$

$$H_2 = v_2^*\varepsilon_2^* - v_{23}^*\varepsilon_{23}^* \quad (A.50.2)$$

$$H_3 = v_{23}^*\varepsilon_{23}^* \quad (A.50.3)$$

$$h_1 = v_{12}^* - v_{23}^* \quad (A.50.4)$$

$$h_2 = v_2^* - v_{23}^* \quad (A.50.5)$$

$$h_3 = v_{23}^* \quad (A.50.6)$$

By simultaneous solution of three non-linear equations of (A.48), (A.49), and (A.50), the unknown parameters of reduced polymer phase density, $\bar{\rho}^{pol}$ and the closed-packed volume fractions of solute components in the polymer phase, ϕ_1^{pol} and ϕ_2^{pol} are calculated. All of the properties of interest are consequently calculated from these parameters, as described hereunder.

A.3.1. Solubility in polymer

According to equation (4.7), the mass fraction of solute *1* and *2* in the amorphous phase of the polymer can be calculated from

$$\omega_{1,am} = \frac{1}{1 + \left(\frac{\rho_2^* v_2^*}{\rho_1^* v_1^*}\right)\left(\frac{\phi_2^{pol}}{\phi_1^{pol}}\right) + \left(\frac{\rho_3^* v_3^*}{\rho_1^* v_1^*}\right)\left(\frac{1 - \phi_1^{pol} - \phi_2^{pol}}{\phi_1^{pol}}\right)} [=] \frac{gr\ sol.1}{gr\ (sol.1 + sol.2 + am.pol)} \quad (A.51)$$

$$\omega_{2,am} = \left[\left(\frac{\rho_2^* v_2^*}{\rho_1^* v_1^*}\right)\left(\frac{\phi_2^{pol}}{\phi_1^{pol}}\right)\right] \omega_{1,am} [=] \frac{gr\ sol.2}{gr\ (sol.1 + sol.2 + am.pol)} \quad (A.52)$$

And consequently

$$\omega_{3,am} = 1 - \omega_{1,am} - \omega_{2,am} [=] \frac{gr\ am.pol}{gr\ (sol.1 + sol.2 + am.pol)} \quad (A.53)$$

The solubility of the species can simply be calculated by

$$S_{1,am} = \frac{\omega_{1,am}}{\omega_{3,am}} [=] \frac{gr\ sol.1}{gr\ am.pol} \quad (A.54)$$

$$S_{2,am} = \frac{\omega_{2,am}}{\omega_{3,am}} [=] \frac{gr\ sol.2}{gr\ am.pol} \quad (A.55)$$

$$S_{12,am} = \frac{\omega_{1,am} + \omega_{2,am}}{\omega_{3,am}} [=] \frac{gr\ (sol.1 + sol.2)}{gr\ am.pol} \quad (A.56)$$

$$S_{12,tot} = S_{12,am}(1 - \chi) [=] \frac{gr\ (sol.1 + sol.2)}{gr\ (am.pol + crys.pol)} \quad (A.57)$$

In addition, the mole fraction of mers of component (*i*) occupying total mers (sites) of the model lattice in closed-packed state can be calculated as

$$x_i^{pol} = \frac{\phi_i^{pol}}{v_i^*} \Big/ \sum_j \left(\frac{\phi_j^{pol}}{v_j^*}\right) [=] \frac{mole\ mer\ (i)}{mole\ total\ mers} \quad (A.58)$$

A.3.2. Swelling of polymer

In order to estimate the extent of swelling of amorphous polymer phase because of sorption of solute species, firstly, the initial density of the amorphous polymer at the same temperature and pressure need to be calculated. This is done by solving equation (A.59) for reduced density of pure amorphous polymer similar to the equation (A.22).

$$\overline{\rho_3} = 1 - \exp\left(-\frac{\overline{\rho_3}^2}{\overline{T_3}} - \frac{\overline{P_3}}{\overline{T_3}} - \overline{\rho_3}\right) \qquad (A.59)$$

where, $\overline{\rho_3}$, is the reduced amorphous polymer density. According to its definition, the amorphous polymer density will be equal to $\overline{\rho_3}\rho_3^*$.

On the other hand, in order to estimate the density of the polymer phase at equilibrium sorption (including solute (*1*, *2*) and polymer (*3*) components), the characteristic density of the polymer phase is defined as

$$\rho^* = \frac{1}{\left(\frac{\omega_{1,am}}{\rho_1^*}\right) + \left(\frac{\omega_{2,am}}{\rho_2^*}\right) + \left(\frac{\omega_{3,am}}{\rho_3^*}\right)} \qquad (A.60)$$

and consequently the density of the amorphous polymer phase will be equal to $\rho^*\bar{\rho}^{\,pol}$.

The extent of swelling of amorphous polymer phase due to the sorption of solute components (*1*, *2*) can be obtained by simple mathematical manipulations to be equal to

$$SW_{12,am} = \frac{\rho_3^*\overline{\rho_3}\left(1 + S_{1,am} + S_{2,am}\right)}{\rho^*\bar{\rho}^{\,pol}} - 1 \qquad (A.61)$$

$$\frac{\rho_3^*\overline{\rho_3}\left(1 + S_{1,am} + S_{2,am}\right)}{\rho^*\bar{\rho}^{\,pol}} [=] \frac{lit\ (am.pol + sol.1 + sol.2)}{lit\ (am.pol)} \qquad (A.61.1)$$

The extent of total polymer swelling considering no solubility in the crystalline phase can be calculated to be equal to

$$SW_{12,tot} = \frac{\chi v_c + \frac{(1-\chi)\left(1 + S_{1,am} + S_{2,am}\right)}{\rho^*\bar{\rho}^{\,pol}}}{\chi v_c + \frac{(1-\chi)}{\rho_3^*\overline{\rho_3}}} - 1 \qquad (A.62)$$

$$\frac{\chi v_c + \frac{(1-\chi)\left(1 + S_{1,am} + S_{2,am}\right)}{\rho^*\bar{\rho}^{\,pol}}}{\chi v_c + \frac{(1-\chi)}{\rho_3^*\overline{\rho_3}}} [=] \frac{lit\ (am.pol + crys.pol + sol.1 + sol.2)}{lit\ (am.pol + crys.pol)} \qquad (A.62.1)$$

in which, v_c, is the specific volume of fully crystalline polymer phase. For fully crystalline polyethylene $v_c = 0.001\ m^3/kg$.

A.3.3. Concentration of solute species in the polymer phase

The concentration of solute (*1*) in the amorphous polymer phase can be easily calculated from

$$C_{1,am} = \frac{\omega_{1,am}\,\rho^*\bar{\rho}^{\,pol}}{MW_1}[=]\frac{mol\ sol.1}{lit\ (am.pol+sol.1+sol.2)} \qquad (A.63)$$

in which, MW_1, is molecular weight of solute species *1* having unite of *gr/mol*.

In order to estimate the concentration of species *1* in the whole polymer including amorphous and crystalline phase, first the volume-based crystallinity of polymer is calculated

$$\chi_v = \frac{\chi v_c}{\chi v_c + \frac{(1-\chi)}{\rho_3^*\bar{\rho}_3}}[=]\frac{lit\ crys.pol}{lit\ (crys.pol + am.pol)} \qquad (A.64)$$

And the concentration of component *1* in total polymer phase can be estimated by

$$C_{1,tot} = C_{1,am}\,\frac{(1+SW_{12,am})}{(1+SW_{12,tot})}\,(1-\chi_v)[=]\frac{mol\ sol.1}{lit(am.pol + crys.pol + sol.1 + sol.2)} \qquad (A.65)$$

A.3.4. The density change in the polymer particle due to the sorption

According to the equation (A.57), the ratio of mass of polymer particles after and before sorption is given by

$$\frac{m_{\substack{swollen\\polymer}}}{m_{\substack{non-swollen\\polymer}}} = 1 + S_{12,tot}[=]\frac{gr\ (sol.1 + sol.2\ + am.pol + crys.pol)}{gr\ (am.pol + crys.pol)} \qquad (A.66)$$

and according to the equation (A.62), the ratio between volumes of swollen and non-swollen polymer particles will be given by

$$\frac{V_{\substack{swollen\\polymer}}}{V_{\substack{non-swollen\\polymer}}} = 1 + SW_{12,tot}[=]\frac{lit\ (sol.1 + sol.2 + am.pol + crys.pol)}{lit\ (am.pol + crys.pol)} \qquad (A.67)$$

The change in the density of polymer particles (including amorphous and crystalline phases) due to the sorption is, as previously given in equation (A.68)

$$\rho_{change} = \frac{\rho_{\substack{swollen \\ polymer}}}{\rho_{\substack{non-swollen \\ polymer}}} - 1 = \frac{\frac{m_{\substack{swollen \\ polymer}}}{V_{\substack{swollen \\ polymer}}}}{\frac{m_{\substack{non-swollen \\ polymer}}}{V_{\substack{non-swollen \\ polymer}}}} - 1 = \frac{\frac{m_{\substack{swollen \\ polymer}}}{m_{\substack{non-swollen \\ polymer}}}}{\frac{V_{\substack{swollen \\ polymer}}}{V_{\substack{non-swollen \\ polymer}}}} - 1 \quad \text{(A.68)}$$

By substituting equation (A.66) and (A.67) into equation (A.68), the change in the density of polymer particles (including amorphous and crystalline phases) due to the sorption will be given by

$$\rho_{change} = \frac{1+S_{12,tot}}{1+SW_{12,tot}} - 1 \quad \text{(A.69)}$$

Appendix B

Nonstandard Finite Difference Scheme

B. Nonstandard finite difference (NSFD) method

Nonstandard finite difference (NSFD) method for the numerical integration of the differential equations, developed by Mickens,[1-4] currently has found a growing applicability in the different fields of science and applied science.[1] It is our intention in the current appendix, firstly, to provide a basic introduction to this method and subsequently to extend its applicability to a reaction-diffusion type of problem in spherical coordinates as the final form of Polymer Flow Model (PFM).

B.1. NSFD method description

The concept of "dynamic consistency" constitutes the core underlying principle of this methodology. Dynamic consistency is defined as follows; consider the differential equation

$$\frac{dx}{dt} = f(x, t, \lambda) \qquad (B.1)$$

where λ is the representative of parameters defining the system modeled by equation (B.1), while *x* and *t* are dependent and independent variables, respectively. Now, let a finite difference scheme for equation (B.1) be

$$x_{k+1} = F(x_k, t_k, h, \lambda) \qquad (B.2)$$

in which *h* is step-size for independent variable i.e. $h = \Delta t$.

Letting the differential equation and/or its solutions have property *P*, the discrete model, equation (B.2), is considered as dynamically consistent with equation (B.1), if it and/or its solutions also has property *P*.

For many systems in engineering science, the dependant variables represent physical variables that cannot take negative values for example they may be concentration or absolute temperature. For such systems the property *P* is referred to "positivity". As a result, in the dynamically consistent schemes with positivity condition, the nonnegative initial and/or boundary data will evolve into nonnegative solutions at later times.

The main issue regarding the numerical solution for differential equations is the possibility to encounter to the "numerical instabilities". Numerical instabilities, in general, are indicative of solutions to the discrete equations which do not correspond to any solution of the corresponding differential equation. One possible mechanism for this to occur is to have the finite difference scheme that does not satisfy some physical principal e.g. positivity on the solutions of PDEs. In simple words, if the solutions of the

PDEs are restricted to have nonnegative values, the numerical instabilities would exist if the finite difference method allows negative values as its solution for nonnegative initial and/or boundary condition.

As a result, the main purpose of Nonstandard Finite Difference (NSFD) method is to construct a "dynamically consistent" scheme in order to avoid such numerical instabilities. In this method, the finite difference scheme for the studied model must be "designed" in a manner that it meets the requirement to be dynamically consistent to avoid the instability problems. This in turn implies that each differential equation has to be treated as a unique mathematical structure and as a result, must be discretized in a unique manner in this method. For instant, if one is dealing with a system model in which the positivity condition is valid for the dependent variable (i.e. negative value for this variable is physically meaningless), the finite difference scheme should be designed in a way that preserves this condition. Mickens[1-3] also has provided further basic rules for appropriate construction of nonstandard finite difference schemes which are skipped here for the brevity reason. For a more comprehensive presentation of this method, interested readers are referred to references [1-3]. Further clarification of this method will be achieved here as its applicability is extended for solving reaction-diffusion type of problem in spherical coordinates as the main interest of this project.

B.2. Application of NSFD scheme to PFM

In order to dynamically calculate concentration gradient through a growing particle by PFM model, one must be able to solve the final form of mass balance in the spherical coordinates as provided in equation (B.3):

$$\frac{\partial M}{\partial \tau} = D\left(\frac{\partial^2 M}{\partial r^2} + \frac{2}{r}\frac{\partial M}{\partial r}\right) - kM \qquad (B.3)$$

with initial and boundary conditions

$$\tau = 0: \qquad M = 0 \qquad 0 \le r \le 1 \qquad (B.4)$$

$$r = 0: \qquad \frac{dM}{dr} = 0 \qquad \tau \ge 0 \qquad (B.5)$$

$$r = 1: \qquad M = 1 \qquad \tau \ge 0 \qquad (B.6)$$

in which *M*, *r*, and τ correspond to dimensionless concentration, radius, and time respectively. In equation (B.3), *D* is a dimensionless constant proportional to the diffusivity of the species through the particle while *k* is also a dimensionless constant proportional to the rate constant for monomer consumption.

A similar equation is obtained for energy balance in order to estimate the temperature gradient through a growing particle. However, the steps taken to construct the nonstandard finite difference scheme only for the mass balance equation are presented here for brevity purpose while similar principles are also being applied for energy balance equation.

The discretization of the normalized particle to the grids of equal thickness, Δr, at each step of the dimensionless time, τ, is represented in Figure B.1. The discrete forms for the first-order time and space derivative, and second-order space derivative are given, respectively, by the usual forward Euler and central difference representations:

$$\frac{\partial M}{\partial \tau} \rightarrow \frac{M_i^{j+1} - M_i^j}{\Delta \tau} \qquad (B.7)$$

$$\frac{\partial M}{\partial r} \rightarrow \frac{M_{i+1}^j - M_i^j}{\Delta r} \qquad (B.8)$$

$$\frac{\partial^2 M}{\partial r^2} \rightarrow \frac{M_{i+1}^j - 2M_i^j + M_{i-1}^j}{(\Delta r)^2} \qquad (B.9)$$

M_i^j represents the dimensionless concentration at grid *i* and dimensionless time step *j*.

As a result the discrete form of the equation (B.3) can be written as:

$$\frac{M_i^{j+1} - M_i^j}{\Delta \tau} = D\left(\frac{M_{i+1}^j - 2M_i^j + M_{i-1}^j}{(\Delta r)^2} + \frac{2}{r_i}\frac{M_{i+1}^j - M_i^j}{\Delta r}\right) - kM_i^{j+1} \qquad (B.10)$$

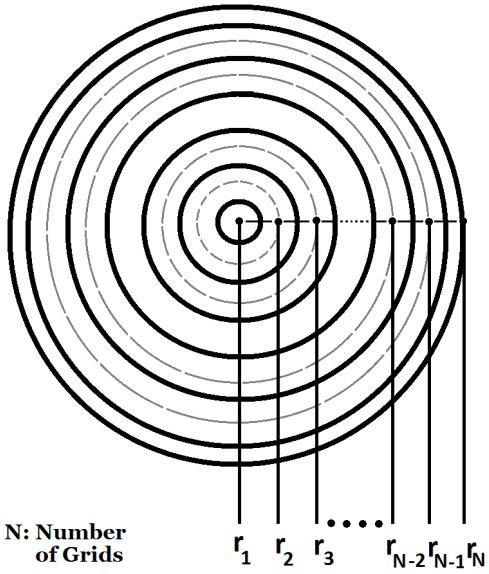

Figure B.1. discretization of the normalized particle at each time step.

It worth mentioning that the component kM in the equation (B.3) is discretized as kM_i^{j+1}in equation (B.10). This is referred to "non-local" discretization, which plays essential role to obtain dynamically consistent schemes and is frequently used in NSFD method.

Rewriting equation (B.10) will result in

$$M_i^{j+1} - M_i^j = D\Delta\tau\left(\frac{M_{i+1}^j - 2M_i^j + M_{i-1}^j}{(\Delta r)^2} + \frac{2}{r_i}\frac{M_{i+1}^j - M_i^j}{\Delta r}\right) - k\Delta\tau M_i^{j+1} \qquad (B.11)$$

and rearranging the equation (B.11) will lead to

$$M_i^{j+1}(1 + k\Delta\tau) = M_{i+1}^j\left(\frac{D\Delta\tau}{(\Delta r)^2} + \frac{2D\Delta\tau}{r_i\Delta r}\right) + M_{i-1}^j\left(\frac{D\Delta\tau}{(\Delta r)^2}\right) + M_i^j\left(1 - \frac{2D\Delta\tau}{(\Delta r)^2} - \frac{2D\Delta\tau}{r_i\Delta r}\right) \qquad (B.12)$$

and finally

$$M_i^{j+1} = \frac{M_{i+1}^j\left(\frac{D\Delta\tau}{(\Delta r)^2} + \frac{2D\Delta\tau}{r_i\Delta r}\right) + M_{i-1}^j\left(\frac{D\Delta\tau}{(\Delta r)^2}\right) + M_i^j\left(1 - \frac{2D\Delta\tau}{(\Delta r)^2} - \frac{2D\Delta\tau}{r_i\Delta r}\right)}{(1 + k\Delta\tau)} \qquad (B.13)$$

At this point, the positivity condition can be applied to the scheme in order to meet the requirement to have a dynamically consistent system i.e. the nonnegative initial and/or boundary data to evolve into nonnegative solutions at later times or in other words $M_i^j \geq 0 \Rightarrow M_i^{j+1} \geq 0$.

It is clear from equation (B.13) that all of terms on the right hand side of the equation have nonnegative value expect for $\left(1 - \frac{2D\Delta\tau}{(\Delta r)^2} - \frac{2D\Delta\tau}{r_i \Delta r}\right)$ which may accept negative value. As a result in order to have dynamically consistent scheme, the positivity condition must be applied to this term

$$1 - \frac{2D\Delta\tau}{(\Delta r)^2} - \frac{2D\Delta\tau}{r_i \Delta r} \geq 0 \qquad \text{(B.14)}$$

which can be rewritten as

$$2D\Delta\tau \left(\frac{1}{(\Delta r)^2} + \frac{1}{r_i \Delta r}\right) \leq 1 \qquad \text{(B.15)}$$

and it can be finally rearranged in the form of

$$\Delta\tau \leq \frac{1}{2D\left(\frac{1}{(\Delta r)^2} + \frac{1}{r_i \Delta r}\right)} \qquad \text{(B.16)}$$

However, it is possible to simplify the equation (B.16) further. As the grid radius, r_i, decreases the value of right hand side of inequality, i.e. $\frac{1}{2D\left(\frac{1}{(\Delta r)^2} + \frac{1}{r_i \Delta r}\right)}$, also decreases. As a result, the value of right hand side of inequality will reach its minimum value at the "applied" grid with minimum radius. According to the Figure B.1, this corresponds to the grid 2, as the grid 1 is subject to the boundary condition of $\left(\frac{\partial M}{\partial r}\right)_1^j = 0$ or in other words $M_1^j = M_2^j$. For grid 2, as depicted in Figure B.1, $r_2 = \Delta r$, and consequently the functional inequality for the space and time steps can be simplified to

$$\Delta\tau \leq \frac{(\Delta r)^2}{4D} \qquad \text{(B.17)}$$

Now, it is possible to summarize what has been obtained in the current appendix. First, the nonstandard finite difference method for equation (B.3) given by equation (B.13) is a dynamically consistent or positivity preserving scheme, if the equation of (B.17) holds true. Second, a functional inequality is found between the space and time step-sizes employing NSFD method, which ensures the

scheme to be numerically stable and finally, the overall developed scheme is explicit. This point can be easily seen by observing that M_i^{j+1}appears only on the left side of equation (B.13).

B.3. References

1. Mickens, R. E. *Advances in the Applications of Nonstandard Finite Difference Schemes;* World Scientific Publishing Co.: **2005**.

2. Mickens, R. E. Dynamic consistency: a fundamental principle for constructing nonstandard finite difference schemes for differential equations. *Journal of Difference Equations and Applications* **2005,** *11* (7), 645-653.

3. Mickens, R. E. Nonstandard Finite Difference Schemes for Differential Equations. *Journal of Difference Equations and Applications* **2002,** *8* (9), 823-847.

4. Mickens, R. E. Nonstandard finite difference schemes for reaction-diffusion equations. *Numer. Methods Partial Differential Eq.* **1999,** *15* (2), 201-214.

Appendix C

Polymer Flow Model

Numerical Solution for Dynamic Mass and Heat Transfer Problem in Spherical Coordinate with Moving Boundary Condition

C. Numerical solution to Polymer Flow Model (PFM)

In this appendix, it is intended to provide the details of calculation steps which have been taken in order to be able to numerically solve the Polymer Flow Model. It is important to note that the Polymer Flow Model itself has not been explained in this appendix. However, where necessary the important assumptions or considerations associated to the different aspects of the model have been highlighted for the purpose of clarity which would also facilitate following the steps related to the development of numerical solution through the appendix.

In the notation used in this appendix, the superscript refers to time step while subscript refers to the number of the grid to which the physical property belongs to. For instance, T_i^j represents the temperature of *i*th grid at the *j*th time step.

In addition, the list of symbols used in this appendix with their brief definitions and units are provided at the end of the appendix.

C.1. Grid generation

In the PFM model, the growing polymer particle is approximated with a pseudo-homogeneous spherical particle in which it is assumed that the polymerization active sites are dispersed homogeneously. At each time step during the numerical solution, the dimensionless normalized radius of the particle, r, is defined by dividing the particle radius at that time step, R_l^j, to itself. In other words

$$r_N = \frac{R_l^j}{R_l^j} = 1 \qquad (C.1)$$

The normalized particle radius is discretized into *N* radial shells having the same thickness of Δr, except for the first and *N*th grid, as shown in Figure C.1. The thickness of first and *N*th grid is considered to be $\frac{\Delta r}{2}$. Regarding Figure C.1, it can be written

$$r = \left(\frac{\Delta r}{2}\right) + (N-2)(\Delta r) + \left(\frac{\Delta r}{2}\right) \qquad (C.2)$$

and consequently

$$r = (N-1)(\Delta r) \qquad (C.3)$$

and as a result, the Δr can be calculated from

$$\Delta r = \frac{r}{N-1} \qquad \text{(C.4)}$$

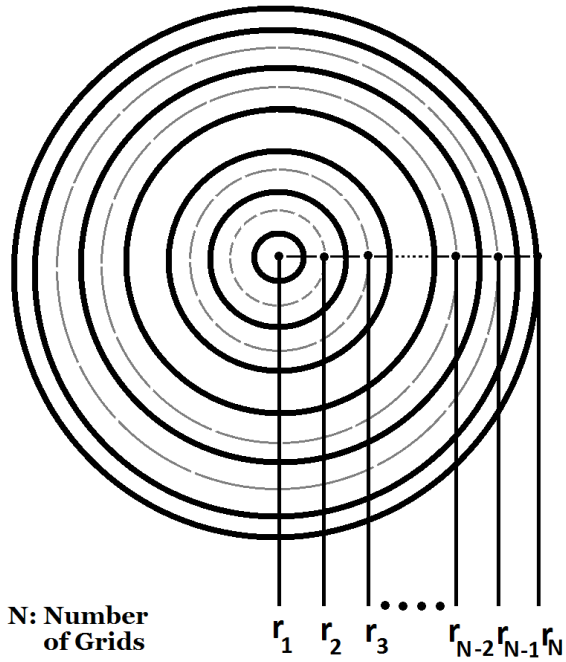

Figure C.1. The discretization of normalized particle radius into *N* shells.

The radial position of each shell is given by

$$r_i = (i-1)(\Delta r) \qquad \text{(C.5)}$$

The dimensionless volume of each grid is calculated by

for *1st* grid

$$v_1 = \frac{4}{3}\pi\left(\frac{\Delta r}{2}\right)^3 \qquad \text{(C.6)}$$

from grid *2* to grid number *N-1*

$$v_i = \frac{4}{3}\pi\left[\left(r_i + \left(\frac{\Delta r}{2}\right)\right)^3 - \left(r_i - \left(\frac{\Delta r}{2}\right)\right)^3\right] \qquad \text{(C.7)}$$

and for *Nth* grid

$$v_N = \frac{4}{3}\pi\left[1-\left(1-\left(\frac{\Delta r}{2}\right)\right)^3\right] \qquad (C.8)$$

Finally, the total dimensionless volume of the spherical particle will be equal to

$$v = \frac{4}{3}\pi \qquad (C.9)$$

By assuming homogeneous distribution of the polymerization active sites immobilized on the surface of the initial catalyst fragments through the growing polymer particle and as a result the normalized particle, the volume of catalyst dispersed in each grid can be calculated from

$$V_{cat_i} = \left(\frac{v_i}{v}\right)V_{cat} \qquad (C.10)$$

in which V_{cat} is the volume of initial fresh catalyst particle calculated from

$$V_{cat} = \frac{4}{3}\pi r_{cat}^3 \qquad (C.11)$$

with r_{cat} being the radius of initial catalyst particle.

C.2. Mass balance for reactant ethylene and development of its numerical solution

C.2.1. Mass balance equation

The mass balance for the reactant of ethylene in the PFM model is given by

$$\frac{\partial[M]_{ov.1}}{\partial t} = \frac{1}{r_l^2}\frac{\partial}{\partial r_l}\left(D_{ov.1}r_l^2\frac{\partial[M]_{ov.1}}{\partial r_l}\right) - R_v \qquad (C.12)$$

with first boundary condition

$$[M]_{ov.1} = [M]_{ov.eq.1} \quad @ \quad r_l = R_l \qquad (C.13)$$

while assuming no external mass transfer resistance through the boundary layer of the particle.

second boundary condition is given by

$$\frac{\partial[M]_{ov.1}}{\partial r_l} = 0 \quad @ \quad r_l = 0 \qquad (C.14)$$

and initial condition is provided by

$$[M]_{ov.1} = 0 \quad @ \quad t = 0 \quad and \quad 0 \le r_l \le R_l \tag{C.15}$$

where $[M]_{ov.1}$ is overall ethylene concentration through the particle, $[M]_{ov.eq.1}$ is the overall equilibrium concentration of ethylene in the particle, $D_{ov.1}$ is the overall ethylene diffusivity through the particle, and R_v is the volumetric rate of ethylene monomer consumption.

The volumetric rate of ethylene polymerization, R_v, is calculated by

$$R_v = R_{pol}\left(\frac{(1-\epsilon)}{\phi^3}\right) \tag{C.16}$$

in which, ϵ, is the particle porosity and ϕ is the overall growth factor defined as

$$\phi = \frac{R_p}{r_{cat}} \tag{C.17}$$

with R_p representing the equivalent radius of "polymer-only" particle at each time step without considering the existing particle porosity.

R_{pol} is the rate of polymerization at the catalyst particle surface given by

$$R_{pol} = k_p C^* [M]_{ov.1} \tag{C.18}$$

with k_p representing the propagation constant at the local particle temperature and C^* being the local concentration of polymerization active sites.

The temperature dependency of propagation constant is described here by Arrhenius-type of correlation

$$k_p = k_{p,ref} e^{-\frac{E_a}{R_g}\left(\frac{1}{T}-\frac{1}{T_{ref}}\right)} \tag{C.19}$$

in which $k_{p,ref}$ is the propagation constant at the reference temperature, T_{ref}. E_a is the activation energy for propagation and R_g is the universal gas constant. T represents the local temperature of active site in the polymer particle.

The deactivation of catalyst active sites during the course of polymerization is considered in the model by

$$C^* = C_1^* e^{-k_d t} + C_2^* \qquad (C.20)$$

which can be rewritten as

$$C^* = C_0^* e^{-k_d t} \qquad (C.21)$$

in which C_0^* is a clustered function defined as

$$C_0^* = C_1^* + C_2^* e^{k_d t} \qquad (C.22)$$

where C_0^* is the concentration of active sites at the time zero as the catalyst particle being exposed to the reaction environment and k_d is the deactivation constant. The temperature dependency of deactivation constant is also described by Arrhenius-type of correlation

$$k_d = k_{d,ref} e^{-\frac{E_d}{R_g}\left(\frac{1}{T}-\frac{1}{T_{ref}}\right)} \qquad (C.23)$$

in which $k_{d,ref}$ is the deactivation constant at the reference temperature, T_{ref}. E_d is the activation energy for the catalyst deactivation.

By substituting equation (C.23) in equation (C.21), the concentration of active sites at each time step will be given by

$$C^* = C_0^* e^{-\left(k_{d,ref} e^{-\frac{E_d}{R_g}\left(\frac{1}{T}-\frac{1}{T_{ref}}\right)}\right)t} \qquad (C.24)$$

By substituting equations (5.11) and (C.24) into equation (5.10), R_{pol} will be given by

$$R_{pol} = \left(k_{p,ref} e^{-\frac{E_a}{R_g}\left(\frac{1}{T}-\frac{1}{T_{ref}}\right)}\right)\left(C_0^* e^{-\left(k_{d,ref} e^{-\frac{E_d}{R_g}\left(\frac{1}{T}-\frac{1}{T_{ref}}\right)}\right)t}\right)[M]_{ov.1} \qquad (C.25)$$

and as a result the volumetric rate of ethylene polymerization, R_v, is calculated by substituting equation (C.25) into equation (5.8) to be

$$R_v = \left(k_{p,ref} e^{-\frac{E_a}{R_g}\left(\frac{1}{T}-\frac{1}{T_{ref}}\right)}\right)\left(C_0^* e^{-\left(k_{d,ref} e^{-\frac{E_d}{R_g}\left(\frac{1}{T}-\frac{1}{T_{ref}}\right)}\right)t}\right)[M]_{ov.1}\left(\frac{(1-\epsilon)}{\phi^3}\right) \quad (C.26)$$

Finally, the mass balance for reactant ethylene provided in equation (5.3) can be rewritten by substituting R_v with equation (C.26)

$$\frac{\partial[M]_{ov.1}}{\partial t} = \frac{1}{r_l^2}\frac{\partial}{\partial r_l}\left(D_{ov.1} r_l^2 \frac{\partial[M]_{ov.1}}{\partial r_l}\right) - \left(k_{p,ref} e^{-\frac{E_a}{R_g}\left(\frac{1}{T}-\frac{1}{T_{ref}}\right)}\right)\left(C_0^* e^{-\left(k_{d,ref} e^{-\frac{E_d}{R_g}\left(\frac{1}{T}-\frac{1}{T_{ref}}\right)}\right)t}\right)[M]_{ov.1}\left(\frac{(1-\epsilon)}{\phi^3}\right) \quad (C.27)$$

C.2.2. Dimensionless form of mass balance equation

In order to transform the mass balance equation of (C.27) to a dimensionless form, the following dimensionless parameters are defined:

(a) dimensionless ethylene concentration in the polymer particle

$$M_1 = \frac{[M]_{ov.1}}{[M]_{ov.eq.1}} \quad (C.28)$$

in which

$$[M]_{ov.eq.1} = [M]_{eq.1}(1-\epsilon) \quad (C.29)$$

$[M]_{eq.1}$ is the equilibrium concentration of ethylene in the polymer phase, while $[M]_{ov.eq.1}$ is the overall equilibrium concentration of ethylene in whole pseudo-homogenous particle considering its porosity, ϵ.

(b) dimensionless time

$$\tau = \frac{t}{t_{char}} \quad (C.30)$$

in which τ is the dimensionless time, t is the time (in seconds), and t_{char} is the constant representing the process characteristic time (in seconds).

(c) dimensionless radial position

$$r = \frac{r_l}{R_l} \qquad \text{(C.31)}$$

in which r is the dimensionless radial position inside the normalized pseudo-homogeneous polymer particle, r_l is radial position in the pseudo-homogeneous polymer particle (in meter) and R_l is the radius of the pseudo-homogeneous polymer particle at each time step during its growth (in meter).

(d) dimensionless temperature

$$T_r = \frac{T}{T_b} \qquad \text{(C.32)}$$

in which T_r is the dimensionless temperature, T is the temperature (in K), and T_b is the bulk temperature (in K).

(e) dimensionless reference temperature

$$T_{r,ref} = \frac{T_{ref}}{T_b} \qquad \text{(C.33)}$$

in which $T_{r,ref}$ is the dimensionless reference temperature, T_{ref} is the reference temperature (in K) , and T_b is the bulk temperature (in K).

By substituting the $[M]_{ov.1}$, t, r_l, T, and T_{ref} with their dimensionless forms in the mass balance equation of (C.27), the dimensionless form of mass balance equation is obtained:

$$\frac{\partial M_1}{\partial \tau} = D_1\left(\frac{\partial^2 M_1}{\partial r^2} + \frac{2}{r}\frac{\partial M_1}{\partial r}\right) - k\, e^{-\frac{E_a}{R_g T_b}\left(\frac{1}{T_r}-\frac{1}{T_{r,ref}}\right)} e^{-\left((k_{d,ref}\, t_{char}) e^{-\frac{E_d}{R_g T_b}\left(\frac{1}{T_r}-\frac{1}{T_{r,ref}}\right)}\right)\tau} M_1 \qquad \text{(C.34)}$$

in which D_1 is the dimensionless diffusivity of ethylene defined as

$$D_1 = \frac{D_{ov.1} t_{char}}{R_l^2} \qquad \text{(C.35)}$$

and k is the dimensionless rate coefficient for ethylene polymerization defined as

$$k = k_{p,ref} C_0^* t_{char} \left(\frac{(1-\epsilon)}{\phi^3} \right) \qquad \text{(C.36)}$$

C.2.3. Discretization

The dimensionless mass balance equation of (C.34) is discretized applying the nonstandard finite difference scheme (NSFD) as described in the previous appendix.

The discrete form of the first-order dimensionless time derivate is provided by the forward Euler representation, while the discrete forms of the first-order and second-order dimensionless space derivatives are given by forward Euler and central difference representations, respectively.

$$\frac{{M_1}_i^{j+1} - {M_1}_i^j}{\Delta\tau^j} = D_1^j \left(\left(\frac{{M_1}_{i+1}^j - 2{M_1}_i^j + {M_1}_{i-1}^j}{(\Delta r)^2} \right) + \left(\frac{2}{r_i} \right) \left(\frac{{M_1}_{i+1}^j - {M_1}_i^j}{(\Delta r)} \right) \right) - k_i^j \, e^{-\frac{E_a}{R_g T_b}\left(\frac{1}{T_{r_i}^j} - \frac{1}{T_{r,ref}} \right)} e^{-\left((k_{d,ref}\, t_{char}) e^{-\frac{E_d}{R_g T_b}\left(\frac{1}{T_{r_i}^j} - \frac{1}{T_{r,ref}} \right)} \right) \tau^j} {M_1}_i^{j+1} \qquad \text{(C.37)}$$

in which D_1^j at each time step is given by

$$D_1^j = \frac{D_{ov.1} t_{char}}{\left(R_l^j \right)^2} \qquad \text{(C.38)}$$

and k_i^j at each time step is provided by

$$k_i^j = k_{p,ref} {C_0^*}_i^j t_{char} \left(\frac{(1-\epsilon)}{(\phi^j)^3} \right) \qquad \text{(C.39)}$$

in which

$${C_0^*}_i^j = C_1^* + C_2^* e^{\left((k_{d,ref}\, t_{char}) e^{-\frac{E_d}{R_g T_b}\left(\frac{1}{T_{r_i}^j} - \frac{1}{T_{r,ref}} \right)} \right) \tau^j} \qquad \text{(C.40)}$$

and

$$\phi^j = \frac{{R_p}^j}{r_{cat}} \qquad (C.41)$$

By rearrangement of equation (C.37), the dimensionless concentration of ethylene in the next time step of *j+1* for each grid of *i*, ${M_1}_i^{j+1}$, can be explicitly calculated from

$$M_{1_i}^{j+1} = \frac{M_{1_{i+1}}^{j}\left(\left(\frac{D_1^j \Delta\tau^j}{(\Delta r)^2}\right)+\left(\frac{2D_1^j \Delta\tau^j}{r_i(\Delta r)}\right)\right) + M_{1_{i-1}}^{j}\left(\frac{D_1^j \Delta\tau^j}{(\Delta r)^2}\right) + M_{1_i}^{j}\left(1-\left(\frac{2D_1^j \Delta\tau^j}{(\Delta r)^2}\right)-\left(\frac{2D_1^j \Delta\tau^j}{r_i(\Delta r)}\right)\right)}{1 + k_i^j \Delta\tau^j\, e^{-\frac{E_a}{R_g T_b}\left(\frac{1}{T_{r_i}^j}-\frac{1}{T_{r,ref}}\right)} e^{-\left(\left(k_{d,ref}\, t_{char}\right) e^{-\frac{E_d}{R_g T_b}\left(\frac{1}{T_{r_i}^j}-\frac{1}{T_{r,ref}}\right)}\right)\tau^j}} \qquad (C.42)$$

For the grid *i=N*, the boundary condition stated in equation (5.4) will be applied as

$${M_1}_N^{j+1} = 1 \qquad (C.43)$$

while for grid *i=1*, the boundary condition provided in equation (5.5) will be applied

$${M_1}_1^{j+1} = {M_1}_2^{j+1} \qquad (C.44)$$

By applying the positivity condition to equation (C.42) and in order to have numerically stable solution, the following mathematical inequality must be valid, as described in detail in the previous appendix

$$1-\left(\frac{2D_1^j \Delta\tau^j}{(\Delta r)^2}\right)-\left(\frac{2D_1^j \Delta\tau^j}{r_i(\Delta r)}\right) \geq 0 \qquad (C.45)$$

This will result in determination of maximum dimensionless time step in order to have numerically stable solution as

$$\Delta\tau^j \leq \frac{(\Delta r)^2}{4D_1^j} \qquad (C.46)$$

By substituting equation (C.38) for D_1^j into (C.46), we will have

$$\Delta\tau^j \leq \frac{\left(R_l^j\right)^2 (\Delta r)^2}{4D_{ov.1}\, t_{char}} \qquad (C.47)$$

or it can be rewritten as

$$\Delta\tau^{j}_{\max,1} = \frac{\left(R_l^j\right)^2 (\Delta r)^2}{4 D_{ov.1} t_{char}} \qquad (C.48)$$

As can be seen from (C.47), the maximum dimensionless time step to have stable numerical solution increases proportionally to the size of the particle. Consequently, as the polymer particle grows due to the accumulation of the produced polymer, the dimensionless time step allowed having stable solution also increases, resulting in faster calculation of the whole polymerization time period while demanding less computational time.

C.3. Mass balance for inert condensing agent (ICA) and development of its numerical solution

C.3.1. Mass balance equation

The mass balance for inert condensing agent (ICA) is given by

$$\frac{\partial [M]_{ov.2}}{\partial t} = \frac{1}{r_l^2} \frac{\partial}{\partial r_l} \left(D_{ov.2} r_l^2 \frac{\partial [M]_{ov.2}}{\partial r_l} \right) \qquad (C.49)$$

with first boundary condition

$$[M]_{ov.2} = [M]_{ov.eq.2} \quad @ \quad r_l = R_l \qquad (C.50)$$

while assuming no external mass transfer resistance through the boundary layer of the particle.

second boundary condition is given by

$$\frac{\partial [M]_{ov.2}}{\partial r_l} = 0 \quad @ \quad r_l = 0 \qquad (C.51)$$

and initial condition is provided by

$$[M]_{ov.2} = 0 \quad @ \quad t = 0 \quad and \quad 0 \le r_l \le R_l \qquad (C.52)$$

where $[M]_{ov.2}$ is overall ICA concentration through the particle, $[M]_{ov.eq.2}$ is the overall equilibrium concentration of ICA in the particle, and $D_{ov.2}$ is the overall ICA diffusivity through the particle.

C.3.2. Dimensionless form of mass balance equation

In order to transform the mass balance equation of (5.14) to a dimensionless form, the following dimensionless parameter is defined in addition to the ones defined in the previous section:

(f) dimensionless ICA concentration in the polymer particle

$$M_2 = \frac{[M]_{ov.2}}{[M]_{ov.eq.2}} \qquad (C.53)$$

in which

$$[M]_{ov.eq.2} = [M]_{eq.2}(1-\epsilon) \qquad (C.54)$$

$[M]_{eq.2}$ is the equilibrium concentration of ICA in the polymer phase, while $[M]_{ov.eq.2}$ is the overall equilibrium concentration of ICA in whole pseudo-homogenous particle considering its porosity, ϵ.

By substituting the $[M]_{ov.2}$, t, and r_l with their dimensionless forms in the mass balance equation of (5.14), the dimensionless form of mass balance equation is obtained:

$$\frac{\partial M_2}{\partial \tau} = D_2\left(\frac{\partial^2 M_2}{\partial r^2} + \frac{2}{r}\frac{\partial M_2}{\partial r}\right) \qquad (C.55)$$

in which D_2 is the dimensionless diffusivity of ICA in the polymer particle, defined as

$$D_2 = \frac{D_{ov.2}t_{char}}{R_l^2} \qquad (C.56)$$

C.3.3. Discretization

The dimensionless mass balance equation of (C.55) is discretized applying the nonstandard finite difference scheme (NSFD) as described in the previous appendix.

The discrete form of the first-order dimensionless time derivate is provided by the forward Euler representation, while the discrete forms of the first-order and second-order dimensionless space derivatives are given by forward Euler and central difference representations, respectively.

$$\frac{{M_2}_i^{j+1} - {M_2}_i^{j}}{\Delta\tau^{j}} = D_2^j \left(\left(\frac{{M_2}_{i+1}^{j} - 2{M_2}_i^{j} + {M_2}_{i-1}^{j}}{(\Delta r)^2} \right) + \left(\frac{2}{r_i} \right) \left(\frac{{M_2}_{i+1}^{j} - {M_2}_i^{j}}{(\Delta r)} \right) \right) \quad \text{(C.57)}$$

in which

$$D_2^j = \frac{D_{ov.2} t_{char}}{\left(R_l^j\right)^2} \quad \text{(C.58)}$$

By rearrangement of equation (C.57), the dimensionless concentration of ICA in the next time step of *j+1* for each grid of *i*, ${M_2}_i^{j+1}$, can be explicitly calculated from

(C.59)

$${M_2}_i^{j+1} = {M_2}_{i+1}^{j} \left(\left(\frac{D_2^j \Delta\tau^{j}}{(\Delta r)^2} \right) + \left(\frac{2D_2^j \Delta\tau^{j}}{r_i(\Delta r)} \right) \right) + {M_2}_{i-1}^{j} \left(\frac{D_2^j \Delta\tau^{j}}{(\Delta r)^2} \right) + {M_2}_i^{j} \left(1 - \left(\frac{2D_2^j \Delta\tau^{j}}{(\Delta r)^2} \right) - \left(\frac{2D_2^j \Delta\tau^{j}}{r_i(\Delta r)} \right) \right)$$

For the grid *i=N*, the boundary condition stated in equation (5.15) will be applied as

$${M_2}_N^{j+1} = 1 \quad \text{(C.60)}$$

while for grid *i=1*, the boundary condition provided in equation (5.16) will be applied

$${M_2}_1^{j+1} = {M_2}_2^{j+1} \quad \text{(C.61)}$$

By applying the positivity condition to equation (C.59) and in order to have numerically stable solution, the following mathematical inequality must be valid, as described in detail in the previous appendix

$$1 - \left(\frac{2D_2^j \Delta\tau^{j}}{(\Delta r)^2} \right) - \left(\frac{2D_2^j \Delta\tau^{j}}{r_i(\Delta r)} \right) \geq 0 \quad \text{(C.62)}$$

This will result in determination of maximum dimensionless time step in order to have numerically stable solution as

$$\Delta\tau^{j} \leq \frac{(\Delta r)^2}{4D_2^j} \quad \text{(C.63)}$$

By substituting equation (C.58) for D_2^j into (C.63), we will have

$$\Delta\tau^{j} \leq \frac{\left(R_l^j\right)^2 (\Delta r)^2}{4D_{ov.2}t_{char}} \qquad (C.64)$$

or it can be rewritten as

$$\Delta\tau_{max,2}^{j} = \frac{\left(R_l^j\right)^2 (\Delta r)^2}{4D_{ov.2}t_{char}} \qquad (C.65)$$

C.4. Energy balance and development of its numerical solution

C.4.1. Energy balance equation

The energy balance for a thin shell of pseudo-homogeneous polymer particle at each instant during the polymerization process, demonstrated in Figure C.2 , can be written as

$$\rho_{ov}V_l C_{p,pol}\frac{\partial T}{\partial t} = \left(-k_{c,p}\left(4\pi r_l^2\right)\left(\frac{\partial T}{\partial r_l}\right)\Big|_{r_l}\right) - \left(-k_{c,p}(4\pi(r_l+dr_l)^2)\left(\frac{\partial T}{\partial r_l}\right)\Big|_{r_l+dr_l}\right) + \left(-\Delta H_{\text{pol}}\right)R_v V_l + \left(-\Delta H_{\text{sorp},2}\right)\frac{\partial}{\partial t}\left([M]_{ov.2}V_l\right) \qquad (C.66)$$

in which ρ_{ov} is the overall particle density given by

$$\rho_{ov} = \rho_{pol}(1-\epsilon) \qquad (C.67)$$

and V_l is the volume of the pseudo-homogeneous polymer shell including its porosity

$$V_l = \frac{V_{pol}}{(1-\epsilon)} \qquad (C.68)$$

with V_{pol} being the volume of the polymer inside the shell.

Regarding Figure C.2, V_l can also be written as

$$V_l = 4\pi r_l^2 dr_l \qquad (C.69)$$

In equation (C.66), $C_{p,pol}$ is the heat capacity of polymer particle, $k_{c,p}$ is the thermal conductivity of polymer particle, ΔH_{pol} is enthalpy of ethylene polymerization, and $\Delta H_{\text{sorp},2}$ representing enthalpy of sorption of ICA from gas phase into polymer phase.

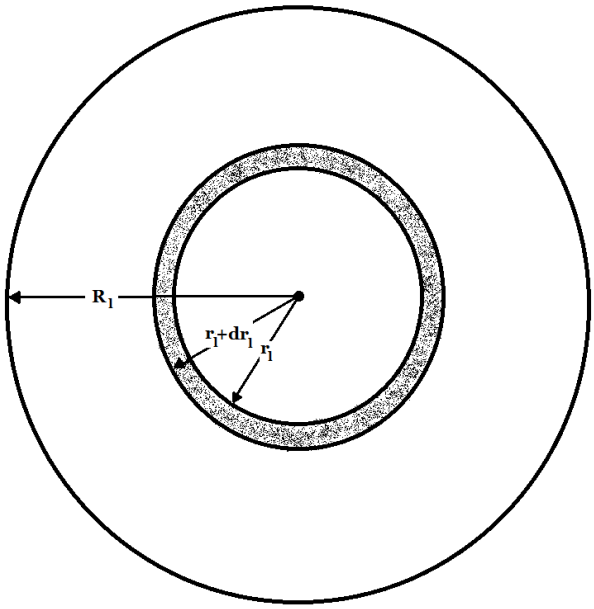

Figure C.2. The energy balance for a shell of pseudo-homogeneous polymer particle.

Rearrangement of equation (C.66) results in

$$\frac{\partial T}{\partial t} = \alpha_{ov}\frac{1}{r_l^2}\frac{\partial}{\partial r_l}\left(r_l^2\left(\frac{\partial T}{\partial r_l}\right)\right) + \left(\frac{-\Delta H_{\text{pol}}}{\rho_{ov}C_{p,pol}}\right)R_v + \left(\frac{-\Delta H_{\text{sorp},2}}{\rho_{ov}C_{p,pol}}\right)\frac{1}{V_l}\frac{\partial}{\partial t}\left([M]_{ov.2}V_l\right) \qquad \text{(C.70)}$$

α_{ov} is the overall thermal diffusivity of the particle defined as

$$\alpha_{ov} = \frac{k_{c,p}}{\rho_{ov}C_{p,pol}} \qquad \text{(C.71)}$$

with first boundary condition

$$-k_{c,p}\frac{\partial T}{\partial r_l}\Big|_{R_l} = h\left(T\Big|_{R_l} - T_b\right) \quad @ \quad r_l = R_l \qquad \text{(C.72)}$$

second boundary condition is given by

$$\frac{\partial T}{\partial r_l} = 0 \quad @ \quad r_l = 0 \tag{C.73}$$

and initial condition is provided by

$$T = T_b \quad @ \quad t = 0 \quad and \quad 0 \le r_l \le R_l \tag{C.74}$$

C.4.2. Dimensionless form of energy balance equation

By substituting the $[M]_{ov.1}$, $[M]_{ov.2}$, t, r_l, T, and T_{ref} with their dimensionless forms in the energy balance equation of (5.19), the dimensionless form of energy balance equation is obtained:

(C.75)

$$\frac{\partial T_r}{\partial \tau} = \alpha \frac{1}{r^2}\frac{\partial}{\partial r}\left(r^2 \frac{\partial T_r}{\partial r}\right) + \beta\, e^{-\frac{E_a}{R_g T_b}\left(\frac{1}{T_r}-\frac{1}{T_{r,ref}}\right)} e^{-\left((k_{d,ref}\, t_{char}) e^{-\frac{E_d}{R_g T_b}\left(\frac{1}{T_r}-\frac{1}{T_{r,ref}}\right)}\right)\tau} M_1 + \gamma \frac{1}{V_l}\frac{\partial}{\partial \tau}(M_2 V_l)$$

which can also be written as

(C.76)

$$\frac{\partial T_r}{\partial \tau} = \alpha\left(\frac{\partial^2 T_r}{\partial r^2} + \frac{2}{r}\frac{\partial T_r}{\partial r}\right) + \beta\, e^{-\frac{E_a}{R_g T_b}\left(\frac{1}{T_r}-\frac{1}{T_{r,ref}}\right)} e^{-\left((k_{d,ref}\, t_{char}) e^{-\frac{E_d}{R_g T_b}\left(\frac{1}{T_r}-\frac{1}{T_{r,ref}}\right)}\right)\tau} M_1 + \gamma\left(\frac{\partial M_2}{\partial \tau}\right) + \left(\frac{\gamma M_2}{V_l}\right)\left(\frac{\partial V_l}{\partial \tau}\right)$$

in which, α is the dimensionless thermal diffusivity of the particle defined as

$$\alpha = \frac{\alpha_{ov} t_{char}}{R_l^2} \tag{C.77}$$

β is a clustered function defined as

$$\beta = \frac{\left(-\Delta H_{pol}\right) k_{p,ref} C_0^* [M]_{ov.eq.1} t_{char} (1-\epsilon)}{\rho_{ov} C_{p,pol} T_b \phi^3} \tag{C.78}$$

and finally the clustered function of γ is provided by

$$\gamma = \frac{\left(-\Delta H_{sorp,2}\right)[M]_{ov.eq.2}}{\rho_{ov} C_{p,pol} T_b} \tag{C.79}$$

C.4.3. Discretization

The dimensionless energy balance equation of (C.76) is discretized applying the nonstandard finite difference scheme (NSFD) as described in the previous appendix.

The discrete form of the first-order dimensionless time derivate is provided by the forward Euler representation, while the discrete forms of the first-order and second-order dimensionless space derivatives are given by forward Euler and central difference representations, respectively.

(C.80)

$$\frac{T_{r_i}^{\,j+1} - T_{r_i}^{\,j}}{\Delta\tau^j} = \alpha^j \left(\left(\frac{T_{r_{i+1}}^{\,j} - 2T_{r_i}^{\,j} + T_{r_{i-1}}^{\,j}}{(\Delta r)^2} \right) + \left(\frac{2}{r_i} \right) \left(\frac{T_{r_{i+1}}^{\,j} - T_{r_i}^{\,j}}{(\Delta r)} \right) \right) + \beta_i^j \, e^{-\frac{E_a}{R_g T_b}\left(\frac{1}{T_{r_i}^{\,j}} - \frac{1}{T_{r,ref}}\right)} e^{-\left((k_{d,ref}\, t_{char}) e^{-\frac{E_d}{R_g T_b}\left(\frac{1}{T_{r_i}^{\,j}} - \frac{1}{T_{r,ref}}\right)} \right) \tau^j} M_{1_i}^{\,j} + \gamma \left(\frac{M_{2_i}^{\,j+1} - M_{2_i}^{\,j}}{\Delta\tau^j} \right) + \left(\frac{\gamma M_{2_i}^{\,j}}{V_{l_i}^{\,j}} \right) \left(\frac{V_{l_i}^{\,j+1} - V_{l_i}^{\,j}}{\Delta\tau^j} \right)$$

in which

$$\alpha^j = \frac{\alpha_{ov} t_{char}}{\left(R_l^j\right)^2} \qquad \text{(C.81)}$$

and

$$\beta_i^j = \frac{\left(-\Delta H_{pol}\right) k_{p,ref} C_{0_i}^{*\,j} [M]_{ov.eq.1} t_{char} (1-\epsilon)}{\rho_{ov} C_{p,pol} T_b (\phi^j)^3} \qquad \text{(C.82)}$$

By rearrangement of equation (C.80), the dimensionless temperature in the next time step of *j+1* for each grid of *i*, $T_{r_i}^{\,j+1}$, can be explicitly calculated from

(C.83)

$$T_{r_i}^{j+1} = T_{r_{i+1}}^{j}\left(\left(\frac{\alpha^j \Delta\tau^j}{(\Delta r)^2}\right)+\left(\frac{2\alpha^j \Delta\tau^j}{r_i(\Delta r)}\right)\right) + T_{r_{i-1}}^{j}\left(\frac{\alpha^j \Delta\tau^j}{(\Delta r)^2}\right) + T_{r_i}^{j}\left(1-\left(\frac{2\alpha^j \Delta\tau^j}{(\Delta r)^2}\right)-\left(\frac{2\alpha^j \Delta\tau^j}{r_i(\Delta r)}\right)\right)$$
$$+ \beta_i^j \Delta\tau^j \, e^{-\frac{E_a}{R_g T_b}\left(\frac{1}{T_{r_i}^j}-\frac{1}{T_{r,ref}}\right)} e^{-\left((k_{d,ref}\, t_{char}) e^{-\frac{E_d}{R_g T_b}\left(\frac{1}{T_{r_i}^j}-\frac{1}{T_{r,ref}}\right)}\right)\tau^j} M_{1_i}^{\,j} + \gamma\left(M_{2_i}^{\,j+1} - M_{2_i}^{\,j}\right)$$
$$+ \frac{\gamma M_{2_i}^{\,j}}{V_{l_i}^{\,j}}\left(V_{l_i}^{\,j+1} - V_{l_i}^{\,j}\right)$$

By applying the positivity condition to equation (C.83) and in order to have numerically stable solution, the following mathematical inequality must be valid, as described in detail in the previous appendix

$$1-\left(\frac{2\alpha^j \Delta\tau^j}{(\Delta r)^2}\right)-\left(\frac{2\alpha^j \Delta\tau^j}{r_i(\Delta r)}\right) \geq 0 \qquad \text{(C.84)}$$

This will result in determination of maximum dimensionless time step in order to have numerically stable solution as

$$\Delta\tau^j \leq \frac{(\Delta r)^2}{4\alpha^j} \qquad \text{(C.85)}$$

By substituting equation (C.81) for α^j into (C.85), we will have

$$\Delta\tau^j \leq \frac{\left(R_l^j\right)^2 (\Delta r)^2}{4\alpha_{ov} t_{char}} \qquad \text{(C.86)}$$

or it can be rewritten as

$$\Delta\tau_{max,3}^{j} = \frac{\left(R_l^j\right)^2 (\Delta r)^2}{4\alpha_{ov} t_{char}} \qquad \text{(C.87)}$$

For the grid *i=1*, the boundary condition stated in equation (5.21) will be applied as

$$T_{r_1}^{\,j+1} = T_{r_2}^{\,j+1} \qquad \text{(C.88)}$$

and for grid *i=N*, the boundary condition stated in equation (5.20) can be written in dimensionless form as

$$-\frac{k_{c,p}}{R_l}\frac{dT_r}{dr}\Big|_{R_l} = h\left(T_r\big|_{R_l} - 1\right) \qquad \text{(C.89)}$$

which can be discretized as

$$-\frac{k_{c,p}}{\left(R_l^j\right)}\frac{T_{r_N}^{\,j+1}-T_{r_{N-1}}^{\,j}}{(\Delta r)}=h^j\left(T_{r_N}^{\,j+1}-1\right) \qquad \text{(C.90)}$$

and consequently $T_{r_N}^{\,j+1}$ can be calculated from

$$T_{r_N}^{\,j+1}=\frac{1+\left(\frac{k_{c,p}}{R_l^j\,h^j\,\Delta r}\right)T_{r_{N-1}}^{\,j}}{1+\left(\frac{k_{c,p}}{R_l^j\,h^j\,\Delta r}\right)} \qquad \text{(C.91)}$$

The heat transfer coefficient, *h*, for the spherical polymer particle is calculated by Ranz-Marshall correlation given as

$$Nu=2+0.6Re^{1/2}Pr^{1/3} \qquad \text{(C.92)}$$

in which

$$Nu=\frac{hd_p}{k_{c,g}} \qquad \text{(C.93)}$$

$$Re=\frac{\rho_g u d_p}{\mu} \qquad \text{(C.94)}$$

$$Pr=\frac{\mu C_{p,g}}{k_{c,g}} \qquad \text{(C.95)}$$

with

$$d_p=2R_l \qquad \text{(C.96)}$$

In these correlations, Nu is Nusselt number, Re is Reynolds number, and Pr is Prandtl number. $k_{c,g}$, ρ_g, μ, $C_{p,g}$ represents thermal conductivity, density, viscosity, and heat capacity of gas phase and finally u is the superficial gas-particle velocity.

As a result, one can calculate the heat transfer coefficient by

$$h=\left(\frac{k_{c,g}}{2R_l}\right)\left(2+0.6Re^{1/2}Pr^{1/3}\right) \qquad \text{(C.97)}$$

or at each time step by

$$h^j = \left(\frac{k_{c,g}}{2R_l^j}\right)\left(2 + 0.6\left(Re^j\right)^{1/2} Pr^{1/3}\right) \qquad (C.98)$$

in which

$$Re^j = \frac{\rho_g u\left(2R_l^j\right)}{\mu} \qquad (C.99)$$

C.5. Polymer generation and particle growth

Obviously, the two mass balance equations of (5.3) and (5.14) and the energy balance equation of (C.66) are simultaneously being solved using the numerical method described in the previous sections. Consequently, the dimensionless time increment at each time step, $\Delta\tau^{j}$, must satisfy the positivity condition for all the three sets of equations, in order to have an overall numerically stable solution scheme . As a result, the $\Delta\tau^{j}$ at each time step will be given by

$$\Delta\tau^{j} = \text{Minimum}\left(\Delta\tau^{j}_{\max,1}, \Delta\tau^{j}_{max,2}, \Delta\tau^{j}_{max,3}\right) \qquad (C.100)$$

After calculation of ethylene concentration and temperature at each grid of *i* inside the normalized polymer particle at time step *j+1* from their values at previous time step *j*, it is possible to calculate the mass of polymer produced at *i*th grid during the dimensionless time step of $\Delta\tau^{j}$ by

$$m_{pol_i}^{j+1} = k_{p,ref}\, e^{-\frac{E_a}{R_g T_b}\left(\frac{1}{T_{r_i}^j} - \frac{1}{T_{r,ref}}\right)} C_{0_i}^{*\,j+1} e^{-\left((k_{d,ref}\, t_{char}) e^{-\frac{E_d}{R_g T_b}\left(\frac{1}{T_{r_i}^j} - \frac{1}{T_{r,ref}}\right)}\right)\tau^j} [M]_{ov.eq.1} M_{1_i}^{j+1}\, MW_1\, V_{cat_i}\, t_{char} \Delta\tau^{j} \qquad (C.101)$$

and as a result the total polymer mass produced during the dimensionless time interval of $\Delta\tau^{j}$ is provided by

$$m_{pol.tot}^{j+1} = \sum_{i=1}^{N} m_{pol_i}^{j+1} \qquad (C.102)$$

while the instantaneous rate of polymerization is given by

$$\left(R_{pol}^{ins}\right)^{j+1} = \left(\frac{m_{pol.tot}^{j+1}}{V_{cat}\,\rho_{cat}\,t_{char}\Delta\tau^{j}}\right)\left(\frac{3600}{1000}\right) \qquad (C.103)$$

having the unit of (gr pol/gr cat.hr).

The volume of total polymer produced during the dimensionless time interval of $\Delta\tau^{j}$ will be simply given by

$$v_{pol.tot}^{j+1} = \frac{m_{pol.tot}^{j+1}}{\left(\rho_{pol} \times 1000\right)} \qquad (C.104)$$

regarding the units used and provided at the end of appendix.

The total volume of polymer produced by the end of *j*th time step or in other words by completion of the dimensionless time interval of $\Delta\tau^{j}$ can be calculated from

$$V_{pol}^{j+1} = V_{pol}^{j} + v_{pol.tot}^{j+1} \qquad (C.105)$$

and similarly the total volume of the particle including its porosity by the end of *j*th time step, can be calculated from

$$V_{tot}^{j+1} = V_{tot}^{j} + \frac{v_{pol.tot}^{j+1}}{(1-\epsilon)} \qquad (C.106)$$

The volume of each grid, $V_{l_i}^{j+1}$, consequently can be calculated by

$$V_{l_i}^{j+1} = \left(\frac{v_i}{v}\right) V_{tot}^{j+1} \qquad (C.107)$$

As a result, the equivalent radius of "polymer-only" particle without considering the existing particle porosity at the end of *j*th time step will be given by

$$R_p^{j+1} = \left(\left(\frac{3}{4\pi}\right) V_{pol}^{j+1}\right)^{1/3} \qquad (C.108)$$

and consequently

$$\phi^{j+1} = \frac{{R_p}^{j+1}}{r_{cat}} \qquad (C.109)$$

Similarly, the particle radius at the end of *j*th time step

$$R_l^{j+1} = \left(\left(\frac{3}{4\pi}\right) V_{tot}^{j+1}\right)^{1/3} \qquad (C.110)$$

C.6. Normalization of particle and update of dimensionless balance equations

After calculation of the particle radius at the end of time step *j*, R_l^{j+1}, the normalized particle radius is obtained similar to the equation (5.30) as

$$r_N = \frac{R_l^{j+1}}{R_l^{j+1}} = 1 \qquad (C.111)$$

the normalized particle is discretized afterwards with the same method explained through equations (C.2) to (C.5).

In order to calculate the dimensionless concentration and temperature gradients in the normalized particle during the next time step of *j+1*, and consequently to be able to estimate the instantaneous polymerization rate and the mass and volume of the polymer produced during the next dimensionless time interval of $\Delta\tau^{j+1}$, the dimensionless mass and energy balance equations need to be updated.

Having the particle radius, R_l^{j+1}, and overall growth factor, ϕ^{j+1}, at the end of time step *j* or beginning of time step *j+1*:

1. The dimensionless mass balance equation for ethylene of (C.37) is updated by

$$D_1^{j+1} = \frac{D_{ov.1} t_{char}}{\left(R_l^{j+1}\right)^2} \qquad (C.112)$$

and

$$k_i^{j+1} = k_{p,ref} C_{0_i}^{*\,j+1} t_{char} \left(\frac{(1-\epsilon)}{(\phi^{j+1})^3}\right) \qquad (C.113)$$

with

$$C_{0_i}^{*\,j+1} = C_1^* + C_2^* e^{\left((k_{d,ref}\, t_{char}) e^{-\frac{E_d}{R_g T_b}\left(\frac{1}{Tr_i^{j+1}} - \frac{1}{T_{r,ref}}\right)}\right)\tau^{j+1}} \qquad (C.114)$$

2. The dimensionless mass balance equation for ICA of (C.57) is updated by

$$D_2^{j+1} = \frac{D_{ov.2} t_{char}}{\left(R_l^{j+1}\right)^2} \qquad \text{(C.115)}$$

3. The dimensionless energy balance equation of (C.80) is updated by

$$\alpha^{j+1} = \frac{\alpha_{ov} t_{char}}{\left(R_l^{j+1}\right)^2} \qquad \text{(C.116)}$$

and

$$\beta_i^{j+1} = \frac{\left(-\Delta H_{pol}\right) k_{p,ref} C_{0_i}^{*\,j+1} [M]_{ov.eq.1} t_{char} (1-\epsilon)}{\rho_{ov} C_{p,pol} T_b (\phi^{j+1})^3} \qquad \text{(C.117)}$$

And for its boundary condition at the particle surface, the Reynolds number and heat transfer coefficient are updated by

$$Re^{j+1} = \frac{\rho_g u \left(2R_l^{j+1}\right)}{\mu} \qquad \text{(C.118)}$$

and

$$h^{j+1} = \left(\frac{k_{c,g}}{2R_l^{j+1}}\right)\left(2 + 0.6\left(Re^{j+1}\right)^{1/2} Pr^{1/3}\right) \qquad \text{(C.119)}$$

4. The maximum dimensionless time intervals obtained from imposing the positivity condition to each of the updated balance equations are recalculated respectively by

$$\Delta\tau_{\max,1}^{j+1} = \frac{\left(R_l^{j+1}\right)^2 (\Delta r)^2}{4 D_{ov.1} t_{char}} \qquad \text{(C.120)}$$

$$\Delta\tau_{max,2}^{j+1} = \frac{\left(R_l^{j+1}\right)^2 (\Delta r)^2}{4 D_{ov.2} t_{char}} \qquad \text{(C.121)}$$

$$\Delta\tau_{max,3}^{j+1} = \frac{\left(R_l^{j+1}\right)^2 (\Delta r)^2}{4 \alpha_{ov} t_{char}} \qquad \text{(C.122)}$$

and similar to the previous time step

$$\Delta\tau^{j+1} = \text{Minimum}\left(\Delta\tau^{j+1}_{\max,1}, \Delta\tau^{j+1}_{max,2}, \Delta\tau^{j+1}_{max,3}\right) \quad \text{(C.123)}$$

After calculation of dimensionless concentration and temperature at each grid *i* and time step of *j+1*, the mass and volume of polymer produced during the time interval of $\Delta\tau^{j+1}$ and consequently the new particle radius is calculated as explained for the previous time step of *j*.

The computational loop for grid normalization, growth, and update is schematically demonstrated in Figure C.3.

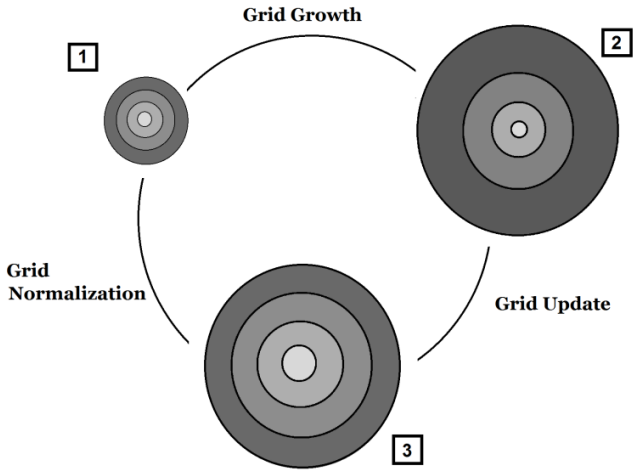

Figure C.3. The schematic representation of computational loop for grid normalization, growth, and update.

The computational loop is repeated until the dimensionless time, τ^j, reaches the dimensionless time for the polymerization reaction,τ_{react}, defined as

$$\tau_{react} = \frac{t_{react}}{t_{char}} \quad \text{(C.124)}$$

in which, t_{react} is the residence time of the catalyst particle in the polymerization reaction environment, from the time of its exposure to the reactor until the time of its withdrawal from the reactor in the form of a fully grown polymer particle.

List of symbols

C^*	concentration of polymerization active sites, (mol site/m^3 cat)
C_0^*	concentration of polymerization active sites at time zero, (mol site/m^3 cat)
$C_{p,g}$	heat capacity of gas phase, (J/kg.K)
$C_{p,pol}$	heat capacity of polymer, (J/kg.K)
D_1	dimensionless diffusivity of ethylene, (dimensionless)
D_2	dimensionless diffusivity of ICA, (dimensionless)
$D_{ov.1}$	overall diffusivity of ethylene through the polymer particle, (m^2/sec)
$D_{ov.2}$	overall diffusivity of ICA through the polymer particle, (m^2/sec)
d_p	diameter of polymer particle, (m)
E_a	activation energy for propagation, (J/mol)
E_d	activation energy for catalyst deactivation, (J/mol)
h	heat transfer coefficient, (J/m^2.sec.K)
k	dimensionless rate coefficient for ethylene polymerization, (dimensionless)
$k_{c,g}$	thermal conductivity of gas phase, (J/m.sec.K)
$k_{c,p}$	thermal conductivity of polymer, (J/m.sec.K)
k_d	deactivation constant, (1/sec)
$k_{d,ref}$	deactivation constant at reference temperature, (1/sec)
k_p	propagation constant, (m^3 tot/mol site.sec)
$k_{p,ref}$	propagation constant at reference temperature, (m^3 tot/mol site.sec)
M_1	dimensionless ethylene concentration in the polymer particle, (dimensionless)
M_2	dimensionless ICA concentration in the polymer particle, (dimensionless)
$[M]_{eq.1}$	equilibrium concentration of ethylene in the polymer phase, (mol/m^3 pol)
$[M]_{eq.2}$	equilibrium concentration of ICA in the polymer phase, (mol/m^3 pol)
$[M]_{ov.1}$	overall concentration of ethylene in the polymer particle, (mol/m^3 tot)
$[M]_{ov.2}$	overall concentration of ICA in the polymer particle, (mol/m^3 tot)
$[M]_{ov.eq.1}$	overall equilibrium concentration of ethylene in whole particle considering its porosity (mol/m^3 tot)
$[M]_{ov.eq.2}$	overall equilibrium concentration of ICA in whole particle considering its porosity (mol/m^3 tot)
MW_1	molecular weight of ethylene, (gr/mol)
m_{pol}	mass of polymer produced, (gr)
N	number of grids, (dimensionless)
Nu	Nusselt number, (dimensionless)

Pr	Prandtl number, (dimensionless)
Re	Reynolds number, (dimensionless)
R_g	universal gas constant, (J/mol.K)
R_l	particle radius, (m)
R_p	equivalent radius of "polymer-only" particle without considering porosity, (m)
R_{pol}	rate of polymerization at the catalyst particle surface, (mol/m^3 cat.sec)
R_{pol}^{ins}	instantaneous rate of polymerization, (gr pol/gr cat.hr)
R_v	volumetric rate of ethylene polymerization inside growing polymer particle, (mol/m^3 tot.sec)
r	dimensionless radial position, (dimensionless)
r_{cat}	radius of initial catalyst particle, (m)
r_l	radial position inside the spherical polymer particle, (m)
T	temperature, (K)
T_b	bulk temperature, (K)
T_r	dimensionless temperature, (dimensionless)
T_{ref}	reference temperature, (K)
$T_{r,ref}$	dimensionless reference temperature, (dimensionless)
t	time, (sec)
t_{char}	characteristic time, (sec)
t_{react}	polymerization reaction time, (sec)
u	gas-particle superficial velocity, (m/sec)
V_{cat}	total catalyst volume, (m^3)
$V_{cat\,i}$	volume of catalyst dispersed in grid i, (m^3)
V_{pol}	volume of polymer, (m^3)
V_{tot}	total particle volume including its porosity, (m^3)
v_i	dimensionless volume of grid i, (dimensionless)

Greek letters

α	dimensionless thermal diffusivity of the particle, (dimensionless)
α_{ov}	overall thermal diffusivity of the particle, (m^2/sec)
β	dimensionless clustered function, (dimensionless)
γ	dimensionless clustered function, (dimensionless)
ΔH_{pol}	enthalpy of ethylene polymerization, (J/mol)

$\Delta H_{sorp,2}$	enthalpy of sorption of ICA in the polymer phase, (J/mol)
ϵ	porosity of polymer particle, (dimensionless)
μ	gas phase viscosity, (kg/m.sec)
ρ_{cat}	catalyst density, (kg/m^3)
ρ_g	gas phase density, (kg/m^3)
ρ_{ov}	overall particle density, (kg/m^3)
ρ_{pol}	polymer density, (kg/m^3)
τ	dimensionless time, (dimensionless)
τ_{react}	dimensionless polymerization reaction time, (dimensionless)
ϕ	overall growth factor, (dimensionless)

Appendix D

Physical and Transport Properties

Calculation Methods

D. Physical and Transport Properties

In this appendix, the methods which have been used in order to estimate the physical and transport properties in different chapters of the thesis are provided. The details of these methods are available in the reference handbooks cited in this appendix.

D.1. Calculation of gas phase viscosity

Calculation of viscosity of pure components at low pressure

First, the viscosity of the pure components of the gas phase in low pressure is calculated in terms of Lennard-Jones parameters

$$\mu_0 = 2.6693 \times 10^{-5} \frac{\sqrt{MT}}{\sigma^2 \Omega_\mu} \qquad (D.1)$$

where if $T[=]K$ and $\sigma[=]Å$, then the $\mu_0[=]g/cm.s$. The dimensionless quantity Ω_μ is a slowly varying function of the dimensionless temperature $\kappa T/\varepsilon$, of order of magnitude of unity. This equation is a useful formula for computing viscosity of nonpolar gases at low pressure (and density) from tabulated values of the intermolecular force parameters σ and ε/κ.[1]

Calculation of viscosity of pure components at reactor conditions

The viscosity of each of components at reactor pressure, is obtained by Reichenberg method[2] from low pressure viscosity values obtained previously.

In the Reichenberg method the ratio of the viscosity of the pure component at higher pressure to its low pressure value (μ/μ_0) is obtained with following correlation

$$\frac{\mu}{\mu_0} = 1 + Q \frac{A\, P_r^{3/2}}{BP_r + \ (1 + CP_r^D)^{-1}} \qquad (D.2)$$

where P_r is reduced pressure for each component, A, B, C, and D are different functions of T_r, reduced temperature of the component, and finally $Q=1$ for nonpolar materials. The error with this method is found to be in the order of few percent and the details of this method can be found in elsewhere[2].

Estimation of the gas phase viscosity as a mixture of pure components

After calculating the viscosity of each pure component at the reactor pressure and temperature, the viscosity of the gas phase of the reactor as a mixture of these components are estimated by the semi-empirical correlation suggested by Wilke[1]. This method has been found to have an average deviation of 2% from experimental measurements. The semi-empirical formula of Wilke is as follows

$$\mu_{mix} = \sum_{\alpha=1}^{N} \frac{x_\alpha \mu_\alpha}{\sum_\beta x_\beta \phi_{\alpha\beta}} \qquad (D.3)$$

where the dimensionless quantity of $\phi_{\alpha\beta}$ is defined as

$$\phi_{\alpha\beta} = \frac{1}{\sqrt{8}}\left(1 + \frac{M_\alpha}{M_\beta}\right)^{-1/2}\left[1 + \left(\frac{\mu_\alpha}{\mu_\beta}\right)^{1/2}\left(\frac{M_\beta}{M_\alpha}\right)^{1/4}\right]^2 \qquad (D.4)$$

N is the number of components in the mixture, x_α is the mole fraction of component α, μ_α is the viscosity of pure component α at the system temperature and pressure, and M_α is the molecular weight of species α.

D.2. Calculation of gas phase density and kinematic viscosity

Mixture of gas is assumed as an ideal gas and the its density is estimated by

$$\rho_{mix} = \frac{P M_{av}}{R_g T} \qquad (D.5)$$

where R_g is the universal gas constant and M_{av} is the average molecular weight of the mixture of components in the gas phase.

$$M_{av} = \sum_{\alpha=1}^{N} x_\alpha M_\alpha \qquad (D.6)$$

Kinematic viscosity of the gas phase is obtained by dividing the viscosity by the density of the fluid

$$\nu_{mix} = \frac{\mu_{mix}}{\rho_{mix}} \qquad (D.7)$$

D.3. Calculation of thermal conductivity of gas phase

Calculation of thermal conductivity of pure components at low pressure

Thermal conductivity of argon at low pressure is calculated directly with the empirical correlation[2] in the format of $k_{c0} = A + BT + CT^2 + DT^3$.

For the rest of components, Roy and Thodos[2] estimation technique was employed. In this method a reduced thermal conductivity is defined as

$$k_{cr} = k_{c0}\Gamma \qquad (D.8)$$

in which Γ is the reduced, inverse thermal conductivity and can be expressed as

$$\Gamma = 210\left(\frac{T_c M^3}{P_c^4}\right)^{1/6} \qquad (D.9)$$

where Γ*[=] (W/(m.K))*$^{-1}$, T_c*[=]K*, *M[=]g/mol*, and P_c*[=]bar*.

Reduced thermal conductivity on the other hand is calculated from

$$k_{cr} = (k_c\Gamma)_{tr} + (k_c\Gamma)_{int} \qquad (D.10)$$

in which

$$(k_c\Gamma)_{tr} = 8.757[\exp(0.0464T_r) - \exp(-0.2412T_r)] \qquad (D.11)$$

$$(k_c\Gamma)_{int} = Cf(T_r) \qquad (D.12)$$

Relations for $f(T_r)$ for different type of materials i.e. saturated hydrocarbons, olefins, etc. are given in Ref. [2]. The constant C is specific for each component and it is estimated by a group contribution method.

By calculating the reduced thermal conductivity, k_{cr}, from equation (D.10) and inverse thermal conductivity, Γ, from equation (D.9), the thermal conductivity of each component at low pressure, k_{c0}, is obtained from equation (D.8).

Calculation of thermal conductivity of pure components at reactor conditions

Stiel and Thodos[2] stablished excess thermal conductivity correlations to consider the effect of pressure in the calculation of thermal conductivity of each component as follows

$$(k_c - k_{c0})\Gamma Z_c^5 = 1.22 \times 10^{-2}[\exp(0.535\rho_r) - 1] \quad for\ \rho_r < 0.5 \qquad (D.13)$$

where k_c and k_{c0} are the thermal conductivity of the component at high pressure and low pressures in the unit of *W/(m.K)*, Z_c is the critical compressibility of the component and ρ_r is the reduced density $\rho_r=\rho/\rho_c$. Parameter Γ is defined in the equation (D.9).

Estimation of the thermal conductivity of gas phase as a mixture of pure components

The thermal conductivity of gas phase as a mixture of pure components is estimated by an analogous method[1] to that previously provided for viscosity:

$$k_{c,mix} = \sum_{\alpha=1}^{N} \frac{x_\alpha k_{c,\alpha}}{\sum_\beta x_\beta \phi_{\alpha\beta}} \qquad (D.14)$$

where coefficients $\phi_{\alpha\beta}$ are identical to those appearing in the viscosity equation (D.4).

D.4. Calculation of specific heat capacity and thermal diffusivity of gas phase

The heat capacity of each component in *J/(mol.K)* is provided in Properties of Gases and Liquids[2] with simple correlation in the format of

$$C_{p,\alpha} = A_\alpha + B_\alpha T + C_\alpha T^2 + D_\alpha T^3 \qquad (D.15)$$

where A_α, B_α, C_α, and D_α are constants specific for each of components, α.

The heat capacity of gas phase as a mixture of pure components in *J/(mol.K)* are calculated by

$$C_{p,mix} = \sum_{\alpha=1}^{N} x_\alpha C_{p,\alpha} \qquad (D.16)$$

Finally, the unit of heat capacity of the gas phase is changed from *J/(mol.K)* to *J/(kg.K)* by following correlation

$$C_{p,mix\left(J/kg.K\right)} = \frac{C_{p,mix\left(J/mol.K\right)}}{M_{av\left(\frac{kg}{mol}\right)}} \qquad (D.17)$$

M_{av} is the average molecular weight of the mixture defined in equation (D.6).

Thermal diffusivity for gas phase, α_{mix}, is calculated according to its definition

$$\alpha_{mix} = \frac{k_{c,mix}}{\rho_{mix} C_{p,mix}} \quad (D.18)$$

D.5. Calculation of diffusivity in gas phase mixture

Calculation of diffusivity of component A in the binary mixture of A and B

The diffusivity of component A in binary mixture of A and B is estimated by:[1]

$$D_{AB} = 0.0018583 \sqrt{T^3 \left(\frac{1}{M_A} + \frac{1}{M_B}\right)} \frac{1}{p\sigma_{AB}^2 \Omega_{D,AB}} \quad (D.19)$$

In the equation above, the units are D_{AB}*[=]*cm^2/s, σ_{AB}*[=]Å*, *T[=]K*, and *p[=]atm*. The dimensionless quantity of $\Omega_{D,AB}$ is a function of the dimensionless temperature $\kappa T/\varepsilon_{AB}$. The parameters σ_{AB} and ε_{AB} are defined as:

$$\sigma_{AB} = \frac{1}{2}(\sigma_A + \sigma_B) \quad (D.20)$$

$$\varepsilon_{AB} = \sqrt{\varepsilon_A \varepsilon_B} \quad (D.21)$$

Calculation of diffusivity of component A in gas phase mixture

The diffusivity of component A in the gas phase as a mixture of different components is calculated by following correlation:[3]

$$D_{A,mix} = \frac{1 - x_A}{\sum_{i=B}^{N} \frac{x_i}{D_{A,i}}} \quad (D.22)$$

where $D_{A,i}$ are the binary diffusivities of component A and component *i*, x_A and x_i are mole fraction of component A and component *i* in the gas phase.

D.6. Estimation of liquid density

It is estimated by the Hankison-Brobst-Thomson technique:[2]

$$\frac{V_s}{V^*} = V_R^{(0)} \left[1 - \omega_{SRK} V_R^{(\delta)}\right] \quad (D.23)$$

$$V_R^{(0)} = 1 + a(1-T_r)^{\frac{1}{3}} + b(1-T_r)^{\frac{2}{3}} + c(1-T_r) + d(1-T_r)^{\frac{4}{3}} \qquad 0.25 < T_r < 0.95 \qquad (D.24)$$

$$V_R^{(\delta)} = [e + fT_r + gT_r^2 + hT_r^3]/(T_r - 1.00001) \qquad 0.25 < T_r < 1.0 \qquad (D.25)$$

Where a,b,c,d,e,f,g, and h are constants.[2] V^* is a characteristic volume of a pure component generally within 1 to 4 percent of the critical volume and ω_{SRK} is the acentric factor. The liquid density is obtained as $\rho_l = \frac{1}{V_s}$.

D.7. Estimation of heat of vaporization

Pitzer acentric factor correlation is used for this purpose. An analytical representation of this correlation is given by:[2]

$$\frac{\Delta H_v}{RT_c} = 7.08(1-T_r)^{0.354} + 10.95\omega(1-T_r)^{0.456} \qquad (D.26)$$

D.8. Estimation of heat capacity of liquid

The Rowlinson modification to the corresponding states methods has been used for estimation of heat capacity of liquid:[2]

$$\frac{C_{pl} - C_p^0}{R} = 1.45 + 0.45(1-T_r)^{-1} + 0.25\omega\left[17.11 + 25.2(1-T_r)^{1/3}T_r^{-1} + 1.742(1-T_r)^{-1}\right] \qquad (D.27)$$

where C_{pl} is the liquid heat capacity for a pure component and $C_p^{\,0}$ is the heat capacity for this component at gas phase at constant pressure as described before.

D.9. Estimation of vapour pressure

The vapour pressure of the components were estimated by the correlation given in Reference.[2]

$$\ln(P_{vp}/P_c) = (1-x)^{-1}(Ax + Bx^{1.5} + Cx^3 + Dx^6) \qquad (D.28)$$

where *A*,*B*,*C*,and *D* are constants specific for each component and *x* is defined as $x = 1 - T_r$.

D.10. References

1. Bird, R. B.; Stewart, W. E.; Lightfoot, E. N. *Transport Phenomena;* 2nd ed.; John Wiley & Sons, Inc.: **2007**.

2. Reid, R. C.; Prausnitz, J. M.; Poling, B. E. *The Properties of Gases and Liquids;* 4th ed.; McGraw-Hill: **1987**.

3. Treybal, R. E. *Mass Transfer Operations;* 3rd ed.; McGraw-Hill: **1987**.